Porins and TonB-like proteins in *Anabaena* sp. PCC 7120

Dissertation

zur Erlangung des Doktorgrades

der Naturwissenschaften

Vorgelegt beim Fachbereich Biowissenschaften

der Johann Wolfgang Goethe-Universität

in Frankfurt am Main

von Hannah Schätzle

aus Hardheim

Frankfurt 2021

(D 30)

vom Fachbereich Biowissenschaften der

Johann Wolfgang Goethe-Universität als Dissertation angenommen.

Dekan: Prof. Dr. Sven Klimpel

Gutachter: Prof. Dr. Enrico Schleiff

Zweitgutachter: Prof. Dr. Claudia Büchel

Datum der Disputation : ...

Table of contents

Zusammenfassung

Cyanobakterien sind photosynthetisch aktive Bakterien, die terrestrisch sowie in Süßwasser- oder Salzwasserlebensräumen vorkommen können. Die Experimente im Rahmen dieser Arbeit wurden am Modell-Cyanobakterium *Anabaena* sp. PCC 7120 durchgeführt (nachfolgend *Anabaena* genannt). *Anabaena* ist ein filamentöses Süßwasser-Cyanobakterium, wobei ein Filament aus mehreren hundert zusammenhängenden Zellen bestehen kann. In Abwesenheit von gebundenem Stickstoff wandelt *Anabaena* etwa jede zehnte bis zwanzigste Zelle in eine sogenannte Heterozyste um. Diese sind spezialisiert auf die Fixierung von Luftstickstoff, was durch den Nitrogenase-Enzymkomplex katalysiert wird. Die Nitrogenase ist sauerstoffempfindlich, weswegen in den Heterozysten, im Gegensatz zu den vegetativen Zellen, keine Photosynthese stattfindet. Zusätzlich schützen spezielle der Äußeren Membran der Heterozysten aufgelagerte Schichten vor dem Eintritt von Sauerstoff in die Zelle, wodurch Heterozysten morphologisch von vegetativen Zellen unterschieden werden können.

Cyanobakterien besitzen eine Gram-negative Zellwandstruktur. Dies schließt das Vorhandensein von zwei die Zelle nach außen hin abgrenzenden Membranen ein (Innere oder Plasmamembran und Äußere Membran). Zwischen diesen befindet sich das Periplasma, mit einer typischerweise dünnen Peptidoglykanschicht. Die Äußere Membran stellt eine Diffusionsbarriere dar, und Parameter wie die Lipopolysaccharid-Struktur oder das Vorhandensein bestimmter Kanalproteine definieren wesentlich ihre Durchlässigkeit. Membranproteine der Inneren und der Äußeren Membran unterscheiden sich in Ihrer Struktur voneinander; während die Membranroteine im ersten Fall eine Beta-Fass Struktur besitzen, sind Proteine der Inneren Membran durch Alpha-Helices in dieser verankert.

Um vom Außenmedium in das Cytosol eines Gram-negativen Bakteriums zu gelangen, müssen Solute und Nährstoffe folglich zwei Membranen überwinden. Je nach Häufigkeit und Größe bestimmter Stoffe gelangen diese durch passive Diffusion oder aktiven Transport über die Äußere Membran ins Periplasma. An der passiven Diffusion bestimmter gelöster Substanzen über die Äußere Membran sind Porine beteiligt. Diese können unspezifisch sein, oder aber eine gewisse Substratspezifität aufweisen, wie zum Beispiel das Maltodextrin-spezifische Porin LamB von *E. coli*. Neben einer Funktion in der diffusionsbasierten Substrataufnahme können Porine auch die Membranintegrität bzw. -stabilität sowie die Sensitivität des Organismus gegenüber bestimmten Antibiotika beeinflussen. Substrate die zum Beispiel zu groß für eine porinvermittelte Diffusion sind, oder nur wenig abundant, müssen aktiv in die Zelle transportiert werden. Der aktive Transport wird von TonB-abhängigen Transportern (TBDT) bewerkstelligt, die durch den Plasmamembran-ständigen

TonB-Komplex energetisiert werden. Der TonB-Komplex besteht aus TonB, ExbB und ExbD Proteinen. TonB interagiert C-terminal mit der sogenannten TonB Box des TBDTs. Der TonB-Komplex kann die Energie, die in Form des Protonengradienten über die Innere Membran gespeichert ist, nutzbar machen und Konformationsänderungen im TBDT induzieren, was einen Substrattransport ins Periplasma ermöglicht. Beispielsweise eisenhaltige Siderophore, Vitamin B12, Nickel oder Häm bilden Substrate für den TonB-abhängigen Transport. Siderophore sind organische Verbindungen die von Mikroorganismen, Pilzen oder Pflanzen sekretiert werden und hochaffin schwer lösliches Eisen binden können, um dann in eisenhaltiger Form wieder in die Zelle transportiert zu werden. Der weitere Transport von Nährstoffen vom Periplasma ins Cytosol über die Innere Membran benötigt in jedem Fall Energie. In dieser Arbeit wurden zum einen TonB-ähnliche Proteine im Cyanobakterium *Anabaena* im Hinblick auf ihre potenzielle Funktion untersucht, und zum anderen wurden Porin-ähnliche Proteine vergleichend analysiert.

In vorangegangenen Analysen wurden vier Proteine in *Anabaena* identifiziert, die eine Aminosäuresequenzähnlichkeit zu TonB Proteinen aufweisen. Die TonB-ähnlichen Proteine in *Anabaena* (TonB1-TonB4) unterscheiden sich in Ihrer Aminosäuresequenz und ihrer Länge. Anhand des im Folgenden beschriebenen Phänotyps der *tonB1*-Mutante (I-*tonB1*[1]), wurde TonB1 (Alr0248) der neuen Funktionalität folgend die Bezeichnung SjdR zugeordnet (*septal junction disc regulator*), welche nun im Weiteren verwendet werden wird. Konservierte funktionelle Aminosäuresequenzen, die in TonB Proteinen anderer Organismen gefunden wurden, sind nur in TonB3, dem längsten putativen TonB Protein in *Anabaena*, vorhanden. Die Im Rahmen der Manuskripte 1 und 2 durchgeführten Transportexperimente zeigten, dass nur die *tonB3*-Mutante signifikant im Transport von eisenhaltigem Schizokinen, dem von *Anabaena* sekretierten Siderophor, beeinträchtigt war. Da eine komplementierende Induktion der Expression der anderen *tonB* Gene in den Mutanten ausgeschlossen werden konnte, scheint nur TonB3 den Schizokinentransport zu energetisieren. Des Weiteren wurde der Transport des Xenosiderophors Ferrichrom getestet, von dem gezeigt werden konnte, dass es für *Anabaena* eine verfügbare Eisenquelle darstellt. In diesem Fall war ebenfalls die *tonB3*-Mutante beeinträchtigt, da das Wachstum dieses Stamms nicht durch die Zugabe von eisenhaltigem Ferrichrom verbessert werden konnte im Vergleich zum Wachstum ohne Eisenquelle. Interessanterweise war auch die *tonB4*-Mutante unfähig eisenhaltiges Ferrichrom als Eisenquelle nutzbar zu machen, in Gegensatz zu I-*tonB2* und I-*sjdR*. In welcher Weise sich das Fehlen von TonB4 auf den Ferrichrom Transport auswirkt konnte nicht abschließend geklärt werden. Die Tatsache, dass trotz des Vorhandenseins von TonB3 in I-*tonB4* (und umgekehrt) kein Wachstumsvorteil durch eisenhaltiges Ferrichrom gezeigt

[1] Alle hier beschriebenen Insertionsmutanten wurden annotiert als „AFS-I-*genX*“ (AFS steht für Arbeitskreis in Frankfurt Enrico Schleiff, I steht für Insertionsmutante). Zur Vereinfachung der Lesbarkeit wurde „AFS-„ im Fließtext ausgeklammert

werden konnte, könnte sowohl für eine gemeinsame Involvierung von TonB3 und TonB4 im Ferrichromtransport als auch für eine Beeinflussung des Ferrichromtransports durch TonB4 auf regulatorischer Ebene sprechen. Es konnte gezeigt werden, dass Eisenmangel sich auf die *tonB4*-Mutante anders auswirkt als auf den Wildtyp. Nach 25 Tagen eisenfreier Kultivierung war der zelluläre Chlorophyllgehalt in der Mutante weniger stark abgesunken als im Wildtyp, was für eine veränderte Anpassung des Stamms an Eisenmangel spricht. Interessanterweise war die Magnesiumkonzentration unter Standard-Wachstumsbedingungen in I-*tonB4* geringer als in Wildtyp, was wiederum die Synthese des Chlorophylls beeinflussen könnte. Zusammengefasst konnten nur TonB3 und putativ TonB4 in Zusammenhang mit dem Siderophortransport in *Anabaena* gebracht werden, exemplarisch gezeigt für Schizokinen und Ferrichrom. SjdR und TonB2 sind hingegen scheinbar nicht involviert, eine eingehende funktionelle Charakterisierung beider Proteine durch die Analyse der Mutanten wurde daher vorgenommen.

Ein Vergleich der Sequenz von SjdR mit den restlichen putativen TonB Proteinen in *Anabaena* zeigte, dass bei SjdR das C-terminale putative Interaktionsmotiv nur teilweise vorhanden ist. Dagegen weist SjdR eine N-terminale Extension ins Cytosol auf, welche bei den anderen TonB-ähnlichen Proteinen nicht vorkommt. Bioinformatische Sequenzanalysen zeigten, dass SjdR Ähnlichkeiten zu ZipA, einem Faktor der an der Zellteilung beteiligt ist, und GltJ, einem Protein das an der Gleitmobilität (*gliding motility*) mitwirkt, besitzt. Die *sjdR*-Mutante zeigte, im Gegensatz zu den Mutanten der anderen *tonB*-Gene, eine starke Beeinträchtigung im Wachstum in Abwesenheit von gebundenem Stickstoff. Eine Expressionsanalyse von *sjdR* kurz nach Transfer von *Anabaena* in stickstoff-freies Medium resultierte in einer verringerten Expression des Gens nach 24 h und 48 h. Dies spricht prinzipiell eher gegen eine direkte Beteiligung von SjdR an der Heterozysten-Differenzierung, da involvierte Gene typischerweise eine verstärkte Expression nach der Induktion von Stickstoffmangel zeigen. Im Gegensatz zur unveränderten Expression der Stickstoffmetabolismus-Markergene *ntcA* und *hepA*, wies I-*sjdR* eine Reduktion des *nifH* Transkripts auf, welches für eine Untereinheit der Nitrogenase codiert. Auch die Nitrogenase-Enzymaktivität war in der *sjdR*-Mutante im Vergleich zum Wildtyp vermindert, was eine ineffiziente Stickstofffixierung in I-*sjdR* impliziert und das vergleichsweise schlechte diazotrophe Wachstum des Stamms erklärt. Eine mikroskopische Analyse ließ eine abnormale Morphologie der I-*sjdR* Heterozysten erkennen. Die Septen zwischen Heterozysten und vegetativen Zellen in *Anabaena* unterscheiden sich normalerweise von den Septen zwischen zwei vegetativen Zellen. Erstere sind stärker verengt, um den Einstrom von Sauerstoff von den photosynthetisch aktiven vegetativen Zellen in die Heterozysten zu minimieren. Die Heterozysten der *sjdR*-Mutante waren elongiert, und die Heterozysten-Septen erschienen weniger eingeschnürt als beim Wildtyp. Des Weiteren wird in

Heterozysten ein Polymer aus Cyanophycin in Septumnähe gebildet, ein zellulärer Stickstoffspeicher, der ebenfalls die molekulare Diffusion zwischen Heterozysten und vegetativen Zellen sterisch verlangsamt. Dieses war in den Heterozysten der *sjdR*-Mutante jedoch nicht oder nur kaum zu erkennen. Die ungewöhnliche Morphologie der Heterozysten-Septen der *sjdR*-Mutante ließ vermuten, dass sich dies auf die molekulare Diffusion zwischen den Zellen auswirken könnte. Wie oben bereits beschrieben sind die Verengung des Septums und die Ausbildung von Cyanophycin wichtige Determinanten der Regulierung der Diffusionsgeschwindigkeit. Um die Geschwindigkeit der interzellulären Diffusion zu ermitteln, wurden die Zellen mit dem fluoreszierenden Marker Calcein gefärbt und anschließend durch FRAP (*Fluorescence recovery after photobleaching*) die Diffusionsgeschwindigkeit bestimmt. Den Annahmen entsprechend war der Molekültransfer zwischen Heterozysten und vegetativen Zellen in der *sjdR*-Mutante vierfach schneller verglichen mit dem Wildtyp. Auch der Calceintransfer zwischen vegetativen Zellen zeigte eine leicht erhöhte Geschwindigkeit in der Mutante im Vergleich zum Wildtyp, jedoch nur um den Faktor 1,5. Um zu analysieren, ob eine veränderte Anzahl der Nanoporen in der Mutante beeinflussender Faktor der veränderten Transfergeschwindigkeit sein könnte, wurden diese elektronenmikroskopisch analysiert und ausgezählt. Aufgrund experimenteller Einschränkungen war dies jedoch nur möglich bei Septen zwischen vegetativen Zellen. Überraschenderweise wurden in den Septen der *sjdR*-Mutante weniger Nanoporen gezählt als beim Wildtyp, was im Hinblick auf die schnellere molekulare Diffusion in I-*sjdR* widersprüchlich erscheint. Außerdem war die Zone, in der sich Nanoporen befanden, relativ zur Gesamtfläche des Septums geringer in der Mutante. Das Fehlen von SjdR beeinflusst folglich die Septen-Morphologie, genauer die des Peptidoglykans. Vermutlich übernimmt SjdR eine Rolle in der Peptidoglykanbildung oder -Anordnung, die in vegetativen Zellen und Heterozysten unterschiedlich stark aktiv oder relevant ist, da sich der Phänotyp der *sjdR*-Mutante besonders in den Heterozysten ausprägt. Die Ursache für die veränderte molekulare Diffusion zwischen den Zellen in der *sjdR*-Mutante kann im Moment nicht genannt werden. Es kann vermutet werden, dass SjdR die Regulation der *septal junctions*, der die Nanoporen auskleidenden Proteinstrukturen, beeinflusst. Deren Regulationspotential in Abhängigkeit von Stress konnte bereits gezeigt werden in *Anabaena*. Vermutlich ist der Sauerstoffeintritt in die Heterozysten der *sjdR*-Mutante verstärkt, wodurch sowohl die Expression des *nif* Gens als auch die Enzymaktivität vermindert würden. Dadurch würde das diazotrophe Wachstum verlangsamt werden. Bemerkenswerterweise konnten hohe $CaCl_2$-Konzentrationen im Wachstumsmedium die Wachstumsverzögerung von I-*sjdR* in Abwesenheit von gebundenem Stickstoff komplementieren. Auch die Peptidoglykanmorphologie in den Septen normalisierte sich in der *sjdR*-Mutante in Gegenwart von 5 mM $CaCl_2$. Dies könnte beispielsweise auf eine Regulierung der

Elongasom-Aktivität durch Calcium zurückgeführt werden, was den Effekt der SjdR Mutation komplementiert. Begründet durch die ungewöhnliche Proteinstruktur und die TonB-untypische Funktionalität in der Peptidoglykan-Modellierung kann SjdR von der Liste putativer TonB Proteine eliminiert werden.

Um putative Funktionen der bis dato uncharakterisierten TonB-ähnlichen Proteine TonB2 und TonB4 zu erhalten, wurde im Rahmen von Manuskript 2 eine Charakterisierung dieser *tonB*-Insertionsmutanten durchgeführt. Es konnte gezeigt werden, dass im Gegensatz zu I-*sjdR*, bei den *tonB2*- und *tonB4*-Mutanten kein Wachstumsdefekt in Abwesenheit einer gebundenen Stickstoffquelle vorlag, ebenso wenig wie eine veränderte Peptidoglykanmorphologie der Septen. Trotzdem wiesen sowohl I-*tonB2* als auch I-*tonB4* eine Reduktion der Nitrogenaseaktivität auf, sowohl in An- als auch in Abwesenheit von Sauerstoff. In beiden Stämmen wurde eine veränderte intrazelluläre Konzentration von Molybdän gemessen, das einen Kofaktor der Nitrogenase darstellt. In I-*tonB2* war die Mo Konzentration verglichen mit dem Wildtyp erhöht, in I-*tonB4* dagegen vergleichsweise verringert. Insbesondere eine Reduktion der Mo Konzentration könnte die Nitrogenaseaktivität negativ beeinflussen. Dennoch scheint sich die Stickstofffixierung in beiden Stämmen zu einem späteren Zeitpunkt (zumindest teilweise) wieder zu normalisieren, da wie bereits erwähnt kein Wachstumsdefekt zu beobachten war. In I-*tonB4* konnte außerdem eine Reduktion der Kobaltkonzentration festgestellt werden, und in I-*tonB2* eine erhöhte Kupferkonzentration. Letzteres könnte eine Folge der vermehrten Produktion von Lipopolysacchariden (LPS) in der *tonB2*-Mutante sein, da die anionischen Gruppen des LPS an der Komplexierung von Metallionen beteiligt sind. Bemerkenswerterweise konnte gezeigt werden, dass die Expression der meisten putativen Poringene in der *tonB2*-Mutante verglichen mit dem Wildtyp heruntergefahren war, was wiederum eine Konsequenz von vermehrter Metalladsorption an der Zelloberfläche des Stamms sein könnte. Eine vermehrte LPS Produktion sowie eine Verringerung der Porinexpression konnte bereits in anderen Organismen in Zusammenhang mit einer Antibiotikaresistenz gebracht werden, und auch I-*tonB2* konnte in Anwesenheit von SDS, Erythromycin oder Neomycin besser wachsen als der Wildtyp. Des Weiteren konnte beobachtet werden, dass Flüssigkulturen von I-*tonB2* eine übermäßige Filamentaggregation und eine gelbliche Färbung aufwiesen verglichen mit dem Wildtyp und den anderen *tonB*-Mutantenstämmen. Ersteres kann vermutlich auf die erhöhte LPS Produktion zurückgeführt werden. Eine Quantifizierung von Chlorophyll und Carotinoiden zeigte, dass I-*tonB2* sowohl unter Starklicht als auch unter Schwachlichtbedingungen ein geringeres Verhältnis von Chlorophyll zu Carotinoiden besaß. Dies war zwar auch bei I-*tonB3* unter Schwach- und Normallichtbedingungen der Fall, jedoch nicht bei Starklicht. In dem Cyanobakterium *Anabaena oryzae* konnte gezeigt werden, dass die Zugabe von bestimmten Metallen (u.a. auch Kupfer) zu einem erhöhten Carotinoidgehalt

in den Zellen führte. Deshalb kann vermutet werden, dass im Fall von I-*tonB2* die Pigmentierung durch die erhöhte Akkumulierung von Kupfer beeinflusst wird. Oxidativer Stress als Ursache der hohen Carotenoidproduktion gilt als unwahrscheinlich, da die Expression der Superoxiddismutasegene in der *tonB2*-Mutante geringer war als im Wildtyp. Das Fehlen von TonB2 verändert folglich die Integrität der Äußeren Membran in *Anabaena*.

Neben TonB-ähnlichen Proteinen wurde im Rahmen dieser Arbeit auch eine vergleichende Analyse der putativen Porine von *Anabaena* vorgenommen. Insgesamt wurden neun Proteine mit Ähnlichkeit zu Porinen in *Anabaena* vorhergesagt. Sieben hiervon wiesen bei der Analyse der Proteindomänen porintypische Eigenschaften auf und wurden daraufhin näher untersucht (hierbei handelt es sich um Alr0834, Alr2231, All4499, Alr4550, Alr4741, All5191 und All7614). Es wurden Mutantenstämme der einzelnen Poringene hergestellt, deren phänotypische Eigenschaften analysiert wurden. Bis auf zwei Insertionsmutanten (I-*alr2231* und I-*all4499*) konnten alle Stämme segregiert werden, was bedeutet, dass eine Plasmidinsertion in alle Kopien des entsprechenden Gens stattfand. In Wachstumsanalysen, bei denen die Mutantenstämme und der Wildtypstamm auf festem Medium in Anwesenheit von hohen Konzentrationen von Metallen oder schädlichen Stoffen wuchsen, konnte gezeigt werden, dass die unterschiedlichen Mutanten in Teilen differenzierte phänotypische Merkmale aufwiesen. Zum einen zeigte die Mutante I-*alr4550* eine generelle extreme Sensitivität gegenüber hohen Metallkonzentrationen, wohingegen die anderen Porinmutantenstämme, mit Ausnahme von I-*alr4741*, eine besonders hohe Resistenz gegenüber hohen Kupferkonzentrationen demonstrierten. Des Weiteren konnte für I-*alr2231* eine erhöhte Resistenz gegenüber hohen Zinkkonzentrationen, und für I-*alr0834*, I-*all4499* und I-*alr4741* eine größere Resistenz in Anwesenheit hoher Mangankonzentrationen verglichen zum Wildtyp gezeigt werden. Davon ausgehend, dass Resistenzen der Mutantenstämme auf eine vergleichsweise verringerte Aufnahme der entsprechenden Stoffe zurückgeführt werden können, könnten ebendiese als putative Substrate der Porine vermutet werden. Wie auch in Gegenwart von hohen Metallkonzentrationen, konnte I-*alr4550* wenn überhaupt nur sehr schlecht wachsen, wenn Salz, Antibiotika, SDS, Lysozym oder Proteinase K im Medium vorhanden waren. Zusammengefasst weist die ausgeprägte Empfindlichkeit der *alr4550*-Mutante gegenüber den genannten Stoffen auf eine beschädigte Integrität der Zellwand und/oder -membranen hin. Die anderen Porinmutantenstämme hingegen wiesen größtenteils eher ein verbessertes Wachstum unter diesen Bedingungen im Vergleich zum Wildtyp auf. Interessanterweise konnte I-*all5191* nur langsam in Abwesenheit von gebundenem Stickstoff wachsen, einer Bedingung bei der *Anabaena* Heterozysten differenziert. Verglichen hierzu wuchsen I-*alr0834* und I-*alr4741* zu einer höheren Dichte als der Wildtyp ohne gebundenen Stickstoff, die Ursache hierfür ist jedoch unklar. Das Vorhandensein von All5191 scheint die Stickstofffixierung in *Anabaena* zu beeinflussen, und

die höhere Heterozystenfrequenz in I-*all5191* verglichen mit dem Wildtyp könnte die Kompensation einer unzureichenden Stickstofffixierung implizieren.

Eine Expressionsanalyse der einzelnen Poringene wurde durchgeführt, nachdem Replikate des Wildtyps 21 Tage jeweils ohne Mangan, Eisen, Kupfer oder Zink herangezogen wurden. Unterschiedliche Effekte auf die Expression der einzelnen Gene konnten hier herausgestellt werden. *Alr4550* zeigte als einziges der getesteten Gene eine verringerte Expression, nachdem der Wildtyp in Abwesenheit der beschriebenen Metalle (mit Ausnahme von Mangan) gewachsen war, verglichen mit Normalbedingungen. Andererseits zeigte sich nach Wachstum in manganfreiem Medium eine erhöhte mRNA-Abundanz von *alr0834*, *alr2231*, *alr4741* und *all5191* verglichen zum Wachstum unter Normalbedingungen, was auf eine gemeinsame Funktion dieser Porine in der Mangandiffusion hinweisen könnte. Auch die Kultivierung in eisenfreiem Medium induzierte die Expression von *alr0834*, *all4499* und *all5191*. Die Rolle von Porinen im Eisentransport ist jedoch unklar, da Eisen als schlecht löslich gilt und siderophorabhängige Eisentransportprozesse in *Anabaena* beschrieben sind. Vermutlich existieren in *Anabaena* mehrere Wege der Eisenaufnahme, wie zu Beispiel für das einzelligen Cyanobakterium *Synechocystis* sp. PCC 6803 gezeigt werden konnte. Interessanterweise konnte bei keinem der Poringene eine vermehrte Transkription gezeigt werden nachdem der Wildtyp in Abwesenheit von Kuper kultiviert worden war verglichen mit Normalbedingungen, obwohl fast alle der Porinmutanten einen Wachstumsvorteil gegenüber dem Wildtyp im Beisein hoher Kuperkonzentrationen aufwiesen. Um eindeutig herauszustellen ob und wenn ja welche der putativen Porine an der Aufnahme von Eisen oder anderer Metalle beteiligt sind, wären spezifischere Experimente erforderlich. Dennoch kann im Rahmen der hier zusammengefassten Ergebnisse eine Differenzierung der putativen Funktionen einzelner Porine vermutet werden. Zusammengefasst kann Alr4550 eine spezielle Rolle innerhalb der Porine von *Anabaena* zugeschrieben werden, da die Anwesenheit dieses Proteins Voraussetzung für eine stabile Membranintegrität ist. Das Fehlen von All5191 wirkt sich in noch unbekannter Weise nachteilig auf die Wachstumskapazität in Abwesenheit von gebundenem Stickstoff aus, was im Gegensatz zum schnelleren Wachstum der Mutanten I-*alr0834* und I-*alr4741* unter diesen Bedingungen steht. Eine Verbindung von Alr2231 zur Zinkaufnahme, sowie anderer Porinkandidaten zur Aufnahme von Mangan oder Kupfer, kann durch die in Rahmen dieser Arbeit durchgeführten Experimente vermutet werden, definitive Schlussfolgerungen benötigen jedoch weitere experimentelle Bestätigung.

1. Introduction

1.1. The cyanobacterial Gram-negative cell envelope

Bacteria can be generally classified by the composition of their cell envelope. Monoderm, Gram-positive bacteria are surrounded by one membrane and a thick, multi layered peptidoglycan (PG) mesh underneath (Silhavy et al., 2010). In contrast, the Gram-negative cell envelope structure comprises an inner or plasma membrane (PM), a flexible but rigid, thin PG layer and an outer membrane (OM, Silhavy et al., 2010). The PG layer of Gram-negative bacteria functions as a determinant of bacterial cell shape and integrity, and is located in the periplasm, an aqueous protein-rich compartment confined by the two membranes (Cabeen and Jacobs-Wagner, 2005). Single glycan strands of different lengths depending on the species are cross-linked to different degrees (Vollmer et al., 2008). The periplasm presents an oxidative environment that is devoid of energy-rich compounds such as ATP or GTP. Whereas the PM constitutes a phospholipid bilayer, the two leaflets of the OM differ in composition and constitute an asymmetric bilayer. The inner leaflet of the OM contains phospholipids, while the outer leaflet consists of lipopolysaccharides (LPS, Kamio and Nikaido, 1977, 1976; Mühlradt and Golecki, 1975). The OM acts as permeability barrier that limits the diffusion of hydrophilic and (due to the presence of LPS) also hydrophobic compounds. The major determinants regulating the barrier function of the OM are therefore the LPS structure and the abundance of proteinaceous pores or transporters (Nikaido, 2003). In contrast to PM-embedded transmembrane proteins, which are embedded via hydrophobic alpha-helices, proteins of the OM constitute beta-barrels (Schulz, 2002).

Cyanobacteria are Gram-negative, photosynthetic bacteria. Next to OM and PM most cyanobacteria possess a thylakoid membrane system, which might be connected to the PM and harbours the membrane embedded photosynthetic machinery (Nickelsen et al., 2011). Both the cyanobacterial OM and the PM host carotenoids (Jürgens and Weckesser, 1985; Resch and Gibson, 1983), which might represent a protection mechanism against oxidation (Hahn and Schleiff, 2014). Cyanobacteria can be grouped into five sections, based on morphological features and the division mode (Rippka et al., 1979). The sections are not monophyletic, and the classification is based on traits that appear to have evolved more than once (Schirrmeister et al., 2015). Unicellular species belong to sections I and II, whereas multicellular filamentous species are classified in sections III-V (Rippka et al., 1979). Notably, multicellularity among the bacterial kingdom is not limited to cyanobacteria, as also representatives of actinomycetes or sulphur bacteria grow in filaments (Lyons and Kolter, 2015). Strains in section III do not differentiate specialized cells in response to environmental stimuli, whereas genera in sections IV and V differentiate heterocysts, cells specialized to

nitrogen fixation, and sometimes also akinetes (spore-like resting cells) or motile hormogonia (Rippka et al., 1979). Genera from section IV divide in one plane, whereas genera from section V divide in several planes (Rippka et al., 1979).

Even though cyanobacteria are considered as Gram-negative bacteria due to the presence of two membranes, their cell envelope structure adopts certain features which are characteristic for Gram-positive bacteria (Hahn and Schleiff, 2014; Hoiczyk and Hansel, 2000). Firstly, the PG layer in cyanobacterial species is thicker compared to that of other Gram-negative species like *E. coli* or *Pseudomonas aeruginosa* (Table 1), and thus consists of more PG layers. This implies a larger distance between OM and PM (Table 1), which sets different requirements for the dimension of trans-envelope machineries. Among envelope proteins, cyanobacteria-specific differences to related proteins in other Gram-negative organisms were discovered, below exemplarily discussed for porins. Not only the thickness, but also the chemical structure of the PG differs between cyanobacteria and other Gram-negative bacteria. The percentage of PG cross-linking with 56% in *Synechocystis* sp. strain PCC 6714 is exceptionally high for a Gram-negative bacterium, considering the *E. coli* PG cross-linking of approximately 30% (Braun et al., 1973; Jürgens et al., 1983). Furthermore the LPS structurally varies, for example the LPS core component 3-deoxy-d-manno-octulosonic acid found in most Gram-negative bacteria is not existing in cyanobacteria, and also the lipid A composition differs (Durai et al., 2015).

Table 1. Dimensions of bacterial cellular compartments in nanometres (nm).

	Escherichia coli[1]	*Pseudomonas aeruginosa*[1]	*Anabaena* sp. PCC 7120[2]	*Oscillatoria princeps*[3]	*Synechocystis* sp. PCC 6714[4]
Periplasm width (OM-PM)	21.0 ± 2.7	23.9 ± 3.9	46 ± 3	ND	ND
PG thickness	6.4 ± 0.5	2.4 ± 0.5	14 ± 2	Up to 700	~ 12
PM thickness	5.8 ± 0.4	6.0 ± 0.9	3.6 ± 0.5	~ 6	ND
OM thickness	6.9 ± 1.0	7.5 ± 0.6	3.8 ± 0.2	~ 6-8	~ 8

[1]Matias et al., 2003, [2]Wilk et al., 2011, [3]Hoiczyk and Baumeister, 1995, [4]Jürgens et al., 1985, ND = not determined, OM = outer membrane, PM = plasma membrane, PG = peptidoglycan.

In some species of Gram-negative bacteria extracellular polysaccharides (EPS) or proteinaceous S-layer subunits are deposited to the outer side of the OM (Ehling-Schulz et al., 1997; Šmarda et al., 2002). Functions of the S-layer or EPS comprise the regulation of cell adhesion, cell protection or virulence (Costa et al., 2018; Sára and Sleytr, 2000). The ability to form these structures is varying among single cyanobacterial species. Some unicellular cyanobacteria were found to form S-layers, whereas in other orders like Nostocales S-layers have not been described until today (Šmarda et al., 2002). EPS

production, however, seems to be a widely distributed feature in cyanobacteria including Nostocales (Pereira et al., 2009; Šmarda et al., 2002).

In filamentous species such as in the model heterocyst-forming bacterium *Anabaena* sp. PCC 7120 (*Anabaena* hereafter), the OM does not enter into the septa between adjacent cells and continuously surrounds the whole filament, which might comprise hundreds of cells (Mariscal et al., 2007). Consequently, a continuous periplasm exists throughout the filament. The PM uniquely surrounds single cells within the filament in contrast to the OM (Mariscal et al., 2007; Flores et al., 2006). In the septum region, the peptidoglycan meshes of adjacent cells come close together and built up “dense circular areas” termed septal disks (Mariscal et al., 2016). Remarkably, peptidoglycan sacculi of connected cyanobacterial cells could be isolated as a whole (Lehner et al., 2011), and in the septal disks small perforations termed nanopores were detected that are crucial for intercellular communication (Lehner et al., 2013; Nürnberg et al., 2015).

1.2. Cell differentiation and intracellular communication in *Anabaena*

Experiments in the frame of this study were conducted with the cyanobacterial model strain *Anabaena*. This species belongs to section IV, since the cells divide in one plane, and heterocysts for dinitrogen fixation are differentiated upon limitation of a combined nitrogen source (Fig. 1; Rippka et al., 1979). Heterocyst development in *Anabaena* already starts a few hours after the cells experience the starvation of combined nitrogen, and the differentiation is tightly regulated through the interplay of conserved transcription factors and signal molecules (Kumar et al., 2010). Important key players in *Anabaena* nitrogen control are the transcription factors NtcA, that indirectly senses the availability of combined nitrogen and initiates differentiation, and HetR, the master regulator of heterocyst development (Herrero et al., 2004, 2001; Kumar et al., 2010).

The nitrogen fixation in heterocysts is facilitated by the nitrogenase enzyme that is highly sensitive to oxygen (Gallon, 1992). However, since oxygen inevitably evolves during photosynthesis, these two processes need to be separated either temporally or spatially, the latter occurs in *Anabaena* (Fay, 1992). Thus, under diazotrophic conditions a division of labour emerges in the *Anabaena* filament. Photosynthesis is restricted to vegetative cells and nitrogen fixation exclusively takes place in heterocysts. Heterocysts, in contrast to vegetative cells, do not divide (Wilcox et al., 1973). They occur in a semi-regular pattern along the *Anabaena* filament, typically every 10^{th}–20^{th} vegetative cell will differentiate (Kumar et al., 2010). Upon terminal differentiation specific genetic and morphological modifications occur, so that a heterocyst cannot become a vegetative cell again. Heterocysts are less pigmented than vegetative cells, and due to the additional envelope layers they appear comparatively

larger (Kumar et al., 2010). The heterocyst-specific layers consist of a glycolipid layer (HGL) on top of the OM, followed by the heterocyst-envelope polysaccharide layer (HEP, Fig. 1) which mechanically protects the HGL coat (Nicolaisen et al., 2009). Thereby the oxygen penetration into heterocysts from the surrounding is diminished and the formation of a micro-oxic environment in the heterocyst, which is a condition for the nitrogenase function, is facilitated. Oxygen evolution is further reduced through the deactivation of photosystem II and an elevated rate of respiration in heterocysts (Wolk et al., 1994). The septum area between vegetative cells and heterocysts is more constricted than the septa between vegetative cells (Fig. 1). Further, the polymeric nitrogen-sink cyanophycin accumulates near the heterocyst poles and reduces the compound exchange between adjacent cells (Mullineaux et al., 2008).

Heterocysts and vegetative cells mutually depend on each other, and thus molecule exchange along the filament is required for diazotrophic growth. The vegetative cells supply the heterocysts with reduced carbon in form of glutamate, alanine and sucrose, which gets rapidly consumed (Jüttner, 1983; López-Igual et al., 2010; Thomas et al., 1977; Wolk et al., 1976). The export of fixed nitrogen from heterocysts into vegetative cells occurs in form of the nitrogen-rich compounds glutamine and beta-aspartyl-arginine, a breakdown product of cyanophycin (Burnat et al., 2014; Thomas et al., 1977; Wolk et al., 1976). The cell specific accumulation of certain metabolites grounds on an asymmetric distribution of certain key enzymes, which are required for the breakdown of specific substrates, between heterocysts and vegetative cells.

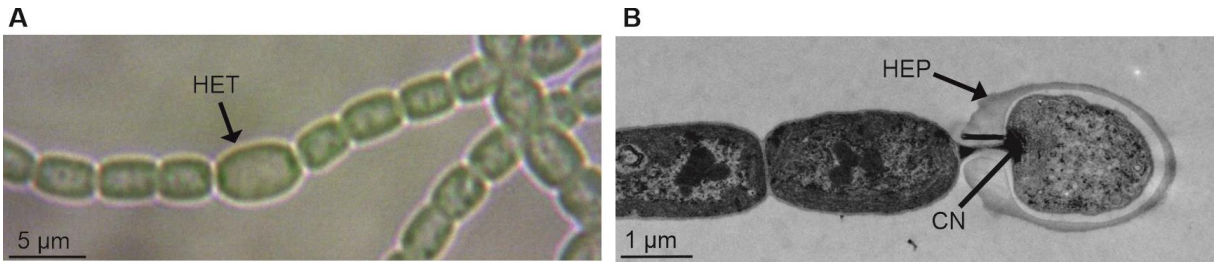

Figure 1. *Anabaena* sp. PCC 7120 heterocysts. **A** Light microscopy image of an *Anabaena* filament consisting of vegetative cells and a heterocyst (HET, marked with arrow). **B** Transmission electron micrograph of an *Anabaena* filament with a terminal heterocyst. The heterocyst specific polysaccharide layer (HEP) and the cyanophycin polymer (CN) are marked.

In *Anabaena*, small solutes between adjacent cells are exchanged in a diffusion-based manner, exemplarily shown for fluorescent model substrates (Mariscal et al., 2011; Mullineaux et al., 2008). This is typically not the case for transport processes across the PM (Nieves-Morión et al., 2017b). The molecules distribute through cell-cell connections termed septal junctions, which are proteinaceous factors traversing the nanopores in the septum (Arévalo et al., 2021; Flores et al., 2018, 2016). Proteins that are considered to build up

septal junctions are for example SepJ (Flores et al., 2007; alternatively termed FraG, Nayar et al., 2007), FraC and FraD (Herrero et al., 2016; Merino-Puerto et al., 2011). Interestingly, today it is assumed that more than one type of septal junction exists, putatively consisting of different proteins (Nürnberg et al., 2015). This hypothesis is based on the observation that mutants of each *ΔsepJ*, *ΔfraC* and *ΔfraD* are compromised in the diffusion of the model substrates calcein and esculin (Merino-Puerto et al., 2010; Mullineaux et al., 2008; Nürnberg et al., 2015). The transfer of 5-carboxyfluorescein (being with 374 Da of lower molecular weight than 622 kDa calcein), however, is only slightly affected in the *ΔsepJ* mutant, but drastically reduced in *ΔfraC, ΔfraD* mutants (Merino-Puerto et al., 2011). Filament fragmentation is a common phenotype of strains where the denoted septal protein encoding genes are mutated, indicating that the septal junctions confer filament stability (Mariscal et al., 2007; Merino-Puerto et al., 2010; Nayar et al., 2007).

1.3. Porins: an overview

Metalloproteins are involved in important cellular processes. Iron is required for the functionality of iron-sulfur clusters, manganese is present in the oxygen evolving centre of photosystem II and structural zinc sites are important for the stability of DNA-binding and ribosomal proteins (Pernil and Schleiff, 2019). A tight regulation of the intracellular metal availability is a perquisite to ensure that proteins are loaded with the correct cofactors, as many metalloproteins can bind several metals with different affinities (Foster et al., 2014). Also, if the concentration of a metal exceeds a critical concentration, the risk of oxidative damage emerges (Ladomersky and Petris, 2015; Touati, 2000). Thus, cellular metal transport, diffusion and export must be tightly controlled (Chandrangsu et al., 2017; Hantke, 2001).

When the supply of certain solutes or metals in the surrounding is sufficient, porins might facilitate the entry of these substrates into the periplasm (Fig. 2). Porins constitute passive diffusion pores that are conserved among Gram-negative bacteria (Nikaido, 2003). Regarding metal ions, in different bacteria the presence of porins involved in the diffusion of inorganic iron (Catel-Ferreira et al., 2016; Gerken et al., 2020; Jones and Niederweis, 2010; Qiu et al., 2021), manganese (Jiang et al., 2020) or copper (González-Sánchez et al., 2018; Haeili et al., 2015; Speer et al., 2013) is assumed. Originally, the name porin referred to OM-channels that lack specificity (Nikaido, 2003). Though, over the last years the term established to describe both unspecific and specific passive diffusion pores; likewise porins will be defined within this thesis. Porins constitute water-filled pores that in general are highly abundant in the OM of bacteria (Choi and Lee, 2019; Galdiero et al., 2013; Nikaido, 1994). Prerequisites for a porin-facilitated solute passage are on the one hand the adequate size of the substrate, which must not exceed the pore size of the porin. On the other hand, as

diffusion is occurring in the direction of a concentration gradient, the solute must be available in sufficient amounts. Porins are mostly homotrimeric proteins, each composed of up to 18 beta-strands (Galdiero et al., 2013). The beta-strands within one barrel are connected through loops of variable lengths. Surface exposed loops may function as contact sites for substrates or phages (Basle et al., 2004; Huff et al., 2009; Wager et al., 2010). Surface exposed loop 2 together with hydrophobic interactions between the monomer is involved in porin trimerization (Phale et al., 1998; Solov'eva et al., 2018). The monomers in a trimer are thought to function as independent pores, whereas the trimerization conveys structural stability (Vergalli et al., 2020). Loop 3, in contrast to the other surface exposed loops, orientates into the barrel contouring the constriction site and pore selectivity characteristics. Residues of Loop 3 contribute to the formation of an electrostatic field that regulates the solute diffusion through the channel (Cowan et al., 1992; Karshikoff et al., 1994).

A structural classification differentiates between general porins, representing 16-stranded barrels that allow the passage of substrates up to a molecular weight of 600 Da, and specific porins (Koebnik et al., 2000). General porins can be selective for cations or anions, examples are the anion channel PhoE or the cation selective OmpF from *E. coli* (Benz et al., 1985). They represent the main entrance for antibiotics with polar nature, such as penicillins or fluoroquinolones, and thus play important roles in antibiotic susceptibility (Vergalli et al., 2020). Specific porins typically consist of 18 beta-strands and are for example specific to certain sugars, such as the sugar specific LamB in *E. coli* (von Meyenburg and Nikaido, 1977). However, a structurally based classification seems impractical, since also porin-like channels with different numbers of beta-strands exist. An example is the 8-stranded OmpW-type porin that mediates iron diffusion in *Acinetobacter baumannii* (Catel-Ferreira et al., 2016).

Apart from nutrient translocation, porins obtain other functionalities such as promoting envelope stability. For instance, the slow OprF porin, which is the major porin in *Pseudomonas aeruginosa,* exists in two distinct conformations (Sugawara et al., 2006). Those are the predominant "closed state", with an 8-stranded barrel and a globular domain in the periplasm, and the less frequent "open state" constituting a 14-16 stranded barrel (Chevalier et al., 2017; Sugawara et al., 2006). The globular domain interacts with a lipoprotein and PG associated components and thereby OprF confers structural stability (Navare et al., 2015; Rawling et al., 1998). The expression of porin genes is often linked to substrate or nutrient availability (Liu and Ferenci, 1998), for instance the expression of phosphate specific PhoE is triggered by phosphate depletion (Overbeeke and Lugtenberg, 1980). Also factors like pH, osmolarity and antibiotic stress can influence porin gene expression (Vergalli et al., 2020).

1.3.1. Cyanobacterial porins

In contrast to proteobacterial porins, porins in cyanobacteria are only sparsely analysed. Cyanobacterial porins are of higher molecular weight (with up to 50 kDa) than proteobacterial representatives, which rarely exceed 40 kDa (Hansel et al., 1994; Nikaido, 2003). This grounds on the presence of an N-terminal S-layer homology (SLH) domain (Hansel and Tadros, 1998), a motif that interacts with PG associated components (Mesnage et al., 2000; Ries et al., 1997). In the genome of *Synechocystis* sp. strain PCC 6803 (*Synechocystis* sp.), six putative porin genes were assigned (F. Huang et al., 2004). Here, the absence of classical, carbohydrate-specific porins was suggested, since the three predominant OM channel proteins Slr1841, Slr1908, and Slr0042 did not mediate the diffusion of organic compounds, whereas the TolC-like protein Slr1270 did (Kowata et al., 2017). The overall permeability of the *Synechocystis* sp. OM was determined to be 20-fold lower than that of *E. coli*. The authors connect this observation to the photosynthetic lifestyle of cyanobacteria, which renders the carbohydrate uptake redundant (Kowata et al., 2017). Only recently, a porin involved in inorganic iron diffusion was described in *Synechocystis* sp. and, moreover, this porin class is considerably conserved among cyanobacteria (Qiu et al., 2021).

In *Anabaena,* it was hypothesized that the uptake of ethidium bromide and erythromycin is porin-dependent (Hahn et al., 2012). Proteomic analyses of the OM revealed that the putative porins Alr4550 and All4499 together with the Omp85 protein Alr2269 represent the most abundant OM proteins (Moslavac et al., 2005). Omp85 proteins like BamA from *E.coli* constitute parts of the beta-barrel assembly machinery, that catalyses the membrane insertion of beta-barrel proteins including porins (Noinaj et al., 2017). In the *Anabaena* genome, three Omp85 homologs were identified: Alr2269, Alr4893 and Alr0075 (Ertel et al., 2005; Inoue and Potter, 2004; Moslavac et al., 2005). Respective single recombinant mutants exhibited in parts specific phenotypes, which led to the conclusion that the three *Anabaena* Omp85 proteins have distinct functionalities (Brouwer et al., 2019; Tripp et al., 2012). It is thought that at least Alr2269 is involved in the insertion of OM proteins, because the interaction with the periplasmic chaperone Tic22 was established, which transfers the unfolded OMP substrates to Alr2269 (Brouwer et al., 2019).

1.4. Iron limitation in cyanobacteria

The demand for specific metal species varies between different bacteria species; regarding the trace metals, iron and zinc are present in the highest concentrations in *E. coli* ($2*10^5$ atoms per cell or 0.1 mM), followed by copper, manganese and molybdenum with concentrations in the range of 10^4 atoms per cell (Finney and O'Halloran, 2003; Fresenborg et al., 2020; Outten and O'Halloran, 2001). Comparative analyses showed that in cyanobacteria the intracellular concentrations of iron and manganese are more than one

order of magnitude higher than in *E. coli* (Fresenborg et al., 2020). The increased iron demand of cyanobacteria can be explained by the prevalence of iron-containing proteins involved in photosynthesis and nitrogen fixation (Kranzler et al., 2013).

In aquatic environments, suitable iron supply is not always guaranteed due to its solubility. The physiologically relevant forms of iron are ferrous iron (Fe^{2+}), which is highly water-soluble, and ferric iron (Fe^{3+}). The solubility of ferric iron is in the range of 10^{-17} M and therefore very low (Andrews et al., 2003). Ferric iron rapidly precipitates out of solution as oxyhydroxides, rendering it bio-inaccessible in theory (Neilands, 1981). Low iron availability can be a factor that limits or co-limits phytoplankton growth in the oceans (Martin and Fitzwater, 1988; Moore et al., 2001; Norman et al., 2014). Iron limitation can induce the development of high nutrient low chlorophyll regions, where high nutrient indicates the sufficient abundance of macronutrients (nitrate, phosphate and potassium) and low chlorophyll refers to the low abundance of phytoplankton (Martin, 1990). In freshwater and marine environments, dissolved iron was found to be abundant in sub-nanomolar levels, and the vast majority of the dissolved iron (>99%) is complexed to organic compounds like humic acids or siderophores (Boyd and Ellwood, 2010; Gledhill and Buck, 2012; Norman et al., 2014). Iron availability and speciation depend on various geochemical and hydrological factors in aquatic environments and both parameters vary along the water column (Boyd and Ellwood, 2010; Gledhill and Buck, 2012).

In cyanobacteria, several adaptation mechanisms to cope with limited iron supply have been detected. For instance, structural rearrangements of the photosynthetic apparatus occur under iron deprivation, such as the expression of the iron-induced genes *isiA* and *isiB* (Leonhardt and Straus, 1994; Razquin et al., 1994; González et al., 2018). The former encodes a chlorophyll-binding protein which colocalizes with photosystem I, functioning as chlorophyll storage and protection against photodamage (Chen et al., 2018). *IsiB* encodes for flavodoxin, which functionally replaces ferredoxin (Leonhardt and Straus, 1992). Thereby, the cellular iron demand is lowered. In addition, the PSI:PSII ratio and the chlorophyll concentration both decrease upon iron starvation (González et al., 2018). Further responses to actively increase the iron incorporation under starvation conditions are the induction of genes encoding for high affinity iron transport proteins and an enhancement of the siderophore secretion (González et al., 2012)

Siderophores are low molecular weight organic compounds (400 Da – 1 kDa) that are capable to coordinate ferric iron with high affinities (dissociation constant of up to 10^{-52} M, Saha et al., 2013). The secretion of siderophores is widely distributed among domains and kingdoms, as species of plants, fungi and bacteria were found to secrete chelators in order to sequester iron (Khan et al., 2018). Siderophores mediate the chelation of the ferric iron with

different groups such as catechols, alpha-hydroxycarboxylic acids and hydroxamates (Khan et al., 2018). Many microorganisms do secrete multiple types of siderophores, which increases the iron scavenging capacity of the strains (Saha et al., 2013). Typically, the siderophore synthesis and secretion in microorganisms is linked to iron availability and gets enhanced when iron is limited (Andrews et al., 2003). Worth mentioning that siderophores also have high affinities for other metals as zinc, copper or manganese, but the physiological relevance of this phenomenon is largely unclear (Johnstone and Nolan, 2015).

Due to their size, siderophores do not cross the OM in a porin mediated fashion, but are translocated actively through a TonB-dependent transport (Fig. 2, described below). Beyond siderophores, also nickel, cobalamin and carbohydrates follow this transport mechanism (Schauer et al., 2008). Different classes of OM TonB-dependent transporters (TBDTs) that are allocated to different substrate classes exist. Besides the cognate substrates, also structural unrelated compounds as colicins, antibiotics or derivates thereof can be transported in a TonB-dependent manner, as shown for *E. coli* FhuA (Ferguson et al., 2001). Once imported into the periplasm, the iron is either released from the siderophore and bound to periplasmic proteins or the ferric siderophore as a whole is further translocated across the PM (Schalk and Guillon, 2013). Translocation of ferric siderophores or metal ions across the PM is energy requiring in any case, which enables the accumulation of metals in the cell relative to the environment (Ferguson and Deisenhofer, 2004). This is achieved by ATP-binding cassette (ABC) transporters or natural resistance-associated macrophage protein (Nramp) transporters (Ma et al., 2009; Fig. 2). In the former case, a cytoplasmic ATPase subunit hydrolyses ATP, and substrate translocation into the cytosol is induced via a permease subunit (Köster, 2001). In contrast to this, Nramp transporters utilize the proton motive force (pmf) as energy source (Nevo and Nelson, 2006).

1.5. TonB-dependent transport

Nutrients that are either too large to passively diffuse through porins, or only abundant in low concentrations, are translocated in an energy-dependent manner. TBDTs in the OM carry out this active transport, where the required energy is harnessed from the pmf. A PM-embedded protein complex consisting of TonB, ExbB and ExbD proteins (referred to as Ton system) acts as energy transducer, and TonB physically interacts with TBDTs (Cadieux and Kadner, 1999; Moeck et al., 1997; Fig. 2). Both ExbB and ExbD are essential for the function of the Ton system (Ahmer et al., 1995; Fischer et al., 1989). ExbB is a polytopic PM protein, its majority is exposed to the cytoplasmic site (Kampfenkel and Braun, 1993). ExbD is anchored to the PM through one N-terminal alpha-helix and, similar to TonB, expands into the periplasmic space (Kampfenkel and Braun, 1992). ExbB presents a scaffold for the TonB-ExbB-ExbD complex formation (Fischer et al., 1989). In contrast to early suggestions, ExbB

is most likely not directly involved in the proton translocation (Baker and Postle, 2013). The precise mechanism of proton translocation by the Ton system is largely unclear until now. The interaction of periplasmic residues of ExbD with TonB might be involved in this process. It is hypothesized that ExbD moves “up and down the ExbB pore axis”, which could effect the proton translocation process (Celia et al., 2019).

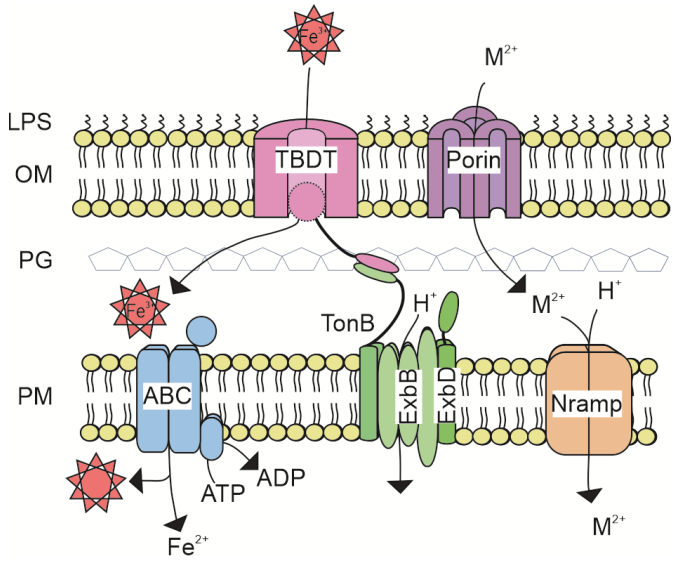

Figure 2. Metal uptake across the cellular envelope. TonB-dependent transporters (TBDTs) extracellularly bind ferric siderophores, and the N-terminal TonB box is exposed. The C-terminal part of the plasma membrane protein TonB binds the TonB box of the TBDT. The Ton complex, consisting of ExbB, ExbD and TonB, translocates a proton in the direction of the proton gradient across the plasma membrane (PM). Structural changes are induced in the TBDT, the plug domain rearranges and the ferric siderophore can enter the periplasm. The transport of the ferric siderophore across the PM is mediated by ATP-binding cassette (ABC) transporters which hydrolyze ATP on the cytoplasmic site. The passive diffusion of metal ions (M^{2+}) into the periplasm is facilitated through porins, further translocation of the metal ions is accomplished by metal transporters such as the natural resistance-associated macrophage protein (Nramp) transporters, which energize the transport by utilizing the proton motive force. OM = outer membrane, PG = peptidoglycan, LPS = lipopolysaccharide.

Today, more than 100 structures of different TBDTs are available in the protein databank. Though, almost all structures represent proteins from proteobacteria. TBDTs are built up of a 22-stranded barrel, where the beta-sheets are connected by extracellular and periplasmic loops, and an N-terminal globular plug domain (Noinaj et al., 2010). The initial step of the transport process is the binding of the extracellular substrate to the TBDT (Nikaido and Saier, 1992). Substrates are recognized and bound by extracellular loop and plug domain residues (Krewulak and Vogel, 2008; Noinaj et al., 2010). Ligand binding was found to come along with structural changes in the plug domain, more precisely with the unwinding of the so-called switch helix and the exposition of a motif called TonB box, making the latter accessible to TonB (Merianos et al., 2000; Xu et al., 2006). The TonB box of the TBDTs FecA and BtuB were found to change the conformation upon ligand binding of the TBDT (Mokdad et al., 2012). The ButB TonB box becomes unfolded and extrudes about 3 nm into the periplasm

(Fanucci et al., 2003). In contrast, wave and pulse EPR spectroscopy experiments with *E. coli* FhuA imply that the TonB box structure of the transporter is dynamic and flexible and does not significantly change the periplasmic exposition in dependence of the FhuA substrate-loading state (Sarver et al., 2018). Thus, apparently the TonB box motifs of different transporters behave differentiated upon substrate binding. Furthermore, also reports about an interaction of TonB with cognate transporters independent of substrate binding status exist (Kenney and Cornelissen, 2002). The interaction of the TonB C-terminal domain with the TonB box of the TBDT occurs via beta-augmentation (Pawelek et al., 2006; Shultis et al., 2006; Josts et al., 2019). Once TonB did bind to the ligand-loaded TBDT, proton translocation across the PM facilitated by the Ton system leads to structural rearrangements in the TBDT, resulting in pore opening and substrate import (e.g. Postle and Larsen, 2007). Several hypotheses emerged trying to explain the mechanism of the TonB-dependent energy transfer, which are briefly outlined in the following section.

The shuttle hypothesis implies that TonB detaches from the PM to subsequently bind and energize the TBDT (Larsen et al., 2003; Letain and Postle, 1997; Postle and Larsen, 2007). Though, at present it is widely accepted that this model proved to be wrong, and TonB resides anchored to the PM throughout the energy coupling process (Gresock et al., 2011). The rotational surveillance and energy transfer (ROSET) model originated through the similarities of the Ton-complex to the flagella motor complex (Klebba, 2016). According to this theory TonB exists as homodimer that binds the PG and thereby locates close to the OM. The pmf energy is harvested through ExbB-ExbD proteins that take over a stator-like function, and transferred to TonB that undergoes rotational movements (Klebba, 2016). A monomeric C-terminal domain binds the TonB box and rearranges the plug domain allowing substrate import (Jordan et al., 2013; Klebba, 2016). Since the Ton-complex is not anchored to the cell wall but is able to move in the PM bilayer, ExbB-ExbD stator function is questionable. Still, it might be inertia due to the higher mass of ExbB-ExbD (compared to TonB) that allows the postulated fast rotation of TonB relative to the ExbB-ExbD subcomplex (Klebba, 2016). Nevertheless, as mentioned above, until now it is unclear if TonB *in vivo* truly exists as dimer or not.

Another theory about the TonB mediated energisation of TBDTs is the pulling model, where TonB is thought to exert a force to the plug domain that consequently unfolds, leading to pore opening and substrate import into the periplasm (Chimento et al., 2005; Shultis et al., 2006). It is assumed that, depending on the direction of the kinetic force, only a relatively weak force is needed to induce conformation changes in a protein (here: the TBDT plug domain, Brockwell et al., 2003; Chimento et al., 2005; Gumbart et al., 2007; Shultis et al., 2006). The interaction between the TonB box and TonB was predicted to be strong enough

to exert such a mechanic force to the plug domain without the dissociation of the two components (Hickman et al., 2017).

Table 2. Stoichiometry of the Ton complex

Stoichiometry	Reference
5ExbB:3ExbD	Maki-Yonekura et al., 2018
6ExbB and 6ExbB:1ExbD	Pramanik et al., 2011
4ExbB:2ExbD	Sverzhinsky et al., 2014
4ExbB:1ExbD:1TonB	Sverzhinsky et al., 2015
5ExbB:2ExbD	Celia et al., 2019
5ExbB:2ExbD:1-2TonB	Celia et al., 2016

Regarding the stoichiometry of the ExbB-ExbD complex with or without TonB, some studies are available that propose different stoichiometric variations, examples are given in Table 2 and summarized in Celia et al., 2020. The most recently obtained crystal structure supports a ExbB:ExbD:TonB stoichiometry of 5:2:(1-2). However, in order to create a pore for proton translocation, further conformational variation of this observed structure would be required (Celia et al., 2020, 2016). The prevalence of pentameric ExbB *in vivo* is also supported by the results of mass spectrometry experiments on native membrane samples (Chorev et al., 2018).

The Ton system shares similarities to another energized PM embedded complex, the TolA-TolQ-TolR system (Tol system). TolQ and TolR are functional homologue to ExbB and ExbD, respectively, and the sequences share considerable similarities (Eick-Helmerich and Braun, 1989). Moreover, ExbB and ExbD as well as TolQ and TolR also share homology with flagellar motor proteins MotA and MotB, respectively (Cascales et al., 2001; Kojima and Blair, 2001). *E. coli* mutants of *tolQ* and *tolR* can be complemented by expression of *exbB* and *exbD*, and vice versa (Braun and Herrmann, 1993). TolA and TonB share the main similarities in the transmembrane part, but are not functionally homologous (Koebnik, 1993). The Tol system components interact with the lipoprotein Pal, the periplasmic soluble proteins TolB and YbgF (CpoB) and connect the PM to the PG and OM (Lloubès et al., 2001). The exact physiological function of the system is not yet elucidated. One function attributed to the Tol system is the energization of OM invagination by harnessing energy from the pmf likewise to the Ton system (Gerding et al., 2007). TolQ and TolR similarly to ExbB-ExbD gather the energy from the pmf and transmit it to TolA. This putatively conducts conformational changes which, with involvement of the Pal protein, lead to OM constriction

initiation (Gerding et al., 2007; Germon et al., 2001; Lloubès et al., 2001). This step is crucial for the divisome-mediated cell division, the maintenance of outer membrane integrity and the PG synthesis regulation (Gray et al., 2015; Szczepaniak et al., 2020). Strains where components of the Tol system were mutated demonstrate an OM instability by releasing OM vesicles or periplasmic proteins and exhibiting hypersensitivity towards antibiotics or salts (Bernadac et al., 1998; Lazzaroni et al., 1989; Llamas et al., 2000). Both the Ton system and the Tol system assist in the entry of different classes of colicins and phages (Kim et al., 2014). Interestingly in *Pseudomonas aeruginosa*, the expression of *tolQRA* is responsive to the iron concentration, putatively regulated through the ferric uptake regulator Fur (Duan et al., 2000; Lafontaine and Sokol, 1998).

1.5.1. TonB proteins in a nutshell

Next to the characterization of porins in *Anabaena*, this study provides a functional characterization of TonB-like proteins. Therefore, an overview about features and characteristics of TonB proteins is given in this section. The analysis of 144 Gram-negative bacteria revealed that the majority of the strains that encode TonB proteins do encode one single copy in the genome (Chu et al., 2007). From the 60 bacteria species that held more than one *tonB* gene, the majority possessed two *tonB*s, making up 20% of all analysed strains (Chu et al., 2007). TonB proteins possess a characteristic domain architecture. They consist of an N-terminal conserved alpha-helix that anchors the protein to the plasma membrane, followed by a flexible linker region that is (often) proline rich, and a C-terminal domain that interacts with TBDTs (Chu et al., 2007). A “YP” motive in the C-terminal linker domain is found in TonB proteins of many species (Chu et al., 2007). Though, also certain differences between TonB proteins of different species were found. Exemplarily, in *E. coli* only one histidine residue within the transmembrane alpha-helix is required to maintain the functionality of TonB when all other residues were substituted by alanine (Larsen et al., 2007). Nevertheless, in functional TonB proteins of other organisms this histidine is not present at all in the N-terminal region (Chu et al., 2007). The TonB C-terminal folded domain is thought to have a general αββαβ-secondary structure, whereas the beta-sheets mediate interaction with the TonB box of the TBDT. C-termini of TonB proteins without TBDT interaction were found to dimerize in crystal structures (Chang et al., 2001; Ködding et al., 2005), however also monomeric structures were observed (Oeemig et al., 2018; Sean Peacock et al., 2005). The dimerization status in solution was observed to be highly variable and dependent on the length of the constructs (Ködding et al., 2005; Koedding et al., 2004). *In vivo* the C-terminal domain of one single TonB protein interacts with the TBDTs (Freed et al., 2013; Pawelek et al., 2006), and if a physiologically relevant homodimerization occurs when TonB is detached from the TonB box is still unclear (Postle et al., 2010).

Pawelek and colleagues (2006) solved the structure of TonB in complex with the ferrichrome-specific TBDT FhuA. They found that an interprotein beta-strand is formed with high affinity between the TonB C-terminal beta-strands β1-β3 and the FhuA TonB box (Pawelek et al., 2006). Here, an arginine residue from TonB is positioned in a way to induce a shearing force in the cork domain of the TBDT, facilitating substrate entrance through pore opening. Also the structure of BtuB:TonB C-terminal domain shows a pairing of one beta-strand of the BtuB TonB box with the three-stranded beta-motif from the C-terminus of TonB, which is accordance with a pulling model of TonB (discussed above, Shultis et al., 2006).

The TonB variants in certain organisms display distinct specificities. HasB from *Serratia marcescens* for example, which represents one out two functionally characterized TonBs in this organism, was found to facilitate heme transport by exclusively interacting with the heme transporter HasR (Paquelin et al., 2001). However, no energy transduction to other heme transporters of *Serratia marcescens* takes place (Benevides-Matos et al., 2008; Paquelin et al., 2001). Structure determination via Nuclear magnetic resonance spectroscopy showed that HasB bears an additional alpha-helix in the C-terminal domain, which is also found in few other TonB or HasB proteins of other organisms (de Amorim et al., 2013). Also, the interaction of HasB with the TonB box was found to be differentiated, since an extended stretch of the TBDT seems to be recognized by HasB compared to TonB. Interestingly, it was observed that the HasB C-terminal domain structure rather resembles TolA than TonB (de Amorim et al., 2013).

Apart from functioning in transport processes, other functions have been assigned to TonB proteins. In *Pseudomonas aeruginosa* and *Pseudomonas putida* one TonB protein influences motility and flagella localization (Ainsaar et al., 2019; Cowles et al., 2013; B. Huang et al., 2004). Further, TonB from the cyanobacterium *Fremyella diplosiphon* was found to play a role in the morphological photoregulation (Pattanaik and Montgomery, 2010a, 2010b). In *Aeromonas hydrophila* and *Pseudomonas aeruginosa*, TonB deletion did impair macrolide export systems (Dong et al., 2021; Zhao et al., 1998; Zhao and Poole, 2002a). *Vibrio* species generally possess more than one TonB copy (Payne et al., 2016), and functional analyses in certain strains indicated that the proteins are only partly redundant. *V. cholerae* TonB1 in combination with ExbB1-ExbD1 energizes schizokinen uptake, whereas the TonB2-system energizes the enterobactin uptake. In addition, both Ton systems are capable to mediate the transport of other siderophores such as ferrichrome or haemin (Occhino et al., 1998; Seliger et al., 2001). Moreover, the *Vibrio* TonB proteins can be conditionally functional; under osmotic stress TonB2 is unable to bridge the enlarged periplasmic space in order to interact with certain TBDTs, whereas TonB1, which is longer than TonB2, retains the interaction capacity (Seliger et al., 2001). This illustrates that multiple TonB proteins can be advantageous for an organism, by providing the ability to regulate the transport capacity in

response to environmental conditions and to increase the efficiency of substrate sequestration.

1.5.2. TonB-dependent siderophore transport in *Anabaena*

Two major strategies exist in cyanobacteria to incorporate ferric iron: the siderophore-based sequestration and the siderophore independent reductive uptake (Sutak et al., 2020). The latter is believed to be the prevalent strategy among cyanobacteria, as in most – especially pelagial – environments siderophore production would be rendered futile by dilution of small substance amounts in large water bodies (Lis et al., 2015; Shaked and Lis, 2012). Reductive uptake involves the reduction of either chelated or inorganic Fe^{3+} to Fe^{2+}, followed by the transport into the cell. In *Synechocystis sp*. for example, the reduction of ferric iron at the PM by the respiratory terminal oxidase and subsequent translocation into the cytosol by the Feo-transporter was shown to be of major importance for high affinity iron uptake (Kranzler et al., 2014, 2011).

In here, the focus will be set on siderophore-based iron incorporation in cyanobacteria. Among cyanobacteria, siderophore-producing strains (e.g. *Anabaena*) as well as non-siderophore producers are represented. In the latter case, however, siderophore incorporation is not excluded. Genes encoding for siderophore translocation proteins were identified in the genome of *Synechocystis* sp., although the strain does not secrete siderophores itself (Ehrenreich et al., 2005). The number of TBDTs in different cyanobacterial strains is highly variable, with genera lacking TBDTs like Prochlorococcus or species that bear an extremely high number like *Gloeobacter violaceus,* which contains 33 TBDTs (Mirus et al., 2009). Compared to this, the number of identified TonB candidates was lower in all strains, with up to 5 putative *tonB* genes in *Nostoc punctiforme* PCC 73012 (Stevanovic et al., 2012). In most analysed cyanobacteria two to four putative *tonB* genes were predicted (Mirus et al., 2009; Stevanovic et al., 2012). Furthermore, FecA-like transporters, which bear an additional N-terminal regulatory motive and typically act as TonB-dependent transducers and were not identified in cyanobacteria (Mirus et al., 2009). This suggests that TBDT-mediated transmembrane signalling is not of relevance in cyanobacteria (Koebnik, 2005; Mirus et al., 2009).

The cyanobacterial TonB-dependent transport is especially well studied in filamentous *Anabaena* and the unicellular freshwater strain *Synechocystis* sp.. In the latter strain, four TBDTs, one TonB protein and three ExbB-ExbD pairs were identified (Stevanovic et al., 2012). A *Synechocystis* sp. strain where all four TBDTs were mutated lost the capacity to transport the xenosiderophore ferric desferrioxamine B (Qiu et al., 2018). In addition, this mutant strain was compromised, albeit to a lesser extent, in inorganic iron transport (Qiu et al., 2018). Interestingly, ExbB and ExbD in *Synechocystis* sp. probably not only mediate the

transport of ferric siderophores but also of inorganic iron, implying that in this species the Ton system is crucial for both inorganic and organic iron uptake (Jiang et al., 2015). For two more xenosiderophores, including schizokinen which is secreted by *Anabaena*, transport in *Synechocystis* sp. was shown to take place in a TonB-dependent manner, independent from a reduction step (Babykin et al., 2018; Obando et al., 2018).

In *Anabaena*, several factors involved in siderophore transport have been identified. Apo-Schizokinen is synthesized in the cytosol and translocated across the plasma membrane via the major facilitator superfamily-like protein SchE (Nicolaisen et al., 2010). Transport across the OM into the extracellular space is conducted by HgdD, a TolC-homolog (Nicolaisen et al., 2010). In *Anabaena* 22 putative TBDTs were identified (Mirus et al., 2009), of those only a few have been functionally characterized. Ferric schizokinen is imported through the TBDT SchT during high starvation conditions, as well as through IutA2 under moderate iron starvation conditions (Nicolaisen et al., 2008; Rudolf et al., 2016). In the same way the xenosiderophore aerobactin, which is structurally related to schizokinen, utilizes those two transporters. A third siderophore that was found to be bioavailable to *Anabaena*, Desferrioxamine B, is not a substrate of SchT (Rudolf et al., 2015). As mentioned above, the transport of ferric siderophores across the plasma membrane into the cytosol is carried out by ATP-binding cassette transporters (Köster, 2001). In *Anabaena* five putative ABC-type transport systems were identified (Stevanovic et al., 2012). Translocation of the three siderophores was found to depend on FhuC, the ATPase that is part of the FhuCDB ABC-type transport system (Rudolf et al., 2016, 2015). In addition, a mutant of the periplasmic binding protein FecB1 exhibited a decreased schizokinen transport capacity (Rudolf et al., 2016).

In contrast to the TBDTs and the ABC-type transporters, only little is known about the function of the four TonB-like proteins detected in *Anabaena*. Those structurally differ from each other; the conserved motifs that were identified by comparison of TonB proteins in other Gram-negative bacteria were exclusively found in TonB3 (Fig. 3; Stevanovic et al., 2012). The YP sequence in the C-terminal domain is thought to be involved in the interaction with TBDTs, whereas the SSG sequence in the TonB C-terminal domain putatively functions in detection of TBDTs (Chu et al., 2007). Further, transcription analyses revealed that *tonB3* expression is induced after iron starvation, and therefore it is assumed that TonB3 is part of the *Anabaena* ferric siderophore transport system (Stevanovic et al., 2013, 2012). The function of the other TonB-like proteins remains to be established. The genes have specific expression patterns; *tonB1* transcription was enhanced after *Anabaena* was grown for seven days in absence or in excess of copper, which appears contradictory, and also under diazotrophic conditions (Stevanovic et al., 2012). *TonB2* mRNA abundance was high after cultivation of wild-type *Anabaena* in medium with high iron concentration, and *tonB4*

exhibited an ambiguous expression profile in response to iron or copper (Stevanovic et al., 2012).

Figure 3. Alignment of *Anabaena* TonB-like sequences. The conserved histidine residue in the transmembrane helix (TM, black box above the alignment) of TonB3 is highlighted, as well as the conserved YP residues in the linker region of TonB3. Predicted beta-sheets and an alpha-helix are indicated below the sequence by pink or orange boxes, respectively. The sequence of TonB3 is truncated at the C-terminus. The alignment was kindly provided by Dr. Oliver Mirus, figure modified from Stevanovic et al., 2012.

1.6. Aim of this study

In this thesis it was aimed to explore and define the roles of specific proteins presumably involved in passive diffusion or active transport processes across the OM in *Anabaena* as an example for Nostocales. In here, especially metals or metal chelates were considered as substrates of major interest, as these were described to enter the cell both though diffusion or in an active manner. Particularly iron is an important factor that determines or influences phytoplankton growth in aquatic environments, next to macronutrient availability (Martin, 1990; Moore et al., 2001; Street and Paytan, 2005). In the scope of this thesis a comparative analysis of (i) TonB-like proteins, presumably energizing the active substrate translocation across the OM, and (ii) porin-like proteins, putatively involved in passive diffusion processes of metals or other solutes across the OM, was targeted.

Firstly, the role of the four TonB-like proteins predicted earlier in *Anabaena* was aimed to be elucidated (Mirus et al., 2009; Stevanovic et al., 2012). The TonB-dependent transport in the cyanobacterium *Anabaena* has been partly described, whereas the research focus was majorly set on the involved transporters (Rudolf et al., 2016, 2015). Even though the expression behaviour of the *tonB*-like genes in response to various metal treatments has been characterized (Stevanovic et al., 2013, 2012), a detailed functional characterization of the *Anabaena* TonB proteins was not provided. It was speculated before that the proteins might take over distinct roles in *Anabaena*, as the expression of the single *tonB* genes is

regulated individually (Stevanovic et al., 2013, 2012). To test the roles of the TonB proteins in ferric siderophore uptake, the bioavailability of the well characterized substrate schizokinen, as well as the in here newly identified substrate ferrichrome to mutant strains of the individual *tonB* genes was examined. Moreover, other phenotypic features of the *tonB* mutants were delineated during this study, in order to reveal presumed functions of single TonB-like proteins besides substrate transport. This included morphological inspections of the individual mutants (e.g. through light and electron microscopy, confocal laser scanning microscopy) and physiological measurements (fluorescence recovery after photobleaching, growth curves, metal and pigment level quantification).

Secondly, a global comparative analysis of the putative porin proteins in *Anabaena* was targeted. Next to the canonical roles of porins in solute uptake, they further influence cellular integrity and growth capacity; porins define the barrier function of the OM, modulate the resistance against harmful compounds or confer envelope stability (Achouak et al., 2001). The role of porins in (inorganic) iron uptake in cyanobacteria just gets apparent, which renders them important players in the acquisition of this growth-limiting factor (Qiu et al., 2018, 2021). The individual porin-like proteins in *Anabaena* have not been examined before, however it was established that *Anabaena* takes up erythromycin and ethidium bromide in a porin-like fashion (Hahn et al., 2012). Apart from this observation porin-mediated diffusion in *Anabaena* remains uncharacterized. To provide a basic comparative characterization of the *Anabaena* porin-like proteins, the transcription of the putative porin-like genes was analysed in response to growth of *Anabaena* in media lacking specific metals, representing putative substrates for porin facilitated diffusion. Further, single insertion mutants of the individual porin genes were created, and growth of the mutant strains under various conditions was analysed. This included the presence of high salt or metal concentrations and toxic compounds in solid medium. Through both approaches it was intended to draw conclusions about possible substrates and specific features of the individual proteins.

2. Manuscripts

2.1. Manuscript 1

A TonB-like protein, SjdR, is involved in the structural definition of the intercellular septa in the heterocyst-forming cyanobacterium *Anabaena*

Status: Published in mBio (2021), 12(3):e00483-21

Contributing Authors: Hannah Schätzle, Sergio Arévalo, Enrique Flores, Enrico Schleiff

Contributions:

Concept and Design	Schätzle, Hannah	60%
	Schleiff, Enrico	40%
Conducting tests and experiments	Schätzle, Hannah (Mutant screening, growth experiments, siderophore transport experiments, expression analysis, ICP-MS, microscopy, FRAP, Vancomycin-FL staining)	90%
	Arévalo, Sergio (Nitrogenase activity measurement, microscopy)	10%
Compilation of data sets and figures	Schätzle, Hannah (Compilation of figures and data of mutant genotyping, growth analysis, expression analysis, ICP-MS measurements, light and electron microscopy, septum properties, fluorescence microscopy, FRAP, nanopore visualization)	60%
	Arévalo, Sergio (Compilation of figure for nanopore visualization)	5%
	Flores, Enrique (Compilation of figure for nanopore visualization)	5%
	Schleiff, Enrico (Compilation of figures and data of bioinformatic analyses, mutant genotyping, growth analysis, expression analysis, ICP-MS measurements, light and electron microscopy, septum properties, fluorescence microscopy, FRAP, nanopore visualization)	30%
Analysis and interpretation of data	Schätzle, Hannah (Analysis and interpretation of all data generated during the study)	55%
	Arévalo, Sergio (Supportive analysis and interpretation of all data generated during the study)	10%
	Flores, Enrique (Supportive analysis and interpretation of all data generated during the study)	5%
	Schleiff, Enrico (Analysis and interpretation of all data generated during the study)	30%
Drafting of manuscript	Schätzle, Hannah	60%
	Schleiff, Enrico	40%

AMERICAN SOCIETY FOR MICROBIOLOGY | mBio®

RESEARCH ARTICLE

A TonB-Like Protein, SjdR, Is Involved in the Structural Definition of the Intercellular Septa in the Heterocyst-Forming Cyanobacterium *Anabaena*

Hannah Schätzle,[a,b] Sergio Arévalo,[c] Enrique Flores,[c] Enrico Schleiff[a,b,d,e]

[a]Institute for Molecular Biosciences, Goethe University Frankfurt, Frankfurt am Main, Germany
[b]FIERCE, Goethe University Frankfurt, Frankfurt am Main, Germany
[c]Instituto de Bioquímica Vegetal y Fotosíntesis, CSIC and Universidad de Sevilla, Seville, Spain
[d]Buchmann Institute for Molecular Life Sciences, Frankfurt am Main, Germany
[e]Frankfurt Institute for Advanced Studies, Frankfurt am Main, Germany

ABSTRACT Cyanobacteria are photosynthetic organisms with a Gram-negative envelope structure. Certain filamentous species such as *Anabaena* sp. strain PCC 7120 can fix dinitrogen upon depletion of combined nitrogen. Because the nitrogen-fixing enzyme, nitrogenase, is oxygen sensitive, photosynthesis and nitrogen fixation are spatially separated in *Anabaena*. Nitrogen fixation takes place in specialized cells called heterocysts, which differentiate from vegetative cells. During heterocyst differentiation, a microoxic environment is created by dismantling photosystem II and restructuring the cell wall. Moreover, solute exchange between the different cell types is regulated to limit oxygen influx into the heterocyst. The septal zone containing nanopores for solute exchange is constricted between heterocysts and vegetative cells, and cyanophycin plugs are located at the heterocyst poles. We identified a protein previously annotated as TonB1 that is largely conserved among cyanobacteria. A mutant of the encoding gene formed heterocysts but was impaired in diazotrophic growth. Mutant heterocysts appeared elongated and exhibited abnormal morphological features, including a reduced cyanophycin plug, an enhanced septum size, and a restricted nanopore zone in the septum. In spite of this, the intercellular transfer velocity of the fluorescent marker calcein was increased in the mutant compared to the wild type. Thus, the protein is required for proper formation of septal structures, expanding our emerging understanding of *Anabaena* peptidoglycan plasticity and intercellular solute exchange, and is therefore renamed SjdR (septal junction disk regulator). Notably, calcium supplementation compensated for the impaired diazotrophic growth and alterations in septal peptidoglycan in the *sjdR* mutant, emphasizing the importance of calcium for cell wall structure.

IMPORTANCE Multicellularity in bacteria confers an improved adaptive capacity to environmental conditions and stresses. This includes an enhanced capability of resource utilization through a distribution of biochemical processes between constituent cells. This specialization results in a mutual dependency of different cell types, as is the case for nitrogen-fixing heterocysts and photosynthetically active vegetative cells in *Anabaena*. In this cyanobacterium, intercellular solute exchange is facilitated through nanopores in the peptidoglycan between adjacent cells. To ensure functionality of the specialized cells, septal size as well as the position, size, and frequency of nanopores in the septum need to be tightly established. The novel septal junction disk regulator SjdR characterized here is conserved in the cyanobacterial phylum. It influences septal size and septal nanopore distribution. Consequently, its absence severely affects the intercellular communication and the strains' growth capacity

Citation Schätzle H, Arévalo S, Flores E, Schleiff E. 2021. A TonB-like protein, SjdR, is involved in the structural definition of the intercellular septa in the heterocyst-forming cyanobacterium *Anabaena*. mBio 12:e00483-21. https://doi.org/10.1128/mBio.00483-21.

Editor Anne K. Vidaver, University of Nebraska—Lincoln

Address correspondence to Enrico Schleiff, schleiff@bio.uni-frankfurt.de.

Received 20 February 2021
Accepted 4 May 2021
Published 8 June 2021

under nitrogen depletion. Thus, SjdR is involved in septal structure remodeling in cyanobacteria.

KEYWORDS cyanobacteria, TonB-like proteins, cell wall, heterocyst, peptidoglycan, cyanobacteria

Cyanobacteria like *Anabaena* sp. strain PCC 7120 (hereinafter *Anabaena*) perform oxygenic photosynthesis and have a Gram-negative type of cell wall. They contain a plasma membrane (PM) and an outer membrane (OM) separated by a peptidoglycan (PG) mesh in the periplasm (1, 2). *Anabaena* is a multicellular organism in which one filament may comprise hundreds of cells. Specialized cells named heterocysts are formed from vegetative cells upon nitrogen starvation (3). In contrast to the vegetative cells that perform oxygenic photosynthesis, oxygen production in heterocysts is avoided due to metabolic adaptations such as photosystem II activity shutdown (4). This, in combination with the formation of additional heterocyst-specific envelope layers, allows the formation of a microoxic environment, which in turn is required for proper nitrogenase activity (5, 6). The nitrogenase catalyzes the fixation of dinitrogen into ammonium. In *Anabaena*, the nitrogenase structural genes are exclusively expressed in heterocysts (7). The spatial separation between carbon and nitrogen fixation results in a mutual dependency of vegetative cells and heterocysts and a requirement for metabolite exchange between the cells. For this, septal junctions exist that allow the intercellular diffusion of certain compounds.

The perforations in the septal PG between adjacent cells are called nanopores (2, 8). SepJ (FraG), FraC and FraD were identified as proteinaceous compounds related to the septal junctions (9, 10). The knockout of either *sepJ* or both *fraC* and *fraD* in *Anabaena* affects intercellular molecular transfer of different fluorescent markers, although to a different extent (8, 11, 12). In addition, SjcF1 was reported to connect PG and septal junction complexes influencing nanopore formation (13). The cell wall amidases AmiC1 and AmiC2 are thought to drill the nanopores in the PG (14). AmiC1 is important for both nanopore formation and septal junction complex integrity, since it influences the localization of septal proteins (14). The deletion of septal or nanopore-related proteins affects diazotrophic growth and filament integrity in *Anabaena*. For example, the inactivation of *sepJ* or *amiC1* impairs heterocyst differentiation in the respective mutant strain (9, 14, 15). Deletion of *sepJ* or the *fraC* and/or *fraD* genes moreover leads to extensive filament fragmentation (9, 10, 12). In addition, a relation between septal proteins and the regulation of cell division and growth can be drawn. It has been reported that SepJ interacts with the divisome proteins ZipN (16) and FtsQ (17) as well as with the two elongasome-associated proteins ZicK and ZacK (18). Divisomal and elongasomal components function in PG formation and thereby in the determination of cell shape (16, 18–20). Whereas the divisome coordinates cell constriction and division, the elongasome incorporates PG along the sidewall and mediates longitudinal cell extension (21, 22). Indeed, inactivation of the *mreB*, *mreC*, and *mreD* genes encoding elongasome components leads to increased septal width and septal PG incorporation (23).

In Gram-negative bacteria, TonB-dependent transport represents a conserved mechanism that mediates the active translocation of compounds across the OM. Siderophores, carbohydrates, vitamin B_{12}, or nickel are substrates for TonB-dependent transporters (TBDT) (24–27). In contrast to the septal junction complex, which is restricted to filamentous cyanobacteria, approximately two thirds of all Gram-negative bacteria bear genes encoding TonB-dependent transport system components (28). The details of the TonB-dependent transport processes in Gram-negative bacteria are partly known. The extracellular binding of the substrate to the TBDT induces the exposition of the TonB box, a semiconserved motif in the N-terminal part of the TBDT (29). The TonB box has a high affinity to bind the C terminus of the PM-embedded TonB protein (30, 31). TonB proteins consist of a conserved N-terminal alpha-helical membrane anchor, a flexible periplasmic linker region that is often proline rich, and a C-terminal TonB box interaction domain that bears

a conserved secondary structure (28). In general, these proteins lack a cytoplasmic domain. ExbB and ExbD harvest the energy of the proton motive force and transmit it to TonB that transduces it to the TBDT. By this mechanism, conformational changes are induced in the transporter, which allows the entrance of the substrate into the periplasmic space (28, 32–34).

Regarding cyanobacteria, the TonB-dependent siderophore transport network has been partially characterized in *Synechocystis* sp. strain PCC 6803 (35–39) and *Anabaena* (40–43). In the *Anabaena* genome, 22 TBDT-encoding genes have been identified, but only 4 genes encode putative TonB proteins, referred to as TonB1 to TonB4 (44). The four presumptive TonB proteins bear disparate structural features and their functional properties have been poorly characterized. *Anabaena* TonB3 (encoded by *all5036*) comprises conserved motifs characteristic for TonB proteins, and its involvement in the transport of ferric siderophores has been shown (44). TonB2 (encoded by *all3585*) and TonB4 (encoded by *alr5329*) are shortened in the C-terminal part compared to TonB3, and TonB1 (encoded by *alr0248* and here renamed SjdR) exhibits the most exceptional domain structure. The latter protein bears an N-terminal extension that is putatively exposed to the cytosol, which is not typically found in TonB proteins. Further, it contains a C-terminal truncation resulting in an incomplete TonB box binding motif (44). Considering this, it remains questionable whether this protein can bridge the periplasm in order to interact with TBDT. The expression of *alr0248* was not enhanced when *Anabaena* was grown in iron-free medium. However, induction of *alr0248* was observed when cells were grown in medium without a combined nitrogen source (44), a condition that in *Anabaena* elicits production of heterocysts. Thus, the available expression data for *alr0248* and the structural composition of the encoded protein raise concerns regarding an involvement of this protein in energizing TBDT-mediated transport.

Consequently, we approached the function of the protein annotated as TonB1 in *Anabaena* by analyzing a mutant strain with a mutant gene. This strain was retarded in growth under diazotrophic conditions due to a low nitrogenase activity, and the mutant heterocysts appeared abnormally elongated. Moreover, the septal PG arrangement and the nanopore zone diameter in the mutant were altered compared to the wild type, which in turn influenced the rate of intercellular molecular diffusion in the mutant strain. This implies that the protein influences PG morphology with an important role in the ultrastructure of the intercellular septa, and therefore, we rename it SjdR (septal junction disk regulator).

RESULTS

SjdR is conserved in cyanobacteria. The amino acid sequence of SjdR (formerly annotated as TonB1) substantially differs from those of TonB2, TonB3, and TonB4 (44), which might suggest a functional diversification. Thus, the prevalence of SjdR within the cyanobacterial phylum was analyzed. Fifty cyanobacterial SjdR-like sequences were identified in seven cyanobacterial orders and 20 families (Fig. 1A). Only in *Gloeobacteria* and *Spirulinales* could a SjdR-like sequence not be identified. A list of all cyanobacterial species where SjdR-like sequences were predicted is provided in Table S5 in the supplemental material. The high conservation of SjdR-like proteins in cyanobacteria implies a significant functionality of SjdR. Moreover, a separation to TonB3 became obvious when BLAST search analysis was performed, as the identified sequences did not overlap.

A conserved domain prediction showed that SjdR contains a cytosolically exposed N-terminal domain of about 65 amino acids, a transmembrane domain in the center of the sequence, and a predicted periplasmic domain rich in Pro (16.9%), Thr (16.2%), Ser (13.8%), and Gln (13.1%; Fig. 1B). This domain shows homology to parts of ZipA, which is involved in cell division by stabilizing the FtsZ ring and anchoring it to the plasma membrane in different bacteria (45). However, the transmembrane domain and the C-terminal domain are similar to a membrane-anchored and periplasm-exposed domain in GltJ/AgmX proteins as well (amino acids 65 to 165; Fig. 1B). These proteins are

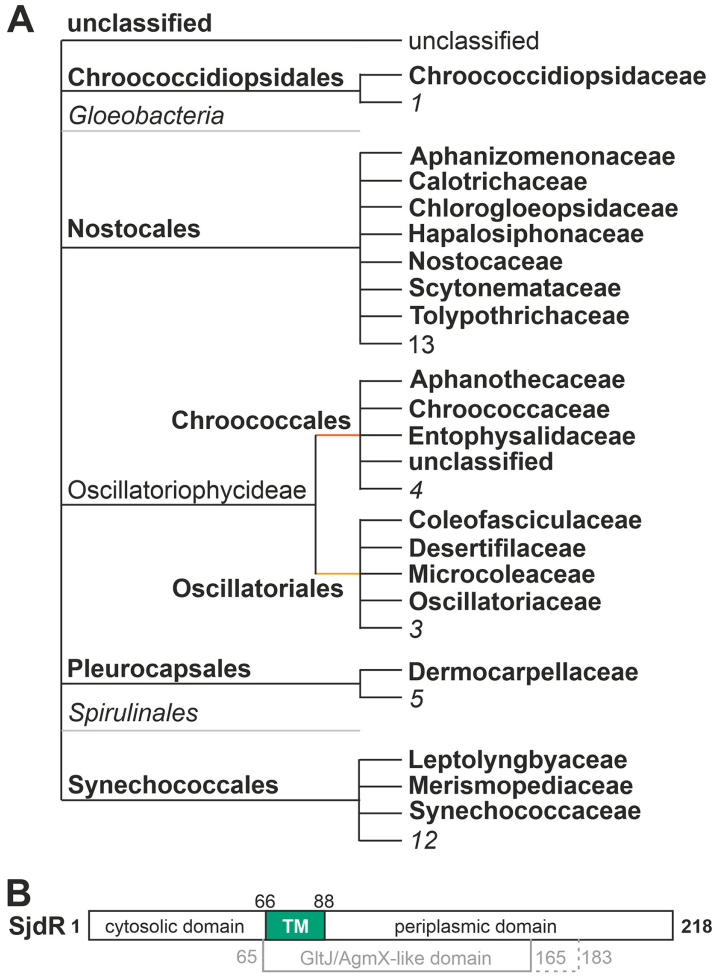

FIG 1 Proteins with similarity to SjdR (formerly named TonB1) from *Anabaena* in cyanobacteria. (A) The cyanobacterial order and the family in which a protein sequence with similarity to SjdR was identified is shown. The numbers of families in which no SjdR-like proteins were identified is indicated as well. (B) Domain architecture of SjdR. The position of the predicted GltJ/AgmX-like domain is shown. The solid line represents the domain deposited in the CDD database. The dashed line indicates the conserved TonB-like region identified by individual alignment. The periplasmic domain also shows homology to a cytoplasmic part of ZipA. The numbers of amino acids that delimit domains are given. TM, transmembrane domain.

related to the so-called adventurous gliding motility that is a pilus-independent mode of motility (46). Remarkably, GltJ proteins bear a C-terminal domain similar to the TonB C terminus (47), but this region does not align to SjdR. To the best of our knowledge, no ZipA or GltJ/AgmX homolog has been discovered in cyanobacteria. Nonetheless, these observations strengthen the assumption that SjdR has function(s) that may not be related to TonB-dependent transport.

SjdR is not involved in transport of the endogenous siderophore. To assess the role of SjdR (previously annotated as a TonB protein) in siderophore transport, a *sjdR* single recombinant mutant was generated by plasmid insertion. The mutant strain was named AFS-I-*sjdR* (*Anabaena* sp. mutant generated in Frankfurt, Germany by the Schleiff lab by plasmid insertion; subsequently termed I-*sjdR*; Fig. 2A; Tables S1 to S3). The strain was segregated after several rounds of dilution. A PCR product of 2,041 bp was obtained with the gene-specific and plasmid-specific oligonucleotide primers on genomic DNA (gDNA) isolated from the mutant (Fig. 2B, lane 1). No fragment was obtained when gDNA from the wild-type strain was utilized as template (lane 3). The product corresponding to a wild-type locus using gene-specific oligonucleotides was

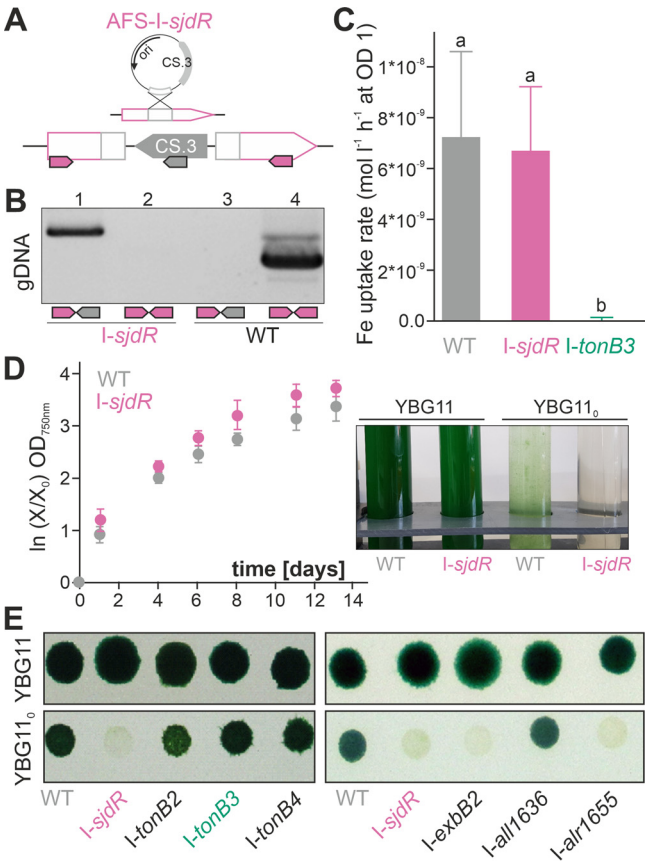

FIG 2 Siderophore transport capacity and diazotrophic growth defects of the *Anabaena sjdR* mutant. (A, top) The strategy of single recombination yielding plasmid insertion into the genome is illustrated. (Bottom) The genotype of the I-*sjdR* mutant is illustrated. The positioning and directionality of oligonucleotides used for the segregation analysis are indicated by arrows. (B) Confirmation of the segregation of I-*sjdR* by PCR on gDNA isolated from I-*sjdR* (lanes 1 and 2) or wild type (WT) (lanes 3 and 4) utilizing oligonucleotides indicated in panel A. (C) The means and standard deviations (error bars) of schizokinen uptake rates of wild-type (WT), I-*sjdR*, and I-*tonB3* strains are shown ($n = 15$ for WT, $n = 6$ for I-*sjdR*, $n = 6$ for I-*tonB3*). Statistical analysis was done with analysis of variance (ANOVA) and Duncan's multiple range test: different letters above the bars indicate statistically significant differences ($P < 0.05$). (D) Growth of wild-type (gray) and I-*sjdR* (pink) strains was monitored in liquid YBG11 for the indicated times. (Right) Cultures grown for 5 days in YBG11 or $YBG11_0$ were photographed. (E) Growth of the indicated mutants on plates composed of YBG11 (top) or $YBG11_0$ (bottom) after spotting of 5 μl (OD_{750} of 1) is shown. Images were taken 7 (right) and 11 days (left) after spotting.

obtained by PCR on gDNA from the wild type (lane 4; 1,433 bp). It should be noted that polar effects of the integration of the inactivating plasmid into the *sjdR* locus are not expected, since individual transcriptional start sites are predicted for *alr0249*, which is localized downstream of the *sjdR* open reading frame (48). Moreover, transcriptome sequencing (RNA-Seq) data imply that *sjdR* is not part of an operon but transcribed individually (49).

In order to examine whether SjdR is involved in energizing the transport of ferric schizokinen, short-term transport uptake measurements were conducted with radiolabeled ferric schizokinen as the substrate. Prior to the uptake measurements, the experimental cultures were depleted for iron, since schizokinen transport is enhanced in iron-starved cells (43). The starvation level was estimated by measuring the chlorophyll *a* (Chl) concentration normalized to the optical density at 750 nm (OD_{750}) (Table S4). The cellular accumulation of the substrate was monitored over time in wild-type, I-*sjdR*, and AFS-I-*tonB3* (I-*tonB3* [44]) strains. An average Fe uptake rate of $(6 \pm 2.5) \times 10^{-9}$ mol liter^{-1} h^{-1} at an OD_{750} of 1 was measured for I-*sjdR*, which is comparable to the average transport rate obtained for the wild type [$(7 \pm 3.4) \times 10^{-9}$ mol liter^{-1} h^{-1} at an OD_{750}

of 1 (Fig. 2C)]. In contrast, the ferric schizokinen transport was severely affected in I-*tonB3* compared to the wild type (Fig. 2C), confirming previous indications that TonB3 mediates the transport of ferric compounds (44). Therefore, schizokinen transport in *Anabaena* depends on TonB3 but not on SjdR.

I-*sjdR* growth is defective under diazotrophic conditions. Previous experiments indicated that the *sjdR* gene is expressed at higher levels in *Anabaena* after growth for 1 week under diazotrophic conditions compared to nitrate-replete conditions (44). Hence, the growth of wild-type and I-*sjdR* strains was examined under diazotrophic conditions in liquid medium and on plates ($YBG11_0$ medium contains no combined nitrogen source). The growth of the two strains in standard (nitrate-containing) liquid or solid medium was used as a control (YBG11). In the presence of nitrate, the growth of both strains in liquid (Fig. 2D) or on solid medium (Fig. 2E, upper panels) was comparable. In the absence of combined nitrogen, I-*sjdR* was severely affected in growth in both liquid (Fig. 2D, right) and solid medium (Fig. 2E, lower panels, Fig. S2A). Different time points for solid and liquid growth are shown because the growth delay of I-*sjdR* becomes obvious earlier in liquid medium, in which the cells typically divide faster, than on plates.

To examine the specificity of the phenotype, the behavior of I-*sjdR* in the absence of combined nitrogen was compared to the growth of the other *tonB* mutants. To control for the conditions used, growth was compared to growth of an *exbB2* mutant (*alr4587*; I-*exbB2*) and mutant strains of two unrelated genes (I-*all1636*; I-*alr1655*). In the presence of nitrate, the growth of all mutants was indistinguishable from wild-type growth (Fig. 2E, upper panels). In the absence of fixed nitrogen, the plasmid insertion mutants of *tonB2*, *tonB3*, and *tonB4* were not impaired in growth (Fig. 2E, lower panel, left). Similarly, the growth of the control mutant I-*all1636* was not affected on $YBG11_0$ plates compared to the wild type (Fig. 2E, lower panel, right). In turn, I-*exbB2* and I-*alr1655* did not grow in the absence of fixed nitrogen (Fig. 2E) similar to I-*sjdR*. Hence, among mutants of the formerly annotated *tonB* genes, only the growth of the *sjdR* mutant was impaired in the absence of combined nitrogen (Fig. 2E).

Nitrogenase activity and transcriptional analysis in the I-*sjdR* mutant strain. The *sjdR* mutant shows a strongly retarded growth in the absence of a source of combined nitrogen (Fig. 2), which might indicate an involvement of SjdR in heterocyst differentiation or function. The transcript levels of *sjdR* were then examined in wild-type cultures grown in $YBG11_0$ medium. Cells were harvested before transfer to $YBG11_0$ medium ("preinduction") and subsequently after 24 h and 48 h of cultivation in $YBG11_0$. During this time frame, heterocyst induction and maturation take place, and the expression of the nitrogenase genes peaks (50); therefore, an induction of *sjdR* expression during this stage might indicate a relation to heterocyst differentiation. The expression was analyzed by quantitative reverse transcription-PCR (qRT-PCR), and for normalization, the values were compared to those of the *rnpB* gene. The *sjdR* mRNA was less abundant in cells that were grown for 24 h or 48 h in $YBG11_0$. After 24 h, only 30% of the transcript was found compared to the preinduction sample (Fig. 3A). After 48 h, the *sjdR* transcript abundance was reduced to about 20% of the preincubation sample (Fig. 3A). Consequently, it seems unlikely that SjdR actively functions in heterocyst differentiation.

In heterocysts, molecular nitrogen is fixed by the nitrogenase complex, which requires a microoxic environment to maintain functionality (6). We intended to assess to which degree the enzyme activity might be affected in I-*sjdR* after 48 h of induction, when heterocyst differentiation is completed. Therefore, the nitrogenase activity in the wild type, I-*sjdR* mutant, and I-*tonB3* mutant as control strain was measured under oxic and anoxic conditions (Fig. 3B). The nitrogenase activity in the I-*sjdR* mutant was null under oxic conditions but increased appreciably, albeit to a low level, under anoxic conditions (Fig. 3B). This suggests a Fox^- Fix^+ phenotype for I-*sjdR* strain, which refers to the inability of the strain to reduce acetylene specifically under oxic conditions (51, 52). In contrast, the nitrogenase activity in the I-*tonB3* mutant was not significantly different from the wild-type activity irrespective of the conditions used (Fig. 3B).

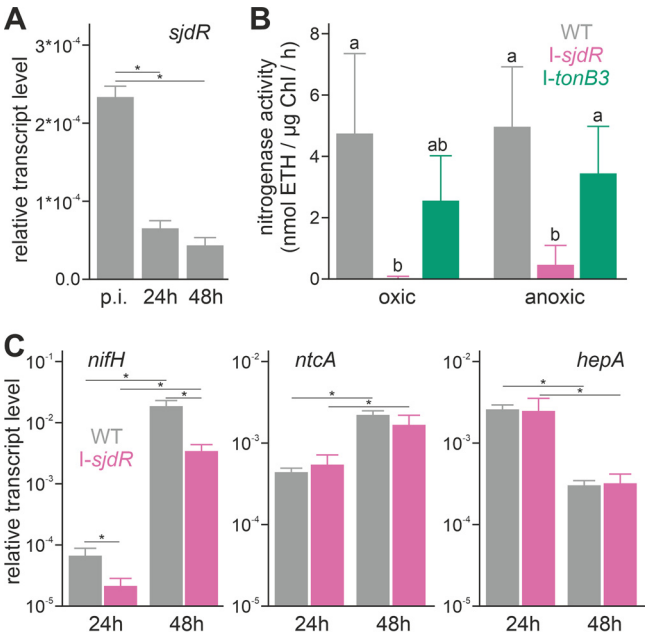

FIG 3 The *sjdR* mutant is impaired in nitrogenase gene expression and enzyme activity. (A) Transcript levels of *sjdR* were determined by qRT-PCR on RNA isolated from the wild type before (preinduction [p.i.]) and 24 h or 48 h after inoculation in nitrate-depleted YBG11$_0$ medium. Error bars represent the standard deviations of three biological replicates per strain. Asterisks above the bars show significant differences to the p.i. sample determined with Student's *t* test ($P < 0.05$). (B) The nitrogenase activity (in nanomoles of ethylene [ETH] per microgram of Chl per hour) was measured in wild-type ($n = 9$; gray), I-*sjdR* ($n = 4$; pink), and I-*tonB3* ($n = 3$; green) strains after 48 h of induction. Error bars represent the standard deviations of independent experiments. Statistical analysis was performed with ANOVA and Duncan's multiple range test; bars that share the same letters are not significantly different from each other ($P < 0.05$). (C) The transcript levels of *nifH*, *ntcA*, and *hepA* were determined in wild-type (gray) and I-*sjdR* (pink) strains and normalized to expression of *rnpB*. Error bars represent the standard deviations of three biological replicates each. Significant differences are indicated by asterisks (Student's *t* test, $P < 0.05$).

The low enzyme activity that, nonetheless, was observed under anoxic conditions might be related to reduced transcription of the nitrogenase-encoding genes. Thus, the mRNA abundance of the gene coding for dinitrogenase reductase (*nifH*), as well as of genes related to nitrogen control (*ntcA*) and heterocyst differentiation (*hepA*) (5), was determined by qRT-PCR. RNA was isolated from wild-type and I-*sjdR* strains 24 h and 48 h after transfer to YBG11$_0$ medium. The expression of *nifH* typically peaks after the heterocysts have maturated (53). Consistent with this, *nifH* transcripts were detected after 24 h, and a significant increase was observed after 48 h, both in the I-*sjdR* mutant and the wild type (Fig. 3C, left). However, compared to the wild type, the *nifH* transcript was less abundant in I-*sjdR* at both time points, indicating a transcriptional delay in the mutant, while the enzyme activity after 2 days was abolished completely. Nonetheless, the abolishment of nitrogenase function under oxic conditions in the I-*sjdR* mutant cannot be completely traced back to the moderate decrease in *nifH* transcription. In contrast, *ntcA* and *hepA* exhibited a similar transcript abundance pattern in both strains (Fig. 3C, middle and right). Thus, SjdR might not have a general impact on the regulation of heterocyst differentiation, but it seems to influence heterocyst function.

Calcium supplementation partially recovers diazotrophic growth of the *sjdR* mutant. In *Anabaena*, the intracellular prevalence of different metals is important for photosynthesis and diazotrophy. The nitrogenase complex possesses a FeMo cofactor, whereas the oxygen-evolving complex of photosystem II contains calcium and manganese ions (54). Thus, altered levels of metals during initial growth under nitrate-replete conditions could contribute to the impaired growth of the *sjdR* mutant upon nitrogen

TABLE 1 Metal concentration in wild-type *Anabaena* and the I-*sjdR* mutant strain[a]

Medium and element	Wild-type		I-*sjdR*		
	Atoms/OD	Atoms/cell[b]	Atoms/OD	Atoms/cell[b]	I-*sjdR*/WT
YBG11					
Ca	$(6.1 \pm 0.7) \times 10^{14}$	$(1.2 \pm 0.2) \times 10^{7}$	$(1.1 \pm 0.2) \times 10^{15}$	$(2.6 \pm 0.9) \times 10^{7}$	***2.1***
Mn	$(5.1 \pm 0.2) \times 10^{14}$	$(1.0 \pm 0.3) \times 10^{7}$	$(1.6 \pm 0.1) \times 10^{14}$	$(3.5 \pm 0.9) \times 10^{6}$	***0.3***
Mg	$(5.0 \pm 0.4) \times 10^{15}$	$(1.0 \pm 0.2) \times 10^{8}$	$(4.6 \pm 1.8) \times 10^{15}$	$(1.0 \pm 0.3) \times 10^{8}$	0.9
Zn	$(5.4 \pm 0.3) \times 10^{13}$	$(1.1 \pm 0.3) \times 10^{6}$	$(1.2 \pm 1.4) \times 10^{14}$	$(2.7 \pm 3.3) \times 10^{6}$	2.2
Mo	$(6.4 \pm 0.2) \times 10^{13}$	$(1.3 \pm 0.3) \times 10^{6}$	$(1.1 \pm 0.1) \times 10^{14}$	$(2.4 \pm 0.7) \times 10^{6}$	***1.7***
Co	$(1.8 \pm 0.1) \times 10^{13}$	$(3.7 \pm 0.8) \times 10^{5}$	$(1.5 \pm 0.1) \times 10^{13}$	$(3.4 \pm 1.0) \times 10^{5}$	***0.8***
Cu	$(5.1 \pm 0.5) \times 10^{13}$	$(1.1 \pm 0.3) \times 10^{6}$	$(5.1 \pm 0.4) \times 10^{13}$	$(1.1 \pm 0.3) \times 10^{6}$	1.0
Ni	$(0.4 \pm 0.2) \times 10^{13}$	$(0.9 \pm 0.4) \times 10^{5}$	$(0.4 \pm 0.1) \times 10^{13}$	$(0.9 \pm 0.2) \times 10^{5}$	0.9

[a]Data are presented as the number of atoms/OD_{750} and the number of atoms/cell. The ratio of the metal content in the wild type and mutant (I-*sjdR*/WT) is also shown. The bold italic values indicate significant changes, as assessed by the Student's *t* test ($P < 0.05$), calculated from the atoms/OD_{750} values.
[b]Note that the value for atom/cell is shown for orientation, since this value is more error-prone than atoms/OD_{750}.

deprivation. Therefore, the intracellular concentration of metal ions was determined in the wild-type (data from reference 55) and I-*sjdR* strains.

Inductively coupled plasma mass spectrometry (ICP-MS) measurements unraveled a significant increase of the calcium and molybdenum concentration, as well as a strong decrease of the manganese concentration in the I-*sjdR* mutant compared to the wild type (Table 1). The cobalt level was lower in the I-*sjdR* mutant as well but to a lesser extent than manganese. This suggests an enhanced uptake of Ca and Mo by the mutant strain, while Mn uptake is likely reduced. Consequently, the growth capacity of wild-type and mutant strains under decreased or enhanced manganese concentrations was tested. Manganese depletion did not yield a significant difference in growth between the I-*sjdR* mutant and the wild type, irrespective of the duration of starvation (Fig. 4A). Therefore, Mn limitation appears not to be problematic for *Anabaena* and I-*sjdR*. In contrast, elevated concentrations of manganese ($100 \times \mathrm{Mn} = 900\,\mu$M) were increasingly detrimental to the I-*sjdR* mutant compared to the wild type (Fig. 4B). To test whether manganese affects the growth of the I-*sjdR* mutant when transferred to nitrate-free medium, manganese was either omitted or the concentration was enhanced (100 μM, 2 mM). However, the altered manganese concentrations did not recover the diazotrophic growth of the I-*sjdR* mutant (Fig. 4C). The measurements of the intracellular zinc concentration showed a high degree of variation in the *sjdR* mutant strain (Table 1), and therefore, alterations in the zinc content between the two strains were omitted from the discussion.

Calcium signaling is essential for heterocyst differentiation and some stress responses in *Anabaena* (56–59). The extracellular calcium concentration strongly influences heterocyst frequency (60, 61) and the expression of heterocyst-specific genes, including the genes coding for the nitrogenase complex (58). Considering the elevated intracellular calcium levels and following the hypothesis of an increased demand for calcium in the I-*sjdR* mutant strain, the impact of an increased calcium supply on the growth of the *sjdR* mutant on $YBG11_0$ plates was analyzed. Notably, supplementation with calcium chloride partially complemented the phenotype of the I-*sjdR* mutant in a concentration-dependent manner (Fig. 4D). The mutant strain regained growth on medium without combined nitrogen when calcium concentrations exceeded the standard concentration of 245 μM, and the biomass produced was highest at 5 mM calcium (Fig. 4D). Notably, a calcium-dependent improvement of I-*sjdR* growth was also observed in diazotrophic liquid cultures (see Fig. S2B in the supplemental material). This phenotypic recovery was not observed for the I-*exbB2* and I-*alr1655* control mutants (Fig. 4D). On the other hand, a similar experiment was conducted with elevated concentrations of molybdenum, but those did not restore growth of the mutant under diazotrophic conditions (Fig. 4E).

The I-*sjdR* mutant exhibits an altered cell morphology and heterocyst pattern. The loss of nitrogenase activity in the I-*sjdR* mutant strain and the reduced growth

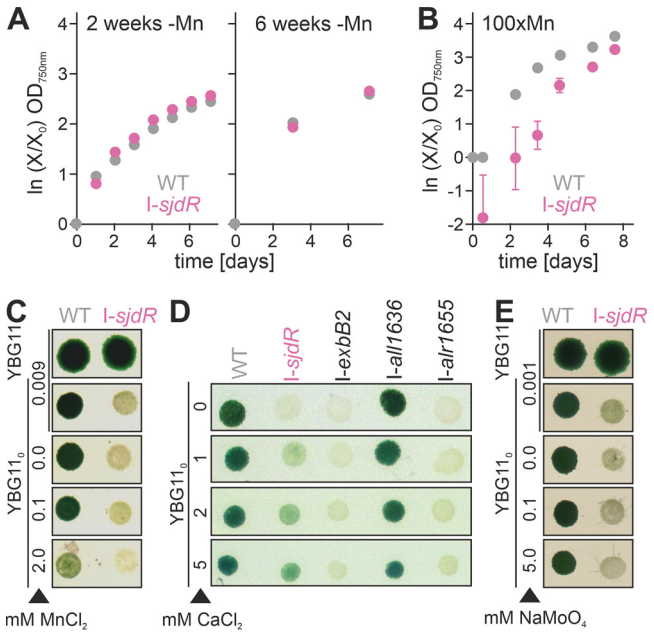

FIG 4 Elevated calcium concentrations stimulate the growth of the I-*sjdR* mutant strain in the absence of combined nitrogen. (A and B) Growth of wild-type (WT) (gray) and I-*sjdR* (pink) strains in YBG11 without Mn (A) or with high Mn concentrations (100 × Mn = 900 μM $MnCl_2$) (B). For Mn starvation, cells were incubated 2 (A, left) or 6 (A, right) weeks in Mn-free medium with dilution to an OD_{750} of 0.05 every 7 days. The average values of ≥3 biological replicates are shown; error bars represent the standard deviations. (C to E) Growth of wild type (WT) and indicated mutants on plates composed of YBG11 or $YBG11_0$ medium containing the indicated concentration of $MnCl_2$ (C), $CaCl_2$ (D), or Na_2MoO_4 (E). Standard YBG11 medium contains 9 μM $MnCl_2$, 245 μM $CaCl_2$, and 1 μM Na_2MoO_4. Cell suspensions were set to an OD_{750} of 1, 5-μl samples were spotted onto the agar plates, and the plates were incubated 7 days under culture conditions. Representative experiments are shown.

in $YBG11_0$ medium prompted us to inspect microscopically the I-*sjdR* filaments. Differentiated heterocysts were observed in the I-*sjdR* strain when grown in $YBG11_0$ medium (Fig. 5A). Heterocyst frequency, determined after 7 days of growth in nitrogen-depleted medium, was higher in the I-*sjdR* mutant than in the wild type (Fig. 5B). On average, 20 vegetative cells were counted between two heterocysts in the wild type, whereas 13 vegetative cells separated two heterocysts in I-*sjdR* (Fig. 5B). A higher heterocyst frequency is consistent with the impaired nitrogenase activity observed in the I-*sjdR* mutant, which leads to insufficient nitrogen assimilation and triggers the differentiation of an increased number of vegetative cells into heterocysts.

Notably, the morphology of the heterocysts in I-*sjdR* filaments was different from wild-type heterocysts (Fig. 5A). In the I-*sjdR* mutant strain, heterocysts appeared elongated and less ovoid in shape compared to heterocysts of the wild type. Moreover, transparent structures inside the heterocysts were observed in larger numbers in I-*sjdR* heterocysts. In transmission electron microscopy images, the characteristic polar neck and the cyanophycin plug near the poles were visible in wild-type heterocysts (Fig. 5C). Heterocysts of the I-*sjdR* mutant exhibited a certain degree of morphological heterogeneity, but they were characterized by (i) a cyanophycin plug that was barely visible or poorly structured, and (ii) a septum that was expanded, with the contact area to adjacent vegetative cells being larger than in the wild type (Fig. 5D). The morphology of I-*sjdR* vegetative cells was altered compared to the wild type, as the vegetative cells of the mutant were more rectangular (Fig. 5D, right; Table 2). The ratio of the width in the center of the cell to the width of the septum was 1.5 ± 0.1 (n = 20) for the wild type and 1.1 ± 0.1 (n = 29) for the I-*sjdR* mutant. Considering the strong morphological alterations of the *sjdR* mutant heterocysts compared to vegetative

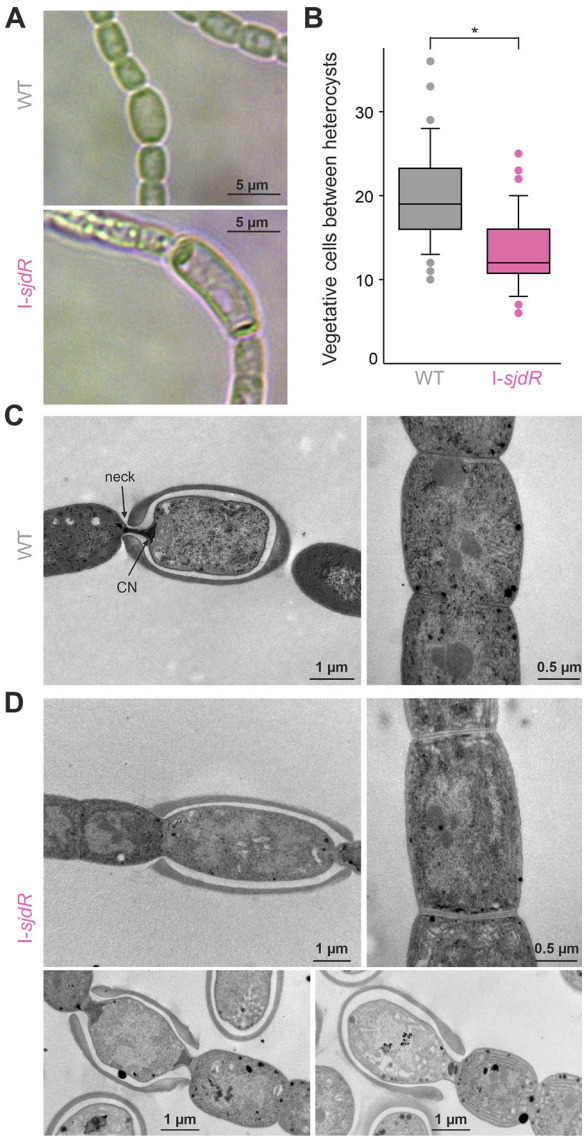

FIG 5 The *sjdR* mutant heterocysts are elongated and have an altered septum structure. (A) Wild-type (WT) and I-*sjdR* filaments were incubated under diazotrophic conditions and inspected by light microscopy. (B) The number of vegetative cells between two heterocysts after growth for 7 days in YBG11$_0$ medium was analyzed ($n = 1{,}389$ for WT cells and $n = 1{,}047$ for I-*sjdR* cells) in $n > 70$ randomly selected filaments. (C and D) Transmission electron microscopy images from wild-type (C) and I-*sjdR* (D) heterocysts (left and bottom) and vegetative cells (right) are shown. In the image of the wild-type heterocyst, the cyanophycin polymer (CN) and the heterocyst neck are indicated. For I-*sjdR*, multiple heterocysts are shown to illustrate the variability of heterocyst's ultrastructure.

cells, we suggest that the absence of SjdR affects a mechanism or activity that is especially important in heterocysts or for heterocyst formation.

SjdR is required for the formation of heterocyst polar structures. Spatial regulation of PG synthesis and distribution is a main determinant of cellular morphology in bacteria (62). Thus, the morphological phenotype of the I-*sjdR* mutant strain might be related to an altered regulation of PG synthesis in the mutant. To test this, PG of the wild-type and mutant strains was fluorescently labeled with vancomycin-FL (63). Cells grown on solid medium were labeled and analyzed by confocal microscopy (Fig. 6). The distribution of the fluorescent dye surrounding a vegetative cell was comparable in the I-*sjdR* mutant and the wild type (Fig. 6A, upper panel). For heterocysts of the wild type, the characteristic polar neck and protuberance of the PG into the adjacent vegetative cell were observed (Fig. 6A, lower panel; yellow arrowheads mark

TABLE 2 Properties of the septa (Fig. 5), septal disks, and nanopores (Fig. 8) in vegetative cells of the wild-type and I-*sjdR* strains

	Value for characteristic[a]			
	NO_3^-		N_2	
Characteristic	WT	I-*sjdR*	WT	I-*sjdR*
Septum width (diam)[b]	1.1 ± 0.2 μm (20)	***1.6 ± 0.3 μm*** (29)	ND	ND
Distance between plasma membranes[b]	32 ± 8 nm (8)	***58 ± 12 nm*** (15)	ND	ND
Disk diam (DD)	1.2 ± 0.2 μm (12)	***1.6 ± 0.6 μm*** (9)	1.4 ± 0.5 μm (14)	2.3 ± 0.8 μm (9)
Nanopore zone diam (NZD)	0.56 ± 0.08 μm (12)	0.5 ± 0.1 μm (9)	0.7 ± 0.2 μm (14)	0.4 ± 0.3 μm (9)
NZD/DD	0.47 ± 0.1 (12)	***0.31 ± 0.1*** (9)	0.51 ± 0.12 (14)	0.15 ± 0.05 (9)
Nanopore diam	23 ± 5 nm (270)	23 ± 6 nm (129)	24 ± 5 nm (349)	21 ± 4 nm (168)
No. of nanopores per disk	39 ± 9 (12)	***28 ± 9*** (8)	63 ± 31 (14)	53 ± 19 (10)

[a]Average values and standard deviations are given, and the number of replicates/measurements is indicated in parentheses. The bold italic values of the mutant shown are significantly different from the wild-type (WT) values (Student's *t* test, $P < 0.05$). ND, not determined; diam, diameter.
[b]Measurements conducted on TEM micrographs as illustrated in Fig. 5, the other parameters were determined from isolated peptidoglycan sacculi as presented in Fig. 8

heterocysts that are magnified in the panel below). The PG distribution in heterocyst septa of the I-*sjdR* mutant resembles, with its increased size, the PG architecture between vegetative cells. Therefore, the common PG area at the intercellular septa, also termed septal disk area, between heterocysts and adjacent vegetative cells was larger in the I-*sjdR* mutant than in the wild type. Thus, septal disks appear to be wider along the filament in the mutant than in the wild type, resulting in aberrant septal disks that do not show the characteristic constriction in vegetative cell-heterocyst septa.

As the supplementation of calcium did complement the growth of the I-*sjdR* mutant strain under diazotrophic conditions (Fig. 4), the impact of calcium on PG formation was analyzed. For both the wild type and the mutant strain, the distribution of the septal PG was comparable when grown on $YBG11_0$ plates or on $YBG11_0$ plates without calcium (Fig. 6B). However, in the presence of 5 mM calcium, the PG distribution in I-*sjdR* heterocyst septa resembled that of the wild type (Fig. 6B). Thus, an enhanced calcium concentration restores the PG morphology in the I-*sjdR* mutant, producing heterocyst septa functional for diazotrophic growth. To quantify this effect, the septum sizes (diameters) were measured for the wild type and I-*sjdR* mutant in the presence and absence of calcium. Interestingly, the analysis of the vegetative cells did not show a difference in septum width between the two strains in $YBG11_0$ or $YBG11_0$ without calcium ($YBG11_0$ -Ca) (Fig. 6C), whereas in YBG11, the I-*sjdR* vegetative cells septa were larger than in the wild type (Table 2); in $YBG11_0$ plus 5 mM $CaCl_2$, the I-*sjdR* septum diameter was also larger than that from the wild type, with average values of 1.8 ± 0.3 μm and 1.6 ± 0.2 μm, respectively (Fig. 6C). The quantification of the size of the septum between vegetative cells and heterocysts confirmed the presence of enlarged septa in the *sjdR* mutant strain, with on average 0.8 ± 0.3 μm in $YBG11_0$ and 0.8 ± 0.2 μm in $YBG11_0$ -$CaCl_2$ (compared to less than 0.4 μm in the wild type; Fig. 6D). When 5 mM $CaCl_2$ was supplemented, the average I-*sjdR* heterocyst septum width decreased to on average 0.3 ± 0.17 μm, similar to the corresponding wild-type value (0.2 ± 0.09 μm [Fig. 6D]). Therefore, calcium supplementation seems to have a differentiated effect on I-*sjdR* septum widths, and the constriction of the heterocyst septum in the presence of 5 mM $CaCl_2$ positively impacts the diazotrophic growth capacity of the strain.

Cell-cell communication is influenced by the disruption of *sjdR*. The septal disk of the I-*sjdR* mutant strain between heterocysts and vegetative cells appears larger than in wild-type *Anabaena* (Fig. 5 and 6), which might have an impact on solute exchange between two adjacent cells. Thus, the rate of solute diffusion was determined using calcein as a fluorescent marker molecule (64). The intercellular diffusion of the marker was recorded after photobleaching of a single cell (Fig. 7A). The fluorescence profiles of the bleached and adjacent cells were determined and analyzed with a 13-cell model (Materials and Methods) providing information for the transfer rate between vegetative cells or between a vegetative cell and a heterocyst.

Under the conditions tested, mean calcein transfer rates between a vegetative cell

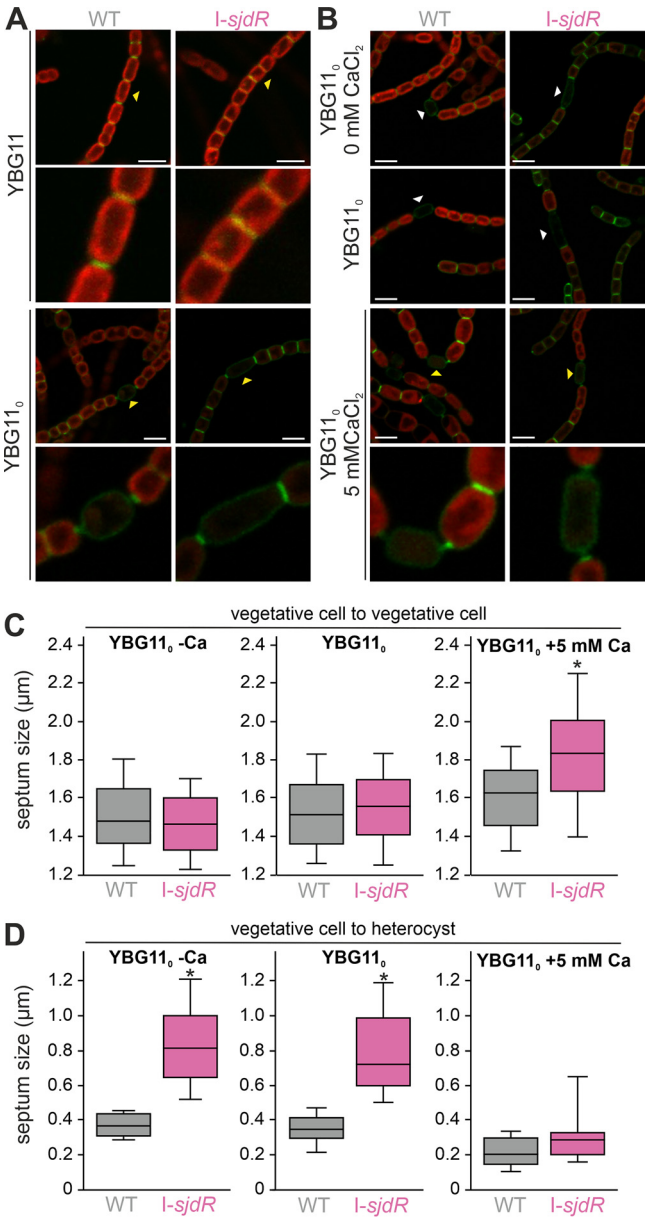

FIG 6 Impaired PG formation during heterocyst differentiation in the I-*sjdR* mutant strain and restoration by an enhanced calcium concentration. (A and B) Wild-type and I-*sjdR* filaments were grown on plates composed of the indicated media and fluorescently labeled with vancomycin-FL for visualizing the peptidoglycan. Merge images of vancomycin-FL fluorescence and autofluorescence are shown. Due to low Chl autofluorescence, in some images of the I-*sjdR* mutant, the intensity was adjusted for better visualization. Representative images are shown. White arrowheads point to heterocysts. Yellow arrowheads point to cells that are fourfold magnified in the panel below. Bars, 5 μm. (C and D) Quantification of the septum sizes between vegetative cells (C) or between vegetative cells and heterocysts (D) from wild-type and I-*sjdR* strains in YBG11$_0$ without $CaCl_2$ (YGB11$_0$ -Ca), YBG11$_0$, or YBG11$_0$ supplemented with 5 mM $CaCl_2$ (YBG11$_0$ +5 mM Ca). The measurements were taken from confocal microscope images (representative images shown in panels A and B); >100 septa of vegetative cells were measured per strain and condition, and >18 heterocyst septa were analyzed. The median values are presented in each box, and the error bars show the 95% confidence interval. Statistical analysis was done with ANOVA and Duncan's multiple range test (independent tests for panels C and D), and the asterisks above the boxes represent the samples that are significantly different from the other sample set (i.e., mutant versus wild type; $P < 0.001$).

and a heterocyst were 0.049 s^{-1} and 0.012 s^{-1} for the I-*sjdR* mutant strain and the wild type, respectively (Fig. 7B and Table 3). Therefore, calcein diffusion from vegetative cells into heterocysts was about fourfold faster in the I-*sjdR* mutant compared to the wild type. Similarly, the diffusion rate between vegetative cells of the I-*sjdR* mutant

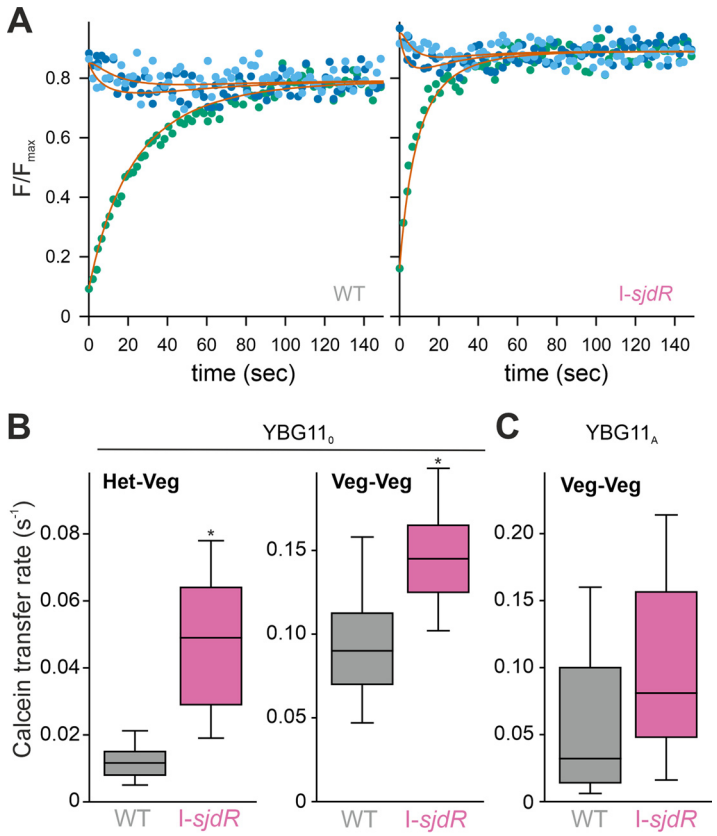

FIG 7 Intercellular calcein transfer rate is increased in the I-*sjdR* mutant strain. (A) The relative fluorescence intensity (F) in single cells was determined after photobleach. Shown is one example for wild-type (WT) (left) and I-*sjdR* (right) strains with the relative fluorescence of the bleached heterocyst visualized in green, the fluorescence of the adjacent vegetative cell in dark blue, and the fluorescence of the second adjacent cell in light blue. The solid line represents the result of the least square fit analysis to the model presented in Materials and Methods for these three cells. (B) The rates of calcein transfer between heterocysts (Het) and vegetative cells (Veg) or between vegetative cells observed for wild type (gray) and I-*sjdR* (pink) strains grown under diazotrophic conditions are shown as box-plots. (C) The calcein transfer rate between vegetative cells in WT (gray) and I-*sjdR* (pink) strains grown in medium containing ammonium is shown. For the box-plots in panels B and C, the central lines indicate the medians, and the error bars represent the 95% confidence intervals.

grown in $YBG11_0$ medium was higher by a factor of about 1.5 compared to the wild type (Fig. 7B and Table 3). This result was confirmed by analyzing the transfer rate between vegetative cells of some filaments of the two strains grown in YBG11 medium (Table 3, NO_3^-) or YBG11 medium supplemented with ammonium ($YBG11_A$) to suppress heterocyst formation (Fig. 7C and Table 3, NH_4^+). These results clearly show an increased intercellular transfer of calcein in the I-*sjdR* mutant between communicating cells.

The I-*sjdR* mutant strain bears alterations in septal nanopore distribution. The augmented intercellular molecular transfer in the I-*sjdR* mutant could be related to the larger septa observed in the mutant (Fig. 5 and 6). In *Anabaena*, the velocity of solute exchange depends on the size and number of nanopores and septal junctions (8, 65, 66), which mediate the efficient intercellular exchange of metabolites (67). In order to examine the properties of the nanopores in the I-*sjdR* mutant compared to the wild type, PG sacculi were isolated, and the septal disks were analyzed.

The periplasm between adjacent vegetative cells was found to be enlarged in the I-*sjdR* mutant strain as deduced from electron microscopy images (Fig. 5), because both the width of the septum and the distance between the centers of two adjacent plasma membranes were enhanced (Table 2). The same holds true for the septal disks (Fig. 8 and Table 2), in which the effect was most pronounced when the strains were grown in

TABLE 3 Calcein transfer rates for the wild-type and I-*sjdR* strains

Cell type[a]	Nitrogen source	Wild type		I-*sjdR*	
		CT rate (s^{-1})[b]	*N*[c]	CT rate (s^{-1})[b]	*N*[c]
VEG-HET	N_2	0.012 ± 0.001	68	0.049 ± 0.003	75
VEG-VEG	N_2	0.094 ± 0.006	53	0.145 ± 0.005	51
VEG-VEG	NO_3^-	0.11 ± 0.01	7	0.16 ± 0.02	6
VEG-VEG	NH_4^+	0.06 ± 0.02	9	0.11 ± 0.06	8

[a]VEG, vegetative cells; HET, heterocysts.
[b]CT rate, calcein transfer rate. The CT rates are shown are as means ± standard errors.
[c]*N* is the number of experiments.

the absence of nitrate. Here, the wild-type septal disks were on average 1.4 ± 0.5 μm in diameter, whereas I-*sjdR* disks had a diameter of 2.3 ± 0.8 μm (Table 2).

Both under nitrate-replete and -deplete conditions, the relative area of the disk in which nanopores were detected was smaller in the *sjdR* mutant. This effect was most drastic in $BG11_0$ medium, in which nanopores were found in 3% of the septal disk area in I-*sjdR* but in about 25% of the disk area in the wild type (calculated from the nanopore zone diameter [NZD] and the disk diameter [DD] in Table 2). In both BG11 and $BG11_0$ media, the number of nanopores per disk was somewhat lower in the I-*sjdR* mutant strain compared to the wild type. The nanopore diameter was comparable between the two strains in the presence of nitrate, whereas in $BG11_0$ medium, the nanopore diameter in the I-*sjdR* mutant was somewhat smaller than in the wild type. Therefore, the increased rate of calcein transfer cannot be explained by an increased number of nanopores in the mutant, but it may result from other factors such as a reduced cyanophycin plug (see Discussion).

In order to investigate the subcellular localization of SjdR, a strain expressing SjdR-GFP was created (Fig. S3). Due to the low expression levels of *sjdR*, the green fluorescent protein (GFP) fluorescence signal was weak under the confocal microscope. A quantification of the fluorescence signal in the septum and the sidewall region showed that GFP was not significantly enriched in the septum (Fig. S3), and SjdR-GFP rather

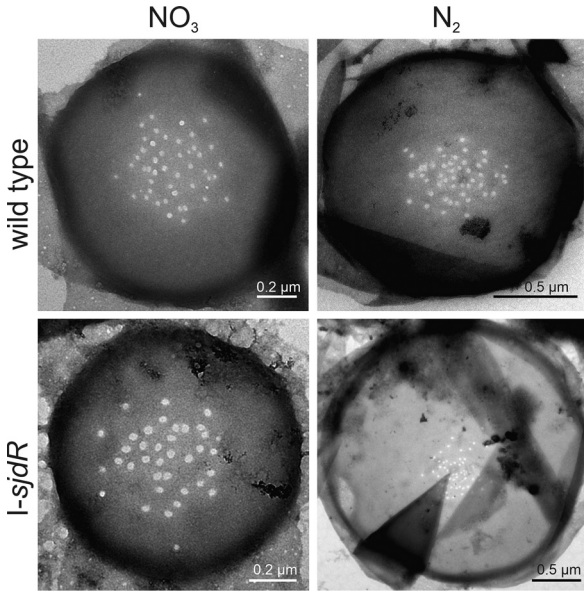

FIG 8 The nanopore distribution in the I-*sjdR* mutant strain. Peptidoglycan sacculi were isolated from BG11-grown filaments or filaments incubated for 48 h in $BG11_0$ medium of the wild type and I-*sjdR* mutant. To visualize the septal disks, the sacculi were inspected by transmission electron microscopy as described in Materials and Methods.

seems to be evenly distributed along the cell envelope. This strengthens the hypothesis that SjdR plays a general role in PG structuring.

DISCUSSION

In *Anabaena*, four proteins have been identified as putative TonB-like proteins (44). However, the previously assigned TonB1 (here denoted SjdR) is exceptionally short, and considering the distance between PM and OM (2), this protein would be unable to interact with OM proteins. In addition, SjdR does not contain a TonB-like periplasmic domain, whereas a similarity to the ZipA divisome protein and GltJ/AgmX superfamiliy proteins is predicted instead (Fig. 1). Whether SjdR contributes to gliding motility in *Anabaena* was not analyzed in this study, but it should be noted that *Anabaena* is described as nonmotile (68).

The periplasmic domain of SjdR is rich in hydroxylated amino acids (serine, threonine) and prolines. Notably these amino acids are enriched as well in the SepJ linker domain and in SepI, both of which are septal proteins in *Anabaena* (9, 18). The absence of SjdR in a plasmid insertion *sjdR* mutant of *Anabaena* does not affect the siderophore transport rate, whereas a *tonB3* mutant generated by the same strategy is drastically impaired in siderophore-dependent iron transport (Fig. 2). This is consistent with the idea that TonB3 is central for energizing the ferric siderophore uptake as previously suggested (44). The involvement of SjdR in TonB-dependent transport was rejected based on the analyzed uptake of schizokinen which is produced by *Anabaena* sp., but a participation in the transport of other substrates cannot be excluded. However, considering its structure and length, we suggest that SjdR takes over a function distinct from TonB-dependent transport in *Anabaena*, perhaps a function as an interaction platform for periplasmic proteins involved in PG maintenance as will be discussed below.

The growth of the *sjdR* mutant (I-*sjdR*) is severely delayed in the absence of nitrate (Fig. 2), although nitrogen step-down does not induce *sjdR* transcription (Fig. 3). This argues against a direct involvement of SjdR in heterocyst differentiation. Despite a substantial expression of nitrogenase-encoding genes (tested with *nifH*), nitrogenase activity is absent under oxic conditions but detectable (albeit at low levels) under anoxic conditions (Fig. 3). This suggests that the phenotype of the mutant is related to a breakdown of the microoxic environment in the heterocyst rather than to the absence of nitrogenase production. Heterocysts of the *sjdR* mutant are morphologically altered, since they are elongated and less ovoid compared to those of the wild type (Fig. 5). Further, the vegetative cell-heterocyst connection shows an abnormal architecture in which a wide heterocyst neck is observed and the cyanophycin plug is reduced or missing (Fig. 5). This could result, at least in part, from the compromised nitrogen fixation capacity of the mutant strain. This morphological phenotype is comparable to those of the *hglK* (67) and *conR* (69, 70) mutants, as well as a strain in which the *sepJ* gene is overexpressed (65).

The diffusion of the fluorescent marker calcein between cells is faster in the *sjdR* mutant than in the wild type, which is most pronounced for the transfer between vegetative cells and heterocysts (Fig. 7), again resembling the phenotype of the *hglK* mutant (71). The transfer of solutes between cells first depends on the number and size of nanopores in the septal PG mesh that connect the cytoplasm of adjacent cells in the filament (8, 66). Notably, the number of nanopores between vegetative cells is somewhat lower in the *sjdR* mutant than in the wild type; thus, the faster transfer in the mutant must be grounded on other factors. In addition to nanopore architecture, also other factors influence molecular transfer in *Anabaena*. For example, the inactivation of *glsP* (encoding a glucoside ABC transporter permease subunit) or of *hepP* (encoding a major facilitator superfamily [MFS] glucoside transporter) decreases the calcein transfer rate, but not the number of nanopores (72). Moreover, septal junctions are gated, since different stress conditions can reversibly reduce the diffusion activity (73). Hence, we hypothesize that SjdR affects the proteinaceous components of the septal junctions in a way such that calcein transfer is influenced as observed in the *sjdR* mutant. In

addition, the reduced cyanophycin plug in the mutant heterocysts might contribute to the increased rate of calcein diffusion (64). An increased molecular influx into heterocysts could in turn contribute to inactivation of nitrogenase by oxygen entering through the wide heterocyst poles in the mutant (6, 74). Whether there is a direct interaction between SjdR and septal proteins remains to be elucidated. However, since an enrichment of SjdR-GFP was not observed near the septum, SjdR function seems to not be limited to the septum area.

The septal PG arrangement at the poles of the heterocyst in the *sjdR* mutant resembles the one between vegetative cells (Fig. 6). This suggests an important role of SjdR in the formation of the vegetative cell-heterocyst septa. Nonetheless, the altered phenotype of the *sjdR* mutant is not restricted to heterocysts, as in YBG11 medium also, the septal disk area between vegetative cells is enlarged compared to the wild type (Fig. 5 and Table 2). Additionally, the zone occupied by the nanopores in the septal disks of vegetative cells is significantly smaller in the *sjdR* mutant than in the wild type, which represents a novel morphological phenotype (unfortunately, no data are available specifically for the heterocyst-vegetative cell septa). These results imply a relation of SjdR with PG formation or remodeling in *Anabaena*. Spatial PG synthesis is a major determinant of cell shape in bacteria (62). We assume that the differential activity of PG metabolism and plasticity in the two cell types (vegetative cells and heterocysts) is the reason for the morphological *sjdR* mutant phenotype, which is mostly visible in heterocysts. SjdR deletion consequently seems to impact mechanisms that are especially active or required for normal heterocyst formation. In *Anabaena*, PG synthesis is stronger during heterocyst differentiation than in vegetative cells and proceeds along the whole cell, whereas in vegetative cells, it is mainly limited to the division site (75). A deregulation of PG arrangement due to lack of SjdR function can explain the alterations in heterocyst morphology and the alterations in the vegetative cell septa, whereas we do not know whether vegetative cell lateral walls are somehow affected. The proper regulation of PG synthesis and elasticity is essential for heterocyst differentiation (76, 77). On the one hand, heterocyst-specific polysaccharides and lipids need to pass through the cell wall (78), and the PG of heterocysts is thicker than that of vegetative cells (75). Thus, a relation of SjdR to PG organization would be consistent with the Fox$^-$ phenotype of the mutant (Fig. 3).

An increase of calcium concentration was observed in the *sjdR* mutant compared to the wild type (Table 1). The growth of the mutant under diazotrophic conditions was largely restored by calcium supplementation (Fig. 4). Since calcium stabilizes the PG and regulates the elongasome activity in some bacteria (79, 80), the *sjdR* mutant might accumulate calcium to compensate for a defect in PG metabolism, with calcium supplementation further enhancing this effect. This is consistent with the reported observations that extracellular calcium has a strong impact on nitrogen metabolism in *Anabaena* (58, 61, 81) and that elevated calcium levels accelerate heterocyst differentiation (81) or enhance the performance of nitrogenase (82). Notably, in *Anabaena*, the intracellular calcium level is about 1 order of magnitude higher in heterocysts than vegetative cells (56, 57).

Proteins with similarity to *Anabaena* SjdR were found to be conserved among cyanobacteria, except for *Gloeobacteria* and *Spirulinales*. As is the case for elangasome- and divisome-related proteins, which define cellular morphology and at the same time are conserved in unicellular and filamentous strains, it is conceivable that the SjdR functionality adapted over time in different cyanobacteria (83, 84).

In summary, the highly conserved SjdR protein (Fig. 1) has a structural role in the maintenance of cell wall morphology in *Anabaena*. SjdR knockout induces an altered PG distribution, which becomes evident in the aberrant morphology of septal PG disks and, more generally, in cell shape alterations and impairment of diazotrophic growth. The latter is likely the consequence of an increased oxic environment in the heterocysts that results from the increased septum size, permitting an elevated influx of solutes, including oxygen.

MATERIALS AND METHODS

***In silico*/bioinformatics analyses.** Cyanobacterial sequences were collected by BLAST search (NCBI with the following settings: BLOSUM62; gap costs: existence, 11, extension, 1; 500 sequences) using the SjdR and TonB3 protein sequences from *Anabaena* sp. strain PCC 7120 as bait (85, 86). All sequences identified were filtered for redundancy using cd-hit (87) with a setting of 90% sequence identity. The distribution of sequences in different species is shown according to the taxonomy nomenclature deposited in NCBI (88). Domains of SjdR were extracted from NCBI (89). The transmembrane domain was predicted by TMHMM (90).

***Anabaena* culture conditions.** *Anabaena* wild type and mutants were stored on BG11 medium agar plates (68) containing 1% (wt/vol) Bacto agar (BD Biosciences). Liquid and solid media for mutants were supplemented to 5 μg ml^{-1} of each spectinomycin dihydrochloride pentahydrate (Duchefa Biochemie) and streptomycin sulfate (Roth). For liquid cultures, BG11 or buffered YBG11 medium was utilized (91). No precipitation of compounds is observed in YBG11, which in experiments that address questions about metal availability is an important condition. For YBG11$_0$ (nitrate-free YBG11), $CoCl_2$ was used instead of $CoNO_3$.

Cultures were grown with constant shaking (90 to 100 rpm) under permanent illumination at 28°C and 70 μmol photons m^{-2} s^{-1} (Frankfurt) or at 30°C and about 25 μmol photons m^{-2} s^{-1} (Seville; for nitrogenase activity determination and septal disk isolation). Bubbling cultures were enriched with CO_2 (1%) and 10 mM $NaHCO_3$ was used for pH stabilization of the medium. Growth analysis was done on agar plates spotted with 5 μl of cell suspensions previously adjusted to an optical density at 750 nm (OD_{750}) of 1 or 0.1 without antibiotics.

DNA extraction and molecular cloning. Genomic DNA from *Anabaena* was isolated as described previously (92) with the following modifications: sodium dodecyl sulfate (SDS) was not added to the samples, and the phenol extraction was done once, followed by two washing steps with 400 μl chloroform.

Generation of *Anabaena* mutants. Single recombinant mutants were created as described previously (93–96). In the case of AFS-I-*sjdR* (I-*sjdR*), an *sjdR*-internal fragment of 532 bp was amplified by PCR (oligonucleotides [see Table S1 in the supplemental material]), and EcoRI and EcoRV restriction sites were inserted at the 5′ and 3′ ends, respectively. The fragment was inserted into EcoRI/EcoRV-digested pCSEL24 that contains a CS.3 cassette (95). The plasmids are listed in Table S3. In the case of AFS-I-*tonB2* (I-*tonB2*) and AFS-I-*tonB4* (I-*tonB4*), fragments of 467 bp and 584 bp, respectively, were amplified, and BglII sites were introduced at both ends. For cloning AFS-I-*exbB2* (I-*exbB2*), an internal fragment of 408 bp was amplified, and BamHI sites were inserted at both ends. All fragments were ligated into BamHI-digested pCSV3. pCSV3 is a modified version of pRL500 (97) bearing the CS.3 resistance cassette (98). The plasmids (Table S3) were transferred to wild-type *Anabaena* by conjugation as previously described (94) utilizing *Escherichia coli* strains HB101 and ED8654. Segregation of mutant strains was tested utilizing an oligonucleotide specific for the plasmid in combination with oligonucleotides annealing outside the internal fragment (Fig. 1; see also Fig. S1 in the supplemental material). All the mutant strains are listed in Table S2. The AFS-I-*all1636* (I-*all1636*) and AFS-I-*alr1655* (I-*alr1655*) mutants were a gift from L. Fresenborg.

To analyze the subcellular localization of SjdR, the superfolder GFP (*sf-gfp*) gene was fused to the 3′ end of the *sjdR* open reading frame, and a sequence encoding a tetraglycine linker was inserted between *sjdR* and *sf-gfp*. Molecular cloning was performed as described previously (71). In brief, the *sf-gfp* sequence was amplified without the start codon (see oligonucleotides in Table S1), an EcoRV site as well as the tetraglycine-encoding sequence was added at the 5′ end, and a KpnI site at the 3′ end. The *gfp-mut2* sequence was excised from plasmid pCSEL21 (95) (Table S3) with KpnI/EcoRV, and *sf-gfp* was inserted instead, yielding pCSEL21-sf-gfp. The *sjdR* sequence was amplified by PCR utilizing *Anabaena* genomic DNA as the template; the stop codon was not included. ClaI and EcoRV sites were inserted at the 5′ and 3′ ends, respectively, and the sequence was inserted into pCSEL21-sf-gfp after restriction digest with ClaI/EcoRV. After the insertion of the *sjdR-sf-gfp* fusion into pCSEl21 was verified by sequencing, *sjdR-sf-gfp* was excised with EcoRI and ligated into EcoRI-digested pCSV3. The resulting plasmid pCSV3-sjdR-sf-gfp (Table S2) was transferred to *Anabaena* (described above), and the genotype of the *sjdR-gfp* strain (Table S2) was analyzed by PCR.

Short-term siderophore transport measurements and chlorophyll measurements. Ferric schizokinen uptake experiments were conducted as described earlier (99, 100). In brief, $^{55}FeCl_3$ (PerkinElmer) was complexed to a threefold excess of iron-free schizokinen (EMC Microcollections). A final concentration of 15 nM ^{55}Fe-schizkonen was utilized as the substrate. For the uptake experiments, the OD_{750} of the culture was adjusted to 0.05. The last samples were taken ~3.5 h after the addition of substrate. *Anabaena* strains were grown in iron-depleted medium prior to the uptake experiments. The cellular concentration of chlorophyll *a* (Chl) is an indicator for the degree of iron deficiency in *Anabaena*, since it constantly decreases with ongoing starvation (43). Chl content was divided by the OD_{750} (Table S4), which allowed a comparison of the starvation levels of different cultures. Only strains that exhibited a comparable Chl at OD_{750} of 1 were utilized. Chl concentration was determined in methanolic extracts as previously described (101) and was calculated with the following formula: Chl (in milligrams per milliliter) = A_{665}/74.5.

Calcein staining and fluorescence recovery after photobleaching. YBG11$_0$ cultures used for calcein staining were grown for 3 days in YBG11$_0$ in shaken flasks. Cultures grown in YBG11$_A$ or YBG11 medium were grown in bubbling cultures for 3 days. Staining of *Anabaena* cells with calcein-AM (Invitrogen) was done according to reference 64. For fluorescence microscopy, 50 to 150 μl of cell suspension was spotted onto YBG11, YBG11$_A$, or YBG11$_0$ agar plates. After drying of the liquid, a small

portion of agar was excised and reversely placed onto a coverslip that was utilized as microscope slide. Fluorescence recovery after photobleaching (FRAP) was measured at 23°C with a Zeiss LSM 780 using a 40× oil immersion objective. Excitation with an argon laser at 488 nm was set at 100% for bleaching, and the laser power was reduced to 20% for further recording. Emission was measured at 500 to 540 nm, and the pinhole diameter was set at 180.5 μm. Two or three scans were recorded prior to bleaching, and recovery was recorded for at least 60 s. Only communicating cells were analyzed, since noncommunicating cells occurred in low frequency both in the wild type and the mutants under the conditions used in this study. The data for calcein transfer between vegetative cells were fitted using a reaction chain of exchange between 13 cells according to the following reaction between two cells: $[C_1 \leftarrow k_V \rightarrow C_2]_{13}$ with C_1 being the fluorescence equivalent to the concentration of calcein in cell 1, C_2 being the fluorescence equivalent to the concentration of calcein in cell 2, and k_V being the rate for the forward and backward transfer of calcein for a chain of 13 vegetative cells with the bleached cell as the center. The values for the bleached and neighboring cells were used as input parameters.

The data for transfer into heterocysts were fitted using a reaction scheme between six vegetative cells on each side of the heterocyst as well as between the heterocyst and the neighboring vegetative cells:

$$[C_1 \leftarrow k_V \rightarrow C_2]_6 \leftarrow k_{\mathrm{VH}} \rightarrow C_H \leftarrow k_{\mathrm{VH}} \rightarrow [C_{1'} \leftarrow k_V \rightarrow C_{2'}]_6$$

with $C_1/C_{1'}$ being the fluorescence equivalent to the concentration of calcein in vegetative cell 1 or cell 1′, $C_2/C_{2'}$ being the fluorescence equivalent to the concentration of calcein in vegetative cell 2 or cell 2′, and k_V being the rate for the forward and backward transfer of calcein for a chain of six vegetative cells with the bleached heterocyst as center. C_H is the fluorescence equivalent to the concentration of calcein in the heterocyst, and k_{VH} is the rate for the forward and backward transfer of calcein between heterocyst and vegetative cell. A similar rate for forward and backward exchange is assumed, as calcein is a nonnative substrate. In the case of a filament with a terminal heterocyst, the reaction was adapted to:

$$[C_1 \leftarrow k_V \rightarrow C_2]_6 \leftarrow k_{\mathrm{VH}} \rightarrow C_H$$

Vancomycin-FL staining and microscopy. For confocal and electron microscopy, the strains were grown for 7 days in the indicated medium, since a suitable cell density was required for performing the experiments. Cells were stained with BODIPY FL vancomycin (Invitrogen) as described previously (63). Following two washing steps, the cells were spotted onto YBG11 or $YBG11_0$ agar plates and incubated for 90 min at 28°C in darkness. A piece of agar was excised afterwards, reversely placed onto a coverslip, and imaged with a Zeiss LSM 780 using a 63× or 40× oil immersion objective. The pinhole diameter was set at 69.4 μm, excitation was done with an argon laser at 488 nm, and fluorescence was tracked between 500 and 550 nm. Chl autofluorescence was monitored in the range of 630 to 700 nm. Light microscope images were taken with Olympus CKX41.

The quantitative analysis of the GFP fluorescence of the *sjdR-gfp* strain was performed as previously described with modifications (72). Since the GFP fluorescence was low in these experiments, the wild-type and *sjdR-gfp* strains were cultured in iron-free medium prior to the analysis, because we observed an increase of the signal compared to normal conditions. The parameter settings are described above. Quantification of the fluorescence was done as follows: the integrated density in squares of 1×1 μm was measured with ImageJ, and a minimum of 120 measurements were taken for each septum and sidewall regions from different filaments. The background value was measured in each picture and subtracted from the corresponding septum or sidewall values. The average wild-type value was subtracted from the average value of the *sjdR-gfp* strain.

Samples for transmission electron microscopy were prepared as reported previously (67) with modifications. In brief, cells were harvested by centrifugation (1,000 × *g*, 5 min), transferred into microcentrifuge tubes, and pelleted again. Cells were resuspended in 2 ml fixation buffer (0.08 M sodium cacodylate [pH 7.3], 2% glutaraldehyde) and incubated for at least 2 h at 4°C. Afterwards, cells were washed twice by centrifugation (1,000 × *g*, 5 min) with wash buffer (0.08 M sodium cacodylate [pH 7.3], 10% [wt/vol] sucrose). Fixation was done in 1% OsO_4 for 1 h, and the dehydration was performed using ethanol gradient series up to 100% ethanol. Then samples were incubated in propylene oxide and infiltrated overnight with a mixture of propylene oxide and araldite (1:1) and embedded in araldite the next day. Ultrathin sections of about 50 nm were stained with uranyl acetate and lead citrate. A Zeiss EM 900 transmission electron microscope was used for visualization.

RNA, cDNA synthesis, and qRT-PCR. RNA extraction was performed as described using TRIzol from Thermo Fisher Scientific (102). The absence of DNA in the RNA sample was tested by PCR using oligonucleotides specific for the *rnpB* gene (Table S1). cDNA synthesis was done with Revert Aid Transcriptase (Thermo Fisher Scientific) according to the manufacturer's instructions using 1.5 μg of total RNA as the template.

qRT-PCR was performed utilizing StepOnePlus Cycler (Thermo Fisher Scientific). Gene-specific oligonucleotides (Table S1) were added to a concentration of 0.3 μM. Template cDNA was diluted at least 1:3, and PowerUp SYBR green Master Mix (Applied Biosystems) was utilized according to the manufacturer's protocol. Cycling conditions were set to 2 min at 50°C and 2 min at 95°C for 2 min initially, followed by 40 cycles with 1 cycle consisting of 15 s at 95°C, 30 s at 60°C, and 30 s at 72°C. As a control housekeeping gene, *rnpB* was used.

Nitrogenase activity. Nitrogenase activity was determined by the acetylene reduction assay (103). Filaments were grown in BG11 medium, harvested by centrifugation, washed with $BG11_0$, inoculated at 1 μg Chl ml^{-1} in 25 ml of $BG11_0$ (without antibiotics), and incubated under culture conditions for 48 h.

Assays were performed with 2 ml of cell suspension (6 μg ml^{-1}) in sealed flasks (total volume, 14 to 17 ml) under both oxic and anoxic conditions. The reaction was started by injecting a saturating amount of acetylene (1 ml). One-milliliter samples for determination of ethylene by gas chromatography were taken for up to 2 h. For anoxic conditions, the cells were supplemented with 10 μM 3-(3,4-dichlorophenyl)-1,1-dimethylurea (DCMU), bubbled with argon for 4 min, and incubated for 60 min before starting the reaction.

Inductively coupled plasma mass spectrometry. Glassware was incubated in 4% HNO_3 overnight. Strains were grown for 7 days in YBG11, harvested by centrifugation (3,000 $\times$ *g*, 10 min), and washed in 20 mM 2-(*N*-morpholino)ethanesulfonic acid (pH 5) and 10 mM ethylenediaminetetraacetic acid (104). After the second washing step, the pellet was resuspended in 5 ml double-distilled water (ddH_2O). For normalization, cells were counted using a Helber bacterial counting chamber (Hawksley), and OD_{750} was measured. Subsequent experiments were conducted in a metal clean laboratory. A volume of 1 ml of each sample was incubated at 120°C in 7 M HNO_3 overnight until dryness. Before measurement, the samples were dissolved in 5% HNO_3. As controls, samples of ddH_2O and culture medium were analyzed.

Peptidoglycan isolation and septal disk visualization. Filaments were grown in liquid BG11 medium (supplemented with antibiotics as required) to about 3 to 4 μg Chl ml^{-1}, harvested, washed with $BG11_0$ medium, inoculated at the same cell density, and incubated in $BG11_0$ medium (without antibiotics) for 48 h. Cultures were harvested by centrifugation and fragmented in a sonication bath, and the sacculi were isolated by boiling in the presence of SDS and treatment with α-chymotrypsin (from bovine pancreas; Sigma) following the protocol described (105). The purified sacculi were deposited on copper grids coated by Formvar/carbon film (Aname) and stained with 1% (wt/vol) uranyl acetate for 15 min. All the samples were examined with a ZEISS LIBRA 120 PLUS electron microscope at 120 kV.

SUPPLEMENTAL MATERIAL

Supplemental material is available online only.

FIG S1, TIF file, 1.3 MB.

FIG S2, TIF file, 1.3 MB.

FIG S3, TIF file, 2.3 MB.

TABLE S1, DOCX file, 0.01 MB.

TABLE S2, DOCX file, 0.01 MB.

TABLE S3, DOCX file, 0.01 MB.

TABLE S4, DOCX file, 0.01 MB.

TABLE S5, DOCX file, 0.02 MB.

ACKNOWLEDGMENTS

We thank Mara Stevanovic for help in preparation and testing of constructs and mutants, Rafael Pernil for useful discussions, and Antonia Herrero for a critical reading of the manuscript. We thank Leonard Fresenborg and Maike Ruprecht for providing the AFS-I-*alr1655* and AFS-I-*all1636* control strains and H.-Michael Seitz for experimental support with ICP-MS.

The work was funded by the Deutsche Forschungsgemeinschaft DFG SCHL585/6-3 to E.S. Work in Seville, Spain, was supported by grant BFU2017-88202-P from Plan Estatal de Investigación Científica y Técnica y de Innovación, Spain, cofinanced by the European Regional Development Fund, to E.F.

We declare that we have no conflicts of interest.

REFERENCES

1. Hahn A, Schleiff E. 2014. The cell envelope, p 29–87. In Flores E, Herrero A (ed), The cell biology of cyanobacteria. Caister Academic Press, Norfolk, United Kingdom.
2. Wilk L, Strauss M, Rudolf M, Nicolaisen K, Flores E, Kühlbrandt W, Schleiff E. 2011. Outer membrane continuity and septosome formation between vegetative cells in the filaments of *Anabaena* sp. PCC 7120. Cell Microbiol 13:1744–1754. https://doi.org/10.1111/j.1462-5822.2011.01655.x.
3. Kumar K, Mella-Herrera RA, Golden JW. 2010. Cyanobacterial heterocysts. Cold Spring Harb Perspect Biol 2:a000315. https://doi.org/10.1101/cshperspect.a000315.
4. Magnuson A, Cardona T. 2016. Thylakoid membrane function in heterocysts. Biochim Biophys Acta 1857:309–319. https://doi.org/10.1016/j.bbabio.2015.10.016.
5. Golden JW, Yoon HS. 1998. Heterocyst formation in *Anabaena*. Curr Opin Microbiol 1:623–629. https://doi.org/10.1016/S1369-5274(98)80106-9.
6. Gallon JR. 1992. Reconciling the incompatible: N_2 fixation and O_2. New Phytol 122:571–609. https://doi.org/10.1111/j.1469-8137.1992.tb00087.x.
7. Elhai J, Wolk CP. 1990. Developmental regulation and spatial pattern of expression of the structural genes for nitrogenase in the cyanobacterium *Anabaena*. EMBO J 9:3379–3388. https://doi.org/10.1002/j.1460-2075.1990.tb07539.x.
8. Nürnberg DJ, Mariscal V, Bornikoel J, Nieves-Morión M, Krauß N, Herrero A, Maldener I, Flores E, Mullineaux CW. 2015. Intercellular diffusion of a fluorescent sucrose analog via the septal junctions in a filamentous cyanobacterium. mBio 6:e02109-14. https://doi.org/10.1128/mBio.02109-14.
9. Flores E, Pernil R, Muro-Pastor AM, Mariscal V, Maldener I, Lechno-Yossef S, Fan Q, Wolk CP, Herrero A. 2007. Septum-localized protein required for filament integrity and diazotrophy in the heterocyst-forming cyanobacterium *Anabaena* sp. strain PCC 7120. J Bacteriol 189:3884–3890. https://doi.org/10.1128/JB.00085-07.

10. Merino-Puerto V, Mariscal V, Mullineaux CW, Herrero A, Flores E. 2010. Fra proteins influencing filament integrity, diazotrophy and localization of septal protein SepJ in the heterocyst-forming cyanobacterium *Anabaena* sp. Mol Microbiol 75:1159–1170. https://doi.org/10.1111/j.1365-2958.2009.07031.x.
11. Mariscal V, Herrero A, Nenninger A, Mullineaux CW, Flores E. 2011. Functional dissection of the three-domain SepJ protein joining the cells in cyanobacterial trichomes. Mol Microbiol 79:1077–1088. https://doi.org/10.1111/j.1365-2958.2010.07508.x.
12. Merino-Puerto V, Schwarz H, Maldener I, Mariscal V, Mullineaux CW, Herrero A, Flores E. 2011. FraC/FraD-dependent intercellular molecular exchange in the filaments of a heterocyst-forming cyanobacterium, *Anabaena* sp. Mol Microbiol 82:87–98. https://doi.org/10.1111/j.1365-2958.2011.07797.x.
13. Rudolf M, Tetik N, Ramos-León F, Flinner N, Ngo G, Stevanovic M, Burnat M, Pernil R, Flores E, Schleiff E. 2015. The peptidoglycan-binding protein SjcF1 influences septal junction function and channel formation in the filamentous cyanobacterium *Anabaena*. mBio 6:e00376-15. https://doi.org/10.1128/mBio.00376-15.
14. Bornikoel J, Carrión A, Fan Q, Flores E, Forchhammer K, Mariscal V, Mullineaux CW, Perez R, Silber N, Peter WC, Maldener I. 2017. Role of two cell wall amidases in septal junction and nanopore formation in the multicellular cyanobacterium *Anabaena* sp. PCC 7120. Front Cell Infect Microbiol 7:386. https://doi.org/10.3389/fcimb.2017.00386.
15. Berendt S, Lehner J, Zhang YV, Rasse TM, Forchhammer K, Maldener I. 2012. Cell wall amidase amic1 is required for cellular communication and heterocyst development in the cyanobacterium *Anabaena* PCC 7120 but not for filament integrity. J Bacteriol 194:5218–5227. https://doi.org/10.1128/JB.00912-12.
16. Camargo S, Picossi S, Corrales-Guerrero L, Valladares A, Arévalo S, Herrero A. 2019. ZipN is an essential FtsZ membrane tether and contributes to the septal localization of SepJ in the filamentous cyanobacterium *Anabaena*. Sci Rep 9:2744. https://doi.org/10.1038/s41598-019-39336-6.
17. Ramos-León F, Mariscal V, Frías JE, Flores E, Herrero A. 2015. Divisome-dependent subcellular localization of cell-cell joining protein SepJ in the filamentous cyanobacterium *Anabaena*. Mol Microbiol 96:566–580. https://doi.org/10.1111/mmi.12956.
18. Springstein BL, Nürnberg DJ, Woehle C, Weissenbach J, Theune ML, Helbig AO, Maldener I, Dagan T, Stucken K. 2020. Two novel heteropolymer-forming proteins maintain the multicellular shape of the cyanobacterium *Anabaena* sp. PCC 7120. FEBS J https://doi.org/10.1111/febs.15630.
19. Zhang CC, Huguenin S, Friry A. 1995. Analysis of genes encoding the cell division protein FtsZ and a glutathione synthetase homologue in the cyanobacterium *Anabaena* sp. PCC 7120. Res Microbiol 146:445–455. https://doi.org/10.1016/0923-2508(96)80290-7.
20. Hu B, Yang G, Zhao W, Zhang Y, Zhao J. 2007. MreB is important for cell shape but not for chromosome segregation of the filamentous cyanobacterium *Anabaena* sp. PCC 7120. Mol Microbiol 63:1640–1652. https://doi.org/10.1111/j.1365-2958.2007.05618.x.
21. Egan AJF, Cleverley RM, Peters K, Lewis RJ, Vollmer W. 2017. Regulation of bacterial cell wall growth. FEBS J 284:851–867. https://doi.org/10.1111/febs.13959.
22. Mahone CR, Goley ED. 2020. Bacterial cell division at a glance. J Cell Sci 133:jcs237057. https://doi.org/10.1242/jcs.237057.
23. Velázquez-Suárez C, Luque I, Herrero A. 2020. The inorganic nutrient regime and the *mre* genes regulate cell and filament size and morphology in the phototrophic multicellular bacterium *Anabaena*. mSphere 5:e00747-20. https://doi.org/10.1128/mSphere.00747-20.
24. Neugebauer H, Herrmann C, Kammer W, Schwarz G, Nordheim A, Braun V. 2005. ExbBD-dependent transport of maltodextrins through the novel MalA protein across the outer membrane of *Caulobacter crescentus*. J Bacteriol 187:8300–8311. https://doi.org/10.1128/JB.187.24.8300-8311.2005.
25. Blanvillain S, Meyer D, Boulanger A, Lautier M, Guynet C, Denancé N, Vasse J, Lauber E, Arlat M. 2007. Plant carbohydrate scavenging through TonB-dependent receptors: a feature shared by phytopathogenic and aquatic bacteria. PLoS One 2:e224. https://doi.org/10.1371/journal.pone.0000224.
26. Schauer K, Gouget B, Carrière M, Labigne A, De Reuse H. 2007. Novel nickel transport mechanism across the bacterial outer membrane energized by the TonB/ExbB/ExbD machinery. Mol Microbiol 63:1054–1068. https://doi.org/10.1111/j.1365-2958.2006.05578.x.
27. Bassford PJ, Bradbeer C, Kadner RJ, Schnaitman CA. 1976. Transport of vitamin B_{12} in *tonB* mutants of *Escherichia coli*. J Bacteriol 128:242–247. https://doi.org/10.1128/JB.128.1.242-247.1976.
28. Chu BCH, Peacock RS, Vogel HJ. 2007. Bioinformatic analysis of the TonB protein family. Biometals 20:467–483. https://doi.org/10.1007/s10534-006-9049-4.
29. Ferguson AD, Hofmann E, Coulton JW, Diederichs K, Welte W. 1998. Siderophore-mediated iron transport: crystal structure of FhuA with bound lipopolysaccharide. Science 282:2215–2220. https://doi.org/10.1126/science.282.5397.2215.
30. Josts I, Veith K, Tidow H. 2019. Ternary structure of the outer membrane transporter FoxA with resolved signaling domain provides insights into TonB-mediated siderophore uptake. Elife 8:e48528. https://doi.org/10.7554/eLife.48528.
31. Shultis DD, Purdy MD, Banchs CN, Wiener MC. 2006. Outer membrane active transport: structure of the BtuB:TonB complex. Science 312:1396–1399. https://doi.org/10.1126/science.1127694.
32. Ogierman M, Braun V. 2003. Interactions between the outer membrane ferric citrate transporter FecA and TonB: studies of the FecA TonB box. J Bacteriol 185:1870–1885. https://doi.org/10.1128/jb.185.6.1870-1885.2003.
33. Pawelek PD, Croteau N, Ng-Thow-Hing C, Khursigara CM, Moiseeva N, Allaire M, Coulton JW. 2006. Structure of TonB in complex with FhuA, *E. coli* outer membrane receptor. Science 312:1399–1402. https://doi.org/10.1126/science.1128057.
34. Skare JT, Ahmer BMM, Seachord CL, Darveau RP, Postle K. 1993. Energy transduction between membranes. TonB, a cytoplasmic membrane protein, can be chemically cross-linked *in vivo* to the outer membrane receptor FepA. J Biol Chem 268:16302–16308. https://doi.org/10.1016/S0021-9258(19)85421-2.
35. Jiang HB, Lou WJ, Ke WT, Song WY, Price NM, Qiu BS. 2015. New insights into iron acquisition by cyanobacteria: an essential role for ExbB-ExbD complex in inorganic iron uptake. ISME J 9:297–309. https://doi.org/10.1038/ismej.2014.123.
36. Lis H, Kranzler C, Keren N, Shaked Y. 2015. A comparative study of iron uptake rates and mechanisms amongst marine and fresh water cyanobacteria: prevalence of reductive iron uptake. Life (Basel) 5:841–860. https://doi.org/10.3390/0life510841.
37. Qiu G-W, Lou W-J, Sun C-Y, Yang N, Li Z-K, Li D-L, Zang S-S, Fu F-X, Hutchins DA, Jiang H-B, Qiu B-S. 2018. Outer membrane iron uptake pathways in the model cyanobacterium *Synechocystis* sp. strain PCC 6803. Appl Environ Microbiol 84:e01512-18. https://doi.org/10.1128/AEM.01512-18.
38. Obando TAS, Babykin MM, Zinchenko VV. 2018. A cluster of five genes essential for the utilization of dihydroxamate xenosiderophores in *Synechocystis* sp. PCC 6803. Curr Microbiol 75:1165–1173. https://doi.org/10.1007/s00284-018-1505-1.
39. Babykin MM, Obando TSA, Zinchenko VV. 2018. TonB-dependent utilization of dihydroxamate xenosiderophores in *Synechocystis* sp. PCC 6803. Curr Microbiol 75:117–123. https://doi.org/10.1007/s00284-017-1355-2.
40. Nicolaisen K, Moslavac S, Samborski A, Valdebenito M, Hantke K, Maldener I, Muro-Pastor AM, Flores E, Schleiff E. 2008. Alr0397 is an outer membrane transporter for the siderophore schizokinen in *Anabaena* sp. strain PCC 7120. J Bacteriol 190:7500–7507. https://doi.org/10.1128/JB.01062-08.
41. Nicolaisen K, Hahn A, Valdebenito M, Moslavac S, Samborski A, Maldener I, Wilken C, Valladares A, Flores E, Hantke K, Schleiff E. 2010. The interplay between siderophore secretion and coupled iron and copper transport in the heterocyst-forming cyanobacterium *Anabaena* sp. PCC 7120. Biochim Biophys Acta 1798:2131–2140. https://doi.org/10.1016/j.bbamem.2010.07.008.
42. Kranzler C, Rudolf M, Keren N, Schleiff E. 2013. Iron in cyanobacteria. Adv Bot Res 65:57–105. https://doi.org/10.1016/B978-0-12-394313-2.00003-2.
43. Rudolf M, Kranzler C, Lis H, Margulis K, Stevanovic M, Keren N, Schleiff E. 2015. Multiple modes of iron uptake by the filamentous, siderophore-producing cyanobacterium, *Anabaena* sp. PCC 7120. Mol Microbiol 97:577–588. https://doi.org/10.1111/mmi.13049.
44. Stevanovic M, Hahn A, Nicolaisen K, Mirus O, Schleiff E. 2012. The components of the putative iron transport system in the cyanobacterium *Anabaena* sp. PCC 7120. Environ Microbiol 14:1655–1670. https://doi.org/10.1111/j.1462-2920.2011.02619.x.
45. Hale CA, De Boer PAJ. 1997. Direct binding of FtsZ to ZipA, an essential component of the septal ring structure that mediates cell division in *E. coli*. Cell 88:175–185. https://doi.org/10.1016/S0092-8674(00)81838-3.

46. Hodgkin J, Kaiser D. 1979. Genetics of gliding motility in *Myxococcus xanthus* (Myxobacterales): two gene systems control movement. Mol Gen Genet 171:177–191. https://doi.org/10.1007/BF00270004.
47. Islam ST, Mignot T. 2015. The mysterious nature of bacterial surface (gliding) motility: a focal adhesion-based mechanism in *Myxococcus xanthus*. Semin Cell Dev Biol 46:143–154. https://doi.org/10.1016/j.semcdb.2015.10.033.
48. Mitschke J, Vioque A, Haas F, Hess WR, Muro-Pastor AM. 2011. Dynamics of transcriptional start site selection during nitrogen stress-induced cell differentiation in *Anabaena* sp. PCC7120. Proc Natl Acad Sci U S A 108:20130–20135. https://doi.org/10.1073/pnas.1112724108.
49. Flaherty BL, Van Nieuwerburgh F, Head SR, Golden JW. 2011. Directional RNA deep sequencing sheds new light on the transcriptional response of *Anabaena* sp. strain PCC 7120 to combined-nitrogen deprivation. BMC Genomics 12:332. https://doi.org/10.1186/1471-2164-12-332.
50. Golden JW, Whorff LL, Wiest DR. 1991. Independent regulation of *nifHDK* operon transcription and DNA rearrangement during heterocyst differentiation in the cyanobacterium *Anabaena* sp. strain PCC 7120. J Bacteriol 173:7098–7105. https://doi.org/10.1128/jb.173.22.7098-7105.1991.
51. Ernst A, Black T, Cai Y, Panoff J-MM, Tiwari DN, Wolk CP. 1992. Synthesis of nitrogenase in mutants of the cyanobacterium *Anabaena* sp. strain PCC 7120 affected in heterocyst development or metabolism. J Bacteriol 174:6025–6032. https://doi.org/10.1128/jb.174.19.6025-6032.1992.
52. Lechno-Yossef S, Fan Q, Wojciuch E, Wolk CP. 2011. Identification of ten *Anabaena* sp. genes that under aerobic conditions are required for growth on dinitrogen but not for growth on fixed nitrogen. J Bacteriol 193:3482–3489. https://doi.org/10.1128/JB.05010-11.
53. Ehira S, Ohmori M, Sato N. 2003. Genome-wide expression analysis of the responses to nitrogen deprivation in the heterocyst-forming cyanobacterium *Anabaena* sp. strain PCC 7120. DNA Res 10:97–113. https://doi.org/10.1093/dnares/10.3.97.
54. Pernil R, Schleiff E. 2019. Metalloproteins in the biology of heterocysts. Life 9:32. https://doi.org/10.3390/life9020032.
55. Schätzle H, Brouwer E-M, Liebhart E, Stevanovic M, Schleiff E. 2021. Comparative phenotypic analysis of *Anabaena* sp. PCC 7120 mutants of porin-like genes. J Microbiol Biotechnol https://doi.org/10.4014/jmb.2103.03009.
56. Zhao Y, Shi Y, Zhao W, Huang X, Wang D, Brown N, Brand J, Zhao J. 2005. CcbP, a calcium-binding protein from *Anabaena* sp. PCC 7120, provides evidence that calcium ions regulate heterocyst differentiation. Proc Natl Acad Sci U S A 102:5744–5748. https://doi.org/10.1073/pnas.0501782102.
57. Shi Y, Zhao W, Zhang W, Ye Z, Zhao J. 2006. Regulation of intracellular free calcium concentration during heterocyst differentiation by HetR and NtcA in *Anabaena* sp. PCC 7120. Proc Natl Acad Sci U S A 103:11334–11339. https://doi.org/10.1073/pnas.0602839103.
58. Walter J, Lynch F, Battchikova N, Aro EM, Gollan PJ. 2016. Calcium impacts carbon and nitrogen balance in the filamentous cyanobacterium *Anabaena* sp. PCC 7120. J Exp Bot 67:3997–4008. https://doi.org/10.1093/jxb/erw112.
59. Torrecilla I, Leganés F, Bonilla I, Fernández-Piñas F. 2001. Calcium transients in response to salinity and osmotic stress in the nitrogen-fixing cyanobacterium *Anabaena* sp. PCC7120, expressing cytosolic apoaequorin. Plant Cell Environ 24:641–648. https://doi.org/10.1046/j.0016-8025.2001.00708.x.
60. Smith RJ, Wilkins A. 1988. A correlation between intracellular calcium and incident irradiance in *Nostoc* 6720. New Phytol 109:157–161. https://doi.org/10.1111/j.1469-8137.1988.tb03703.x.
61. Torrecilla I, Leganés F, Bonilla I, Fernández-Piñas F. 2004. A calcium signal is involved in heterocyst differentiation in the cyanobacterium *Anabaena* sp. PCC7120. Microbiology (Reading) 150:3731–3739. https://doi.org/10.1099/mic.0.27403-0.
62. Typas A, Banzhaf M, Gross CA, Vollmer W. 2011. From the regulation of peptidoglycan synthesis to bacterial growth and morphology. Nat Rev Microbiol 10:123–136. https://doi.org/10.1038/nrmicro2677.
63. Lehner J, Berendt S, Dörsam B, Pérez R, Forchhammer K, Maldener I. 2013. Prokaryotic multicellularity: a nanopore array for bacterial cell communication. FASEB J 27:2293–2300. https://doi.org/10.1096/fj.12-225854.
64. Mullineaux CW, Mariscal V, Nenninger A, Khanum H, Herrero A, Flores E, Adams DG. 2008. Mechanism of intercellular molecular exchange in heterocyst-forming cyanobacteria. EMBO J 27:1299–1308. https://doi.org/10.1038/emboj.2008.66.
65. Mariscal V, Nürnberg DJ, Herrero A, Mullineaux CW, Flores E. 2016. Overexpression of SepJ alters septal morphology and heterocyst pattern regulated by diffusible signals in *Anabaena*. Mol Microbiol 101:968–981. https://doi.org/10.1111/mmi.13436.
66. Arévalo S, Nenninger A, Nieves-Morión M, Herrero A, Mullineaux CW, Flores E. 2021. Coexistence of communicating and noncommunicating cells in the filamentous cyanobacterium *Anabaena*. mSphere 6:e01091-20. https://doi.org/10.1128/mSphere.01091-20.
67. Black K, Buikema WJ, Haselkorn R. 1995. The *hglK* gene is required for localization of heterocyst-specific glycolipids in the cyanobacterium *Anabaena* sp. strain PCC 7120. J Bacteriol 177:6440–6448. https://doi.org/10.1128/jb.177.22.6440-6448.1995.
68. Rippka R, Deruelles J, Waterbury JB, Herdman M, Stanier RY. 1979. Generic assignments, strain histories and properties of pure cultures of cyanobacteria. J Gen Microbiol 111:1–61. https://doi.org/10.1099/00221287-111-1-1.
69. Fan Q, Lechno-Yossef S, Ehira S, Kaneko T, Ohmori M, Sato N, Tabata S, Wolk CP. 2006. Signal transduction genes required for heterocyst maturation in *Anabaena* sp. strain PCC 7120. J Bacteriol 188:6688–6693. https://doi.org/10.1128/JB.01669-05.
70. Mella-Herrera RA, Neunuebel MR, Golden JW. 2011. *Anabaena* sp. strain PCC 7120 conR contains a LytR-CpsA-Psr domain, is developmentally regulated, and is essential for diazotrophic growth and heterocyst morphogenesis. Microbiology (Reading) 157:617–626. https://doi.org/10.1099/mic.0.046128-0.
71. Arévalo S, Flores E. 2020. Pentapeptide-repeat, cytoplasmic-membrane protein HglK influences the septal junctions in the heterocystous cyanobacterium *Anabaena*. Mol Microbiol 113:794–806. https://doi.org/10.1111/mmi.14444.
72. Nieves-Morión M, Lechno-Yossef S, López-Igual R, Frías JE, Mariscal V, Nürnberg DJ, Mullineaux CW, Wolk CP, Flores E. 2017. Specific glucoside transporters influence septal structure and function in the filamentous, heterocyst-forming cyanobacterium *Anabaena* sp. strain PCC 7120. J Bacteriol 199:e00876-16. https://doi.org/10.1128/JB.00876-16.
73. Weiss GL, Kieninger A-K, Maldener I, Forchhammer K, Pilhofer M. 2019. Structure and function of a bacterial gap junction analog. Cell 178:374–384.e15. https://doi.org/10.1016/j.cell.2019.05.055.
74. Walsby AE. 2007. Cyanobacterial heterocysts: terminal pores proposed as sites of gas exchange. Trends Microbiol 15:340–349. https://doi.org/10.1016/j.tim.2007.06.007.
75. Zhang JY, Lin GM, Xing WY, Zhang CC. 2018. Diversity of growth patterns probed in live cyanobacterial cells using a fluorescent analog of a peptidoglycan precursor. Front Microbiol 9:791. https://doi.org/10.3389/fmicb.2018.00791.
76. Lázaro S, Fernández-Piñas F, Fernández-Valiente E, Blanco-Rivero A, Leganés F. 2001. *pbpB*, a gene coding for a putative penicillin-binding protein, is required for aerobic nitrogen fixation in the cyanobacterium *Anabaena* sp. strain PCC7120. J Bacteriol 183:628–636. https://doi.org/10.1128/JB.183.2.628-636.2001.
77. Sakr S, Jeanjean R, Zhang C-C, Arcondeguy T. 2006. Inhibition of cell division suppresses heterocyst development in *Anabaena* sp. strain PCC 7120. J Bacteriol 188:1396–1404. https://doi.org/10.1128/JB.188.4.1396-1404.2006.
78. Zhu J, Jäger K, Black T, Zarka K, Koksharova O, Wolk CP. 2001. HcwA, an autolysin, is required for heterocyst maturation in *Anabaena* sp. strain PCC 7120. J Bacteriol 183:6841–6851. https://doi.org/10.1128/JB.183.23.6841-6851.2001.
79. Thomas KJ, Rice CV. 2014. Revised model of calcium and magnesium binding to the bacterial cell wall. Biometals 27:1361–1370. https://doi.org/10.1007/s10534-014-9797-5.
80. Szatmári D, Sárkány P, Kocsis B, Nagy T, Miseta A, Barkó S, Longauer B, Robinson RC, Nyitrai M. 2020. Intracellular ion concentrations and cation-dependent remodelling of bacterial MreB assemblies. Sci Rep 10:12002. https://doi.org/10.1038/s41598-020-68960-w.
81. Singh S, Mishra AK. 2014. Regulation of calcium ion and its effect on growth and developmental behavior in wild type and *ntcA* mutant of *Anabaena* sp. PCC 7120 under varied levels of $CaCl_2$. Microbiology 83:235–246. https://doi.org/10.1134/S002626171403014X.
82. Giraldez-Ruiz N, Mateo P, Bonilla I, Fernandez-Piñas F. 1997. The relationship between intracellular pH, growth characteristics and calcium in the cyanobacterium *Anabaena* sp. strain PCC7120 exposed to low pH. New Phytol 137:599–605. https://doi.org/10.1046/j.1469-8137.1997.00864.x.

83. Springstein BL, Nürnberg DJ, Weiss GL, Pilhofer M, Stucken K. 2020. Structural determinants and their role in cyanobacterial morphogenesis. Life 10:355. https://doi.org/10.3390/life10120355.
84. Springstein BL, Weissenbach J, Koch R, Stücker F, Stucken K. 2020. The role of the cytoskeletal proteins MreB and FtsZ in multicellular cyanobacteria. FEBS Open Bio 10:2510–2531. https://doi.org/10.1002/2211-5463.13016.
85. NCBI Resource Coordinators. 2014. Database resources of the National Center for Biotechnology Information. Nucleic Acids Res 42:D7–D17. https://doi.org/10.1093/nar/gkt1146.
86. Johnson M, Zaretskaya I, Raytselis Y, Merezhuk Y, McGinnis S, Madden TL. 2008. NCBI BLAST: a better web interface. Nucleic Acids Res 36:W5–W9. https://doi.org/10.1093/nar/gkn201.
87. Huang Y, Niu B, Gao Y, Fu L, Li W. 2010. CD-HIT Suite: a web server for clustering and comparing biological sequences. Bioinformatics 26:680–682. https://doi.org/10.1093/bioinformatics/btq003.
88. Schoch CL, Ciufo S, Domrachev M, Hotton CL, Kannan S, Khovanskaya R, Leipe D, Mcveigh R, O'Neill K, Robbertse B, Sharma S, Soussov V, Sullivan JP, Sun L, Turner S, Karsch-Mizrachi I. 2020. NCBI Taxonomy: a comprehensive update on curation, resources and tools. Database (Oxford) 2020:baaa062. https://doi.org/10.1093/database/baaa062.
89. Yang M, Derbyshire MK, Yamashita RA, Marchler-Bauer A. 2020. NCBI's Conserved Domain Database and tools for protein domain analysis. Curr Protoc Bioinformatics 69:e90. https://doi.org/10.1002/cpbi.90.
90. Krogh A, Larsson B, Von Heijne G, Sonnhammer ELL. 2001. Predicting transmembrane protein topology with a hidden Markov model: application to complete genomes. J Mol Biol 305:567–580. https://doi.org/10.1006/jmbi.2000.4315.
91. Shcolnick S, Shaked Y, Keren N. 2007. A role for mrgA, a DPS family protein, in the internal transport of Fe in the cyanobacterium *Synechocystis* sp. PCC6803. Biochim Biophys Acta 1767:814–819. https://doi.org/10.1016/j.bbabio.2006.11.015.
92. Cai Y, Wolk CP. 1990. Use of a conditionally lethal gene in *Anabaena* sp. strain PCC 7120 to select for double recombinants and to entrap insertion sequences. J Bacteriol 172:3138–3145. https://doi.org/10.1128/jb.172.6.3138-3145.1990.
93. Wolk CP, Vonshak A, Kehoe P, Elhai J. 1984. Construction of shuttle vectors capable of conjugative transfer from *Escherichia coli* to nitrogen-fixing filamentous cyanobacteria. Proc Natl Acad Sci U S A 81:1561–1565. https://doi.org/10.1073/pnas.81.5.1561.
94. Elhai J, Wolk CP. 1988. Conjugal transfer of DNA to cyanobacteria. Methods Enzymol 167:747–754. https://doi.org/10.1016/0076-6879(88)67086-8.
95. Olmedo-Verd E, Muro-Pastor AM, Flores E, Herrero A. 2006. Localized induction of the *ntcA* regulatory gene in developing heterocysts of *Anabaena* sp. strain PCC 7120. J Bacteriol 188:6694–6699. https://doi.org/10.1128/JB.00509-06.
96. Moslavac S, Reisinger V, Berg M, Mirus O, Vosyka O, Plöscher M, Flores E, Eichacker LA, Schleiff E. 2007. The proteome of the heterocyst cell wall in *Anabaena* sp. PCC 7120. Biol Chem 388:823–829. https://doi.org/10.1515/BC.2007.079.
97. Elhai J, Wolk PC. 1988. A versatile class of positive-selection vectors based on the nonviability of palindrome-containing plasmids that allows cloning into long polylinkers. Gene 68:119–138. https://doi.org/10.1016/0378-1119(88)90605-1.
98. Valladares A, Rodríguez V, Camargo S, Martínez-Noël GMA, Herrero A, Luque I. 2011. Specific role of the cyanobacterial pipX factor in the heterocysts of *Anabaena* sp. strain PCC 7120. J Bacteriol 193:1172–1182. https://doi.org/10.1128/JB.01202-10.
99. Kranzler C, Lis H, Shaked Y, Keren N. 2011. The role of reduction in iron uptake processes in a unicellular, planktonic cyanobacterium. Environ Microbiol 13:2990–2999. https://doi.org/10.1111/j.1462-2920.2011.02572.x.
100. Rudolf M, Stevanovic M, Kranzler C, Pernil R, Keren N, Schleiff E. 2016. Multiplicity and specificity of siderophore uptake in the cyanobacterium *Anabaena* sp. PCC 7120. Plant Mol Biol 92:57–69. https://doi.org/10.1007/s11103-016-0495-2.
101. Salomon E, Bar-Eyal L, Sharon S, Keren N. 2013. Balancing photosynthetic electron flow is critical for cyanobacterial acclimation to nitrogen limitation. Biochim Biophys Acta 1827:340–347. https://doi.org/10.1016/j.bbabio.2012.11.010.
102. Stevanovic M, Lehmann C, Schleiff E. 2013. The response of the TonB-dependent transport network in *Anabaena* sp. PCC 7120 to cell density and metal availability. Biometals 26:549–560. https://doi.org/10.1007/s10534-013-9644-0.
103. Stewart WD, Fitzgerald GP, Burris RH. 1967. *In situ* studies on N_2 fixation using the acetylene reduction technique. Proc Natl Acad Sci U S A 58:2071–2078. https://doi.org/10.1073/pnas.58.5.2071.
104. Sharon S, Salomon E, Kranzler C, Lis H, Lehmann R, Georg J, Zer H, Hess WR, Keren N. 2014. The hierarchy of transition metal homeostasis: iron controls manganese accumulation in a unicellular cyanobacterium. Biochim Biophys Acta 1837:1990–1997. https://doi.org/10.1016/j.bbabio.2014.09.007.
105. Lehner J, Zhang Y, Berendt S, Rasse TM, Forchhammer K, Maldener I. 2011. The morphogene AmiC2 is pivotal for multicellular development in the cyanobacterium *Nostoc punctiforme*. Mol Microbiol 79:1655–1669. https://doi.org/10.1111/j.1365-2958.2011.07554.x.

2.2. Manuscript 2

Functional diversity of TonB-like proteins in the heterocyst-forming cyanobacterium *Anabaena* sp. PCC 7120

Status: Accepted for publication in mSphere (2021)

Contributing Authors: Hannah Schätzle, Sergio Arévalo, Enrique Flores, Enrico Schleiff

Contributions:

Concept and Design	Schätzle, Hannah	70%
	Schleiff, Enrico	30%
Conducting tests and experiments	Schätzle, Hannah (Mutant screening, growth experiments, siderophore transport experiments, expression analysis, ICP-MS, microscopy, LPS analysis, pigment analysis)	95%
	Arévalo, Sergio (Nitrogenase activity measurement)	5%
Compilation of data sets and figures	Schätzle, Hannah (Compilation of figures and data of mutant genotyping, growth analysis, LPS and expression analysis, ICP-MS measurements, nitrogenase activities, fluorescence microscopy, iron uptake and pigmentation)	80%
	Arévalo, Sergio (Compilation of figure for nitrogenase activity)	5%
	Flores, Enrique (Compilation of figure for nitrogenase activity)	5%
	Schleiff, Enrico (Compilation of figures and data of bioinformatic analyses, mutant genotyping, growth analysis, LPS and expression analysis, ICP-MS measurements, nitrogenase activities, fluorescence microscopy, iron uptake and pigmentation)	10%
Analysis and interpretation of data	Schätzle, Hannah (Analysis and interpretation of all data generated during the study)	70%
	Schleiff, Enrico (Analysis and interpretation of all data generated during the study)	30%
Drafting of manuscript	Schätzle, Hannah	70%
	Schleiff, Enrico	30%

Functional diversity of TonB-like proteins in the heterocyst-forming cyanobacterium *Anabaena* sp. PCC 7120

Hannah Schätzle[a,b,c], Sergio Arévalo[d], Enrique Flores[d] and Enrico Schleiff[a,b,c,e,#]

[a]Institute for Molecular Biosciences, Goethe University Frankfurt, Max von Laue Str. 9, 60438 Frankfurt, Germany;

[b]FIERCE, Goethe University Frankfurt, Altenhöferallee 1, 60438 Frankfurt am Main, Germany

[c]Buchmann Institute for Molecular Life Sciences; Max von Laue Str. 11, 60438 Frankfurt, Germany.

[d]Instituto de Bioquímica Vegetal y Fotosíntesis, CSIC and Universidad de Sevilla, Américo Vespucio 49, Seville, E-41092, Spain

[e]Frankfurt Institute for Advanced Studies, Ruth-Moufang-Straße 1, 60438 Frankfurt, Germany.

[#]Correspondence to: schleiff@bio.uni-frankfurt.de

Running title: *Characterization of Anabaena TonB-like proteins*

Abstract word count: 234

Text word count: 4570

Abstract

The TonB-dependent transport of scarcely available substrates across the outer membrane is a conserved feature in Gram-negative bacteria, in which energy from the plasma membrane proton gradient is utilized to facilitate the substrate transport in the outer membrane. The plasma membrane embedded TonB-ExbB-ExbD complex functions as energy transducer by physically interacting with TonB-dependent outer membrane transporters (TBDT). TonB mediates structural rearrangements in the substrate-loaded TBDT that are required for substrate translocation into the periplasm. In the model heterocyst-forming cyanobacterium *Anabaena* sp. strain PCC 7120, four TonB-like proteins have been identified. Out of these TonB3 accomplishes the transport of ferric schizokinen, the siderophore secreted by *Anabaena* to scavenge iron. TonB1 presumably does not act as canonical TonB protein because it is exceptionally short and the TBDT-interaction motif is missing, and the function of TonB2 and TonB4 is yet unknown. Here we examined *tonB2* and *tonB4* mutants for siderophore transport capacities and other specific phenotypic features. Both mutants were not or only slightly affected in schizokinen transport, whereas they showed decreased nitrogenase activity in apparently normal heterocysts. Moreover, the cellular metal concentrations and pigment contents were altered in the mutants, most pronouncedly in the *tonB2* mutant. This strain showed an altered susceptibility towards antibiotics and SDS and formed cell aggregates when grown in liquid culture, a phenotype associated with an elevated LPS production. Thus, the TonB-like proteins in *Anabaena* appear to take over distinct functions, and the mutation of TonB2 strongly influences outer membrane integrity.

Importance

The genomes of many organisms encode more than one TonB protein, and their number does not necessarily correlate with that of TonB-dependent outer membrane transporters. Consequently, specific as well as redundant functions of the different TonB proteins have been identified. In addition to a role in uptake of scarcely available nutrients, including iron complexes, TonB proteins are related to virulence, flagella assembly, pili localization or envelope integrity including antibiotic resistance. The knowledge about the function of TonB proteins in cyanobacteria is limited. Here we compare the four TonB proteins of *Anabaena* sp. strain PCC 7120 providing evidence that their functions are in part distinct, since mutants of these proteins exhibit specific features but also show some common impairments.

Introduction

Cyanobacteria possess a Gram-negative type of cell envelope containing an outer membrane (OM), a peptidoglycan layer (PG) and a plasma (cytoplasmic or inner) membrane (PM) (1). Macromolecular complexes that reside in the two membranes facilitate the assembly of the cell wall components as well solute exchange and signalling (2). Among them, the OM-embedded TonB-dependent transport machinery is widely distributed in Gram-negative bacteria (3). The TonB-dependent transport system is important for growth under iron starvation conditions, since iron is an essential but lowly bioavailable nutrient (3–7). Iron-loaded proteins carry out functions in important cellular activities such as electron transport and DNA synthesis (8). This holds particularly true for cyanobacteria, in which iron is required for the synthesis of phycobiliproteins (9) and chlorophyll *a* (10), as well as for photosynthetic complexes that in total require approximately 22-23 iron atoms (11). Moreover in certain cyanobacterial species that are capable of nitrogen fixation, the nitrogenase enzyme is also dependent on iron (12).

Due to its low solubility under oxic conditions at neutral pH, iron rapidly forms insoluble aggregates that are inaccessible to many microorganisms (6, 13). Only a very small amount of dissolved iron exists as inorganic iron, whereas the largest proportion is bound to organic ligands such as siderophores (6). Siderophores are low molecular weight compounds that chelate ferric iron with high affinities. The production and secretion of sidereophores is a widespread strategy of bacteria, fungi and plants to cope with iron-limiting conditions (14). Siderophores are divided into three classes depending on the chemical nature of iron coordination, namely catecholates, hydroxamates or mixed-types that contain another iron complexing group such as hydroxy-carboxylate (15).

The TonB-dependent transport system involves a PM-localized energising TonB-ExbB-ExbD complex and OM-localized TonB-dependent transporters (TBDT). TBDTs constitute gated channels that facilitate the transport of substrates into the periplasm (16). The translocation process is energy-dependent, as the substrates are typically large and rarely abundant (17, 18). Examples besides siderophores are carbohydrates, vitamin B_{12} (cobalamin) and heme (16, 19). The energy for transport is derived from the proton motive force (pmf) across the PM (20, 21). ExbB and ExbD build up a proton channel that converts the pmf into energy for the translocation process (22). The TonB protein transfers the energy to the TBDT through direct interaction with both, ExbB/ExbD and the TBDT (23–26).

TonB proteins contain a transmembrane α-helix and a conserved C-terminal motif that interacts with the so-called TonB-box of the TBDTs (16, 27). Remarkably, more than 40% of the organisms that possess a TonB-dependent system have more than one *tonB* gene copy (3). For instance, *Pseudomonas aeruginosa* possesses three TonB proteins (28–30). Here, TonB1 and likely TonB2 facilitate the transport of iron-containing compounds and are required for growth under iron-limiting conditions, while TonB3 is crucial for motility and pili assembly (28–32). In *Pseudomonas putida,* one of the two TonB proteins energizes the transport of siderophores, whereas the other TonB protein is important for maintaining the integrity of the cell envelope and flagella localization (33–35). Also, *Vibrio* species typically contain multiple *tonB* copies in the genome. Here, distinct TonB proteins facilitate the transport of both common and individual substrates (36). Thus, multiple TonB proteins in one organism can take over redundant as well as unique functions. They can function in protein complex assembly, cell wall integrity regulation or in global or substrate-specific transport processes.

Little is known about the functionality of TonB proteins in cyanobacteria, which are photoautotrophic organisms that can be found in terrestrial, marine or freshwater habitats. The number of putative TBDT, TonB or ExbB/D proteins in the genomes of analysed cyanobacteria is highly variable (37, 38). For example, in the genome of the filamentous cyanobacterium *Anabaena* sp. strain PCC 7120 (*Anabaena* hereafter) 22 different TBDTs were predicted (37). In contrast, only four genes with *tonB*-signature were assigned by bioinformatics methods (38). TonB1 contains an exceptionally short periplasmic domain that is likely not sufficient in size to reach OM-embedded factors. In contrast, TonB3 is supposed to be a central component of the ferric siderophore transport system (38). The *tonB3* mRNA abundance increases in iron limited conditions, and a single recombinant mutant can be generated only in the presence of enhanced iron concentrations (38). The growth of this mutant in the absence of iron is reduced, and siderophore synthesis genes are upregulated in this genetic background (38).

TonB2 encoded by *all3585* or TonB4 encoded by *alr5329* have a domain structure comparable to the TonB proteins from *E.coli* or TonB3 from *Anabaena* (38). However, the distance between the transmembrane domain and the TonB-box binding domain is smaller than in TonB3 (Figure 1). Estimation of the size assuming an extended helix suggests a dimension of 12 nm for TonB4 and 22 nm for TonB2, while for TonB3 32 nm are estimated. The latter fits to the determined distance between OM and PM in *Anabaena*, as well as to the estimated size of the TolC system (39, 40). Both, *tonB2* and *tonB4* are expressed at highest levels in low-density cultures and lowest in the stationary phase (41). Their expression is enhanced at all growth stages in the presence of elevated iron (38, 41), while the expression of *tonB4* is also enhanced in the presence of elevated copper concentrations (38, 41).

We aimed to functionally characterize the TonB-like proteins focussing on TonB2 and TonB4, since the role of those proteins in *Anabaena* is unclear (38). Insertion mutants of *tonB2*, *tonB3* and *tonB4* demonstrated alterations in cellular metal levels as well as in carotenoid or chlorophyll *a* concentrations compared to the wild type, although to different extents. Moreover the *tonB2* mutant filaments aggregated in liquid cultures, which might be related to an enhanced production of lipopolysaccharide in this strain. Also, the outer membrane integrity as well as the expression of porins was affected in the *tonB2* mutant. On the other hand, the *tonB2* mutant as well as the *tonB4* mutant retains the siderophore transport capacity, which suggests a functional diversity of *Anabaena* TonB proteins.

Results

The *Anabaena tonB*-mutants bear pigment alterations

To analyse putative functions of the individual TonB proteins, the growth behaviour of mutants of the corresponding genes was examined. The mutant strains, I-*tonb1*, I-*tonB2*, I-*tonB3* and I-*tonB4*, were generated through single recombinant insertion of a plasmid in the gene of interest (Figure 2A), as described before (38). I-*tonb1* and I-*tonB2* are segregated mutants, as no wild-type copy of the respective genes was detectable in the mutants (Figure 2B). In contrast, I-*tonB3* and I-*tonB4* could not be segregated, as even after repeated dilution on plates with antibiotics, the wild-type genes were detectable in the corresponding gDNA by PCR (Figure 2A (38)). For I-*tonB3* this is agreement with the previous report, where full segregation was only obtained in the presence of enhanced iron (38). This suggests that TonB3 and TonB4 are important for viability under the conditions used in this study.

None of the *tonB* mutants exhibited an altered growth behaviour when compared to wild type under standard conditions (YBG11 medium, Figure 2C). However, I-*tonB2* cells

frequently formed aggregates in liquid medium (Figure 2D). The enhanced tendency of I-*tonB2* to aggregate was also verified by sedimentation analysis (Figure S1). In addition, the colour of I-*tonB2* was considerably different from that of the wild type (Figure 2E), suggesting a modification in the cellular pigment content.

The synthesis of carotenoids and Chl in *Anabaena* is differentially regulated in response to growth temperature and light intensity (42–45). Therefore, the concentrations of these pigments in the mutants and the wild type were determined after growth of the cultures for seven days under ambient light as well as under high-light or low-light conditions.

In general the pigment concentrations under ambient light and low light were comparable. When grown under ambient or low light conditions, the Chl concentration in the wild type was 10.1±0.5 µg ml^{-1} and 9.7±0.4 µg ml^{-1} at OD_{750}=1, and the carotenoid concentration was 2.7±0.2 µg ml^{-1} or 2.8±0.1 µg ml^{-1} at OD_{750}=1, respectively. Compared to that, the I-*tonB1*, I-*tonB3* and I-*tonB4* strains were diminished in their cellular Chl content under both conditions (Table 1), whereas the Chl concentration in I-*tonB2* was comparable to wild type. TonB3 is presumably involved in siderophore transport (38) and, because a reduction in Chl is an indicator of iron starvation in *Anabaena*, the decrease in Chl likely mirrors a fast iron starvation (46, 47). For TonB1, however, is unlikely that the protein participates in TBDT-mediated transport (38), and therefore the observed reduction of the Chl content should not be related to iron uptake.

Notably, I-*tonB2* and I-*tonB3*, with 3.9±0.6 µg ml^{-1} and 3.3±0.1 µg ml^{-1}, respectively, exhibited an elevated carotenoid concentration under ambient light when compared to wild type. Under low-light, only in I-*tonB2* the carotenoid concentration was significantly enhanced. In contrast to that, I-*tonB4* had a comparatively lower carotenoid level under

both ambient and low light conditions, and I-*tonB1* under low light. These alterations led to a lower Chl:Car ratio under ambient light in I-*tonB1*, I-*tonB2* and I-*tonB3* strains compared to the wild-type strain (Table 1). The decrease was strongest in I-*tonB2*, in which a colour change was already visible by eye (Figure 2). Under low light, a significantly lower Chl:Car ratio was observed in I-*tonB2* and I-*tonB3* when compared to the wild type (Table 1).

The Chl concentration was higher in all strains under normal (ambient) light or low-light conditions when compared to high light (Table 1). For the wild-type strain an average Chl concentration per OD_{750} 4.7±0.8 µg ml^{-1} was determined under high light. The carotenoid level in the wild-type cultures was lower under high light compared to ambient light as well (Table 1), but the difference between these conditions was not as drastic as in case of Chl. This resulted in a compromised ratio of Chl:Car, which in the wild type was 2.0 under high light. These data are consistent with previous observations (48–50). Only in I-*tonB1* the Chl as well as carotenoid content was significantly decreased compared to the wild type, whereas I-*tonB2* exhibited an elevated carotenoid level (Table 1). Notably the reduction in Chl in I-*tonB1* did not result in a compromised growth (Fig.1). Thus, I-*tonB2* is the only *tonB*-mutant that, compared to the wild type, also displays a diminished Chl:Car ratio under high light.

In summary, I-*tonB2* contained an enhanced level of carotenoids irrespective of the light condition leading to a reduced Chl:Car ratio, while under ambient light the strains I-*tonB1* and I-*tonB3* showed a lower Chl:Car ratio as well. Therefore, the colour alterations observed for I-*tonB2* result from the observed alterations in cellular pigmentation.

The cellular metal content is altered in *tonB*-mutants

The carotenoid concentration in cyanobacteria is affected by metal availability. Elevated Cu, Zn or Co concentrations result in an elevation of the carotenoid content in *Anabaena oryzae* (51). Similarly, Ca supplementation enhances the level of pigments in *Anabaena* (52, 53). Thus, the cellular concentrations of metals were determined by ICP-MS analyses in cells of the wild type, I-*tonB2,* I-*tonB3* and I-*tonB4*. The metal concentration of I-*tonB1* will be discussed elsewhere.

Remarkably, alterations in metal concentrations were observed for all *tonB*-mutants when compared to the wild type. (I) I-*tonB3* and I-*tonB4* exhibited a decrease in cellular Mg and Co concentration when compared to the wild type (Table 2). (II) In I-*tonB2* and I-*tonB3* the Mn concentration was decreased. In I-*tonB4* the level of Mn showed a large variation, but was always at a lower level than in the wild type. (III) The Mo concentration was enhanced in I-*tonB2* and (IV) reduced in I-*tonB4*. (V) In I-*tonB2* cells an elevated Cu concentration was observed compared to the wild type. Notably, after seven days of growth in YBG11 medium an alteration in the Fe concentration was not observed, although TonB3 is supposed to be related in ferric siderophore transport.

Ca and Zn levels were not drastically altered in the mutants. In contrast Cu, which influences the carotenoid content in cyanobacteria (51), was enhanced in I-*tonB2*, in which the carotenoid level was found to be enhanced as well (Table 1,2). In turn, in I-*tonB3* and I-*tonB4* the Co levels were reduced, which also could be related to reduced levels of carotenoids in these mutants (Table 1,2). In summary all *tonB*-mutants exhibited alterations in the cellular metal levels compared to wild type to different extents. Whereas I-*tonB3* and I-*tonB4* were reduced in Co, Mn (I-*tonB3*) or Mo (I-*tonB4*), only I-*tonB2* did, besides the observed reduction in Mn, significantly enrich metals, namely Cu and Mo.

Membrane properties and transcriptional alterations in I-*tonB2*

Considering the relative accumulation of Cu and Mo in I-*tonB2* and the tendency of the strain to form aggregates in solution, a modification in the cell surface could cause the mentioned effects. Therefore, lipopolysaccharide (LPS) was extracted from the wild-type and I-*tonB2* strain and separated by SDS-PAGE. Reproducibly enhanced signals for the O-antigen ladder were observed for the *tonB2* mutant compared to wild type, in which the O-chain was barely visible when similar amounts of LPS extracts were loaded (Fig. 3A, Fig. S2). This confirms an increased synthesis of LPS in the mutant strain that could result from an aberrant regulation.

LPS structure as well as carotenoids are known to influence membrane properties (54–58). In cyanobacteria, carotenoids are found in all membranes including the outer membrane (59–61). Therefore, the integrity of the OM in the *tonB*-mutants was tested by spotting suspensions of the strains on plates containing antibiotics or SDS.

Interestingly, I-*tonB2* exhibited an increased resistance towards SDS, erythromycin and neomycin when compared to the wild type (Figure 3A). In addition, I-*tonB3* and I-*tonB4* were more resistant towards the selected antibiotics, but the effect was not as pronounced as for I-*tonB2*. Moreover, I-*tonB1* grew in a similar manner as I-*tonB2* in the presence of SDS, but was as sensitive towards the tested antibiotics as the wild type.

The reduced susceptibility of I-*tonB2* suggests a limited uptake of the selected compounds into the cell and confirms an alteration ot the cell envelope. Typically, porins mediate the transport of certain antibiotics across the OM, and thus porin mutants often display hyper-resistance towards those compounds (62). Although it has been discussed that lipophilic macrolide antibiotics likely enter the cell though diffusion across the membranes and not through porins (17), for *Anabaena* a relation to porin function has

been proposed (63). Thus, the transcript abundance of nine genes coding for porin-like proteins (1, 64) was examined in I-*tonB2*.

Remarkably, the transcript abundance of six genes coding for putative porins was reduced in I-*tonB2* compared to the wild type after 7 days of growth in YBG11 medium (Figure 3B). Among those, the transcript abundance of *all7614, all4499* and *alr4550* was most drastically reduced by 54-, 37- and 36-fold, respectively. The transcript level of the three genes *alr4741*, *alr3608* and *alr3917* was higher in the mutant compared to wild type. The maximum increase was, however, five-fold (*alr3917*), which appears to be only moderate compared to the drastic down-regulation of other putative porin-encoding genes (Figure 3B).

In addition to their impact on membranes, carotenoids are involved in the protection of the photosynthetic apparatus from reactive oxygen species. Thus, an increased carotenoid concentration might result from an elevated level of oxidative stress. To test whether I-*tonB2* exhibits a higher oxidative stress level, the expression of superoxide dismutase A (SodA, MnSOD) and B (SodB, FeSOD) was analysed. Both enzymes confer resistance to oxidative stress under distinct nitrogen regimes (65). The abundance of both transcripts was reduced in I-*tonB2* in comparison to the wild type after 7 days of cultivation in YBG11 medium (Figure 3C). This suggests that the *tonB2*-mutant does not suffer from increased oxidative stress and that the enhanced carotenoid level is caused by other factors.

I-*tonB2* and I-*tonB4* are impaired in nitrogenase activity

The nitrogenase enzyme in *Anabaena* has Mo as a cofactor (12). Notably I-*tonB2* and I-*tonB4* were altered in the cellular Mo concentration compared to wild type (Table 2), and the abundance of the *tonB4* transcript was found to be enhanced in the absence of

combined nitrogen (38) Therefore the nitrogenase activity was determined for I-*tonB2* and I-*tonB4* by means of the acetylene reduction assay. Under oxic conditions, a nitrogenase activity of 0.8 ± 0.7 or 1.3 ± 0.9 nmol ethylene/µg Chl*h was measured in I-*tonB2* and I-*tonB4*, respectively (Figure 4A), which was significantly lower than in the wild type (4.7 ± 2.6 nmol ethylene/µg Chl*h). Under anoxic conditions, the nitrogenase activity in both mutants was enhanced compared the oxic conditions. However, the average values of 2 ± 2 and 3 ± 2 nmol ethylene/µg Chl*h for I-*tonB2* and I-*tonB4*, respectively, were again significantly lower than the nitrogenase activity of the wild type. Hence, both strains showed a reduced but not abolished nitrogen fixation capacity.

Considering the alterations in nitrogenase activity, the heterocysts of the *tonB*-mutants were analysed under the light microscope and compared to those of the wild type. I-*tonB2* and I-*tonB4* mutants differentiated wild-type-like heterocysts as judged from light microscopy (Figure 4B), and the formation of the constricted heterocyst pole was not altered as determined with fluorescently labelled vancomycin (Figure 4C). Therefore, TonB2 and TonB4 are not essential for heterocyst differentiation, although *tonB4* expression is upregulated under nitrogen starvation (38) and nitrogenase activity in the mutants is somewhat reduced compared to the wild type (see Figure 4A).

Iron-starvation and siderophore transport capacities of *tonB*-mutants

Next, we addressed the question if TonB2 and TonB4 are involved in the transport of ferric siderophores, as proposed for TonB3 (38). First, a potential complementation of single *tonB*-insertions through enhanced expression of other *tonB* genes was analysed by qRT-PCR. TonB1 was excluded from this analysis, since an interaction with TBDTs and thus a relation to siderophore transport is not assumed (38). The transcript abundance of the non-mutated *tonB*-genes was determined after seven days of iron starvation and

normalized against the expression of the housekeeping gene *rnpB*. Starvation was applied since the expression of genes involved in TonB-dependent transport in *Anabaena* is triggered in the absence of iron (38, 41, 47, 66).

The abundance of *tonB2* transcripts in I-*tonB3* and I-*tonB4* mutants was not significantly different from the wild-type level, both under standard conditions and after iron starvation (Figure 5A, left). Further, no significant alteration of *tonB2* expression was observed in response to iron starvation in any of the strains tested. Similarly, the expression of *tonB4* was not significantly affected by iron starvation (Figure 5A, right), but was enhanced in I-*tonB2* compared to the wild type when strains were grown in YBG11 medium.

The *tonB3* transcript was increased under iron-starvation in all strains (Figure 5A, middle), although the change in I-*tonB4* was not significant (Figure 5A, middle). Moreover, *tonB3* expression in I-*tonB2* was enhanced compared to the wild type when cells were grown in YBG11 medium, but not after iron starvation. This may suggest an early level of starvation in I-*tonB2*, since *tonB3* expression is triggered upon iron depletion. However, no changes in Chl (as indicator of iron starvation) and no significant alteration in the cellular iron content were observed in I-*tonB2* compared to the wild type (Tables 1, 2), which does not support iron starvation in I-*tonB2*.

In contrast, *tonB3* expression was not as drastically enhanced after iron starvation in I-*tonB4* as observed in the wild type or I-*tonB2*. This suggests a comparatively lower level of starvation in the *tonB4*-mutant. To test this, wild-type and mutant cultures were grown for 25 days in iron-free medium and the Chl level was determined as indicator for the degree of starvation. Indeed, the Chl content was more drastically decreased in the wild type (0.38 µg ml^{-1} at OD_{750} 1) compared to I-*tonB4* (1.4 µg ml^{-1} at OD_{750} 1; Figure 5B).

Thus, the *tonB4*-mutant shows an unusually weak iron starvation phenotype, which explains the reduced induction of *tonB3* expression during starvation.

In conclusion, no drastic alterations of *tonB* transcript abundance were observed between the mutants and the wild type after iron starvation. Thus, complementation effects between the *tonB* genes appear not to take place according to the analysis of the phenotypes under iron starvation. Thus the growth behaviour in iron-free medium was analysed for I-*tonB2* and I-*tonB4* (Figure 5C). The cultures were pre-starved prior to monitoring growth, since iron starvation in *Anabaena* including the expression of relevant uptake systems requires acclimation (66). We did not observe a compromised growth of the mutants compared to the wild type, which argues against a direct function of TonB2 and TonB4 in iron uptake. To support this conclusion, the transport rates of schizokinen loaded with ^{55}Fe were determined. Although the normalized uptake rates of $4.9*10^{-9}$ mol Fe /l*h for I-*tonB2* and $7.0*10^{-9}$ mol Fe /l*h for I-*tonB4* were slightly lower compared to the wild-type rates ($8.5*10^{-9}$ mol Fe /l*h), no significant difference could be established (Figure 5D). Thus, TonB2 and TonB4 do not seem to function in schizokinen transport in *Anabaena*.

Discussion

The TonB-ExbB-ExbD system is conserved among Gram-negative bacteria, as approximately two thirds of these bacteria have at least one TonB-encoding gene (3). Notably many species encode multiple TonB copies in the genome (3), and diverse functions have been assigned to the different genes in one species (30, 31, 36).

In *Anabaena* four genes have been annotated as encoding possible TonB proteins. With respect to the three TonB-like proteins of *Anabaena* that exhibit a conserved domain architecture (Figure 1), TonB3 likely represents the central component of the siderophore-

dependent iron uptake system (38). In contrast, TonB2 and TonB4 are likely not related to iron uptake, since schizokinen uptake is not impaired in their mutants (Figure 5). The abnormal iron starvation behaviour of I-*tonB4* requires further investigation and cannot be explained at this stage. Noteworthy *Anabaena* is capable of transporting other siderophores besides the endogenously synthesized schizokinen, such as aerobactin, ferrioxamine B (47, 66, 67) or ferrichrome (unpublished data). Aerobactin penetrates through the same TBDT as schizokinen does (66), therefore it is likely that this transport is TonB3-dependent as well (38). If TonB2 or TonB4 are involved in the TonB-dependent transport of other iron-containing substrates cannot be excluded. However, because the growth of the mutant cultures is not affected in the absence of iron, a relation to ferric siderophore transport seems unlikely. Besides ferric siderophores also other substrates such as cobalamin, nickel or sugars are transported in a TonB-dependent manner in some organisms (16, 19). This further broadens the spectrum of possible functions for TonB2 and TonB4 that will need to be investigated, especially considering the high number of 22 TBDTs that are predicted from the *Anabaena* genome (37).

The phenotypes of I-*tonB2* and I-*tonB4* were investigated in order to figure out possible functions. Differential characteristics of the strains were unveiled, including alterations of the cellular metal concentrations that were observed, albeit to different extents, for all *tonB*-mutants. Both I-*tonB3* and I-*tonB4* show decreased cellular contents of Mg and Co, and I-*tonB4* also of Mo (Table 2). Molybdenum is the cofactor of the nitrogenase enzyme (12), which might contribute to the reduced nitrogenase activity in I-*tonB4* (Figure 4). Moreover, in I-*tonB3* and I-*tonB4* the Chl level is comparatively decreased (Table 1), which in turn might be a consequence of the reduced Mg content in these strains. Notably in I-

tonB4 the regulation of Chl synthesis seems to be generally affected, considering the remarkably high Chl concentration after iron starvation.

Besides a decrease in Mn in I-*tonB2* and I-*tonB3*, an accumulation of Cu and Mo was observed in I-*tonB2* that might be caused by altered outer membrane properties. The anionic LPS surface is involved in metal binding in bacteria (68–71), and it was reported that cyanobacterial negatively charged exopolysaccharides are capable of binding metals (72) and might even accumulate trace metals under starvation conditions. Thus, the enhanced LPS production in I-*tonB2* might (i) lead to an enhanced adsorption of certain metals that subsequently diffuse into the cell and (ii) cause the formation cell aggregates.

LPS is thought to have an important role in porin trimerization, stability and conductance (73–75). In the so called deep rough mutants, strains that are compromised in LPS synthesis and thus only produce truncated LPS, a lower amount of proteins is abundant in the OM (17). Additionally, those mutants are increasingly susceptible towards SDS or hydrophobic antibiotics (76, 77). An opposite effect might take place in I-*tonB2*, in which the excessive LPS production might result in the monitored decrease in susceptibility towards drugs, possibly reinforced by the reduction of the expression of genes encoding porins observed in this strain. Although it has been speculated that aminoglucoside antibiotics cross the OM through a diffusion-based self-promoted pathway in which the LPS surface is involved (17, 78), for *Anabaena* a relation of erythromycin uptake to porin function has been established (63). In the I-*tonB2* mutant most of the genes coding for porins are downregulated, among them the porins described to be most abundant in *Anabaena* (39, 64). The decreased porin expression could display a feedback transcriptional response to a putatively enhanced substrate (metal) diffusion into the cell,

reflected by a higher metal adsorption in I-*tonB2.* Hence, considering these characteristics a TolA-like function could be proposed for TonB2 rather than a TonB-like function.

The TolA-TolQ-TolR system embedded in the PM (Tol-system hereinafter, (79)) is structurally related to the TonB-system. The C-terminal domains of TonB and TolA are structurally analogous (80) and it is assumed that the Tol-system is involved in maintaining OM integrity (81–83). TolA interacts with trimeric porins of *E. coli* (84, 85) and the Tol-Pal system constitutes a component of the divisome involved in cell constriction and peptidoglycan remodelling (86, 87). Moreover, TolA might modulate the expression of LPS components in *E. coli* (88, 89), which also might be the case for TonB2.

The lack or low dosage of any TonB-like protein induces pigment alterations in *Anabaena* (Table 1). The enhancement of the carotenoid level in I-*tonB2*, and thus the reduction of the Chl:Car ratio, is also reflected in the comparatively bright colour of its cultures (Figure 2). Carotenoids are accessory pigments that harvest light and transfer energy to Chl. In addition, carotenoids have important functions in photoprotection or membrane stability. A possible explanation for the modifications in pigment content are the observed alterations in cellular metal contents, because different metal treatments are known affect cyanobacterial pigment concentrations. The treatment of *Anabaena oryzae* with 1-100 ppm Cu resulted in an increased carotenoid concentration after six to eight days of incubation (51). As the Cu treatment likely increases the cellular Cu concentration, the treatment with enhanced Cu in the medium likely mimics the situation of I-*tonB2*. Thus, the enhanced carotenoid concentration in the *tonB2*-mutant may be a consequence of copper enrichment.

In summary, the four TonB-like proteins found in *Anabaena* apparently take over distinct functions. Neither I-*toB2* nor I-*tonB4* is drastically reduced in schizokinen uptake

capacity, which suggests that TonB3 exclusively mediates schizokinen transport in *Anabaena*. On the other hand, both *tonB2* and *tonB4* mutants are compromised in the production of full nitrogenase activity, especially under oxic conditions, although heterocyst differentiation seems not affected. TonB2 influences OM properties, including LPS synthesis, with an effect on susceptibility towards antibiotics and porin abundance (as deduced from porin gene expression), and its role might be related to that of the Tol-system as discussed above. The role of TonB4 is elusive, consistent with its peculiar predicted structure (Fig. 1), although we note that its mutant is affected in the cellular levels of several metals including Mo that may result in the observed low nitrogenase levels.

Material and Methods

Anabaena culture conditions

Anabaena (also known as *Nostoc)* sp. strain PCC 7120 was stored on plates of BG11 medium with 1% (w/v) bacto agar (BD Biosciences; (90)). For liquid culturing either BG11 (90) or YBG11 medium (91) was used. *Anabaena* cultures were grown under constant shaking at 90-100 rpm and constant illumination (ambient light: 70 µmol photons m^{-2} s^{-1}; OSRAM L 58 W/954-LUMILUX de Luxe, Daylight) at 28°C. In case of mutant strains 5 µg ml^{-1} of both spectinomycin dihydrochloride pentahydrate (Sp; Duchefa Biochemie) and streptomycin sulfate (Sm; Roth) were added. The growth was monitored spectrophotometrically in terms of optical density at 750 nm (OD_{750}). For growth analysis on plates 5 µl of cell suspensions with OD_{750}=1 were spotted in a dilution series (1; 1:10; 1:100), and representative results are shown.

DNA extraction, molecular cloning and generation of *Anabaena* mutants

Transformation of *E. coli* and isolation and manipulation of plasmid DNA were performed

according to standard protocols (92). *Anabaena* genomic DNA (gDNA) was isolated as described previously (93) with modifications: sodium dodecyl sulfate was not added, the phenol extraction was done once followed by two washing steps with 400 µl of chloroform.

The *Anabaena tonB* mutants AFS-I-*tonB1*, AFS-I-*tonB2*, AFS-I-*tonB3* and AFS-I-*tonB4* were utilized in this study, whereas AFS-I-*tonB3* has been introduced previously (38). The annotation stands for *Anabaena* mutant generated in Frankfurt, Germany by the Schleiff Lab by plasmid insertion, for better readability *"*AFS-" was omitted throughout the text. In brief, internal fragments of the single genes were ligated into vector pCSV3 (94, 95) in case of I-*tonB2*, I-*tonB3* and I-*tonB4* or pCSEL24 (96) in case of I-*tonB1,* both carrying spectinomycin- and streptomycin-resistance markers. The oligonucleotides and the plasmids used in this study are listed in Table S1 and S2, respectively. Plasmids were transferred to *Anabaena* with the triparental mating method as previously described (39, 96–98). The *Anabaena* strains analysed in this study are listed in Table S3. The genotype of the exconjugants was tested by PCR, in which an oligonucleotide specific for the plasmid in combination with an oligonucleotide specific for the gene region was used.

Short-term siderophore transport measurements

The transport rates of ferric schizokinen were determined as described earlier (66, 99). Schizokinen was ordered from EMC Microcollections and $^{55}FeCl_3$ was purchased from Perkin Elmer. A final concentration of 15 nM ^{55}Fe-Schizokinen was used in single measurements, and the final cell suspension utilized for measuring was inoculated at OD_{750}=0.05. Cultures were pre-starved in iron-free YBG11 before the measurements were conducted and the degree of starvation was estimated by the chlorophyll *a* (Chl) concentration at OD_{750}=1, as previous studies indicated that the Chl concentration per cell decreases in *Anabaena* with ongoing iron starvation (47). The Chl concentrations of

experiment cultures are given in Table S4.

Inductively coupled plasma mass spectrometry (ICP-MS)

The cellular metal concentrations in *Anabaena* were determined as described earlier (100). In brief, cultures grown for seven days in YBG11 were harvested by centrifugation and washed twice with 20 mM 2-(N-Morpholino)ethanesulfonic acid (pH 5), 10 mM ethylenediaminetetraacetic acid. Cells were resuspended in 5 ml double distilled water and 1 ml was subjected to ICP-MS measurement. The OD_{750} of the suspension was measured and cells were counted for normalization. Samples were digested overnight at 120 °C in 7 M HNO_3 and dissolved in 5% HNO_3 for measurement.

Pigment extraction

The measurements of Chl and carotenoid (Car) concentrations were performed with methanolic extracts as previously described (101, 102). The Chl concentration was determined with the formula:

$$\text{Chl [µg/ml]} = 12.9447(A_{665nm} - A_{720nm})$$

and the carotenoid concentration was calculated with the formula:

$$\text{Car [µg/ml]} = (1000(A_{470nm} - A_{720nm}) - 2.86 * (\text{Chl [µg/ml]}))/221$$

To estimate the Chl concentration for experimental cultures a simplified equation was utilized, as follows:

$$\text{Chl [mg/ml]} = A_{665nm} / 74.5$$ (103).

Vancomycin-FL staining and microscopy

For visualization of peptidoglycan, the filaments were stained with BODIPY™ FL Vancomycin (Van-FL) (Invitrogen) as previously described (104). For microscopy a piece of agar was excised and reversely placed onto a coverslip that was utilized as microscope slide. Images were recorded with a Zeiss LSM 780 using 63x or 40x objectives with

immersion oil. Diameter of the pinhole was set to 69.4 µM, and a 488-nm laser source was used for excitation. Specific Van-FL fluorescence was recorded between 500-550 nm, Chl autofluorescence was recorded between 630-700 nm. Light microscopy images were recorded with a Thorlabs DCC1645C-HQ camera.

RNA extraction, RT-PCR and qRT-PCR

RNA was isolated either from strains that had been grown for 7 days in YBG11 medium or, in the case of iron-starvation, from samples incubated for 7 days under culture conditions in iron-free YBG11 medium. RNA was extracted with TRIzol (Thermo Fisher Scientific) according to described protocols (41). After DNase I digestion the absence of DNA in RNA samples was verified by PCR. Revert Aid Reverse transcriptase was used for first strain cDNA synthesis (Thermo Fisher Scientific). qPCR was performed with a StepOnePlus Cycler from Thermo Fisher Scientific, the cycling conditions were set as: 50°C, 2 min and 95°C, 2 min followed by 40 cycles at 95°C,15 s; 60°C, 30 s; 72°C, 30 s. Experiments were performed with PowerUp SYBR Green Master Mix from Applied Biosystems. *rnpB* served as housekeeping gene. The Ct value of the gene of interest was normalized to *rnpB* Ct-value (Δct) and, if indicated, further normalized to the corresponding Δct of the wild type (ΔΔct) (105).

Extraction and analysis of lipopolysaccharide

Lipopolysacharide (LPS) was extracted from wild type and I-*tonB2*, the cultures were grown in flasks with constant shaking for 8 days or in tubes with supplementation of 1% CO_2 in YBG11 medium for 7 days (Fig. S2). Cells corresponding to an OD_{750} of 3 in 1 ml were harvested for LPS extraction. LPS was extracted as described previously (106) with modifications. In brief, the cells were harvested by centrifugation (6000 *g*, 5 min), washed with 1 ml of phosphate buffered saline (137 mM NaCl, 2.7 mM KCl, 10 mM Na_2HPO_4 , 1.8

mM KH_2PO_4) and resuspended in 50 µl lysing buffer (2% sodium dodecyl sulfate, 4% β-mercaptoethanol, 10% glycerol,1 M Tris-HCl pH 6.8, bromphenol blue). After the samples were heated at 100°C for 10 min, 10 µl of lysing buffer containing 100 µg Proteinase K was added, followed by 60 min incubation at 60°C.

The LPS was subjected to denaturing SDS polyacrylamide electrophoresis utilizing a 12% acrylamide gel, afterwards the gel was silver stained (107). For the loading control (large subunit of Rubisco is shown in figures) cells were treated as described for LPS extraction omitting proteinase K.

Nitrogenase activity

Nitrogenase activity was determined by the acetylene reduction assay (108) carried out under both oxic and anoxic conditions. Cells grown in 25 ml of liquid BG11 medium (supplemented with Sp/Sm when necessary) were harvested by centrifugation, washed with liquid $BG11_0$ medium and incubated at 1 µg Chl ml^{-1} (without antibiotics) in 25 ml of liquid $BG11_0$ medium for 48 hours. Cell suspensions of 2 ml at 6 µg Chl ml^{-1} were transferred to sealed small flasks in which the nitrogenase activity assay was carried out. In both oxic and anoxic conditions 2 ml of acetylene was injected. For the assays under oxic conditions, the sealed flasks were incubated for 30 min (30ºC and shaking) before taking 1-ml samples for determination of ethylene by gas chromatography. For anoxic conditions, the sealed flasks were supplemented with 10 µM 3-(3,4-dichlorophenyl)-1,1-imethylurea (DCMU; from Sigma), bubbled with argon for 4 min and incubated for 60 min (30ºC and shaking) before acetylene injections, and then 1-ml samples were taken for ethylene determination. In both conditions, samples for ethylene determination were taken for up to 2 hours.

Acknowledgements

We thank Rafael Pernil for useful discussions, Sotirios Fragkostefanakis for a critical reading of the manuscript, H.-Michael Seitz for experimental support with ICP-MS. The work was funded by the Deutsche Forschungsgemeinschaft DFG SCHL585/6-3 to ES. Work in Seville was supported by grant number BFU2017-88202-P from Plan Estatal de Investigación Científica y Técnica y de Innovación, Spain, co-financed by the European Regional Development Fund, to Enrique Flores.

Conflict of interest

The authors declare that they have no conflict of interests.

References

1. Hahn A, Schleiff E. 2014. The Cell Envelope, p. 29–87. *In* Flores, E, Herrero, A (eds.), The Cell Biology of Cyanobacteria. Caister Academic Press, U.K., Norfolk.
2. Mirus O, Hahn A, Schleiff E. 2010. Outer membrane proteins, p. 175–228. *In* König, H, Claus, H, Varma, A (eds.), Prokaryotic Cell Wall Compounds: Structure and Biochemistry. Springer Berlin Heidelberg.
3. Chu BCH, Peacock RS, Vogel HJ. 2007. Bioinformatic analysis of the TonB protein family. BioMetals 20:467–483.
4. Andrews SC, Robinson AK, Rodríguez-Quiñones F. 2003. Bacterial iron homeostasis. FEMS Microbiol Rev 27:215–237.
5. Wandersman C, Delepelaire P. 2004. Bacterial iron sources: from siderophores to hemophores. Annu Rev Microbiol 58:611–658.
6. Gledhill M, Buck KN. 2012. The organic complexation of iron in the marine environment: A review. Front Microbiol 3:1–17.
7. Street JH, Paytan A. 2005. Iron, phytoplankton growth, and the carbon cycle, p. 153–193. *In* Metal Ions in Biological Systems.
8. Ratledge C, Dover LG. 2000. Iron metabolism in pathogenic bacteria. Annu Rev Microbiol 54:881–941.
9. Dammeyer T, Frankenberg-Dinkel N. 2008. Function and distribution of bilin biosynthesis enzymes in photosynthetic organisms. Photochem Photobiol Sci 7:1121–1130.
10. Pushnik JC, Miller GW, Manwaring JH. 1984. The role of iron in higher plant chlorophyll biosynthesis, maintenance and chloroplast biogenesis. J Plant Nutr 7:733–758.

11. Raven JA, Evans MCW, Korb RE. 1999. The role of trace metals in photosynthetic electron transport in O_2-evolving organisms. Photosynth Res 60:111–150.
12. Pernil R, Schleiff E. 2019. Metalloproteins in the Biology of Heterocysts. Life 9.
13. Norman L, Cabanesa DJE, Blanco-Ameijeiras S, Moisset SAM, Hassler CS. 2014. Iron Biogeochemistry in Aquatic Systems: From Source to Bioavailability. Chim Int J Chem 68:764–771.
14. Khan A, Singh P, Srivastava A. 2018. Synthesis, nature and utility of universal iron chelator – Siderophore: A review. Microbiol Res 212–213:103–111.
15. Saha M, Sarkar S, Sarkar B, Sharma BK, Bhattacharjee S, Tribedi P. 2016. Microbial siderophores and their potential applications: a review. Environ Sci Pollut Res 23:3984–3999.
16. Noinaj N, Guillier M, Barnard TJ, Buchanan SK. 2010. TonB-dependent transporters: regulation, structure, and function. Annu Rev Microbiol 64:43–60.
17. Nikaido H. 2003. Molecular Basis of Bacterial Outer Membrane Permeability Revisited. Microbiol Mol Biol Rev 67:593–656.
18. Vergalli J, Bodrenko I V., Masi M, Moynié L, Acosta-Gutiérrez S, Naismith JH, Davin-Regli A, Ceccarelli M, van den Berg B, Winterhalter M, Pagès JM. 2020. Porins and small-molecule translocation across the outer membrane of Gram-negative bacteria. Nat Rev Microbiol 18:164–176.
19. Schauer K, Rodionov DA, de Reuse H. 2008. New substrates for TonB-dependent transport: do we only see the “tip of the iceberg”? Trends Biochem Sci 33:330–338.
20. Hancock REW, Braun V. 1976. Nature of the energy requirement for the irreversible adsorption of bacteriophages T1 and *Φ*80 to *Escherichia coli*. J

Bacteriol 125:409–415.

21. Holroyd C, Bradbeer C. 1984. Cobalamin transport in *Escherichia coli*, p. 21–23. *In* Leive, L, Schlessinger, D (eds.), Microbiology-1984. American Society for Microbiology, Washington, D.C.
22. Celia H, Botos I, Ni X, Fox T, De Val N, Lloubes R, Jiang J, Buchanan SK. 2019. Cryo-EM structure of the bacterial Ton motor subcomplex ExbB–ExbD provides information on structure and stoichiometry. Commun Biol 2.
23. Skare JT, Ahmer BMM, Seachord CL, Darveau RP, Postle K. 1993. Energy transduction between membranes. TonB, a cytoplasmic membrane protein, can be chemically cross-linked *in vivo* to the outer membrane receptor FepA. J Biol Chem 268:16302–16308.
24. Cadieux N, Kadner RJ. 1999. Site-directed disulfide bonding reveals an interaction site between energy-coupling protein TonB and BtuB, the outer membrane cobalamin transporter. Proc Natl Acad Sci U S A 96:10673–10678.
25. Ollis AA, Manning M, Held KG, Postle K. 2009. Cytoplasmic membrane protonmotive force energizes periplasmic interactions between ExbD and TonB. Mol Microbiol 73:466–481.
26. Ollis AA, Postle K. 2012. Identification of functionally important TonB-ExbD periplasmic domain interactions *In vivo*. J Bacteriol 194:3078–3087.
27. Ferguson AD, Deisenhofer J. 2002. TonB-dependent receptors - Structural perspectives. Biochim Biophys Acta - Biomembr 1565:318–332.
28. Poole K, Zhao Q, Neshat S, Heinrichs DE, Dean CR. 1996. The *Pseudomonas aeruginosa tonB* gene encodes a novel TonB protein. Microbiology 142:1449–1458.

29. Zhao Q, Poole K. 2000. A second *tonB* gene in *Pseudomonas aeruginosa* is linked to the *exbB* and *exbD* genes. FEMS Microbiol Lett 184:127–132.
30. Huang B, Ru K, Yuan Z, Whitchurch CB, Mattick JS. 2004. tonB3 is required for normal twitching motility and extracellular assembly of type IV pili. J Bacteriol 186:4387–4389.
31. Shirley M, Lamont IL. 2009. Role of TonB1 in pyoverdine-mediated signaling in *Pseudomonas aeruginosa*. J Bacteriol 191:5634–5640.
32. Takase H, Nitanai H, Hoshino K, Otani T. 2000. Requirement of the *Pseudomonas aeruginosa tonB* gene for high-affinity iron acquisition and infection. Infect Immun 68:4498–4504.
33. Ainsaar K, Tamman H, Kasvandik S, Tenson T, Hõrak R. 2019. The $TonB_m$-pocAB system is required for maintenance of membrane integrity and polar position of flagella in *Pseudomonas putida*. J Bacteriol 201.
34. Bitter W, Tommassen J, Weisbeek PJ. 1993. Identification and characterization of the *exbB*, *exbD* and *tonB* genes of *Pseudomonas putida* WCS358: their involvement in ferric-pseudobactin transport. Mol Microbiol 7:117–130.
35. Godoy P, Ramos-González MI, Ramos JL. 2001. Involvement of the TonB system in tolerance to solvents and drugs in *Pseudomonas putida* DOT-T1E. J Bacteriol 183:5285–5292.
36. Kuehl CJ, Crosa JH. 2010. The TonB energy transduction systems in *Vibrio species*. Future Microbiol 5:1403–1412.
37. Mirus O, Strauss S, Nicolaisen K, von Haeseler A, Schleiff E. 2009. TonB-dependent transporters and their occurrence in cyanobacteria. BMC Biol 7:68.
38. Stevanovic M, Hahn A, Nicolaisen K, Mirus O, Schleiff E. 2012. The components

of the putative iron transport system in the cyanobacterium *Anabaena* sp. PCC 7120. Environ Microbiol 14:1655–1670.

39. Moslavac S, Reisinger V, Berg M, Mirus O, Vosyka O, Plöscher M, Flores E, Eichacker LA, Schleiff E. 2007. The proteome of the heterocyst cell wall in *Anabaena* sp. PCC 7120. Biol Chem 388:823–829.
40. Wilk L, Strauss M, Rudolf M, Nicolaisen K, Flores E, Kühlbrandt W, Schleiff E. 2011. Outer membrane continuity and septosome formation between vegetative cells in the filaments of *Anabaena* sp. PCC 7120. Cell Microbiol 13:1744–1754.
41. Stevanovic M, Lehmann C, Schleiff E. 2013. The response of the TonB-dependent transport network in *Anabaena* sp. PCC 7120 to cell density and metal availability. BioMetals 26:549–560.
42. Steiger S, Schäfer L, Sandmann G. 1999. High-light-dependent upregulation of carotenoids and their antioxidative properties in the cyanobacterium *Synechocystis* PCC 6803. J Photochem Photobiol B Biol 52:14–18.
43. Kłodawska K, Bujas A, Turos M, Malec P. 2016. Low temperature induced accumulation of keto-carotenoids canthaxanthin and echinenone in cyanobacterium *Anabaena* 7120. N Biotechnol 33:S196.
44. Várkonyi Z, Masamoto K, Debreczeny M, Zsiros O, Ughy B, Gombos Z, Domonkos I, Farkas T, Wada H, Szalontai B. 2002. Low-temperature-induced accumulation of xanthophylls and its structural consequences in the photosynthetic membranes of the cyanobacterium *Cylindrospermopsis raciborskii*: An FTIR spectroscopic study. Proc Natl Acad Sci U S A 99:2410–2415.
45. Muramatsu M, Hihara Y. 2012. Acclimation to high-light conditions in cyanobacteria: From gene expression to physiological responses. J Plant Res

125:11–39.

46. Guikema JA, Sherman LA. 1983. Organization and Function of Chlorophyll in Membranes of Cyanobacteria during Iron Starvation. Plant Physiol 73:250–256.
47. Rudolf M, Kranzler C, Lis H, Margulis K, Stevanovic M, Keren N, Schleiff E. 2015. Multiple modes of iron uptake by the filamentous, siderophore-producing cyanobacterium, *Anabaena* sp. PCC 7120. Mol Microbiol 97:577–588.
48. Grant CS, Louda JW. 2010. Microalgal pigment ratios in relation to light intensity: Implications for chemotaxonomy. Aquat Biol 11:127–138.
49. Lakatos M, Bilger W, Büdel B. 2001. Carotenoid composition of terrestrial cyanobacteria: Response to natural light conditions in open rock habitats in Venezuela. Eur J Phycol 36:367–375.
50. Schagerl M, Müller B. 2006. Acclimation of chlorophyll a and carotenoid levels to different irradiances in four freshwater cyanobacteria. J Plant Physiol 163:709–716.
51. Chakilam SR. 2012. Metal effects on carotenoid content of Cyanobacteria. Int J Bot 8:192–197.
52. Tiwari A, Singh P, Asthana RK. 2016. Role of calcium in the mitigation of heat stress in the cyanobacterium *Anabaena* PCC 7120. J Plant Physiol 199:67–75.
53. Singh S, Mishra AK. 2016. Unraveling of cross talk between Ca^{2+} and ROS regulating enzymes in *Anabaena* 7120 and *ntcA* mutant. J Basic Microbiol 56:762–778.
54. Ehling-Schulz M, Bilger W, Scherer S. 1997. UV-B-Induced Synthesis of Photoprotective Pigments and Extracellular Polysaccharides in the Terrestrial Cyanobacterium *Nostoc commune*. J Bacteriol 179:1940–1945.

55. Gruszecki WI, Strzałka K. 2005. Carotenoids as modulators of lipid membrane physical properties. Biochim Biophys Acta - Mol Basis Dis 1740:108–115.
56. Mohamed HE, Van De Meene AML, Roberson RW, Vermaas WFJ. 2005. Myxoxanthophyll is required for normal cell wall structure and thylakoid organization in the cyanobacterium *Synechocystis* sp. strain PCC 6803. J Bacteriol 187:6883–6892.
57. Nakao R, Senpuku H, Watanabe H. 2006. *Porphyromonas gingivalis* galE is involved in lipopolysaccharide O-antigen synthesis and biofilm formation. Infect Immun 74:6145–6153.
58. Dirienzo JM, Inouye M. 1983. Effect of reduced membrane lipid fluidity on the biosynthesis of lipopolysaccharide of *Escherichia coli*. Eur J Biochem 135:351–357.
59. Jürgens UJ, Weckesser J. 1985. Carotenoid-containing outer membrane of *Synechocystis* sp. strain PCC6714. J Bacteriol 164:384–389.
60. Resch CM, Gibson J. 1983. Isolation of the carotenoid-containing cell wall of three unicellular cyanobacteria. J Bacteriol 155:345–350.
61. Masamoto K, Riethman HC, Sherman LA. 1987. Isolation and Characterization of a Carotenoid-Associated Thylakoid Protein from the Cyanobacterium *Anacystis nidulans* R2. Plant Physiol 84:633–639.
62. Fernández L, Hancock REW. 2012. Adaptive and mutational resistance: Role of porins and efflux pumps in drug resistance. Clin Microbiol Rev 25:661–681.
63. Hahn A, Stevanovic M, Mirus O, Schleiff E. 2012. The TolC-like protein HgdD of the cyanobacterium *Anabaena* sp. PCC 7120 is involved in secondary metabolite export and antibiotic resistance. J Biol Chem 287:41126–41138.

64. Moslavac S, Bredemeier R, Mirus O, Granvogl B, Eichacker LA, Schleiff E. 2005. Proteomic analysis of the outer membrane of *Anabaena* sp. strain PCC 7120. J Proteome Res 4:1330–1338.

65. Raghavan PS, Rajaram H, Apte SK. 2011. Nitrogen status dependent oxidative stress tolerance conferred by overexpression of MnSOD and FeSOD proteins in *Anabaena* sp. strain PCC7120. Plant Mol Biol 77:407–417.

66. Rudolf M, Stevanovic M, Kranzler C, Pernil R, Keren N, Schleiff E. 2016. Multiplicity and specificity of siderophore uptake in the cyanobacterium *Anabaena* sp. PCC 7120. Plant Mol Biol 92:57–69.

67. Goldman SJ, Lammers PJ, Berman MS, Sanders-Loehr J. 1983. Siderophore-Mediated Iron Uptake in Different Strains of *Anabaena* sp. J Bacteriol 156:1144–1150.

68. Oh ET, Yun HS, Heo T-R, Koh S-C, Oh K-H, So J-S. 2002. Involvement of lipopolysaccharide of *Bradyrhizobium japonicum* in metal binding. J Microbiol Biotechnol 12:296–300.

69. Langley S, Beveridge TJ. 1999. Effect of O-side-chain-lipopolysaccharide chemistry on metal binding. Appl Environ Microbiol 65:489–498.

70. Strain SM, Fesik SW, Armitage IM. 1983. Structure and metal-binding properties of lipopolysaccharides from heptoseless mutants of *Escherichia coli* studied by ^{13}C and ^{31}P nuclear magnetic resonance. J Biol Chem 258:13466–13477.

71. Ferris FG, Beveridge TJ. 1986. Site specificity of metallic ion binding in *Escherichia coli* K-12 lipopolysaccharide. Can J Microbiol 32:52–55.

72. De Philippis R, Colica G, Micheletti E. 2011. Exopolysaccharide-producing cyanobacteria in heavy metal removal from water: Molecular basis and practical

applicability of the biosorption process. Appl Microbiol Biotechnol 92:697–708.

73. Arunmanee W, Pathania M, Solovyova AS, Le Brun AP, Ridley H, Baslé A, Van Den Berg B, Lakey JH. 2016. Gram-negative trimeric porins have specific LPS binding sites that are essential for porin biogenesis. Proc Natl Acad Sci U S A 113:E5034–E5043.

74. Buehler LK, Kusumoto S, Zhang H, Rosenbusch JP. 1991. Plasticity of *Escherichia coli* porin channels: Dependence of their conductance on strain and lipid environment. J Biol Chem 266:24446–24450.

75. Schindler H, Rosenbusch JP. 1981. Matrix protein in planar membranes: clusters of channels in a native environment and their functional reassembly. Proc Natl Acad Sci U S A 78:2302–2306.

76. Chang V, Chen L-Y, Wang A, Yuan X. 2010. The Effect of Lipopolysaccharide Core Structure Defects on Transformation Efficiency in Isogenic *Escherichia coli* BW25113 *rfaG*, *rfaP*, and *rfaC* Mutants. J Exp Microbiol Immunol 14:101–107.

77. Schnaitman CA, Klena JD. 1993. Genetics of Lipopolysaccharide Biosynthesis in Enteric Bacteria. Microbiol Rev 57:655–682.

78. Hancock REW. 1984. Alterations in Outer Membrane Permeability. Annu Rev Microbiol 38:237–264.

79. Braun V, Herrmann C. 1993. Evolutionary relationship of uptake systems for biopolymers in *Escherichia coli*: cross-complementation between the TonB-ExbB-ExbD and the TolA-TolQ-TolR proteins. Mol Microbiol 8:261–268.

80. Witty M, Sanz C, Shah A, Grossmann JG, Mizuquchi K, Perham RN, Luisi B. 2002. Structure of the periplasmic domain of *Pseudomonas aeruginosa* TolA: Evidence for an evolutionary relationship with the TonB transporter protein. EMBO

J 21:4207–4218.

81. Davies JK, Reeves P. 1975. Genetics of resistance to colicins in *Escherichia coli* K-12: cross-resistance among colicins of group A. J Bacteriol 123:102–117.
82. Fognini-Lefebvre N, Lazzaroni JC, Portalier R. 1987. tolA, tolB and excC, three cistrons involved in the control of pleiotropic release of periplasmic proteins by *Escherichia coli* K12. MGG Mol Gen Genet 209:391–395.
83. Bernadac A, Gavioli M, Lazzaroni JC, Raina S, Lloubès R. 1998. *Escherichia coli tol-pal* mutants form outer membrane vesicles. J Bacteriol 180:4872–4878.
84. Derouiche R, Gavioli M, Bénédetti H, Prilipov A, Lazdunski C, Lloubès R. 1996. TolA central domain interacts with *Escherichia coli* porins. EMBO J 15:6408–6415.
85. Rigal A, Bouveret E, Lloubes R, Lazdunski C, Benedetti H. 1997. The TolB protein interacts with the porins of *Escherichia coli*. J Bacteriol 179:7274–7279.
86. Gerding MA, Ogata Y, Pecora ND, Niki H, de Boer PAJ. 2007. The trans-envelope Tol–Pal complex is part of the cell division machinery and required for proper outer-membrane invagination during cell constriction in *E. coli*. Mol Microbiol 63:1008–1025.
87. Yakhnina AA, Bernhardt TG. 2020. The Tol-Pal system is required for peptidoglycan-cleaving enzymes to complete bacterial cell division. Proc Natl Acad Sci U S A 117:6777–6783.
88. Gaspar JA, Thomas JA, Marolda CL, Valvano MA. 2000. Surface expression of O-specific lipopolysaccharide in *Escherichia coli* requires the function of the TolA protein. Mol Microbiol 38:262–275.
89. Rivera M, Hancock REW, Sawyer JG, Haug A, McGroarty EJ. 1988. Enhanced binding of polycationic antibiotics to lipopolysaccharide from an aminoglycoside-

supersusceptible, *tolA* mutant strain of *Pseudomonas aeruginosa* . Antimicrob Agents Chemother 32:649–655.

90. Rippka R, Deruelles J, Waterbury JB, Herdman M, Stanier RY. 1979. Generic Assignments, Strain Histories and Properties of Pure Cultures of Cyanobacteria. J Gen Microbiol 111:1–61.

91. Shcolnick S, Shaked Y, Keren N. 2007. A role for mrgA, a DPS family protein, in the internal transport of Fe in the cyanobacterium *Synechocystis* sp. PCC6803. Biochim Biophys Acta - Bioenerg 1767:814–819.

92. Sambrook J, Fritsch EF, Maniatis T. 1989. Molecular cloning: a laboratory manual2nd ed. Cold Spring Harbor Laboratory, Cold Spring Harbor N.Y.

93. Cai Y, Wolk CP. 1990. Use of a conditionally lethal gene in *Anabaena* sp. strain PCC 7120 to select for double recombinants and to entrap insertion sequences. J Bacteriol 172:3138–3145.

94. Elhai J, Wolk PC. 1988. A versatile class of positive-selection vectors based on the nonviability of palindrome-containing plasmids that allows cloning into long polylinkers. Gene 68:119–138.

95. Valladares A, Rodríguez V, Camargo S, Martínez-Noël GMA, Herrero A, Luque I. 2011. Specific role of the cyanobacterial pipX factor in the heterocysts of *Anabaena* sp. strain PCC 7120. J Bacteriol 193:1172–1182.

96. Olmedo-Verd E, Muro-Pastor AM, Flores E, Herrero A. 2006. Localized induction of the *ntcA* regulatory gene in developing heterocysts of *Anabaena* sp. strain PCC 7120. J Bacteriol 188:6694–6699.

97. Wolk CP, Vonshak A, Kehoe P, Elhai J. 1984. Construction of shuttle vectors capable of conjugative transfer from *Escherichia coli* to nitrogen-fixing filamentous

cyanobacteria. Proc Natl Acad Sci U S A 81:1561–1565.

98. Elhai J, Wolk CP. 1988. Conjugal Transfer of DNA to Cyanobacteria. Methods Enzymol 167:747–754.

99. Kranzler C, Lis H, Shaked Y, Keren N. 2011. The role of reduction in iron uptake processes in a unicellular, planktonic cyanobacterium. Environ Microbiol 13:2990–2999.

100. Sharon S, Salomon E, Kranzler C, Lis H, Lehmann R, Georg J, Zer H, Hess WR, Keren N. 2014. The hierarchy of transition metal homeostasis: Iron controls manganese accumulation in a unicellular cyanobacterium. Biochim Biophys Acta - Bioenerg 1837:1990–1997.

101. Sinetova MA, Červený J, Zavřel T, Nedbal L. 2012. On the dynamics and constraints of batch culture growth of the cyanobacterium *Cyanothece* sp. ATCC 51142. J Biotechnol 162:148–155.

102. Zavřel T, Sinetova MA, Červený J. 2015. Measurement of Chlorophyll a and Carotenoids Concentration in Cyanobacteria. Bio-protocol 5.

103. Salomon E, Bar-Eyal L, Sharon S, Keren N. 2013. Balancing photosynthetic electron flow is critical for cyanobacterial acclimation to nitrogen limitation. Biochim Biophys Acta - Bioenerg 1827:340–347.

104. Lehner J, Berendt S, Dörsam B, Pérez R, Forchhammer K, Maldener I. 2013. Prokaryotic multicellularity: A nanopore array for bacterial cell communication. FASEB J 27:2293–2300.

105. Livak KJ, Schmittgen TD. 2001. Analysis of relative gene expression data using real-time quantitative PCR and the $2^{-\Delta\Delta CT}$ method. Methods 25:402–408.

106. Apicella MA, Griffiss JM, Schneider H. 1994. Isolation and characterization of

lipopolysaccharides, lipooligosaccharides, and lipid A. Methods Enzymol 235:242–252.

107. Kavran JM, Leahy DJ. 2014. Silver staining of SDS-polyacrylamide gel, p. 169–176. *In* Methods in Enzymology. Academic Press Inc.

108. Stewart WD, Fitzgerald GP, Burris RH. 1967. *In situ* studies on N_2 fixation using the acetylene reduction technique. Proc Natl Acad Sci U S A 58:2071–2078.

Figures

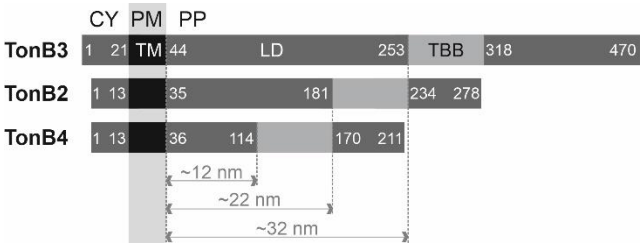

Figure 1. Domain architecture of TonB proteins in *Anabaena*. TonB3, TonB2 and TonB4 contain an N-terminal cytosolic region (CY), a transmembrane region (TM), a linker domain (LD), the TonB-box binding region (TBB) and a C-terminal extension. Indicated are the amino acids at the border of the cytosolic region, the LD and the C-terminal extension. The length of the linker domain was calculated assuming an extended helix (3.6 amino acids and 0.54 nm per turn). PM, plasma membrane; PP, periplasm.

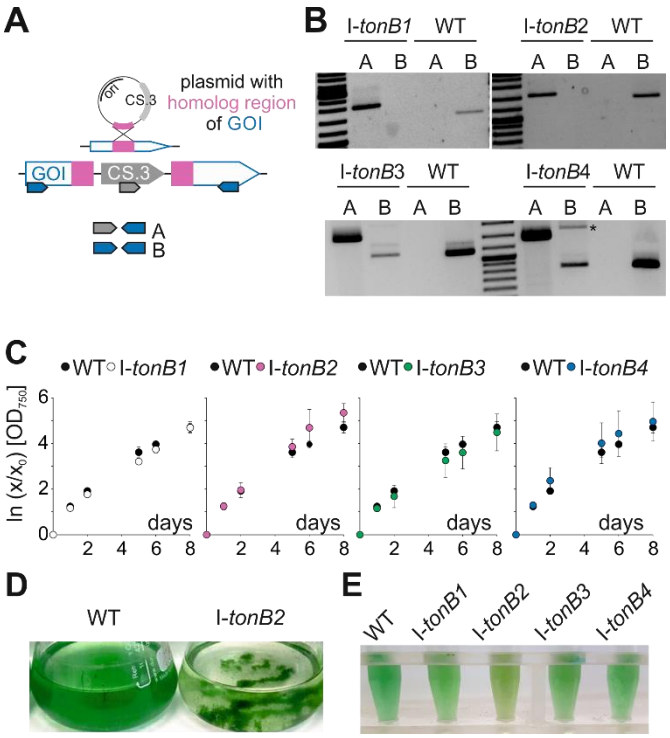

Figure 2. Growth phenotype of the *tonB* mutant strains. (A) Illustration of the single recombination strategy, a portion of the gene of interest (GOI) is cloned into a plasmid which bears the Sp^R Sm^R cassette (CS.3). After the recombination event the GOI in the mutant is interrupted by plasmid insertion. The oligonucleotide pairs utilized for mutant screening are indicated, primer combination A results in a product when the plasmid is integrated into the genome, combination B can only generate a product when the GOI is intact. (**B**) Segregation analysis of I-*tonB3* was introduced before (38). Either an oligonucleotide pair specific for the insertion fragment was used (lanes A), or an oligonucleotide pair specific for the wild-type gene (lanes B). The asterisk marks an unspecific PCR product **(C)** The growth of the indicated strains in YBG11 medium was determined by analysis of the OD_{750}, the wild type experiment is shown in the four diagrams for better comparability to the behaviour of each mutant. Values were normalized to initial OD_{750} of the culture and values are expressed as natural logarithm.

The mean of at least three biological replicates is shown with the standard deviation as error bar. **(D)** Wild-type and I-*tonB2* cultures photographed after growth for 7 days in YBG11 medium. **(E)** Wild-type and mutant cultures photographed after growth for 5 days in YBG11 medium, the I-*tonB2* sample was homogenized by pipetting up and down prior to the photographing in order to reduce clumping.

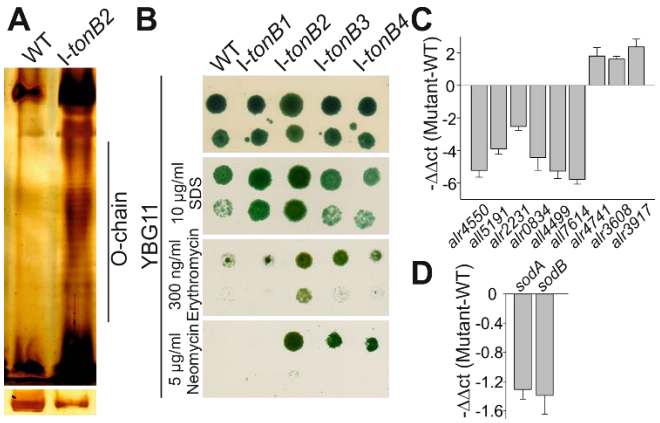

Figure 3. Outer membrane integrity of the *tonB* mutants and expression patterns in I-*tonB2*. (A) LPS extracted from the wild type (WT) and I-*tonB2* was separated on SDS-PAGE and silver stained. The O-antigen fragments are indicated. The loading control (large subunit of Rubisco) is given in the bottom panel where whole cell lysate of both strains was separated in amounts proportional to the LPS extract. **(B)** The wild type (WT) and the *tonB* mutants were spotted on plates of YBG11 medium supplemented with the indicated compounds. 5 µl of a cell suspension with OD_{750}=1 (upper row in each plate) or OD_{750}=0.1 (bottom row in each plate) were spotted. Images were taken after 10 days of incubation, and representative images are shown. **(C, D)** The relative expression (I-t*onB2* versus WT) in terms of -ΔΔct is shown for the putative *Anabaena* porin genes (C) and the superoxide dismutase genes (D). The Δct-value was normalized to the housekeeping gene *rnpB* (giving the Δct) and the respective Δct of the wild type (giving the ΔΔct). Average values of three independent replicates are shown, error bars indicate the standard deviation.

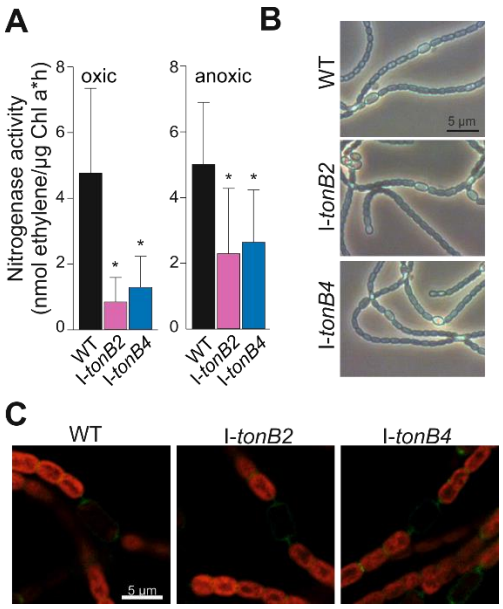

Figure 4. Heterocyst formation and nitrogenase activity in I-*tonB*2 and I-*tonB4*. (A) Nitrogenase activity was determined under oxic and anoxic conditions in the wild type (WT), I-*tonB2* and I-*tonB4*. Average values of 9 (Wild type), 4 (I-*tonB2*) and 5 (I-*tonB4*) measurements are given, and error bars represent the standard deviation. (B) Light microscopy images of cultures grown for 3 days on $BG11_0$ medium plates. (C) The peptidoglycan of cells grown for 7 days on $BG11_0$ medium plates was labelled with the fluorescent dye Vancomycin-FL that specifically binds to the cell wall (see Materials and methods for details). Fluorescence images were recoded with a confocal laser scanning microscope, a merge of the Vancomycin-FL fluorescence (green) and the Chlorophyll autofluorescence (red) is shown.

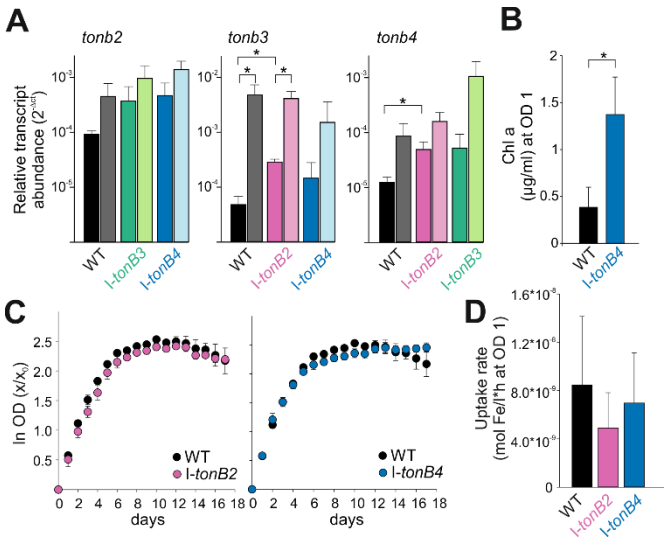

Figure 5. Gene expression, growth and siderophore transport in the *tonB*-mutants. (A) RNA isolated from wild-type and *tonB* mutant strains after growth in YBG11 medium (left brightly coloured bars in black, dark green and dark blue and pink) and after 7 days of iron-starvation (right bars with pale colours in grey, light green, light blue and rose). Gene expression was normalized to *rnpB*. Significant changes between the mutants and the wild type or the two conditions tested in one strain are marked with an asterisk (Student's *t*-test, $p<0.05$). Three independent replicates per strain were analysed, and the error bars represent the standard deviation. (B) Cultures were grown for 25 days in iron-free medium and Chl was extracted; averages of three different replicates per strain with standard deviation are shown. Asterisk indicates $p<0.05$ (Student's *t*-test). (C) Wild-type, I-*tonB2* and I-*tonB4* cultures were pre-starved, diluted afterwards to OD_{750} = 0.05 and growth was monitored. The growth of three cultures per strain was analysed; for better visualization and comparison, the wild-type values are present in both diagrams. Standard deviations are indicated. (D) Ferric schizokinen transport was measured with the wild type, I-*tonB2*

and I-*tonB4*. Average values of 8 (wild type), 7 (I-*tonB2*) and 7 (I-*tonB4*) measurements are presented, and standard deviations are given.

Tables

Table 1. Chlorophyll *a* (Chl) and carotenoid concentrations in the wild type and the *tonB* mutants. Given are the concentrations in cultures grown for seven days under high, ambient or low light (140, 70 or 15 µmol photons m^{-2} s^{-1}, respectively) in YBG11 medium. The average of four replicates and the standard deviation in given normalized to OD_{750} = 1. Values in the mutants that significantly differ from wild-type values are indicated in bold ($p<0.05$, Student's *t*-test).

	High light			Ambient light			Low light		
	Chl/OD_{750} (µg ml^{-1})	Car/OD_{750} (µg ml^{-1})	Ratio Chl:Car	Chl/OD_{750} (µg ml^{-1})	Car/OD_{750} (µg ml^{-1})	Ratio Chl:Car	Chl/OD_{750} (µg ml^{-1})	Car/OD_{750} (µg ml^{-1})	Ratio Chl:Car
Wild type	4.7±0.8	2.4±0.1	2.0	10.1±0.5	2.7±0.2	3.7	9.7±0.4	2.8±0.1	3.5
I-*tonB1*	**3.6±0.4**	**1.9±0.1**	2.0	**8.6±0.4**	2.9±0.02	**3.0**	**7.8±0.5**	**2.4±0.3**	3.3
I-*tonB2*	4.3±0.4	**3.2±0.2**	**1.4**	9.8±1.0	**3.9±0.6**	**2.5**	9.7±0.6	**4.0±0.3**	**2.5**
I-*tonB3*	3.9±0.9	1.9±0.5	2.2	**8.6±0.3**	**3.3±0.1**	**2.6**	**6.5±0.6**	2.5±0.3	**2.7**
I-*tonB4*	4.1±0.3	2.1±0.2	2.0	**7.4±0.8**	**2.1±0.3**	3.6	**8.0±0.8**	**2.2±0.3**	3.8

Table 2. Metal concentration in wild-type *Anabaena* and the mutants I-*tonB2*, I-*tonB3* and I-*tonB4* expressed as atoms per OD_{750}. The ratio of the metal content in wild type and mutants is shown. The values represent averages and standard deviation of three biological measurements. The bold letters indicate significant changes in the ratio column ($p<0.05$, student's t-test).

	*10^{13} atoms/OD				Ratio (mutant/WT)		
	WT	I-*tonB2*	I-*tonB3*	I-*tonB4*	I-*tonB2*	I-*tonB3*	I-*tonB4*
Mg	500 ± 40	410 ± 20	350 ± 40	280 ± 10	0.82	**0.70**	**0.56**
Ca	61 ± 7	70 ± 50	60 ± 20	40 ± 20	1.15	0.98	0.66
Mn	51 ± 2	17 ± 1	11 ± 1	30 ± 20	**0.33**	**0.22**	0.59
Fe	34 ± 2	35 ± 5	29 ± 3	30 ± 8	1.03	0.85	0.88
Co	1.8 ± 0.1	1.8 ± 0.1	1.2 ± 0.1	1.3 ± 0.1	1.00	**0.66**	**0.72**
Cu	5.1 ± 0.5	6.7 ± 0.6	5 ± 2	6 ± 1	**1.31**	0.98	1.18
Zn	5.4 ± 0.3	6.1 ± 0.4	5 ± 4	7 ± 3	1.13	0.93	1.29
Mo	6.4 ± 0.2	9.8 ± 0.7	7.3 ± 0.6	4.8 ± 0.4	**1.53**	1.14	**0.75**

2.3. Manuscript 3

Comparative phenotypic analysis of *Anabaena* sp. PCC 7120 mutants of porin-like genes

Status: Published in Journal of Microbiology and Biotechnology (2021), 31(5): 645-658

Contributing Authors: Hannah Schätzle, Eva-Maria Brouwer, Elisa Liebhart, Mara Stevanovic, Enrico Schleiff

Contributions:

Concept and Design	Schätzle, Hannah	50%
	Schleiff, Enrico	50%
Conducting tests and experiments	Schätzle, Hannah (Mutant generation and screening, growth analysis, microscopy, expression analysis)	40%
	Brouwer, Eva-Maria (Mutant generation and screening, density gradient analysis)	25%
	Liebhart, Elisa (Mutant generation and screening, growth analysis)	15%
	Stevanovic, Mara (Expression analysis)	20%
Compilation of data sets and figures	Schätzle, Hannah (Compilation of figures and data of mutant genotyping, expression analysis, microscopy)	60%
	Schleiff, Enrico (Compilation of figures and data of bioinformatic analysis, rate zonal centrifugation, genotyping, expression analysis)	40%
Analysis and interpretation of data	Schätzle, Hannah (Analysis and interpretation of all data generated during the study)	60%
	Schleiff, Enrico (Analysis and interpretation of all data generated during the study)	40%
Drafting of manuscript	Schätzle, Hannah	45%
	Schleiff, Enrico	45%
	Brouwer, Eva-Maria	10%

JMB Journal of Microbiology and Biotechnology

J. Microbiol. Biotechnol. 2021. 31(5): 645–658
https://doi.org/10.4014/jmb.2103.03009

Comparative Phenotypic Analysis of *Anabaena* sp. PCC 7120 Mutants of Porin-like Genes

Hannah Schätzle[1,2,3], Eva-Maria Brouwer[1#], Elisa Liebhart[1##], Mara Stevanovic[1], and Enrico Schleiff[1,2,3,4]*

[1]*Institute for Molecular Biosciences, Goethe University, Frankfurt am Main, Germany*
[2]*FIERCE, Goethe University, Frankfurt am Main, Germany*
[3]*Buchmann Institute for Molecular Life Sciences, Goethe University, Frankfurt am Main, Germany*
[4]*Frankfurt Institute of Advanced Studies, Frankfurt am Main, Germany*

Porins are essential for the viability of Gram-negative bacteria. They ensure the uptake of nutrients, can be involved in the maintenance of outer membrane integrity and define the antibiotic or drug resistance of organisms. The function and structure of porins in proteobacteria is well described, while their function in photoautotrophic cyanobacteria has not been systematically explored. We compared the domain architecture of nine putative porins in the filamentous cyanobacterium *Anabaena* sp. PCC 7120 and analyzed the seven candidates with predicted OprB-domain. Single recombinant mutants of the seven genes were created and their growth capacity under different conditions was analyzed. Most of the putative porins seem to be involved in the transport of salt and copper, as respective mutants were resistant to elevated concentrations of these substances. In turn, only the mutant of *alr2231* was less sensitive to elevated zinc concentrations, while mutants of *alr0834, alr4741* and *all4499* were resistant to high manganese concentrations. Notably the mutant of *alr4550* shows a high sensitivity against harmful compounds, which is indicative for a function related to the maintenance of outer membrane integrity. Moreover, the mutant of *all5191* exhibited a phenotype which suggests either a higher nitrate demand or an inefficient nitrogen fixation. The dependency of porin membrane insertion on Omp85 proteins was tested exemplarily for Alr4550, and an enhanced aggregation of Alr4550 was observed in two *omp85* mutants. The comparative analysis of porin mutants suggests that the proteins in parts perform distinct functions related to envelope integrity and solute uptake.

Keywords: Cyanobacteria, β-barrel proteins, Omp85 function, outer membrane biogenesis, porins

Received: March 4, 2021
Accepted: April 6, 2021

First published online:
April 9, 2021

**Corresponding author*
Phone: +49 69 798 29287
Fax: +49 69 798 29286
E-mail: Schleiff@bio.uni-frankfurt.de

[#]Current address: Eva-Maria Brouwer, University of Rostock, Albert-Einstein-Straße 3, 18059 Rostock, Germany
[##]Current address: Elisa Liebhart, Eberhard Karls University, Auf der Morgenstelle 28, 72076 Tübingen, Germany

Supplementary data for this paper are available on-line only at http://jmb.or.kr.

pISSN 1017-7825
eISSN 1738-8872

Introduction

Cyanobacteria are Gram-negative bacteria, as they possess an outer membrane (OM) that acts as diffusion barrier, a peptidoglycan mesh (PG) and a plasma membrane (PM). The cyanobacterial envelope in certain aspects differs from that of other Gram-negative heterotrophs [1]. Exemplarily the PG layer in filamentous *Anabaena* sp. strain PCC 7120 (*Anabaena* sp.) is approximately 14 nm thick, and the distance between PM and OM is about 45 nm [2]. Here, the outer membrane continuously surrounds the whole filament by not penetrating into the septum area between two cells [2]. Compared to that the PG of *E. coli* is approximately 6 nm thick and the distance between PM and OM is in the range of 20 nm [3]. The denoted dimensions of the cell envelope might be even disparate within certain cyanobacterial species, as some multicellular cyanobacteria species possess different cell types with distinct cell envelope properties.

Membrane proteins regulate transport processes across membranes and define the susceptibility of an organism against harmful compounds and antibiotics. A protein class that is highly abundant in the OM are porins. Porins are membrane embedded β-barrel proteins that allow diffusion of substrates with low or high specificities (reviewed *e.g.* in [4, 5]). Their functions are not only related to diffusion and solute transport, but porins are also crucial for outer membrane integrity including antibiotic resistance [6] or pathogenesis [4]. Porins that lack specificity are termed general or non-specific porins. They typically consist of 16β-strands and facilitate diffusion of small hydrophilic compounds [7]. In addition, substrate specific porins exist, typically composed of 18β-strands [8]. Porins with less than 16β-strands are described as well, for example the monomeric OmpG from *Escherichia coli* is composed of 14β-strands [9]. Although monomeric porins have been reported, porins most often occur as trimers [5]. Porins and other outer membrane β-barrel proteins are integrated into the OM by the β-

barrel assembly machinery [10]. An Omp85 protein constitutes the main pore of this protein complex. The N-terminal part of the Omp85 protein bears polypeptide transport-associated domains (POTRA) that recognize the non-folded membrane proteins. Moreover, the POTRA domains interact with periplasmic chaperones or other proteins involved in the insertion and folding process [11].

The freshwater cyanobacterium *Anabaena* sp. is a model organism with regard to bacterial cell differentiation, as in the absence of a combined nitrogen source specialized cells called heterocysts are formed. Heterocysts are morphologically distinct from vegetative cells, including the structure of the cell envelope [12]. They are surrounded by a polysaccharide layer that mechanically protects the underneath glycolipid layer. The prevalence of certain proteins in the outer membrane only mildly differs between vegetative cells and heterocysts [13]. Information on cyanobacterial porins is rather limited compared to proteobacteria. Cyanobacterial porins were found to be relatively large with about 30–50 kDa per monomer, whereas most proteopbacterial porin monomers have a molecular weight lower than 40 kDa [14-16]. The enlargement results from the presence of an additional cyanobacteria specific N-terminal domain [17]. This domain is related to the conserved surface layer homology (SLH) domain, which is involved in targeting and linking proteins to cell-wall associated components [18-21].

Examinations of SomA and SomB, two out of six porin-like proteins in the unicellular cyanobacterium *Synechocystis* sp. strain PCC 6803 (*Synechocystis* sp.), indicated that the permeability of organic compounds is relatively low (0.4 and 0.9 nS) [17]. Hence, it is hypothesized that *Synechocystis* sp. lacks classical porins. The major OM proteins did not allow diffusion of organic substances, whereas inorganic molecules could penetrate the pores [22]. Thus the overall permeability of the *Synechocystis* sp. OM was around 20-fold lower than that of *E. coli*. The authors claim that this might be a consequence of the photoautotrophic lifestyle of *Synechocystis* sp., which renders an import of sugars dispensable. Cyanobacteria that are living in symbiosis with plants seem to represent an exception, as the photosynthetic activity in those organisms is often diminished. In a symbiotic species of the cyanobacterium *Nostoc punctiforme* the sugar-specific porin OprB was found to be required for proper uptake of sugars [23]. Notably an OprB-type porin together with the Omp85 protein and LptD, a protein that is involved in the transfer of lipid A, was found to be globally conserved among cyanobacterial OM proteins [24]. However, there is no indication whether those porins are truly carbohydrate-selective or not. Recently it was described that in *Synechocystis* sp. the porin Slr1908 mediates the transport of inorganic iron [25]. Slr1908-like sequences were identified in many cyanobacterial species, indicating a porin-dependent iron uptake in cyanobacteria

Nine porin-like genes were assigned based on sequence alignments and amino acid sequence properties in the genome of *Anabaena* sp. [26-28], and previous analyses showed that porins might be involved in ethidium bromide and presumably erythromycin uptake in *Anabaena* sp. [29]. The central Omp85 proteins of *Anabaena* sp. are encoded by *alr0075*, *alr2269* and *alr4893*. Proteomic analyses revealed that Alr2269 is the most abundant among the three Omp85 proteins, whereas Alr4550, All4499 and Alr3608 are the most abundant among the putative porins [28].

Here, we comparatively characterize the seven genes coding porin-like proteins in *Anabaena* sp. by analyzing the transcript abundance of the genes under standard and starvation conditions. Although the function of these protein has not been biochemically characterized, for simplification and easier reading we subsequently refer to the proteins as "porins" based on the sequence and motif similarity to characterized proteins in proteobacteria. Moreover, mutants of the single porin-like genes were phenotypically analyzed in presence of high metal, salt and drug concentrations. The results indicate that the highly abundant porin Alr4550 plays an important structural role in *Anabaena* sp., since the corresponding mutant was strongly defected in OM integrity. Further, a function in the transport of manganese, zinc or cobalt is suggested for specific porins. Interestingly a mutant of *all5191* was altered in growth under diazotrophic conditions, which suggests an insufficient nitrogen fixation capacity or an enhanced nitrogen demand of the strain. Moreover, we show that Alr2269 and Alr4893 affect the membrane integration of the porin Alr4550, which was analyzed as model substrate. This implies a functional diversification of the three Omp85 proteins.

Materials and Methods

Bioinformatics

Sequences and sequence information were extracted from NCBI database [30]. Logo plots were created using the WebLogo online tool (http://weblogo.berkeley.edu/logo.cgi, [31]). The sequence alignment for determination of the sequence identities was performed with Clustal Omega [32, 33].

Generation of *Anabaena* sp. PCC 7120 Mutants

An internal fragment of the gene of interest was amplified by PCR with gene specific oligonucleotides (Table S1). BglII-sites were introduced at 5' and 3'-ends of the fragment. This fragment was inserted into BamHI-digested pCSV3 carrying a CS.3 cassette (kind gift from Prof. E. Flores, [34, 35]) yielding the final plasmid for conjugation (Table S2). Single-recombinant insertion mutants of *Anabaena* sp. were created with the triparental mating method [36-38] utilizing *E. coli* strains HB101 (gets transformed with the plasmid of interest) and ED8654 (carries the conjugative plasmid). In short the two *E. coli* strains were mixed with *Anabaena* sp. wild type, and the plasmid of interest bearing a homolog region to the gene of interest is transferred to *Anabaena* sp. by conjugation. A single recombination event happens where the whole plasmid bearing the homolog region gets integrated into the genome, resulting in cells that are resistant towards spectinomycin and streptomycin.

The genotype of the exconjugants was tested by PCR utilizing oligonucleotides that anneal outside of the internal homologous fragment in combination with a vector-specific oligonucleotide (Table S1). The mutant strains are listed in Table S3.

Phenotypic Analysis of the Porin Mutants

Anabaena sp. strains were stored on BG11 plates [39] with 1% (w/v) bacto-agar (BD Biosciences) until use. For expression analysis by qRT-PCR *Anabaena* sp. wild type and mutants were grown in buffered liquid YBG11 medium [40]. In case of mutants the medium was supplemented with 5 μg ml^{-1} spectinomycin dihydrochloride pentahydrate (Duchefa Biochemie) and streptomycin sulfate (Roth).

For the phenotyping on plates, cultures were washed and suspended at a final concentration OD_{750nm}=1. 5 μl of the non-diluted suspension and of a 1:10 dilution was spotted onto YBG11 plates containing given amounts of supplements or on $YBG11_0$ plates ($YBG11_0$: YBG11 medium without $NaNO_3$). Plates were incubated under constant illumination (70 μmol photons m^{-2} s^{-1}) at 28-29°C for 7 days. Each spotting assay was repeated with independent cultures at least three times. Representative images are shown in the results. All strains depicted in one line were grown on the same plate.

Microscopy

Light microscope images were taken with Olympus CKX41 using a 40x objective and a Thorlabs DCC1645C-HQ camera. Heterocysts were stained with alcian blue to improve visibility. A*nabaena* sp. suspension was mixed in a 1:1 ratio with the alcian blue staining solution (0.5% alcian blue in 50% ethanol, [41]) and incubated for 5 min. After three washing steps with $YBG11_0$ medium (centrifugation at 1500 *g*, 5 min) filaments were inspected under the microscope.

RNA Isolation and qRT-PCR Analysis

RNA isolation, cDNA synthesis and qRT-PCR with the corresponding oligonucleotides (Table S1) was performed as previously described [42]. Three independent wild-type and mutant cultures grown for 5 days were used for RNA isolation, while for starvation experiments three week-old cultures were used. qRT-PCR was performed on cDNA from three biological replicates. The Ct values for the genes were normalized to Ct values of the *rnpB* transcript in the corresponding sample, yielding the ΔCt. For the calculation of the ΔΔCt-value the ΔCt for each sample was normalized to the ΔCt of wild type grown under control conditions [43].

Membrane Isolation and Rate Zonal Centrifugation

OM from *Anabaena* sp. was isolated as described [30] with slight modifications. *Anabaena* sp. cultures were grown in BG11 to exponential growth phase, 500 ml were harvested and washed with 5 mM 4-(2-hydroxyethyl)-1-piperazineethanesulfonic acid (HEPES), pH 7.6 supplemented with 1 mM phenylmethylsulfonyl fluoride (PMSF). Cell lysis and harvesting of membrane fractions was performed as described [30]. The membrane fraction was resuspended in 30 % sucrose containing 20 mM HEPES, pH 7.6 and 0.2 mM PMSF. It was layered on top of a 55% (w/v) sucrose cushion. The OM was sedimented by centrifugation (130,000 ×*g*, 16 h, 4°C). The OM pellet was washed with 20 mM HEPES, pH 7.6 supplemented with 0.2 mM PMSF and collected by centrifugation (130,000 ×*g*, 1 h, 4°C). Membranes were resuspended in 20 mM HEPES, pH 7.6 with 0.2 mM PMSF and stored at -80°C.

100 μg protein of the membrane fraction was loaded on top of a linear sucrose gradient (10 to 70%; w/v) and centrifuged (100,000 ×*g*, 16 h, 4°C). The gradient was fractionated into ten fractions of 1 ml. Proteins were precipitated with 0.02% (w/v) Na-deoxycholate and 15% (v/v) trichloroacetic acid. Precipitates were resolved in 6-fold SDS-Urea loading buffer containing 200 mM Tris HCl pH 6.8; 8M Urea; 0.1 mM ethylenediaminetetraacetic acid (EDTA); 5% sodium dodecyl sulfate (SDS) and 0.03% bromophenol blue and subjected to SDS-PAGE followed by immunoblotting. Blotting membranes were stained with direct blue 71 (DB71) as described [44].

For total protein extract 1 ml of exponential phase culture was harvested by centrifugation (10,000 ×*g*, 5 min) and the pellet was resuspended in 6-fold SDS-Urea loading buffer (recipe given above). Samples were incubated at 42°C for 5 min and centrifuged afterwards to pellet insoluble cell debris, the supernatant was used for SDS PAGE.

Antibodies against the peptides specific for Alr4450 were generated by Peptide Specialty Laboratories (Germany) and previously described [45], the following peptides were used: Peptide 1: ASGQGLQTFQVGSTGNNC, Peptide 2: PITEDTKVIDQVNRYSNEGKGNAQ. Antibodies against Alr2269 and Tic22 have also been previously described [30,46].

Inductively Coupled Plasma Mass Spectrometry (ICP-MS)

The intracellular metal concentration of *Anabaena* sp. wild type grown for seven days in YBG11 medium was analysed. The procedure was adapted [47] with modifications. The cells were sedimented by centrifugation (3,000 g, 10 min) and subsequently washed twice with 20 mM 2-(N-morpholino)ethanesulfonic acid (pH 5) and 10 mM EDTA. The final pellet was resuspended in double-distilled water (ddH_2O). For normalization the OD_{750} was determined and the cells were counted using a Helber bacteria counting chamber (Hawksley). From here on experiments were conducted in a metal clean laboratory. 1 ml of each sample was incubated at 120°C in 7 M HNO_3 overnight until dryness. Before measurement, the samples were resolved in 5% HNO_3. As controls, samples of ddH_2O and cultivation medium were analysed. Glassware used during the experiment was incubated in 4% HNO_3 overnight prior to use.

Results

Seven Proteins in *Anabaena* sp. Contain a Porin-like Domain Architecture

In previous studies, the nine putative porin-candidates *alr0834*, *alr2231*, *all4499*, *alr4550*, *alr4741*, *all5191*, *all7614*, *alr3917* and *alr3608* were identified in the *Anabaena* sp. genome [30, 48]. In addition, All3289 and

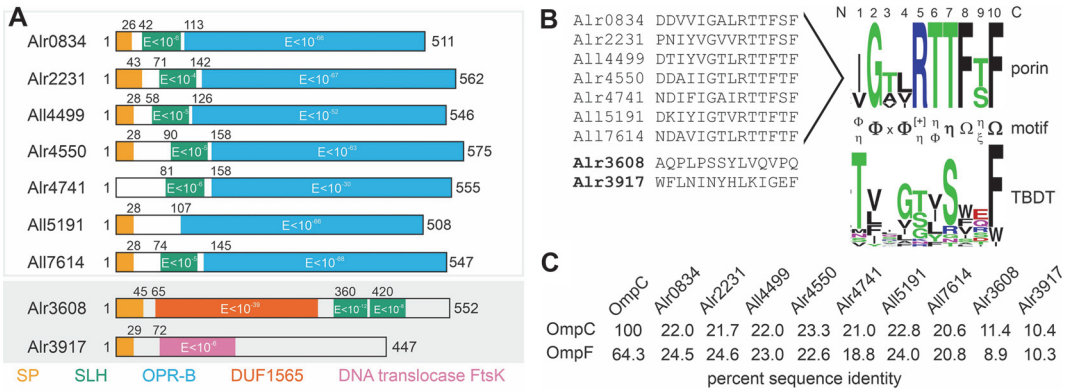

Fig. 1. Domain structure of the putative porins in *Anabaena* sp. PCC 7120. (**A**) Shown is the domain structure of the nine predicted porins highlighting the signal peptide (SP, orange; predicted with Signal P 5.0), the SLH domain (green, extracted from the CCD server, the E-value for prediction is given), the OPR-B domain (blue), the Domain of unknown function 1565 (red) and the provisional DNA translocase FtsK domain fragment (purple). (**B**) The last 14 C-terminal amino acids of the predicted porins are shown in the alignment. The LOGO plot for the seven proteins with OPR-B domain and for the predicted 22 TBDTs is shown. The motif of the last β-strand found in the putative porins and the TBDTs is highlighted with the following nomenclature: Ω aromatic amino acids, η hydroxylated amino acids, Φ hydrophobic/small amino acids, ξ hydrophilic amino acids, [+] positively charged amino acids, x any amino acid. (**C**) The amino acid sequence of the indicated proteins was aligned and the percent identity is shown.

Alr5049 were assigned as OmpA-like proteins [48]. OmpA-type porins are thought to perform structural functions related to membrane integrity [8, 49]. However, *all3289* codes for a protein with 1289 amino acids. The C-terminal region might form an OM anchor for the large soluble domain that contains characteristics of glycoproteins. Hence, we suggest that this protein should not be considered as typical OmpA. In turn, *alr5049* codes for a protein with 169 amino acids lacking the characteristic domains of an OmpA [48]. Thus, based on the small size, the absence of domains characteristic for OmpA proteins and considering that the outer membrane localization can be confirmed in future, the protein might represent a functional OmpX [50].

Seven of the nine putative porins (Alr0834, Alr2231, All4499, Alr4550, Alr4741, All7614, Alr3608) contain an S-layer homology domain (SLH) which is also found in other cyanobacterial porins [19]. In Alr3608, the two predicted SLH-domains are located in the C-terminal region, whereas in other porins they are found in the N-terminal part of the protein (Fig. 1A). Moreover, seven of the putative porin proteins contain an OPR-B domain that is characteristic for carbohydrate-selective porins (Fig. 1A). This domain could not be identified in Alr3608 and Alr3917. In turn, a domain of unknown function (DUF) and a short region characteristic for a DNA translocase FtsK were identified in Alr3608 and Alr3917, respectively. However, a BLAST search with the Alr3917 sequence against cyanobacterial genomes in the NCBI-database did not yield a similarity to cyanobacterial FtsK sequences. Notably, *Anabaena* sp. FtsK is encoded by *all7666*.

The comparison of the amino acid sequence of the last β-strand in the seven porins with OPR-B fold shows a high degree of conservation, while Alr3608 and Alr3917 are somewhat distinct (Fig. 1B). It is proposed that the most C-terminal region of proteobacterial outer membrane proteins with β-barrel fold contains the signal for membrane insertion and Omp85 interaction [51-54]. In addition, the so called β-signal initiates the association with Omp85 (BamA; [55, 56]). The comparison of the identified motif to that of the 22 TonB-dependent transporters (TBDT) in the outer membrane uncovers a common motif in the last β-strand: hydrophobic/small amino acid (Φ) – x – Φ – x – hydroxylated/ hydrophobic/small amino acids (Φ/η) – x – aromatic amino acids (Ω) – x – Ω. This motif might be important for the insertion of the proteins into the outer membrane, as it was reported that an aromatic amino acid at the last position of the sequence is important for proteobacterial outer membrane protein insertion [53]. In addition, the insertion of mitochondrial β-barrel proteins depends on a hydrophobic signal in the last strand as well [57]. Comparison of the amino acid sequence of the seven porin-like proteins to the amino acid sequence of the two most abundant *E. coli* porins, namely OmpC and OmpF [5], yielded a sequence identity between 18.8% to 24.6% (Fig. 1C). This indicates that the cyanobacterial proteins do not share a high sequence similarity to proteobacteriual porins.

In summary, the bioinformatics inspection revealed that seven out of the nine predicted porins in *Anabaena* sp. contain a domain architecture consistent with a porin-like function, although no secretion signal was predicted for Alr4741. The other two proteins previously assigned to the porin-like family (Alr3608, Alr3917) contain a domain architecture that is rather atypical for porins. As it is questionable whether these two proteins constitute porins, they were excluded from the subsequent analyses.

Genotyping of Porin Mutants and Growth under Standard Conditions

In order to assess specific mutant phenotypes, single-recombinant mutants were created by integration of a plasmid bearing the CS.3 cassette into the porin genes. Five mutants had the plasmid insertion in forward

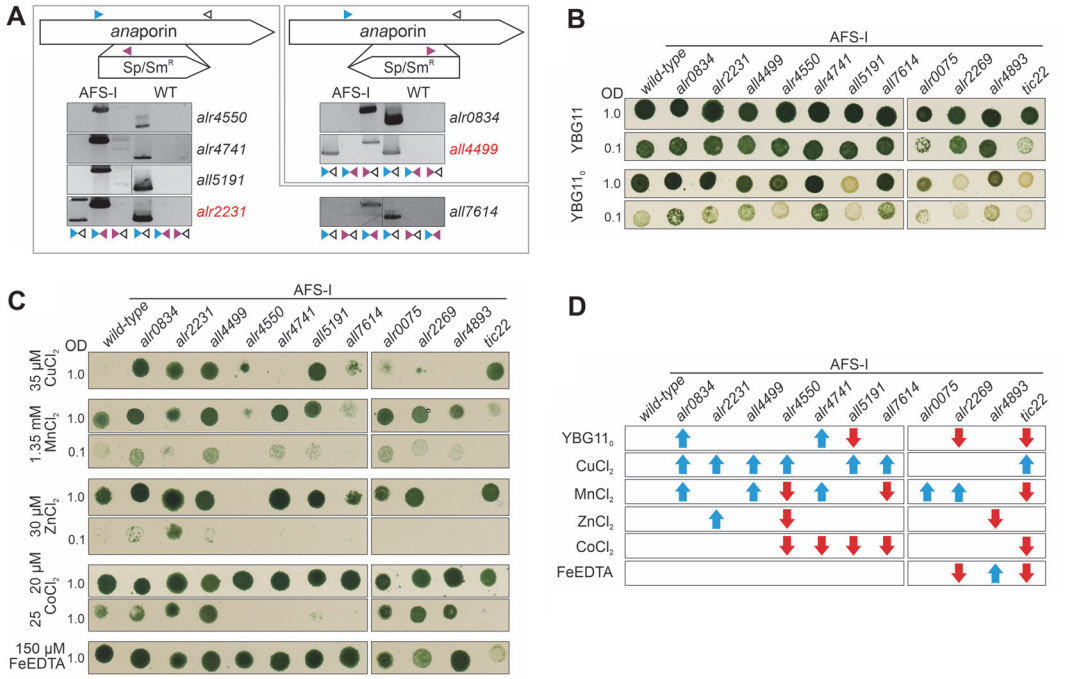

Fig. 2. Metal sensitivity of porin mutants. (**A**) Genotype of the porin-insertion mutants. The orientation of the cassette (on top) and annealing position of oligonucleotides (colored arrowheads) are indicated. Panels show PCR products on gDNA of mutant strains (lane 1–3; AFS-I) or wild type (lane 4–6; WT) using the gene specific forward (blue) or reverse (black), or the plasmid specific oligonucleotide (magenta) as indicated. Mutants that are not segregated because a wild type gene fragment could be amplified are highlighted in red. (**B**, **C**) 5 µl of wild type and mutant strains (names on top) at OD_{750} = 1.0 (or 0.1 if indicated) were spotted on plates of YBG11 (**B**), $YBG11_0$ (**B**) or YBG11 containing indicated concentrations of divalent metals (**C**). Representative images after 7 days of growth are shown, the test was conducted three times. (**D**) The increased (blue arrow) or decreased (red arrow) growth capacity of a mutant strains on $YBG11_0$ or YBG11 with the indicated ingredient in comparison to wild type is presented as model.

direction, while the plasmid was inserted in the opposite direction into *alr0834* and *all4499* loci (Fig. 2A). Mutants of *all4499* and *alr2231* were not segregated, as wild-type copies of the genes were present after repeatedly diluting the cultures on medium containing antibiotics (Fig. 2A, first lane). This might indicate an essential function of the two gene products under the given conditions. For all other genes, segregated mutants were obtained.

The growth behavior of the porin mutants was compared to wild type. In addition, mutants exhibiting alterations in outer membrane integrity, bearing either an insertion in *Anabaena* sp. *omp85* genes (AFS-I-*alr0075*, AFS-I-*alr2269* and AFS-I-*alr4893;* AFS stands for *Anabaena* mutant created in Frankfurt by the Schleiff group*)* [58] or the *tic22* gene (AFS-I-*tic22, alr0114*, [45, 46, 59]) were used as additional controls. As reported before, AFS-I-*alr0075,* AFS-I-*alr2269* and AFS-I-*alr4893* could not be segregated since wild-type copies could be amplified even after exposing the strains to increased concentrations of antibiotics [58] (Fig. S1).

On standard YBG11 plates only AFS-I-*alr0075* and AFS-I-*tic22* grew to a lower density compared to wild type (Fig. 2B, first and second panel). This behavior was not described before [45, 46, 59] as the effect was only visible when the culture was sufficiently diluted (Fig. 2B, second panel). However, the strains with plasmid insertion in the porin-like genes did not show any phenotype under this condition (Fig. 2B).

The Mutants of Three Porin-Like Genes Are Affected in Growth in Absence of Combined Nitrogen

On plates without a combined nitrogen source ($YBG11_0$), a condition where *Anabaena* sp. fixes atmospheric nitrogen in heterocysts, AFS-I-*alr2269* and AFS-I-*tic22,* but not AFS-I-*alr0075* and AFS-I-*alr4893* were impaired in growth (Fig. 2B, third panel) as previously reported [46]. With respect to the with respect to the porin mutants, AFS-I-*all5191* grew to a lower density than wild type on $YBG11_0$ plates (Fig. 2B, third panel). In addition, AFS-I-*alr4741* and AFS-I-*alr0834* grew to slightly higher densities under diazotrophic conditions compared to wild type.

Consequently, filaments of wild type, AFS-I-*alr0834*, AFS-I-*alr4741* and AFS-I-*all5191* grown in YBG11 or $YBG11_0$ were microscopically inspected. In standard YBG11 medium the filaments of all strains appeared morphologically comparable to wild-type cells (Fig. 3, $+NO_3$). Heterocysts were not detected in the mutant and wild-type strains grown in the presence of nitrate. After a seven-day cultivation in $YBG11_0$ medium heterocysts were visible in wild type, AFS-I-*alr0834*, AFS-I-*alr4741* and AFS-I-*all5191* (Fig. 3, $-NO_3$). Thus the defective growth of AFS-I-*all5191* is not due to an inability of this strain to differentiate heterocysts. Though, since in general the cells of AFS-I-*all5191* looked comparatively pale in the absence of nitrate (Fig. 2B), we assume that

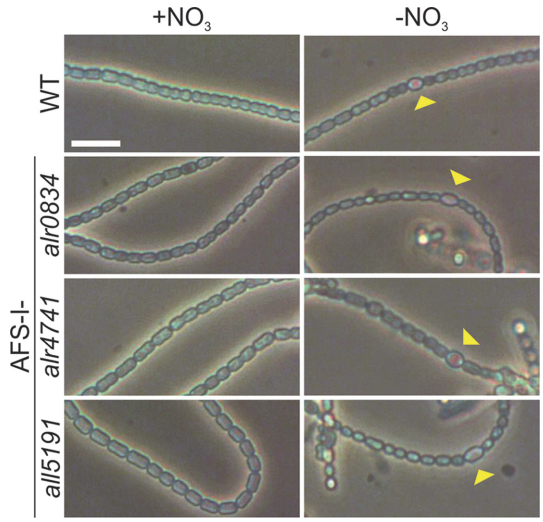

Fig. 3. Filaments of wild type (WT) and the three mutant strains AFS-I-*alr0834*, AFS-I-*alr4741* and AFS-I-*all5191*. Strains were grown in the presence or absence of nitrate (YBG11 and YBG11$_0$, respectively). Heterocysts observed in absence of nitrate are marked with a yellow arrowhead. The reference bar indicates 5 μm.

nitrogen fixation might not work properly in this strain.

The heterocyst pattern was determined by counting the vegetative cells between two heterocysts in the three strains and significance of the difference to wild type was assessed with Student's t-test. In AFS-I-*alr0834* and AFS-I-*alr4741* on average 16.2 ± 4.6 and 16.7 ± 4.7 vegetative cells were found between two heterocysts respectively (>1500 cells were counted for each strain). Hence there was no significant difference compared to wild type, where on average 15.4 ± 6.4 vegetative cells existed between heterocysts (n > 600 cells). In AFS-I-*all5191* however on average 11.8 ± 4.6 vegetative cells were found between two heterocysts (n > 1200 cells) after 7 days of growth without nitrate, which significantly differs from the wild type (Student's t-test $p = 4.3 \times 10^{-6}$). This suggests a necessity of AFS-I-*all5191* to increase the relative number of heterocysts per filament to compensate for either an inefficient nitrogen fixation or an increased demand of the strain.

Most of the Genes Coding for Porin-like Proteins are Upregulated by Metal Starvation

The regulation of porin-mediated solute diffusion in bacteria is governed by distinct parameters. For instance, the extracellular nutrient supply status and the osmolarity might trigger transcriptional responses [60]. *Anabaena* sp. performs photosynthesis and is therefore not obligatorily dependent on sugar uptake. Thus, the potential changes in gene expression of porins in response to altered metal concentrations in the growth medium were examined. For this, *Anabaena* sp. wild type was grown in YBG11 with modified metal concentrations by omitting either manganese (Mn), iron (Fe), zinc (Zn) or copper (Cu) from the medium. These metals were used since *Anabaena* sp. accumulates $(5.0 \pm 0.3) \times 10^{14}$ atoms Mn in cells equivalent to 1 ml culture at $OD_{750} = 1$, $(0.5 \pm 0.05) \times 10^{14}$ atoms Cu/1 ml ($OD_{750} = 1$) and $(0.5 \pm 0.03) \times 10^{14}$ atoms Zn/1 ml ($OD_{750} = 1$) as determined by ICP-MS. By that, the cellular concentration of these metals is in the similar range to that of iron ($(3.4 \pm 0.2) \times 10^{14}$ atoms Fe/1 ml ($OD_{750} = 1$)), which is considered to be a limiting factor for cyanobacterial growth and is especially important for N_2-fixing cyanobacteria [61, 62].

Thus, RNA was isolated from wild-type cells grown for 21 days in the indicated media (Table 1) and qRT-PCR

Table 1. qRT-PCR analysis of expression of porin genes.

	Anabaena sp. PCC 7120				
	YBG11	YBG11$_{-Mn}$	YBG11$_{-Fe}$	YBG11$_{-Cu}$	YBG11$_{-Zn}$
	-ΔCt	-ΔΔCt	-ΔΔCt	-ΔΔCt	-ΔΔCt
alr0834	-10.8 ± 0.3	**1.7 ± 0.1**	**1.6 ± 0.1**	0.1 ± 0.2	0.8 ± 0.1
alr2231	-12.3 ± 0.3	**1.9 ± 0.1**	0.0 ± 0.1	0.5 ± 0.3	0.9 ± 0.1
all4499	-9.4 ± 0.2	0.5 ± 0.1	**1.4 ± 0.2**	-0.6 ± 0.2	0.2 ± 0.2
alr4550	-6.4 ± 0.1	-0.5 ± 0.1	***-3.5 ± 0.2***	***-3.3 ± 0.2***	***-2.8 ± 0.2***
alr4714	-11.5 ± 0.4	**1.3 ± 0.2**	0.2 ± 0.2	-0.3 ± 0.2	0.6 ± 0.2
all5191	-12.1 ± 0.5	**1.8 ± 0.1**	**1.1 ± 0.1**	0.0 ± 0.2	**1.7 ± 0.1**
all7614	-8.3 ± 0.2	0.3 ± 0.1	-0.5 ± 0.1	-0.8 ± 0.2	-0.3 ± 0.1

The -ΔCt value based on the housekeeping gene *rnpB* is given for YBG11 and the -ΔΔCt based on the YBG11 values is shown for the treatments, the standard deviation is indicated. Values in bold represent changes with $p < 0.05$ (Student's *t*-test) and an absolute fold-change higher or lower (italics) than one.

was performed on cDNA. The high transcript abundance of *alr4550* in standard YBG11 medium corresponds to proteomic analyses in which Alr4550 and All4499 were identified as the highest abundant porins in the OM of *Anabaena* sp. [30].

The mRNA abundance of *all7614* was not affected after 21 days of culturing wild type in media lacking either manganese, iron, copper or zinc (Table 1). Manganese deprivation resulted in an increase of the transcripts of *alr0834, alr2231, alr4741* and *all5191* when compared to YBG11 (Table 1). The transcript of *alr0834* was further increased under iron limitation, whereas the transcript of *all5191* was increased under iron and zinc limitation. Moreover, iron deprivation yielded in an elevated *all4499* transcript level when compared to cultivation in YBG11.

Notably *alr4550* demonstrated an exceptional behavior. On the one hand, it is highly expressed in YBG11 when normalized to *rnpB*. On the other hand, among all tested genes, only *alr4550* transcripts decreased in medium lacking Fe, Cu or Zn (Table 1). Only Mn deprivation did not significantly alter *alr4550* transcript levels (Table 1).

In conclusion, the expression of the genes coding for the seven porin-like proteins does not show a common regulation after 21 days in media without individual trace metals. This might indicate distinct functions of the analyzed proteins. Altogether, manganese and iron depletion resulted in increased abundance of four and three transcripts, respectively. Zn depletion led to enhanced mRNA levels of only *all5191*.

The Mutants of Porin-like Genes Show a Differential Sensitivity to Divalent Metal Stress

The sensitivity against elevated metal concentrations was tested with the porin mutants, as it is expected that strains with defected transport capacities of certain substrates display hyper-resistance towards increased concentrations of these substrates. Interestingly, virtually all mutant strains except AFS-I-*alr4741* exhibited a resistance towards elevated copper concentrations (35 µM) compared to the wild type. AFS-I-*alr4550* and AFS-I-*all7614* grew to a slightly lower density under those conditions compared to the other mutant strains (Fig. 2C, first panel). Also, the growth of the two *omp85* mutants, AFS-I-*alr2269* and AFS-I-*alr4893,* was inhibited under elevated copper concentrations, while AFS-I-*alr0075* grew to a lower density (Fig. 2C, first panel). Thus, the *omp85* mutants exhibited a similar sensitivity against the selected copper concentration compared to wild type, while AFS-I-*tic22* showed an enhanced resistance. It can be concluded that copper entry into the porin mutants is largely limited compared to wild type. Notably, none of the porin transcripts was increased after copper depletion, leading to the assumption that this effect might not be specifically related to a single porin (Table 1).

On plates with an excess of manganese (1.35 mM $MnCl_2$; Fig. 2C, second & third panel) AFS-I-*alr4550* and AFS-I-*all7614* grew to lower densities when compared to wild type, while AFS-I-*alr0834,* AFS-I-*all4499* and AFS-I-*alr4714* appeared to be more resistant as they grew to higher densities. AFS-I-*alr0075* and AFS-I-*alr2269* were more resistant than wild type, while AFS-I-*tic22* showed a higher sensitivity (Fig. 2C, second & third panel). Interestingly AFS-I-*alr2231* grew better than wild type when the zinc concentration was enhanced (Fig. 2C, fifth panel). With respect to the control strains, only AFS-I-*alr4893* was hyper-sensitive towards this zinc concentration (Fig. 2C, fourth panel).

In addition to the mentioned divalent metals, the growth in the presence of enhanced cobalt concentrations was determined as well. The ICP-MS measurements showed that cobalt was about ten-fold less abundant in cells then the other metals ($(1.79 \pm 0.04) \times 10^{13}$ atoms Co/1 ml ($OD_{750} = 1$)). AFS-I-*alr4550*, AFS-I-*alr4741*, AFS-I-*all5191* and AFS-I-*all7614* were hypersensitive towards 25 µM $CoCl_2$ (Fig. 2C, seventh panel), but not towards 20 µM $CoCl_2$ (Fig. 2C, sixth panel). Notably AFS-I-*tic22* was already reduced in growth when 20 µM $CoCl_2$ was present (Fig. 2C, sixth panel). On plates with an excess iron (150 µM $FeCl_2$-EDTA) no clear phenotype could be observed for any of the tested porin mutants, while AFS-I-*alr2269* and AFS-I-*tic22* were more sensitive to the elevated iron levels than wild type (Fig. 2C, eighth panel).

Taken together most porin mutants were more resistant to enhanced copper concentrations when compared to wild type, while their behavior in response to enhanced iron levels was comparable to wild type (Fig. 2D). In *Anabaena* sp. ferric iron chelates typically get transported by TBDTs, however the expression of the siderophore transport system gets triggered mainly under starvation conditions [63]. It is hypothesized that soluble iron diffuses through porins under replete conditions, as shown for the unicellular cyanobacterium *Synechocystis* sp. [27]. Remarkably, only AFS-I-*alr2231* was more resistant towards high zinc concentrations, which might lead to the assumption that Alr2231 facilitates zinc transport. To support this conclusion, the expression of other porins

Table 2. qRT-PCR analysis of porin genes in individual porin mutants.

	AFS-I-			
	alr0834	*alr2231*	*all4499*	*alr4741*
	-ΔΔCt			
alr0834	n.d.	**1.8 ± 0.4**	**4.4 ± 0.5**	0.9 ± 0.4
alr2231	0.7 ± 0.3	n.d.	0.9 ± 0.5	**2.8 ± 0.5**
all4499	-0.2 ± 0.1	**3.3 ± 0.4**	n.d.	0.2 ± 0.2
alr4550	**-1.5 ± 0.2**	**2.0 ± 0.4**	0.7 ± 0.3	-0.3 ± 0.1
alr4741	-0.1 ± 0.2	**2.5 ± 0.3**	0.0 ± 0.5	n.d.
all5191	**1.0 ± 0.1**	**2.2 ± 0.3**	0.7 ± 0.4	**1.3 ± 0.3**
all7614	**-2.5 ± 0.1**	**1.6 ± 0.4**	0.5 ± 0.2	0.1 ± 0.2

The -ΔΔCt based on the *rnpB* expression and BG11 values are shown for the mutants. Values in bold are changes with $p < 0.05$ (Student's t-test) compared to wild type.

in this mutant strain was analyzed. Interestingly, the transcript abundance of all other porin-coding genes was increased in this mutant (Table 2). This strengthens the hypothesis that zinc resistance is mediated by *alr2231*-insertion and not by the diminished transcription of another putative porin gene.

In addition, in the presence of enhanced concentrations of manganese, the mutants of *alr0834, all4499* and *alr4741* were more resistant than wild type. Interestingly, *all4499* was comparatively high expressed under standard conditions and the transcript abundance did not change after manganese deprivation. However, the expression of *alr0834* and *alr4741* was upregulated in the absence of manganese (Table 1). Analyzing the transcript abundance of the other porins in the respective mutants revealed a downregulation of *alr4550* and *all7614* expression in AFS-I-*alr0834* (Table 2). The mutants of *alr4550* and *all7614* were the only strains showing a hypersensitivity towards an elevated manganese concentration. Therefore, this downregulation does not explain the manganese resistance of AFS-I-*alr0834*. In AFS-I-*all4499* and AFS-I-*alr4741* no other gene coding for a porin-like protein was found to be downregulated (Table 2). Thus, the resistance of AFS-I-*all4499* and AFS-I-*alr4741* against elevated manganese can be attributed to the mutated gene.

The Mutant of *alr4550* Shows a Reduced Integrity of the Outer Membrane

Next, the integrity of the outer envelope was analyzed in the porin mutants. To this end, lysozyme that catalyzes peptidoglycan hydrolysis was added to the medium (Fig. 4A, first panel). AFS-I-*alr4550*, and AFS-I-*tic22* were hampered in growth in presence of 250 µg ml^{-1} lysozyme when compared to wild type. For AFS-I-*tic22*, this is in line with earlier findings [46]. In turn, AFS-I-*alr0075* grew similar to wild type, while all other porin mutants showed an improved growth compared to wild type. This was observed as well for the *omp85* mutants AFS-I-*alr2269* and AFS-I-*alr4893*. On plates containing 10 µg ml^{-1} SDS, the porin mutants followed a comparative trend as in presence of lysozyme; the porin mutants grew somewhat better than wild type, which in turn did grow better as in presence of lysozyme (Fig. 4A, second panel). Here AFS-I-*alr4550* did grow, but only to a low density. The mutants AFS-I-*alr2269* and AFS-I-*tic22* were inhibited in growth in the presence of SDS, while AFS-I-*alr4893* was less affected than wild type. In the presence of 50 µg ml^{-1} proteinase K the porin mutants behaved again similar as in the presence of lysozyme, while only AFS-I-*all7614* behaved similar to wild type (Fig. 4A, third panel). AFS-I-*alr0075* and AFS-I-*tic22* were inhibited in growth in presence of proteinase K. Instead, AFS-I-*alr2269* growth was comparable to wild type and AFS-I-*alr4893* grew better than wild type. In presence of the antibiotic erythromycin again all porin mutants except AFS-I-*alr4550* showed an enhanced growth compared to wild type (Fig. 4A, fourth panel), with the exception of AFS-I-*alr2269* which exhibited growth inhibition.

Next, the cells were grown under salt stress, which is known to alter the abundance of porins [64]. In the presence of 100 mM KCl a similar growth of the porin mutants as in the presence of proteinase K was observed, while the growth of the *omp85* mutants was enhanced. Growth of AFS-I-*tic22* on the other hand was severely affected (Fig. 4A, fifth panel). The addition of 100 mM NaCl reduced the growth of AFS-I-*alr4550*, AFS-I-*all7614* and AFS-I-*tic22* when compared to wild type (Fig. 4A, sixth panel). When 150 mM NaCl was added, wild type, AFS-I-*alr4550*, AFS-I-*all7614*, AFS-I-*alr2269* and AFS-I-*tic22* were defective in growth, while AFS-I-*alr0834*, AFS-I-*alr2231*, AFS-I-*all4499*, AFS-I-*alr4714*, AFS-I-*all5191*, AFS-I-*alr0075* and AFS-I-*alr4893* were able to grow on this medium (Fig. 4A, seventh panel).

Our results demonstrate that the mutants of five porin-like genes (*alr0834, alr2231, all4499, alr4741* and *all5191*) were more resistant towards the selected compounds, which is indicative for alterations in the outer membrane integrity. AFS-I-*tic22* for instance, a previously characterized mutant with alterations in OM biogenesis, exhibited severe growth defects (Fig. 4). In contrast, mutation of the highest expressed porin-like gene *alr4550* causes a phenotype that is consistent with an impaired outer membrane integrity in general (Figs. 2 and 4). AFS-I-*all7614* showed an intermediate phenotype. On the one hand, the strain was sensitive to divalent metals and sodium chloride (Figs. 2 and 4), on the other hand the mutant presented a higher resistance to SDS and lysozyme.

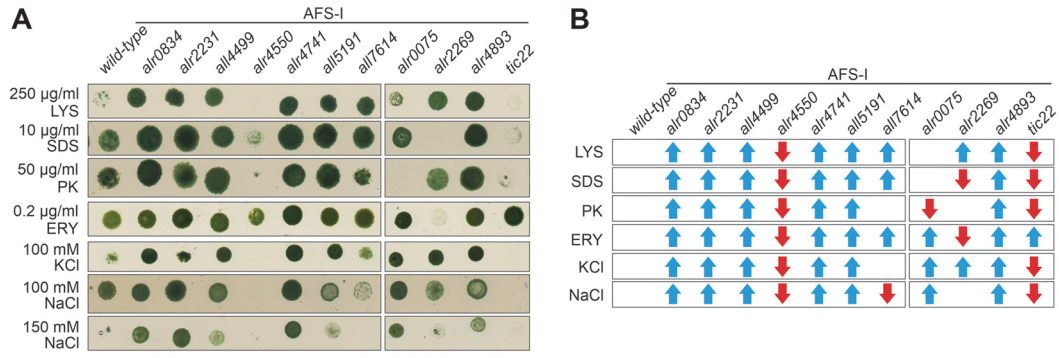

Fig. 4. Outer membrane integrity of porin mutants. (**A**) 5 µl of wild type, the porin, the *omp85* and the *tic22* insertion mutants (indicated on top) at OD_{750} = 1.0 were spotted onto media composed of YBG11 supplemented with indicated divalent metals. Images were taken after 7 days of growth. Representative results (n = 3) are shown. (**B**) The increased (blue arrow) or decreased (red arrow) growth capacity of a mutant strain on YBG11 with the indicated ingredient in comparison to wild type is indicated. LYS = lysozyme, SDS = sodium dodecyl sulfate, PK = proteinase K, ERY = erythromycin.

Table 3. qRT-PCR analysis of expression of porin genes in *omp85* mutants.

	AFS-I-		
	alr0075	*alr2269*	*alr4893*
		-ΔΔC	
alr0834	-1.2 ± 0.6	**-2.2 ± 0.1**	-0.2 ± 0.1
alr2231	-0.7 ± 0.1	-2.5 ± 2.1	0.2 ± 0.1
all4499	**-2.1 ± 0.6**	0.0 ± 0.1	0.3 ± 0.1
alr4550	-1.8 ± 1.2	0.7 ± 0.3	**2.0 ± 0.3**
alr4741	0.2 ± 0.1	0.5 ± 0.3	**1.4 ± 0.3**
all5191	**-2.3 ± 0.7**	**-2.3 ± 0.1**	-0.8 ± 0.5
all7614	-1.5 ± 0.9	**1.5 ± 0.1**	**-13 ± 11**

The -ΔΔC based on *rnpB* expression and BG11 values is shown for the mutants. Values in bold are changes with $p < 0.05$ (Student's t-test) compared to wild type.

Omp85 Proteins are Distinct in Their Function In Porin Biogenesis

Altogether these results can be seen as first hint towards a putative functional relation between the Omp85 protein Alr4893 and most of the porins, as the mutant phenotypes were consistent under many conditions (Figs. 2 and 4). In order to assess the influence of the *omp85* gene mutations on the porins, the expression of the putative porin-coding genes was analyzed in the three *omp85* mutants (Table 3). In AFS-I-*alr0075* a reduction of the transcripts of *all4499* and *all5191* was observed. In AFS-I-*alr2269* a reduction in transcript abundance of *alr0834* and *all5191* was detected, while the abundance of *all7614* was enhanced (Table 3). In turn, the transcript abundance of *all7614* was strongly reduced in AFS-I-*alr4893*, while the transcript levels of *alr4550* and *alr4741* were increased. The mRNA levels of *alr2231* were not affected by the mutation of *omp85* genes.

To determine the importance of the Omp85 protein function for porin-insertion into the outer membrane, the protein abundance of a porin was examined in wild type and the *omp85* mutants. As Alr4550 was found to be the most abundant protein component of the *Anabaena* sp. outer membrane [30] the abundance of this protein was tested. Total protein was extracted from wild type, AFS-I-*alr0075*, AFS-I-*alr2269* and AFS-I-*alr4893*. The

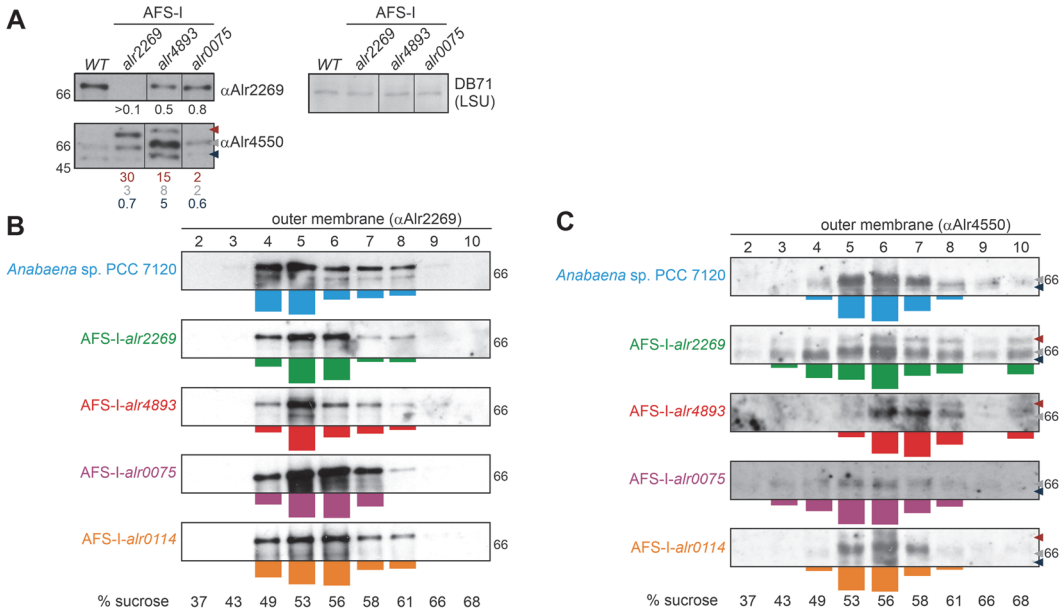

Fig. 5. Relation between Omp85 function and porin biogenesis. (**A**) A representative result ($n = 3$) for the outer membrane protein content in wild type (first lane) and the three indicated *omp85* mutants (lane 2-4) is shown. Total protein extract was probed with specific antibodies against Alr2269 or Alr4550 as indicated. DB71 staining of the large subunit of Rubisco (LSU) was used as loading control. The average of the ratio of the protein density in mutants and wild type is shown as analyzed with ImageJ. The standard deviation is smaller than 25%. All lanes come from the same gel and have been developed simultaneously. (**B**, **C**) Outer membrane vesicles were isolated from the indicated strains and subjected to rate zonal ultracentrifugation. Fractions 2-10 of the sucrose gradient (25% to 70% (v/w)) were probed with an antibody against Alr2269 (**B**) or Alr4550 (**C**). Note: in B the result for AFS-I-*alr2269* was longer exposed than other blots to visualize the bands. In (**B**) and (**C**) one of two repetitions is shown. The densitometric protein distribution of both experiments normalized to the highest intensity is shown on the bottom of each panel as bar diagram. In (**A**) and (**C**) the blue arrowhead marks the presumed degradation product of Alr4550, the grey arrowhead marks the full length protein and the red arrowhead points at a fragment that likely represents a non- native state of the protein. The migration of the 66 kDa molecular weight standard is indicated.

presence of outer membranes in the total protein fractions was confirmed by detection of Alr2269 using a specific antibody. The protein was detected in the cell lysate of all strains except AFS-I-*alr2269* (Fig. 5A, panel 1). Thus, Alr2269 could not be detected in AFS-I-*alr2269* lysate although the strain is not segregated (Fig. S1). The relatively small amount of outer membrane proteins in total cell lysate and the reduced protein abundance in the mutant are possible explanations for this. The loading of lysate was comparable between all four strains as controlled by DB71 staining (Fig. 5A, panel 3, LSU). Probing for Alr4550 in wild type resulted in two apparent signals (Fig. 5A, panel 2). The upper band corresponds to the full length protein, whereas the lower molecular weight signal most likely represents a degradation product. Both fragments have been detected in wild type in previous experiments [45]. The size of the lowest fragment is consistent with the molecular weight of Alr4550 lacking the periplasmic S-layer homology domain.

Alr4550 was more abundant in the *omp85* mutants AFS-I-*alr2269* and AFS-I-*alr4893* compared to the wild type. Especially in AFS-I-*alr4893* the protein amount was comparatively increased. Moreover, the protein band of higher molecular weight than the mature protein was more abundant in the mutants when compared to wild type (Fig. 5A, panel 2). This apparent fragment likely represents an SDS-resistant unfolded or aggregated intermediate, which likewise has been reported for other outer membrane β-barrel proteins [65, 66]. In AFS-I-*alr2269* the high molecular weight fragment was the dominating species, whereas in AFS-I-*alr4893* the form migrating as intermediate predominated. Hence, our results might suggest that the plasmid-insertion in *alr2269* or *alr4893* leads to an increased protein production of Alr4550 as well as an increased detection of misfolded or degraded proteins. The increase in Alr4550 protein amount was found to be reflected by an enhanced mRNA abundance of *alr4550* in AFS-I-*alr4893*, but not AFS-I-*alr2269* (Table 3).

Alterations in the outer membrane integrity and biogenesis as well as an alteration of the protein to lipid ratio can result in an aberrant membrane density which can be examined by rate zonal centrifugation [67-69]. The effects of the *omp85* mutations on membrane protein integrity were examined by analyzing the outer membrane protein density in the single insertion mutants. The sedimentation behavior of outer membranes was analyzed by rate zonal centrifugation. Gradient fractions were collected and subjected to SDS-PAGE. To detect non-porin type OM-proteins the antibody against Alr2269 was utilized (Fig. 5B). As AFS-I-*alr2269* is not segregated a signal was obtained in this sample as well.

Isolated outer membranes from *Anabaena* sp. that contained Alr2269 sedimented in the range of 49% to 61% sucrose. The largest quantity of Alr2269 was detected between 49% and 53% (Fig. 5B, top panel). The same distribution of Alr2269 was detected when outer membrane preparations of the *omp85* mutants or AFS-I-*tic22* were analyzed. However, in AFS-I-*alr0075,* AFS-I-*alr2269* and AFS-I-*tic22* the majority of the protein migrated between 53% and 56% sucrose (Fig. 5B).

In wild type outer membrane fractions Alr4550 was more broadly dispersed than Alr2269. Similar to Alr2269, the largest quantity of Alr4550 was found between 49% to 61% sucrose as well. The peak was shifted to the fractions between 53% and 56% sucrose (Fig. 5C, top). Interestingly, the distribution of Alr4550 in the membrane fractions isolated form AFS-I-*alr0075* (Fig. 5C, fourth panel) and AFS-I-*tic22* (Fig. 5C, bottom) was comparable to that of wild type. Hence, Alr4550 synthesis and integrity seems not affected in AFS-I-*alr0075*. This is also underlined by the fact that the Alr4550-fragment which putatively represents the aggregated form of the protein was not detectable in AFS-I-*alr0075* (Fig. 5A and 5C, fourth panel). In turn, in AFS-I-*tic22* the aggregated form was detectable (Fig. 5C, bottom, red arrowhead).

The sedimentation behavior of Alr4550 in samples from AFS-I-*alr2269* and AFS-I-*alr4893* showed clear distinctions compared to wild type. While the general distribution profile of the membrane fractions containing Alr4550 from AFS-I-*alr2269* was more disperse than in wild type (ranging from 43% to 61%), the peak fraction was found at a comparable density (Fig. 5C, second panel). However, an enrichment of the porin in fractions of higher density that possibly represents aggregated protein was observed (Fig. 5C, second panel, fraction 10). The migration of the membrane fractions isolated from AFS-I-*alr4893* that contained Alr4550 was shifted to higher density compared to wild type (56%–61% sucrose; Fig. 5C, third panel). Just like observed in AFS-I-*alr2269* samples, a significant portion of Alr4550 was found in the last gradient fractions. In both strains the high molecular-weight fragment that likely represents the aggregated form was identified, whereas in wild type samples it was not detected in this experiment. This is consistent with earlier reports documenting the aggregation of unfolded, not inserted proteins at the outer membrane [70].

Taken together these results indicate that outer membrane biogenesis or integrity is affected in AFS-I-*alr0075,* AFS-I-*alr2269* and AFS-I-*tic22,* as judged from the sucrose gradient centrifugation analysis and detection of Alr2269 and Alr4550, whereas AFS-I-*alr0075* samples only exhibited an aberrant distribution of Alr2269, but not Alr4550. Factors that could cause the increased density of the vesicles could be for example an increased protein to lipid ratio, an altered (enhanced) co-migration of peptidoglycan with the proteins or variations in LPS production [69, 71, 72].

Discussion

Porins have an important function in the regulation of solute uptake and further contribute to the maintenance of envelope integrity [8]. The degree of specificity of certain porin classes is highly diverse [6]. In proteobacteria a distinction between *e.g.* OmpA-type porins (structural function) and OmpF-type porins (transport function) can be made [8]. In the genome of the filamentous cyanobacterium *Anabaena* sp. a typical OmpA-like porin, namely Alr4550, was identified. Expression analysis revealed that among all the porins in *Anabaena* sp. the *alr4550*-transcript was high abundant under standard conditions (Table 1). Remarkably AFS-I-*alr4550* was hypersensitive compared to wild type under virtually all tested conditions (except elevated copper levels). Growth of AFS-I-

alr4550 in the absence of fixed nitrogen was not inhibited, hence Alr4550 dysfunction seems not to affect heterocyst development (Figs. 2 and 3). Thus, Alr4550 might have a prominent structural function in *Anabaena* sp. that is distinct from the function of the other porin-like proteins, considering the exceptionality of the mutant phenotype. This could be for instance mediated by the interaction of Alr4550 with cell wall (components) and thereby connecting the OM to the peptidoglycan, as described for OmpA in *E. coli* [49, 73].

Most of the porin mutants were increasingly resistant towards elevated potassium chloride and sodium chloride concentrations compared to the wild type. The same was observed when the macrolide erythromycin was added. In contrast to other antibiotics, macrolide antibiotics are generally not thought to penetrate through porins, therefore the enhanced resistance might point towards altered membrane properties (Fig. 3) [18, 74]. Interestingly AFS-I-*all5191* was the only strain that did barely grow in the absence of a combined nitrogen source (Fig. 2). Apparently, this strain was able to differentiate heterocysts as judged from microscopic analyses, showing that the protein might not play a role in heterocyst development. We rather suggest that the absence of All5191 generates a condition that complicates nitrogen fixation. Consequently, the percentage of heterocysts increases is AFS-I-*all5191* filaments. AFS-I-*alr0834* and AFS-I-*alr4741* grew better on $YBG11_0$ compared to wild type (Fig. 2). An alteration in the heterocyst pattern of the two strains was not observed, thus the reason for the enhanced growth of the mutants remains to be elucidated. Noteworthy the transcript of *all5191* was increasingly abundant in AFS-I-*alr0834* and AFS-I-*alr4741*. Since AFS-I-*all5191* was defected in growth in absence of a combined nitrogen source, an increased production of the protein might on the other hand have beneficial effects on the growth capacity in $YBG11_0$, as observed in AFS-I-*alr0834* and AFS-I-*alr4741*.

With respect to the uptake of divalent ions, a relation to iron uptake could not be established in this study. Ferric iron ions are prevalently complexed to organic ligands like siderophores [75]. However, the transport of siderophores in *Anabaena* is rather dependent on functional TBDTs instead of porins [63, 76]. It was shown that inorganic iron is highly bioavailable to cyanobacteria [77, 78]. Moreover, homologues of the iron-transporting porin Slr1908 in *Synechocystis* sp. are found in many freshwater and marine cyanobacteria species [27]. This generally suggests an important role of porin-mediated iron transport among cyanobacteria, which needs to be further examined in *Anabaena* sp.

Also for cobalt uptake, no relation to a porin in *Anabaena* sp. could be made, as mutation of porins did not lead to a resistance against elevated concentrations (Fig. 2). Cobalt also might be taken up in *Anabaena* sp. in form of cobalamin. This uptake is dependent on the BtuB proteins of the TBDT-family, which are predicted to exist in *Anabaena* sp. as well [79]. Similarly, two TBDTs but none of the porin-like genes investigated here have been found to be regulated by the zinc starvation sensor Zur in *Anabaena* sp. [80]. This is consistent with the earlier identification of the zinc transporter ZnuD in proteobacteria, which belongs to the TonB-dependent transporter (TBDT) family [81, 82]. However, AFS-I-*alr2231* shows a high resistance to elevated levels of zinc (Fig. 2), which might link the Alr2231 function to the uptake of zinc when the trace metal is present in sufficient amounts. Such function would be consistent with the identification of a cyanobacterial porin as zinc binding protein [83]. An adequate zinc supply is important for organisms as for example the carbonic anhydrase depends on zinc. This enzyme is involved in conversion of CO_2 to bicarbonate, which is important for the regulation of the pyruvate conversion to oxaloacetate and thus central for the cyanobacterial metabolism.

The uptake of other divalent metals like manganese and copper is discussed to depend on porin-like proteins in Gram-negative bacteria [84–88]. The importance of manganese is associated with the regulation of the pyruvate pool as phosphoenolpyruvate carboxykinase and pyruvate carboxylase are Mn-dependent metalloenzymes. Moreover, the oxygen evolving complex in photosystem II bears manganese as cofactor [89]. In turn, the manganese content is tightly regulated and 50 fold excess leads to growth inhibition [90]. Three porin mutant strains were resistant against enhanced manganese concentrations, namely AFS-I-*alr0834*, AFS-I-*alr4741* and AFS-I-*all4499* (Fig. 2). Interestingly, *alr0834* and *alr4741* are upregulated in the absence of manganese, while *all4499* belongs to the three most abundant transcripts among the porins (Table 1). No significant downregulation of the other two genes was observed in the three mutants (Table 2), this suggests that the three porins might act in parallel in manganese uptake. The interplay between these three porins remains to be further explored.

Copper is a globally important co-factor, *e.g.* for respiration and photosynthesis. Consistent with reports for other bacteria [84, 88] most of the mutant strains showed an increased survival on medium with high copper concentrations (Fig. 2). Thus, many porins might be involved in copper uptake under replete conditions. In contrast, for *Anabaena* sp. the TBDT IacT was identified which might be involved in copper uptake under highly limiting conditions [91].

Interestingly, only the *tic22*-mutant, but not the three *omp85* mutants exhibits an elevated resistance towards high copper concentrations (Fig. 2). Omp85 proteins are involved in membrane insertion of OM-proteins [92,93] and Tic22 acts as periplasmic shuttle [45]. The phenotype of AFS-I-*alr4893* showed the highest accordance to the phenotypes of most porin mutants (except to that of AFS-I-*alr4550*, Fig. 4), which could suggest a direct function of Alr4893 in porin insertion.

Moreover, in AFS-I-*alr2269* and AFS-I-*alr4893* the accumulation of the denatured form and a high abundance of aggregated Alr4550 were observed. Based on these results two interpretations are possible, which need to be explored in future. One could suggest that both Alr2269 and Alr4893 are involved in membrane insertion of porins, which would explain the rather moderate correlation between the phenotypes of porin mutants and *omp85* mutants. Alternatively, the data would also be consistent with a functional diversification of the two Omp85 proteins. By this means Alr2269 could be specialized on the insertion of larger OM-proteins such as members of the Omp85 family, LptD or the TBDTs. On the other hand, Alr4893 could be specifically inserting porins into the OM. This could explain the observed diversity in the C-terminal amino acid composition between

TBDTs and porins (Fig. 1) and the high correlation of the phenotypes of the porin mutants with AFS-I-*alr4893,* but not AFS-I-*alr2269*. The occurrence of the aggregated porin form in AFS-I-*alr2269* would be the consequence of a reduced insertion of Alr4893. Both explanations suggest that Alr0075 only plays a minor role in porin insertion. Thus, Tic22 might globally act as periplasmic transfer protein including porins as substrate.

Our results imply diverse functions of single porin-like proteins, reflected by the specific phenotypes of the mutants. Most prominently AFS-I-*alr4550* exhibited a unique phenotype by sowing hypersensitivity towards metals, salt and harmful compounds. Also the strong transcription of *alr4550* suggests a crucial function of the protein, which apparently involves the maintenance of envelope integrity. First associations between single porin candidates and manganese, zinc or copper transport as well as diazotrophic growth capacity could be drawn, thus these connections need to be further examined. The density gradient centrifugation experiments showed that the three *omp85* mutants in *Anabaena* sp. are affected in the migration of Alr2269 and Alr4550, but to different extents. The presence of aggregated intermediates of Alr4550 in the two *omp85* mutants AFS-I-*alr2269* and AFS-I-*alr4893*, but not in AFS-I-*alr0075*, suggests a functional specification on certain substrates for membrane insertion.

Author Contributions

ES conceptualized and HS, EMB and ES designed the study. HS, EMB, EL, and MS conducted experiments. HS, EMB and ES performed analysis and interpretation of data. HS and ES wrote the original manuscript. All authors critically revised and approved the article.

Acknowledgments

We would like to thank Prof. Enrique Flores for providing material used for mutant generation. We thank Dr. Sotirios Fragkostefanakis and Julia Graf for comments on the manuscript. Moreover, we thank Dr. H.-Michael Seitz and Prof. Dr. Horst Marschall for support with the ICP-MS analysis. The work was funded by the Deutsche Forschungsgemeinschaft DFG SCHL585/7-2 to ES. HS received a stipend of the Buchmann Foundation.

Conflict of Interest

The authors have no financial conflicts of interest to declare.

References

1. Jürgens UJ, Drews G, Weckesser J. 1983. Primary structure of the peptidoglycan from the unicellular cyanobacterium *Synechocystis* sp. strain PCC 6714. *J. Bacteriol.* **154:** 471-478.
2. Wilk L, Strauss M, Rudolf M, Nicolaisen K, Flores E, Kühlbrandt W, *et al.* 2011. Outer membrane continuity and septosome formation between vegetative cells in the filaments of *Anabaena* sp. PCC 7120. *Cell. Microbiol.* **13:** 1744-1754.
3. Matias VRF, Al-Amoudi A, Dubochet J, Beveridge TJ. 2003. Cryo-transmission electron microscopy of frozen-hydrated sections of *Escherichia coli* and *Pseudomonas aeruginosa*. *J. Bacteriol.* **185:** 6112-6118.
4. Galdiero S, Falanga A, Cantisani M, Tarallo R, Elena Della Pepa M, D'Oriano V, *et al.* 2013. Microbe-Host Interactions: Structure and Role of Gram-Negative Bacterial Porins. *Curr. Protein Pept. Sci.* **13:** 843-854.
5. Nikaido H. 1994. Porins and specific diffusion channels in bacterial outer membranes. *J. Biol. Chem.* **269:** 3905-3908.
6. Choi U, Lee CR. 2019. Distinct roles of outer membrane porins in antibiotic resistance and membrane integrity in *Escherichia coli*. *Front. Microbiol.* **10:** 953.
7. Novikova OD, Solovyeva TF. 2009. Nonspecific porins of the outer membrane of Gram-negative bacteria: Structure and functions. *Biochem. Suppl. Ser. A: Membr. Cell. Biol.* **3:** 3-15.
8. Schirmer T, Keller TA, Wang YF, Rosenbusch JP. 1995. Structural basis for sugar translocation through maltoporin channels at 3.1 Å resolution. *Science* **267:** 512-516.
9. Conlan S, Zhang Y, Cheley S, Bayley H. 2000. Biochemical and biophysical characterization of OmpG: A monomeric porin. *Biochemistry* **39:** 11845-11854.
10. Kim KH, Aulakh S, Paetzel M. 2012. The bacterial outer membrane β-barrel assembly machinery. *Protein Sci.* **21:** 751-768.
11. Simmerman RF, Dave AM, Bruce BD. 2014. Structure and Function of POTRA Domains of Omp85/TPS Superfamily. pp. 1-34. In *International Review of Cell and Molecular Biology,* Elsevier Inc.
12. Kumar K, Mella-Herrera RA, Golden JW. 2010. Cyanobacterial heterocysts. *Cold Spring Harb. Perspect. Biol.* **2:** a000315.
12. Moslavac S, Reisinger V, Berg M, Mirus O, Vosyka O, Plöscher M, *et al.* 2007. The proteome of the heterocyst cell wall in *Anabaena* sp. PCC 7120. *Biol. Chem.* **388:** 823-829.
14. Hancock REW. 1987. Role of porins in outer membrane permeability. *J. Bacteriol.* **169:** 929-933.
15. Jap BK, Walian PJ. 1990. Biophysics of the structure and function of porins. *Q. Rev. Biophys.* **23:** 367-403.
16. Nikaido H. 2003. Molecular basis of bacterial outer membrane prmeability revisited. *Microbiol. Mol. Biol. Rev.* **67:** 593-656.
17. Hansel A, Tadros MH. 1998. Characterization of two pore-forming proteins isolated from the outer membrane of *Synechococcus* PCC 6301. *Curr. Microbiol.* **36:** 321-326.
18. Brechtel E, Bahl H. 1999. In *Thermoanaerobacterium thermosulfurigenes* EM1 S-layer homology domains do not attach to peptidoglycan. *J. Bacteriol.* **181:** 5017-5023.
19. Ilk N, Kosma P, Puchberger M, Egelseer EM, Mayer HF, Sleytr UB, *et al.* 1999. Structural and functional analyses of the secondary cell wall polymer of *Bacillus sphaericus* CCM 2177 that serves as an S-layer-specific anchor. *J. Bacteriol.* **181:** 7643-7646.
20. Kern J, Ryan C, Faull K, Schneewind O. 2010. *Bacillus anthracis* surface-layer proteins assemble by binding to the secondary cell wall polysaccharide in a manner that requires csaB and tagO. *J. Mol. Biol.* **401:** 757-775.
21. Lupas A, Engelhardt H, Peters J, Santarius U, Volker S, Baumeister W. 1994. Domain structure of the *Acetogenium kivui* surface layer revealed by electron crystallography and sequence analysis. *J. Bacteriol.* **176:** 1224-1233.
22. Kowata H, Tochigi S, Takahashi H, Kojima S. 2017. Outer membrane permeability of cyanobacterium *Synechocystis* sp. strain PCC 6803: Studies of passive diffusion of small organic nutrients reveal the absence of classical porins and intrinsically low permeability. *J. Bacteriol.* **199:** e00371-17.
23. Ekman M, Picossi S, Campbell EL, Meeks JC, Flores E. 2013. A *Nostoc punctiforme* sugar transporter necessary to establish a cyanobacterium-plant symbiosis. *Plant. Physiol.* **161:** 1984-1992.

24. Simm S, Keller M, Selymesi M, Schleiff E. 2015. The composition of the global and feature specific cyanobacterial core-genomes. *Front. Microbiol.* **6:** 219.
25. Qiu G, Jiang H, Lis H, Li Z, Deng B, Shang J, *et al.* 2020. A unique porin meditates iron-selective transport through cyanobacterial outer membranes. *Environ. Microbiol.* **23:** 376-390.
26. Hahn A, Schleiff E. 2014. The Cell Envelope. In *The Cell Biology of Cyanobacteria*, Flores E, Herrero A, eds. pp. 29-87. Caister Academic Press, U.K., Norfolk.
27. Oliveira P, Martins NM, Santos M, Couto NAS, Wright PC, Tamagnini P. 2015. The *Anabaena* sp. PCC 7120 exoproteome: Taking a peek outside the box. *Life* **5:** 130-163.
28. Moslavac S, Bredemeier R, Mirus O, Granvogl B, Eichacker LA, Schleiff E. 2005. Proteomic analysis of the outer membrane of *Anabaena* sp. strain PCC 7120. *J. Proteome. Res.* **4:** 1330-1338.
29. Hahn A, Stevanovic M, Mirus O, Schleiff E. 2012. The TolC-like protein HgdD of the cyanobacterium *Anabaena* sp. PCC 7120 is involved in secondary metabolite export and antibiotic resistance. *J. Biol. Chem.* **287:** 41126-41138.
30. Acland A, Agarwala R, Barrett T, Beck J, Benson DA, Bollin C, *et al.* 2014. Database resources of the National Center for Biotechnology Information. *Nucleic Acids Res.* **42:** D7-D17.
31. Crooks GE, Hon G, Chandonia J-M, Brenner SE. 2004. WebLogo: A sequence logo generator. *Genome Res.* **14:** 1188-1190.
32. Sievers F, Wilm A, Dineen D, Gibson TJ, Karplus K, Li W, *et al.* 2011. Fast, scalable generation of high-quality protein multiple sequence alignments using Clustal Omega. *Mol. Syst. Biol.* **7:** 539.
33. Madeira F, Park YM, Lee J, Buso N, Gur T, Madhusoodanan N, *et al.* 2019. The EMBL-EBI search and sequence analysis tools APIs in 2019. *Nucleic Acids Res.* **47**: W636-W641.
34. Valladares A, Rodríguez V, Camargo S, Martínez-Noël GMA, Herrero A, Luque I. 2011. Specific role of the cyanobacterial pipX factor in the heterocysts of *Anabaena* sp. strain PCC 7120. *J. Bacteriol.* **193:** 1172-1182.
35. Elhai J, Wolk PC. 1988. A versatile class of positive-selection vectors based on the nonviability of palindrome-containing plasmids that allows cloning into long polylinkers. *Gene* **68:** 119-138.
36. Elhai J, Wolk CP. 1988. Conjugal transfer of DNA to cyanobacteria. *Methods Enzymol.* **167:** 747-754.
37. Olmedo-Verd E, Muro-Pastor AM, Flores E, Herrero A. 2006. Localized induction of the *ntcA* regulatory gene in developing heterocysts of *Anabaena* sp. strain PCC 7120. *J. Bacteriol.* **188:** 6694-6699.
38. Wolk CP, Vonshak A, Kehoe P, Elhai J. 1984. Construction of shuttle vectors capable of conjugative transfer from *Escherichia coli* to nitrogen-fixing filamentous cyanobacteria. *Proc. Natl. Acad. Sci. USA* **81:** 1561-1565.
39. Rippka R, Deruelles J, Waterbury JB, Herdman M, Stanier RY. 1979. Generic assignments, strain histories and properties of pure cultures of cyanobacteria. *J. Gen. Microbiol.* **111:** 1-61.
40. Shcolnick S, Shaked Y, Keren N. 2007. A role for mrgA, a DPS family protein, in the internal transport of Fe in the cyanobacterium *Synechocystis* sp. PCC6803. *Biochim. Biophys. Acta–Bioenerg.* **1767:** 814-819.
41. Videau P, Cozy LM. 2019. *Anabaena* sp. strain PCC 7120: Laboratory Maintenance, Cultivation, and Heterocyst Induction. *Curr. Protoc. Microbiol.* **52:** e71.
42. Stevanovic M, Hahn A, Nicolaisen K, Mirus O, Schleiff E. 2012. The components of the putative iron transport system in the cyanobacterium *Anabaena* sp. PCC 7120. *Environ. Microbiol.* **14:** 1655-1670.
43. Livak KJ, Schmittgen TD. 2001. Analysis of relative gene expression data using real-time quantitative PCR and the $2^{-\Delta\Delta CT}$ method. *Methods* **25:** 402-408.
44. Zeng L, Guo J, Xu HB, Huang R, Shao W, Yang L, *et al.* 2013. Direct Blue 71 staining as a destaining-free alternative loading control method for Western blotting. *Electrophoresis* **34:** 2234-2239.
45. Brouwer EM, Ngo G, Yadav S, Ladig R, Schleiff E. 2019. Tic22 from *Anabaena* sp. PCC 7120 with holdase function involved in outer membrane protein biogenesis shuttles between plasma membrane and Omp85. *Mol. Microbiol.* **111:** 1302-1316.
46. Tripp J, Hahn A, Koenig P, Flinner N, Bublak D, Brouwer EM, *et al.* 2012. Structure and conservation of the periplasmic targeting factor Tic22 protein from plants and cyanobacteria. *J. Biol. Chem.* **287:** 24164-24173.
47. Sharon S, Salomon E, Kranzler C, Lis H, Lehmann R, Georg J, *et al.* 2014. The hierarchy of transition metal homeostasis: Iron controls manganese accumulation in a unicellular cyanobacterium. *Biochim. Biophys. Acta – Bioenerg.* **1837:** 1990-1997.
48. Nicolaisen K, Hahn A, Schleiff E. 2009. The cell wall in heterocyst formation by *Anabaena* sp. PCC 7120. *J. Basic Microbiol.* **49:** 5-24.
49. Samsudin F, Ortiz-Suarez ML, Piggot TJ, Bond PJ, Khalid S. 2016. OmpA: A flexible clamp for bacterial cell wall attachment. *Structure* **24:** 2227-2235.
50. Koebnik R, Locher KP, Van Gelder P. 2000. Structure and function of bacterial outer membrane proteins: Barrels in a nutshell. *Mol. Microbiol.* **37:** 239-253.
51. Bosch D, Scholten M, Verhagen C, Tommassen J. 1989. The role of the carboxy-terminal membrane-spanning fragment in the biogenesis of *Escherichia coli* K12 outer membrane protein PhoE. *Mol. Gen. Genet. MGG* **216:** 144-148.
52. De Cock H, Struyvé M, Kleerebezem M, Van Der Krift T, Tommassen J. 1997. Role of the carboxy-terminal phenylalanine in the biogenesis of outer membrane protein PhoE of *Escherichia coli* K-12. *J. Mol. Biol.* **269:** 473-478.
53. Struyvé M, Moons M, Tommassen J. 1991. Carboxy-terminal phenylalanine is essential for the correct assembly of a bacterial outer membrane protein. *J. Mol. Biol.* **218:** 141-147.
54. Paramasivam N, Habeck M, Linke D. 2012. Is the C-terminal insertional signal in Gram-negative bacterial outer membrane proteins species-specific or not? *BMC Genomics* **13:** 510.
55. Gessmann D, Chung YH, Danoff EJ, Plummer AM, Sandlin CW, Zaccai NR, *et al.* 2014. Outer membrane β-barrel protein folding is physically controlled by periplasmic lipid head groups and BamA. *Proc. Natl. Acad. Sci. USA* **111:** 5878-5883.
56. Robert V, Volokhina EB, Senf F, Bos MP, Van Gelder P, Tommassen J. 2006. Assembly factor Omp85 recognizes its outer membrane protein substrates by a species-specific C-terminal motif. *PLoS Biol.* **4:** e377.
57. Kutik S, Stojanovski D, Becker L, Becker T, Meinecke M, Krüger V, *et al.* 2008. Dissecting Membrane Insertion of Mitochondrial β-Barrel Proteins. *Cell* **132:** 1011-1024.
58. Nicolaisen K, Mariscal V, Bredemeier R, Pernil R, Moslavac S, López-Igual R, *et al.* 2009. The outer membrane of a heterocyst-forming cyanobacterium is a permeability barrier for uptake of metabolites that are exchanged between cells. *Mol. Microbiol.* **74:** 58-70.
59. Hsueh YC, Brouwer EM, Marzi J, Mirus O, Schleiff E. 2015. Functional properties of LptA and LptD in *Anabaena* sp. PCC 7120. *Biol. Chem.* **396:** 1151-1162.
60. Liu X, Ferenci T. 1998. Regulation of porin-mediated outer membrane permeability by nutrient limitation in *Escherichia coli*. *J. Bacteriol.* **180:** 3917-3922.
61. Berman-Frank I, Cullen JT, Shaked Y, Sherrell RM, Falkowski PG. 2001. Iron availability, cellular iron quotas, and nitrogen fixation in Trichodesmium. *Limnol. Oceanogr.* **46:** 1249-1260.
62. Paerl HW, Crocker KM, Prufert LE. 1987. Limitation of N_2 fixation in coastal marine waters: Relative importance of molybdenum, iron, phosphorus, and organic matter availability. *Limnol. Oceanogr.* **32:** 525-536.
63. Rudolf M, Kranzler C, Lis H, Margulis K, Stevanovic M, Keren N, Schleiff E. 2015. Multiple modes of iron uptake by the filamentous, siderophore-producing cyanobacterium, *Anabaena* sp. PCC 7120. *Mol. Microbiol.* **97:** 577-588.

64. Barron A, May G, Bremer E, Villarejo M. 1986. Regulation of envelope protein composition during adaptation to osmotic stress in *Escherichia coli*. *J. Bacteriol.* **167:** 433-438.
65. Dekker N, Tommassen J, Lustig A, Rg J, Rosenbusch P, Verheij HM. 1997. Dimerization regulates the enzymatic activity of *Escherichia coli* outer membrane Phospholipase A. *J. Biol. Chem.* **272:** 3179-3184.
66. Volokhina EB, Beckers F, Tommassen J, Bos MP. 2009. The β-barrel outer membrane protein assembly complex of *Neisseria meningitidis*. *J. Bacteriol.* **191:** 7074-7085.
67. Braun M, Silhavy TJ. 2002. Imp/OstA is required for cell envelope biogenesis in *Escherichia coli*. *Mol. Microbiol.* **45:** 1289-1302.
68. Genevrois S, Steeghs L, Roholl P, Letesson J-J, van der Ley P. 2003. The Omp85 protein of *Neisseria meningitidis* is required for lipid export to the outer membrane. *EMBO J.* **22:** 1780-1789.
69. Steeghs L, de Cock H, Evers E, Zomer B, Tommassen J, van der Ley P. 2001. Outer membrane composition of a lipopolysaccharide-defcient *Neisseria meningitidis* mutant. *EMBO J.* **20:** 6937-6945.
70. Sklar JG, Wu T, Kahne D, Silhavy TJ. 2007. Defining the roles of the periplasmic chaperones SurA, Skp, and DegP in *Escherichia coli*. *Genes Dev.* **21:** 2473-2484.
71. Smit J, Kamio Y, Nikaido H. 1975. Outer membrane of *Salmonella typhimurium*: chemical analysis and freeze fracture studies with lipopolysaccharide mutants. *J. Bacteriol.* **124:** 942-958.
72. Osborn MJ, Gander JE, Parisi E, Carson J. 1972. Mechanism of assembly of the outer membrane of *Salmonella typhimurium*. Isolation and characterization of cytoplasmic and outer membrane . *J. Biol. Chem.* **247:** 3962-3972.
73. Smith SGJ, Mahon V, Lambert MA, Fagan RP. 2007. A molecular Swiss army knife: OmpA structure, function and expression. *FEMS Microbiol. Lett.* **273:** 1-11.
74. Pagès J-M, James CE, Winterhalter M. 2008. The porin and the permeating antibiotic: a selective diffusion barrier in Gram-negative bacteria. *Nat. Rev. Microbiol.* **6:** 893-903.
75. Gledhill M, Buck KN. 2012. The organic complexation of iron in the marine environment: A review. *Front. Microbiol.* **3:** 69.
76. Rudolf M, Stevanovic M, Kranzler C, Pernil R, Keren N, Schleiff E. 2016. Multiplicity and specificity of siderophore uptake in the cyanobacterium *Anabaena* sp. PCC 7120. *Plant. Mol. Biol.* **92:** 57-69.
77. Lis H, Kranzler C, Keren N, Shaked Y. 2015. A comparative study of Iron uptake rates and mechanisms amongst marine and fresh water Cyanobacteria: prevalence of reductive Iron uptake. *Life* **5:** 841-860.
78. Morel FMM, Kustka AB, Shaked Y. 2008. The role of unchelated Fe in the iron nutrition of phytoplankton. *Limnol. Oceanogr.* **53:** 400-404.
79. Fresenborg LS, Graf J, Schätzle H, Schleiff E. 2020. Iron homeostasis of cyanobacteria: advancements in siderophores and metal transporters. pp. 85-117. In *Advances in Cyanobacterial Biology,* Elsevier.
80. Napolitano M, Rubio MÁ, Santamaría-Gómez J, Olmedo-Verd E, Robinson NJ, Luque I. 2012. Characterization of the response to Zinc deficiency in the Cyanobacterium *Anabaena* sp. strain PCC 7120. *J. Bacteriol.* **194:** 2426-2436.
81. Calmettes C, Ing C, Buckwalter CM, El Bakkouri M, Chieh-Lin Lai C, Pogoutse A, *et al.* 2015. The molecular mechanism of Zinc acquisition by the neisserial outer-membrane transporter ZnuD. *Nat. Commun.* **6**: 7996.
82. Stork M, Bos MP, Jongerius I, de Kok N, Schilders I, Weynants VE, *et al.* 2010. An outer membrane receptor of *Neisseria meningitidis* involved in zinc acquisition with vaccine potential. *PLoS Pathog.* **6:** e1000969.
83. Barnett JP, Scanlan DJ, Blindauer CA. 2014. Identification of major zinc-binding proteins from a marine cyanobacterium: Insight into metal uptake in oligotrophic environments. *Metallomics* **6:** 1254-1268.
84. González-Sánchez A, Cubillas CA, Miranda F, Dávalos A, García-de los Santos A. 2018. The *ropAe* gene encodes a porin-like protein involved in copper transit in *Rhizobium etli* CFN42. *Microbiologyopen* **7:** e00573.
85. Haeili M, Speer A, Rowland JL, Niederweis M, Wolschendorf F. 2015. The role of porins in copper acquisition by mycobacteria. *Int. J. Mycobacteriol.* **4:** 91-92.
86. Hohle TH, Franck WL, Stacey G, O'Brian MR. 2011. Bacterial outer membrane channel for divalent metal ion acquisition. *Proc. Natl. Acad. Sci. USA* **108:** 15390-15395.
87. Lutkenhaus JF. 1977. Role of a major outer membrane protein in *Escherichia coli*. *J. Bacteriol.* **131:** 631-637.
88. Speer A, Rowland JL, Haeili M, Niederweis M, Wolschendorf F. 2013. Porins increase copper susceptibility of *Mycobacterium tuberculosis*. *J. Bacteriol.* **195:** 5133-5140.
89. Eisenhut M. 2019. Manganese homeostasis in cyanobacteria. *Plants (Basel)* **9:** 18.
90. Gandini C, Schmidt SB, Husted S, Schneider A, Leister D. 2017. The transporter SynPAM71 is located in the plasma membrane and thylakoids, and mediates manganese tolerance in *Synechocystis* PCC6803. *New Phytol.* **215:** 256-268.
91. Nicolaisen K, Hahn A, Valdebenito M, Moslavac S, Samborski A, Maldener I, *et al.* 2010. The interplay between siderophore secretion and coupled iron and copper transport in the heterocyst-forming cyanobacterium *Anabaena* sp. PCC 7120. *Biochim. Biophys. Acta – Biomembr.* **1798:** 2131-2140.
92. Schleiff E, Maier UG, Becker T. 2011. Omp85 in eukaryotic systems: One protein family with distinct functions. *Biol. Chem.* **392:** 21-27.
93. Webb CT, Heinz E, Lithgow T. 2012. Evolution of the β-barrel assembly machinery. *Trends Microbiol.* **20:** 612-620.

3. Additional Results

3.1. Material and Methods

3.1.1. *Anabaena* culture conditions

Anabaena sp. PCC 7120 strains were stored on BG11 plates (Rippka et al., 1979) that contained 1% (w/v) bacto agar (BD Biosciences, Franklin Lakes, USA). Liquid and solid samples were cultured under permanent illumination (70 µmol photons m^{-2} s^{-1}) at 28-29 °C, liquid flasks were constantly shaken at 90-100 rpm. In case of mutants, a final concentration of 5 µg ml^{-1} spectinomycin dihydrochloride pentahydrate (Duchefa Biochemie, Haarlem, Netherlands) and streptomycin sulfate (Carl Roth, Karlsruhe, Germany) each was added to the medium. All insertion mutant strains were annotated AFS-I-*geneX*, due to an easier readability the 'AFS-' is omitted throughout the whole text. The mutants I-*tonB3* and I-*SchT* were introduced previously (Nicolaisen et al., 2008; Stevanovic et al., 2012), and the generation of I-*sjdR* (previously annotated as I-*tonB1*), I-*tonB2* and I-*tonB4* is described in Manuscripts 1 and 2 in detail.

3.1.2. Growth curves

Mutant and wild-type cultures were grown in YBG11 without iron (YBG11 -Fe, absence of solution 2, Shcolnick et al., 2007) in order to pre-starve the cells. The cultures were pre-starved minimum two weeks prior to the start of the growth monitoring. After the pre-starvation, the cultures were washed three times in YBG11 -Fe, split in two and inoculated to OD at 750 nm (OD_{750}) 0.03 in YBG11 -Fe in separate flasks. To one of the two cultures ferric ferrichrome was added to a final concentration of 500 nM (EMC Microcollections, Tübingen, Germany), whereas no iron source was added to the other culture. The growth of the cultures was monitored by measuring OD_{750}.

3.1.3. Inductively coupled plasma mass spectrometry (ICP-MS)

Glassware utilized for *Anabaena* culturing was incubated in 4% HNO_3 overnight. Cultures of *Anabaena* wild type and I-*tonB4* were grown for 14 days in YBG11 -Fe. ICP-MS measurements were conducted as described in Manuscripts 1, 2 and 3 and Sharon et al., 2014. In brief, cells grown in YBG11 -Fe in acid-treated flasks were harvested after two weeks of growth (3,000 *g,* 10 min) and washed twice with washing buffer (20 mM 2-(N-Morpholino)ethanesulfonic acid pH 5 and 10 mM ethylenediaminetetraacetic acid). Afterwards, cells were resuspended in double distilled water. Cells in the water suspension were counted and OD_{750} was measured. Prior to the measuring, samples were digested in 7 M HNO_3 at 120°C over night until dryness and dissolved in 5% HNO_3 for measurement.

3.2. Results

3.2.1. The availability of ferrichrome

In order to test the functionality of the Ton system in *Anabaena* for a substrate other than schizokinen, the bioavailability of the fungal siderophore ferrichrome was tested. Ferrichrome is structurally not related to schizokinen, however like schizokinen it belongs to the hydroxamate-type siderophore group (Al Shaer et al., 2020). In *Anabaena,* several TBDTs were assigned to be hydroxamate-type transporters (Mirus et al., 2009). Iron is an essential nutrient for all organisms, and in *Anabaena* the continuous growth in the absence of iron results in an increase of the oxidative stress level and a reduction of growth rate, until at one point cell division stops and the cells die (Latifi et al., 2005). To test if ferrichrome-chelated ferric iron is available to *Anabaena*, cells were pre-starved for iron for about two weeks, the cultures were split afterwards and ferric ferrichrome was subsequently added to one culture as iron source. The other culture served as control and was grown further in the absence of iron. For wild type, a growth stimulation was observed after ferric ferrichrome was added to the culture, reflected in an increased growth of this culture compared to the control culture grown without iron. This result was obtained in several independent experiments for wild type, a representative plot is shown in Fig. 4. To test if ferric ferrichrome also presents a suitable iron source for the *tonB* mutants and I-*sjdR*, the experiment was repeated with the mutant cultures (minimum of four replicates). Representative growth curves are depicted in Fig. 4. For I-*sjdR*, a wild-type like growth stimulation through ferric ferrichrome was observed. Also I-*tonB2* cultures grew better in presence of ferric ferrichrome than in the absence of iron, although the growth promotion was slightly less pronounced compared to wild type. For I-*tonB3* and I-*schT*, no or only a very weak difference in growth between the two conditions was observed, implying that ferric ferrichrome might not be incorporated by these strains to serve as an iron source. Also, these two strains were retarded in growth in iron-free medium compared to wild type, which confirms previous observations (Stevanovic et al., 2012). Interestingly, also I-*tonB4* cultures were, if at all, very slightly boosted in growth through ferric ferrichrome supplementation, which also in this case suggests that iron bound to ferrichrome is not available to this strain. Hence, the *tonB4* mutant cultures are able to utilize ferric schizokinen (Manuscript 2, Fig. 5D), but not ferrichrome as iron source.

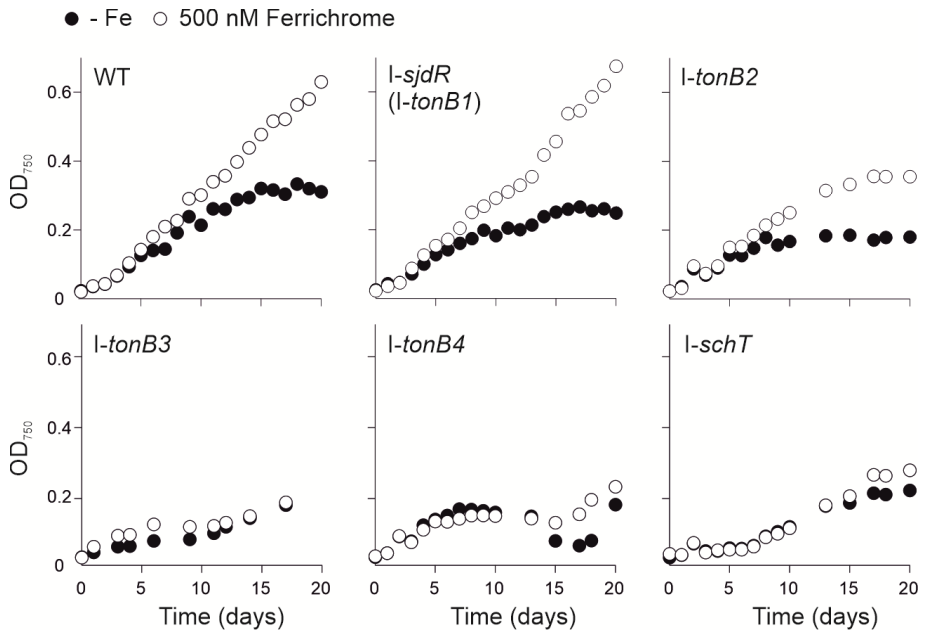

Figure 4. Growth stimulation of iron-starved cultures by ferric ferrichrome. The *Anabaena* wild type (WT) and indicated strains were grown in iron-free medium for minimum two weeks (pre-starvation), afterwards the culture was split in two and diluted into fresh iron-free medium. To one culture ferric ferrichrome was added as iron source (final concentration of 500 nM, white circles). The other culture was grown further without iron source (-Fe, black circles). Representative graphs out of minimum four independent experiments are shown.

3.2.2. The cellular metal content in I-*tonB4* and wild type after iron starvation

In I-*tonB4*, the chlorophyll concentration after iron starvation was found to be enhanced compared to wild type (Manuscript 2, Fig. 5B). This proposes an altered iron uptake or starvation regulation in the mutant. To test whether the iron concentration of I-*tonB4* and wild type is different after the cultures were grown in iron-free medium for two weeks, ICP-MS measurements were conducted. The concentration of all tested metals including iron in I-*tonB4* was comparable to wild type after two weeks of growth in iron-free medium (Table 3), suggesting an altered starvation adaptation in I-*tonB4*.

Table 3. Cellular metal concentrations of *Anabaena* wild type and I-*tonB4*. The average metal concentrations measured after the cells were grown for 14 days in medium without an iron source are listed. The experiment was conducted with three cultures per strain. Values represent the atoms/OD, the standard deviation is given. No significant differences between wild type and I-*tonB4* values were observed (Student's t-test).

Metal	Wild type	I-*tonB4*
Mg	$(2.6\pm0.5)*10^{15}$	$(3.7\pm1.4)*10^{15}$
Ca	$(1.8\pm0.7)*10^{14}$	$(5.2\pm2.0)*10^{14}$
Mn	$(8.6\pm1.8)*10^{13}$	$(1.1\pm0.4)*10^{14}$
Fe	$(1.4\pm1.0)*10^{13}$	$(2.9\pm1.1)*10^{13}$
Co	$(1.5\pm0.3)*10^{13}$	$(1.8\pm0.4)*10^{13}$
Cu	$(2.7\pm1.2)*10^{13}$	$(3.0\pm0.9)*10^{13}$
Zn	$(6.4\pm5.8)*10^{13}$	$(4.2\pm1.9)*10^{13}$
Mo	$(3.0\pm2.6)*10^{13}$	$(9.8\pm4.3)*10^{13}$

4. Discussion

4.1. TonB proteins in *Anabaena*: variations on a theme

An active transport of substrates like siderophores across the OM is mediated by the Ton complex, formed by TonB, ExbB and ExbD proteins that harness energy from the pmf (Klebba, 2016; Noinaj et al., 2010). TonB physically interacts with TBDTs and induces conformational changes in the OM transporters, followed by substrate translocation (described in detail in section 1.3.3). The four predicted TonB-like proteins in *Anabaena* reveal a great variety in length and domain architecture (Fig. 3). With respect to the observed novel function of TonB1 (described below in detail, Manuscript 1) a new annotation was introduced: TonB1 is named SjdR (septal junction disc regulator) hereinafter. TonB3 is the longest protein among the *Anabaena* TonBs, where in addition conserved motifs such as the Histidine in the transmembrane helix or the YP sequence in the linker domain are present (Fig. 3; Chu et al., 2007; Larsen et al., 2007). These conserved residues are absent in the other *Anabaena* TonB candidates. SjdR, TonB2 and TonB4 are considerably shorter than TonB3. Here, the TonB box interaction site can be found 16 nm, 22 nm and 12 nm distant from the transmembrane helix, respectively, premising an extended helix configuration (Fig. 5). Though, the distance between the PM and the OM in *Anabaena* was determined to be 46±3 nm (Wilk et al., 2011), posing the question if SjdR, TonB2 and TonB4 could even reach the TonB box of TBDTs.

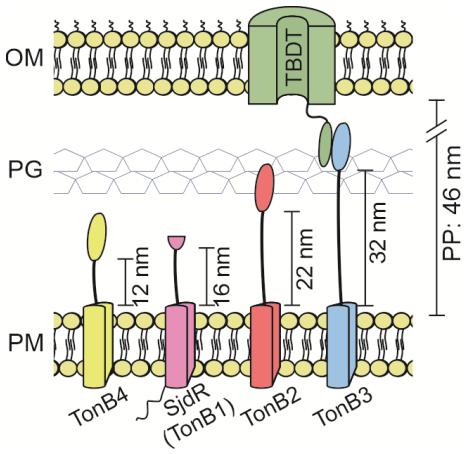

Figure 5. Length of the periplasmic linker domain to the annotated TonB box interaction site of the *Anabaena* TonB-like protein and SjdR. The lengths were calculated assuming an extended helix formation of the periplasmic linker domain, figure modified from Fig. 1 in Manuscript 2. TBDT = TonB-dependent transporter, OM = outer membrane, PG = peptidoglycan, PM = plasma membrane, PP = periplasmic space.

Possibilities for shorter TonB proteins to bind OM TBDTs could be that under certain conditions the distance between OM and PM decreases. The regulation of the OM-PM

distance is important for cellular signalling processes and stress response (Asmar et al., 2017). Periplasm width was found to be variable, for example it can be influenced by the osmotic conditions or the presence of lipoproteins or protein complexes hosted in both OM and PM (Cohen et al., 2017; Mathelié-Guinlet et al., 2020; Stock et al., 1977). Examples therefore are the Type-I secretion system or the capsular polysaccharide export machinery, that span the periplasm and connect both membranes (Collins et al., 2007; Miller and Salama, 2018). Also, lipoproteins residing in the inner leaflet of the OM regulate the periplasm width, by binding to the PG and tethering or attaching the OM to the cell wall (Cohen et al., 2017; Mathelié-Guinlet et al., 2020). In proteobacteria, such as the model strain *E. coli*, lipoproteins such as Lpp are extremely abundant (Li et al., 2014). Lpp length was found to regulate the periplasm width and thereby to influence flagella morphology and the motility of the cell (Cohen et al., 2017). Interestingly, the Pal protein, which is interacting with TolA and the PG, is able to partially complement the phenotype of an *lpp* mutant strain (Cascales et al., 2000). Further, in *Vibrio cholerae*, a differential activity of the two Ton systems in dependence on the periplasm width is described. Here, the relatively longer TonB1 is active under osmotic conditions, when the periplasmic space is enlarged, whereas the shorter TonB2 protein can only reach the OM under low-osmolarity conditions (Seliger et al., 2001). Therefore, for short TonB proteins a conditional functionality in OM transport cannot be excluded completely.

In order to investigate the function of the individual *Anabaena* TonB-like proteins in the frame of this study, single insertion mutants of *sjdR*, *tonB2*, *tonB3* and *tonB4* were analysed. For *sjdR*, as well as *tonB2*, segregated mutants were available (I-*sjdR* and I-*tonB2*, respectively). Here, the plasmid was inserted into all gene copies of *Anabaena* (Manuscript 1, Fig. 2B and Manuscript 2, Fig. 2B). In contrast, *tonB3* and *tonB4* each could not get eliminated completely in the respective mutants I-*tonB3* and I-*tonB4* (Manuscript 2, Fig. 2B). For TonB3 an essential functionality was described before under iron starvation conditions (Stevanovic et al., 2012), and the incomplete segregation suggests that also TonB4 is essential for cell viability under standard cultivation conditions. The individual *tonB* mutants and I-*sjdR* shared some common phenotypic features, but also displayed specific characteristics. For example, an insertion in any of the mentioned genes in *Anabaena* leads to certain alterations in the pigment level, the cellular concentration of specific metals and nitrogenase activity (Manuscript 1, Fig. 1B and Table 1; Manuscript 2, Fig. 4A and Tables 1 and 2), and possible reasons therefore are discussed below.

4.1.1. Siderophore transport in *Anabaena:* the key role of TonB3 and the enigmatic role of TonB4

The understanding of TonB-dependent substrate transport in cyanobacteria is only emerging, a few species have been analysed in this regard so far. In *Anabaena*, 22 TBDTs, 4 TonB proteins, 2 ExbB-ExbD clusters and one additional single ExbB were predicted (Mirus et al., 2009; Stevanovic et al., 2012). The data obtained during this study associate only TonB3 with a direct role in energization of translocation processes across the OM, as schizokinen transport was abolished in the respective mutant strain (Manuscript 1, Fig. 2C). In contrast to this, I-*sjdR* and I-*tonB2* strains were not impaired in schizokinen transport. For I-*tonB4* a slightly decreased average schizokinen uptake rate was obtained which, however, was not significantly different from the average rate calculated for wild type (Manuscript 2, Fig. 5D). Further, a significant induction of transcription after iron depletion was only observed for *tonB3*, and not for the other *tonB*-like genes (Manuscript 2, Fig. 5A). Also, the growth defects of the *tonB3* mutant during iron starvation strengthens the relation of TonB3 to the energization of ferric siderophore transport (Stevanovic et al., 2012).

A transcriptional induction of genes involved in high affinity siderophore transport under iron starvation is a conserved phenomenon conveyed by the ferric uptake regulator Fur. Fur is a conserved transcriptional repressor that senses the cellular iron concentration (Bagg and Neilands, 1987; Hantke, 1981). Notably, also a limited number of genes are identified that are activated by Fur (González et al., 2014). Three Fur homologs were identified in *Anabaena*, out of those FurA regulates target genes in response to the iron concentration (Kaushik et al., 2016). Targets for FurA-mediated repression in *Anabaena* are for instance genes encoding for TBDTs like *schT* (González et al., 2012, 2010) or the porin-like gene *alr0834* (González et al., 2014). Interestingly, in an *Anabaena* strain where *furA* expression was turned off, *tonb2* expression was moderately induced, whereas *sjdR*, *tonB3* and *tonB4* transcription was only mildly affected (González et al., 2016). Currently it is not clear if *tonB3* is a direct target of FurA, or if the expression in response to iron starvation is regulated in a different way. Beyond the FurA-mediated transcriptional control also *cis*- and *trans*-acting small RNAs are described to orchestrate iron responsive expression regulation (Fresenborg et al., 2020), illustrating a complex regulatory system of expression control.

It was shown that the TBDTs SchT and IutA2 mediate schizokinen and aerobactin transport in *Anabaena*, whereas ferrioxamine B is putatively taken up through another TBDT (Rudolf et al., 2016). Considering the presence of 22 putative TBDTs in the *Anabaena* genome, among them 14 presumable FhuA-type hydroxamate transporters (Mirus et al., 2009), it is likely that the number of putative substrates for the TonB-dependent transport in *Anabaena* exceeds that of the currently characterized compounds. Hence, the bioavailability of the fungal

hydroxamate-type siderophore ferrichrome was tested in the frame of this study. Regarding cyanobacteria, the availability of ferric ferrichrome to *Trichodesmium* was established (Achilles et al., 2003), which is a filamentous marine species. When ferric ferrichrome was present as iron source in the medium, growth of *Anabaena* wild-type, I-*sjdR* and I-*tonB2* cultures was enhanced compared to growth in iron-free medium (Fig. 4). Though, this was not observed for I-*tonB3*, I-*tonB4* and I-*schT*, indicating that these strains are unable to utilize ferric ferrichrome as iron source, presumably due to an impeded transport into the cell. Assuming this, apparently both TonB3 and the TBDT SchT are required for transport of schizokinen and ferric ferrichrome, whereas *tonB4* knock-down only affects ferrichrome transport. Moreover, the absence of ferrichrome-mediated growth stimulation in I-*tonB4* cannot be traced back to an altered expression of *tonB3* (Manuscript 2, Fig. 4A). Thus, since a complementation of the TonBs on an expression level was not observed, ferrichrome sequestration could depend on the combined function of TonB3 and TonB4, which might involve a function of the proteins as heterodimer. Regarding the length of TonB4 it remains questionable if this protein could physically connect to TBDTs under normal conditions (Fig. 5; Manuscript 2, Fig. 1). Nevertheless, assuming the existence of a TonB3-TonB4 heterodimer, it could be sufficient for energy transduction if only TonB3 binds to TBDTs. The impact of TonB4 on ferrichrome utilization could also take place on a regulation level, however, further investigation and experiments are required to establish the exact role of TonB4. Also, it did not yet become clear why the chlorophyll level per cell, which can serve as marker for iron starvation in *Anabaena*, decreases slower in I-*tonB4* compared to the wild type (Manuscript 2, Fig. 5B). On the one hand, the magnesium concentration was comparatively low in I-*tonB4* under normal conditions (Manuscript 2, Table 2), which could affect chlorophyll synthesis. On the other hand, ICP-MS measurements after two weeks of iron starvation did not show an altered magnesium concentration in I-*tonB4* compared to wild type (Table 3), and the growth behaviour of the strain under normal conditions or iron starvation was comparable to wild type (Manuscript 2, Fig. 5C). This argues against a compromised photosynthetic capacity and rather suggests a modulated iron starvation adaptation in I-*tonB4*. Further, although a certain raise in transcription was observed, the *tonB3* mRNA abundance in I-*tonB4* did not significantly differ between growth in YBG11 or YBG11 without iron source. In wild type or I-*tonB2*, in contrast, the induction of *tonB3* transcription after iron starvation was significant (Manuscript 2, Fig. 5A). Also, schizokinen uptake was not affected in the *tonB4* mutant, and the iron concentration after two weeks of starvation was similar to that of wild type (Table 3 and Manuscript 2, Fig. 5D). Therefore, it can be assumed that iron sequestration is not considerably impacted in I-*tonB4*. These observations strengthen the hypothesis about a modulation of iron starvation sensing or adaptation in I-*tonB4.*

After 48 h cultivation in $BG11_0$ medium, the nitrogenase activity of I-*tonB2*, I-*tonB4* and I-*sjdR* was significantly lower than that of the wild type (Manuscript 1, Fig. 3B; Manuscript 2, Fig. 4A). Nevertheless, only I-*sjdR* showed a visible growth defect when grown in absence of a combined nitrogen source, whereas growth of I-*tonB2* and I-*tonB4* was comparable to wild type (Manuscript 1, Fig. 2D, E and Fig. 3B; Manuscript, 2 Fig. 4A). Moreover, the heterocysts of the *tonB2* and *tonB4* mutants appeared normal in morphology (Manuscript 2, Fig. 4B, C). A decrease in the cellular concentration of molybdenum was measured for I-*tonB4* cultures, whereas in I-*tonB2* the molybdenum level was enhanced (Manuscript 2, Table 2). One hypothesis could be that the insufficient molybdenum abundance in I-*tonB4* causes a lower enzyme activity, as the enzyme bears an iron-molybdenum cofactor (Pernil and Schleiff, 2019). During ongoing growth, however, the enzyme activity seems to recover in a way that diazotrophic growth is not noticeably affected in both I-*tonB2* and I-*tonB4*. A developmental delay could exist in both mutant strains, leading to a retarded nitrogenase activity. Time resolved activity measurements would be required to verify this theory.

Altogether, siderophore transport in *Anabaena* depends on TonB3 and, in case of ferrichrome, presumably also on TonB4. Thus, whether TonB4 is directly involved in ferrichrome translocation across the OM cannot be concluded from the available data. The high number of TBDTs in *Anabaena* suggests that the organism might take up other substrates in a TonB-dependent manner, such as cobalamin or heme. If also TonB3 or one of the other TonB proteins (or both) energize these transport processes remains unclear and should be addressed in future.

4.1.2. The influence of TonB2 on outer membrane integrity

The phenotype of I-*tonB2* displays certain alterations of the OM integrity. The LPS production was shown to be enhanced, and the expression of porin genes was decreased in I-*tonB2* under standard cultivation conditions (Manuscript 2, Fig. 3A, C). Further, the strain is less vulnerable towards harmful compounds compared to wild type (Manuscript 2, Fig. 3). These features can be related; exemplarily it is conceivable that the boosted LPS production supports the adsorption of certain metals. The anionic LPS groups are known to mediate metal binding in bacteria (Coughlin et al., 1983; Strain et al., 1983). A mutant of *Bradyrhizobium japonicum,* where the O-polysaccharide portion of the LPS was absent, demonstrated a reduction in the binding of metals including copper (Oh et al., 2002). Since an elevated copper and molybdenum concentration was observed in I-*tonB2* (Manuscript 2, Table 2), it can be hypothesized that the augmented biosorption of metals further facilitates the diffusion of those into the cell, simply by increasing the substrate concentration at the cell surface. Also, cellular pigmentation is influenced by metal availability; for instance the exposition of *Anabaena oryzae* to high copper, cobalt or zinc concentrations induces an

elevated carotenoid production (Chakilam, 2012). I-*tonB2* displayed a lower chlorophyll to carotenoid ratio under high light, ambient light and low light (Manuscript 2, Table 1). Also, both I-*tonB4* and I-*tonB3* were altered in chlorophyll or carotenoid levels under ambient or low light. Only in case of I-*tonB2*, however, an accumulation of carotenoids was observed under all tested conditions (Manuscript 2, Table 1), which could correspond to the excessive adsorption of e.g. copper. On the other hand, excessive metal chelation might induce changes in envelope components such as the LPS. For example, copper exposure reduced the biofilm formation capacity in *Acidithiobacillus ferrooxidans* by diminishing the extracellular polysaccharide production (Vargas-Straube et al., 2020). Thus, following the philosophic question about what came first, the chicken or the egg, deciphering cause and effect of phenotypic features cannot be provided in here and would require further investigations.

A factor that is also known to cause changes in cellular carotenoid concentration is the oxidative stress level, as carotenoids hold antioxidant properties (Wada et al., 2013). Cyanobacterial species increased the relative amount of carotenoids upon exposure to high light or UV light (Izuhara et al., 2020; Wachi et al., 1995). Therefore, the oxidative stress level in I-*tonB2* compared to wild type was assessed by testing the expression of the superoxide dismutase genes *sodA* and *sodB.* Previous findings established that *sodB* expression gets induced after treatment of the cells with methyl viologen, which induces oxidative stress (Li et al., 2002). Though, in both cases the expression under normal conditions in I-*tonB2* was comparable to wild type (Manuscript 2, Fig. 3D). Thus, it can be assumed that the *tonB2* mutant strain does not suffer from increased stress.

Porins from *E. coli* were found to bind LPS specifically, and LPS prevalence seems to affect porin assembly and trimerization (Arunmanee et al., 2016; De Cock and Tommassen, 1996). The influence of LPS on envelope integrity is illustrated by the phenotype of bacterial mutants that lack LPS or specific parts as the O-polysaccharide (deep-rough mutants), which are highly susceptible towards antibiotics (Nikaido and Vaara, 1985). A decrease in porin expression combined with an alteration in LPS synthesis, as observed in I-*tonB2*, is found in bacteria that demonstrated multiresistance towards antibiotics (Fernández and Hancock, 2012; Rosenfeld and Shai, 2006; Thiolas et al., 2005). In case of *Anabaena*, single recombinant mutants of virtually all porin-like genes (except *alr4550*) did grow better than wild type in presence of SDS, lysozyme or erythromycin (Manuscript 3, Fig. 4A). Hence, the reduction in porin transcription could explain the resistance of I-*tonB2* towards the harmful compounds.

Adverse effects of mutations in *tonB* genes on OM integrity and antibiotic or drug resistance are repeatedly described in literature (Calvopiña et al., 2020; Dong et al., 2021; Godoy et al., 2001; Zhao and Poole, 2002a), which stands in contrast to the monitored resistance of I-

tonB2. Different explanations exist about the high vulnerability of *tonB* mutants towards antibiotics: in *Pseudomonas aeruginosa* and *Aeromonas hydrophila* it is hypothesized that the sensitivity towards antibiotics bases on an influence of *tonB* mutation on multidrug export system (Dong et al., 2021; Zhao et al., 1998; Zhao and Poole, 2002a), whereas in *Stenotrophomonas maltophilia* beat-lactam antibiotics are supposed to enter the cell via TBDTs energized by TonB (Calvopiña et al., 2020). All this implies a great variety in phenotypes of *tonB* mutants regarding antibiotic/drug resistance, and the impacts apparently cannot be generalized. No connection between LPS synthesis regulation and TonB proteins is described in literature, whereas mutations in the related *tol-pal* genes were found to affect the lipid and LPS composition of the OM in *Salmonella* and *E*. *coli*. Mutant strains lacking the Tol-Pal system exhibited an abnormal lipid composition of the OM and it is assumed that the Tol system is involved in the phospholipid transport from the OM to the PM (Masilamani et al., 2018; Shrivastava et al., 2017). Moreover, in *E. coli,* TolA influences the expression of O-antigen subunits (Gaspar et al., 2000), and mutants of the Tol system demonstrated a modulated expression of porin genes (Heyde et al., 1988). The connection of TonB2 to LPS production and porin expression in combination with the maintained schizokinen transport capacity of I-*tonB2* proposes a functioning of *Anabaena* TonB2 related to Tol proteins. As the Tol system is absent from cyanobacteria, it could be assumed that other proteins (such as TonB2?) adopt associated functions.

4.1.3. SjdR is involved in the modulation of peptidoglycan structure

As mentioned previously, in accordance with the novel role of TonB1 that will be explained below, the annotation of the protein was changed to septal junction disc regulator (SjdR). The periplasmic part of SjdR is rather short, and additionally the protein bears an N-terminal extension of 66 amino acids that stretches into the cytosol (Fig. 3; Manuscript 1, Fig. 1B). N-terminal extensions with lengths between 50-100 amino acids as well as very long extensions (lengths around 300 amino acids) were identified in TonB proteins of other bacteria (Chu et al., 2007). For example, the N-terminal extension in *Pseudomonas aeruginosa* TonB1, which is yet not similar to that of SjdR, is crucial for the function of the protein and its stability (Zhao and Poole, 2002b). A conserved domain prediction assigns a gliding GltJ-superfamily-like domain in SjdR, as well as a similarity to ZipA (Manuscript 1, Fig. 1B). To the best of my knowledge, no ZipA homologue was identified among cyanobacteria. ZipA is participating in cell division and stabilizes FtsZ polymers by connecting them to the PM (Haeusser and Margolin, 2016). Interestingly, according to predictions the SjdR ZipA domain is periplasmic and does not stretch into the cytosol, where the canonical ZipA interacts with FtsZ. GltJ is a PM-embedded component of a multiprotein complex required for adventurous gliding motility, which is an active movement of cells over surfaces not mediated by flagella or pili (McBride, 2001). Gliding motility is a conserved mechanism in many

cyanobacteria species, whereas *Anabaena* is characterized as non-motile (Rippka et al., 1979). In *Myxococcus xanthus* the pmf was found to drive bacterial gliding (Nan et al., 2011). Remarkably, homologs to the Tol system and the MreB cytoskeleton are involved in *M. xanthus* gliding motility (Youderian et al., 2003). Thus, harnessing the energy from the pmf in order to initiate mechanical forces might occur through conserved mechanisms, which entails a certain degree of structural similarity of the factors involved (Faure et al., 2016). If SjdR is involved in *Anabaena* gliding was not tested in here, but considering that only a small portion of GltJ overlaps with SjdR it can be assumed that SjdR does not occupy a GltJ-like function.

The *sjdR* mutant maintained the schizokinen transport capacity, similar to wild type, I-*tonB2* and I-*tonB4* (Manuscript 1, Fig. 2C). Thus, SjdR seems not to participate in schizokinen transport. In contrast, I-*sjdR* exhibited severe growth retardations under diazotrophic conditions both in liquid and on solid medium (Manuscript 1, Fig. 2D, E). This can be explained through an insufficient ability to fix nitrogen, due to a compromised nitrogenase enzyme expression and activity in the mutant (Manuscript 1, Fig. 3B, C). Transcriptional analysis revealed that nitrogen metabolism marker genes (*ntcA*, *hepA*) obtained a wild type like expression pattern in I-*sjdR* (Manuscript 1, Fig. 3C). Additionally, *sjdR* transcription was lower after transfer of wild type cultures into medium lacking a combined nitrogen source (Manuscript 1, Fig. 3A, C), which however would be expected for a gene where the corresponding protein is involved in heterocyst differentiation initiation. These findings implicate that SjdR is not directly involved in heterocyst development and metabolism. Instead, the absence of SjdR in the null mutant creates a condition that impedes the proper heterocyst formation.

The septa between adjacent vegetative cells (in presence of nitrate), but most prominently the septa between heterocysts and vegetative cells (in absence of nitrate) were found to be abnormally large in I-*sjdR* compared to that of wild type (Manuscript 1, Fig. 5,6). So apparently the septal PG formation is affected through SjdR malfunction. The gas exchange between neighbouring cells might primarily occur through the septal pores in *Anabaena* (Walsby, 2007). Therefore, the entrance of oxygen into heterocysts might be enhanced in I-*sjdR* through the wide septa, which damages the nitrogenase. And indeed, between both adjacent vegetative cells and between vegetative cells and heterocysts a faster molecular diffusion was measured in the *sjdR* mutant strain (as exemplarily shown for the fluorescent marker molecule calcein, Manuscript 1, Fig. 7 and Table 3). Again, the effect was more pronounced in the latter case. Interestingly, the vegetative cell septa of I-*sjdR* contained less nanopores than wild type, which in this case rejects the assumption that the faster transfer originates from an increased number of nanopores (Manuscript 1, Fig. 8).

In *Anabaena*, considerable research was done on understanding the molecular basis of intracellular communication, nanopore and septal junction formation and regulation. Thus, on the basis of the current knowledge in this field, some explanations about the rationale behind the *sjdR* mutant phenotype can be proposed. Next to nanopore size and number, additional factors can influence the intercellular molecular transfer in *Anabaena*. This is illustrated through a mutant of the glucoside transporter subunit GlsC, that exhibited a decreased calcein transfer velocity but was not altered in the number of nanopores (Nieves-Morión et al., 2017a). In I-*sjdR*, the sparsely developed cyanophycin polymer might facilitate rapid molecular diffusion between heterocysts and vegetative cells, whereas in wild type the polymer acts as physical barrier (Manuscript 3, Fig. 5C, D). An influence of cyanophycin plugs on intercellular diffusion velocity was described before in the cyanobacterium *Anabaena variabilis* (Mullineaux et al., 2008). However, this explanation is not valid for the accelerated transfer between vegetative cells, since cyanophycin granules are only present in heterocysts (Sherman et al., 2000). Interestingly, the velocity of calcein diffusion between vegetative cells was faster after *A. variabilis* cells were transferred into medium without nitrogen source, and thus the nitrogen source in the medium affects molecular diffusion velocity (Mullineaux et al., 2008). To specify in which way the nitrogen status influences the cellular communication in I-*sjdR* would require further investigation.

The activity in terms of the “open state” of the septal junctions, constituting the proteinaceous compounds traversing the nanopores (Flores et al., 2016), can be regulated by external factors. Treatment with an ionophore reversibly impaired the molecular diffusion in *Anabaena* (Weiss et al., 2019). SepJ (FraG), FraC and FraD were proposed to build up the septal junctions in *Anabaena* (Flores et al., 2007; Merino-Puerto et al., 2010). Therefore, an aberrant regulation (of the septal junctions?) in the *sjdR* mutant that modulates the calcein diffusion independent of the nanopore number could present another possible explanation for the observed phenotype. It should be noted that it is not likely that SjdR constitutes a component of the septal junctions, because no polar localization of the SjdR-GFP protein was observed (Manuscript 1, Fig. S3).

Next to the unusually fast molecular diffusion in I-*sjdR*, the aberrant PG morphology of the septa, especially in heterocysts, needs to be explained. Peptidoglycan synthesis determines bacterial cell shape, which is intricately connected to the divisome and elongasome functions (Cabeen and Jacobs-Wagner, 2005). Cell wall plasticity is a prerequisite for proper heterocyst development. *Anabaena* mutant strains lacking proteins involved in cell wall remodelling were found to be compromised in diazotrophic growth, as shown for mutants of the cell wall amidases AmiC1 and AmiC2, the PG synthesis proteins MurB and MurC, or a penicillin binding protein (Berendt et al., 2012; Bornikoel et al., 2017; Lázaro et al., 2001; Lehner et al., 2013; Videau et al., 2016). In *Anabaena*, AmiC1 and AmiC2 are involved in

pore formation and an *amiC1/amiC2* double mutant presents an enlarged septum diameter, which fairly resembles the phenotype of I-*sjdR* (Berendt et al., 2012; Bornikoel et al., 2017). Therefore, it can be speculated that one of these factors is impaired or functionally dysregulated in the *sjdR* mutant. Notably, the regulation of PG synthesis differs between vegetative cells and heterocysts, whereas vegetative cell PG synthesis majorly takes place at the constriction and division points. In heterocysts, PG synthesis is comparatively stronger, and next to the septum sites it is active along the whole cell (Zhang et al., 2018). The heterocyst PG mesh is presumably thicker than that of vegetative cells (Zhang et al., 2018). Regarding the abnormally wide septum of the I-*sjdR* heterocysts, SjdR seems to affect certain processes (e.g. related to PG synthesis regulation) that have differentiated activities in heterocysts and vegetative cells, in this case making the effect more visible in heterocysts.

The calcium concentration was augmented in I-*sjdR*, but not in the other *tonB* mutants (Manuscript 1, Table 2; Manuscript 3, Table 1). Calcium in cyanobacteria influences important cellular mechanisms such as nitrogen fixation (Smith et al., 1987; Singh and Mishra, 2014; Torrecilla et al., 2004b) or photosynthesis (Torrecilla et al., 2004a; Walter et al., 2016). In *Nostoc* sp. PCC 6720, calcium supplementation could improve the performance of the nitrogenase and the assimilation of dinitrogen, whereas the concentration applied in the experiments conducted during this study (5 mM) can be considered as relatively high and therefore rather detrimental for the cells (Smith et al., 1987). Interestingly, an excess of calcium in the medium could partly compensate the growth defects of I-*sjdR* in absence of a combined nitrogen source. In the presence of 5 mM $CaCl_2$ the cellular morphology of *sjdR* mutant cells changed; (i) the septa between vegetative cells increased in diameter, and (ii) the heterocyst septa were more constricted than under normal conditions ($YBG11_0$ contains 245 µM $CaCl_2$; Manuscript 1, Fig. 6 and Table 2). In the first case, the enlargement of the septa is limited to I-*sjdR*, whereas the septum width of wild type was found to be constant, independent of the tested calcium concentration. In the latter case, *sjdR* mutant septa in standard $YBG11_0$ are enlarged, and when 5 mM $CaCl_2$ is present the size normalizes, meaning it gets closer to wild type phenotype. Therefore, in I-*sjdR* calcium in both cases influences the septum morphology, most likely the PG synthesis regulation. Only recently it was observed that the calcium concentration influences and putatively regulates the MreB polymerization and remodelling (Szatmári et al., 2020). The actin-like MreB occupies a key role in cell morphology determination being part of the elongasome, a multiprotein complex conveying cell elongation (Shi et al., 2018). Thus, it is conceivable that *sjdR* mutation in *Anabaena* causes cell wall synthesis regulatory effects, which are partly abrogated through calcium mediated PG rearrangement. In which way the maintenance of septum integrity in conferred by SjdR remains elusive. It would be of interest if the *sjdR* mutant under high

calcium conditions also reduces (normalizes) the velocity of molecular diffusion. If so, this could explain the regenerated growth capacity. Considering the outlined findings about the *sjdR* mutant phenotype, we do not any longer include this protein in the set of potential TonB like proteins. We suggest that SjdR constitutes a novel factor that is involved in PG ultrastructure formation and conserved among cyanobacteria.

4.2. Relevance of the *Anabaena* porin-like proteins

Porin proteins play important roles in nutrient uptake and membrane integrity including antibiotic resistance, and might thereby considerably shape the fitness and stress resistance potential of organisms (Galdiero et al., 2013; Pagès et al., 2008; Vergalli et al., 2020). Bioinformatic predictions assigned nine porin-like proteins in *Anabaena*, whereas the seven candidates that contained the expected structural features were analysed in this study (Manuscript 3, Fig. 1; in the following also termed “porins”). The aim of this analysis was to gain first hints about the potential substrates and the functional specificity of the single proteins. A comparison of transcriptional patterns of the porin genes in response to metal starvation, as well as a collating phenotypic analysis of the respective single recombinant mutants is provided in the frame of Manuscript 3, and the implications will be discussed below.

In seven putative porin proteins from *Anabaena* an OprB-domain was predicted (Nicolaisen et al., 2009). OprB from *Pseudomonas aeruginosa* is a carbohydrate selective porin (Wylie and Worobec, 1995). *Anabaena* is able to grow mixotrophically, and growth can be stimulated through sugar supplementation (Nieves-Morión and Flores, 2018; Stebegg et al., 2012). In our hands the growth of *Anabaena* wild type was similar in presence and absence of sugars (not shown), and hence the focus of the analysis of the porin-like genes was set on metal and salt substrates. Except All5191, all analysed porins contain an S-layer homology like domain (SLH domain) in the N-terminal region, which might represent a site of interaction with PG related components (Manuscript 3, Fig. 1). SLH domains are also described in OM channel proteins of other organisms, such as *Selenomonas ruminantium* (Kojima et al., 2016). Here, the SLH domain is thought to confer stability by interaction with the PG. *Selenomonas ruminantium* lacks the Tol-Pal machinery, similarly to cyanobacteria, and it can be speculated that SLH-containing porins might take over the Tol-Pal function of attaching the OM to the cell wall (Kojima et al., 2016). As mentioned above, only in All5191 an SLH domain was not identified. Also, the related mutant I-*all5191* was the only strain retarded in diazotrophic growth (Manuscript 3, Fig. 2B). This, in combination with the increased heterocyst frequency in I-*all5191,* suggests an inefficient nitrogen assimilation in this strain. It can be assumed that All5191 is not specifically localized in the heterocyst OM, because in earlier studies heterocyst and vegetative cells OM could not be discriminated through protein

composition (Moslavac et al., 2007). Thus, All5191 appears to impact nitrogen fixation, or any factor impacting diazotrophic growth, in a yet unknown way which does not require an SLH-mediated interaction with the cell wall.

The transcription of the seven porin genes was analysed after growth of wild type cultures for 21 days in different media depleted of single metals (Manuscript 3). In case of manganese, copper and zinc the degree of starvation after this time period is unknown, due to the lack of specific starvation markers. In contrast, iron starvation is described to have an impact on the cells at an early time point, meaning already a few days after the cells were transferred to iron-free medium (as measured from the cellular chlorophyll concentration decrease, Narayan et al., 2011; Rudolf et al., 2016). The cultivation of *Anabaena* in manganese-free medium does not impact growth even after several weeks of starvation (Manuscript 1, Fig. 4A), highlighting the diversity of metal requirements and starvation perception in *Anabaena*. Considering this, the observed expression induction of porin-like genes in iron-free (*alr0834*, *all4499*, *all5191*) or manganese-free medium (*alr0834*, *alr2231*, *alr4741*, *all5191*) might imply a role of the related proteins in the diffusion of the compounds but does not exclude other genes to be involved as well, as only one time point during depletion growth was investigated.

Alr2231 is described as a protein unique to cyanobacteria, without orthologs in other bacteria classes (Martin et al., 2003). An insertional mutant of *alr2231* did grow to a comparatively higher density than wild type in presence of high zinc concentrations, which was a unique observation among the porin mutants (Manuscript 3, Fig. 2C, D). This proposes zinc as a putative substrate for Alr2231. The zinc demand of cyanobacteria might differ from that of heterotrophic bacteria because it is required for heterocyst function and carbon fixation (Cavet et al., 2003; Pernil and Schleiff, 2019). Porin expression connected to zinc availability is not (only) described in cyanobacteria, but also in other genera as *Mycobacterium smegmatis* (Goethe et al., 2020) or *Pseudomonas* (Lim et al., 2013; Marguerettaz et al., 2014).

Although an altered expression of the porin genes was not observed after *Anabaena* was grown in copper depleted medium, copper excess might lead to the decrease of the porin mRNA abundance. All porin mutants except I-*alr4741* were comparatively more resistant towards wild type toxic copper concentrations (Manuscript 3, Fig. 2C, D). Interestingly, exactly these genes (again with exception of *alr4741*) were decreased in expression in I-*tonB2,* a strain that accumulates copper intracellularly (Manuscript 2, Table 2 and Fig. 3C). This supports a general effect of copper on porin gene expression, which might be mirrored in the I-*tonB2* phenotype.

For two putative porin-like genes in *Anabaena*, namely *alr4550* and *alr0834*, as well as for the Omp85 encoding gene *alr2269*, a transcriptional regulation by the conserved small RNA Yfr1 was suggested, since Yfr1 did bind to the respective mRNAs (Brenes-Álvarez et al., 2020). Yfr1 interaction diminished the expression of these genes, as well as of other genes related to cell wall integrity and synthesis. It is suggested that Yfr1 modulated cell envelope stability and remodelling during differentiation in *Anabaena* (Brenes-Álvarez et al., 2020). An *yfr1* overexpression strain was increasingly sensitive towards antibiotics as vancomycin and erythromycin and against SDS, whereas in our studies I-*alr4550* but not I-*alr0834* was hypersensitive towards SDS and erythromycin (Manuscript 3, Fig. 4). Alr4550 is a special candidate among *Anabaena* porins, because is displays exclusive features: (i) the protein is among the highest abundant OM proteins in *Anabaena* (Moslavac et al., 2005), (ii) *alr4550* expression was decreased after growth in medium depleted of iron, zinc or copper and (iii) the respective mutant, I-*alr4550*, shows a general and high susceptibility towards high metal and detergent concentrations (Manuscript 3, Table 1 and Fig. 4A). Therefore, Alr4550 might take over a structurally important role in *Anabaena*, possibly via connecting the OM to the cell wall via the SLH domain, conferring stability to the cells as described for OmpA-like channels (Samsudin et al., 2016). An increased vulnerability towards salt and harmful compounds is described for strains mutated in *ompA* e.g. in *Acinetobacter baumannii* and *E. coli* (Choi and Lee, 2019; Smani et al., 2014; Wang, 2002). Furthermore, it should be mentioned that the investigation of the three Omp85 mutants in *Anabaena* led to the hypothesis that Alr4893 and Alr2269 might be involved in the membrane insertion of porins, whereas the third Omp85 protein, Alr0075, seems not to be participating. In the respective mutants an elevated amount of presumably degraded and aggregated products of Alr4550 were detected, and the densiometric distribution of Alr4550 was altered (Manuscript 3, Fig. 5).

4.3. Putative roles of TonB- and porin-like proteins in *Anabaena*: a summary

During this study, components putatively involved in the active translocation of metal chelates across the OM, TonB-like proteins, as well as porins presumably facilitating the diffusion of solutes were examined. An initial assessment about putative roles of the porins in *Anabaena* was presented in here, through the analysis of porin gene expression and the comparative mutant phenotyping. It became apparent that certain porin mutants showed exclusive features that were not observed in other mutants, and thus a special position was ascribed to the respective candidate proteins. The absence of Alr4550 strongly affects the envelope integrity, suggesting that this protein confers membrane stability, possibly by anchoring the OM to the cell wall through the SLH domain (Fig. 6A). Further, All5191 in a yet unknown way is required for normal diazotrophic growth, as the respective mutant exhibited

a strong growth delay under these conditions. The results of expression analyses in combination with the mutant phenotyping might suggest the involvement of certain porin candidates in uptake of salts, zinc, manganese, cobalt or antibiotics (Fig. 6A). Certainly, deeper investigations, including for example diffusion rate measurements, would be required to concretely assign substrates to the single porins.

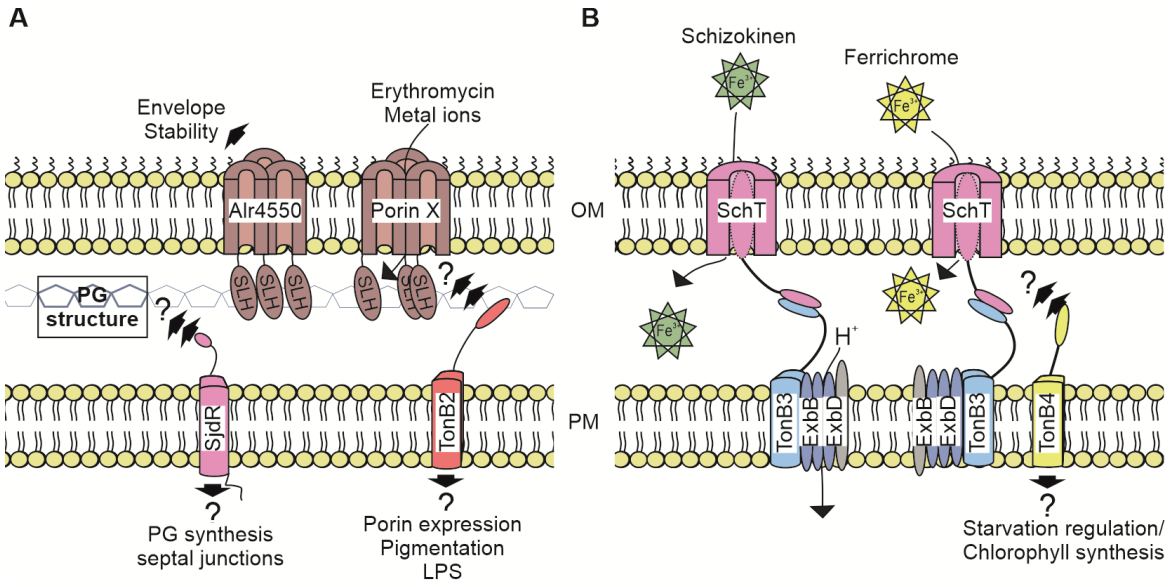

Figure 6. Properties of porins and TonB-like proteins in *Anabaena*. **A** The porin Alr4550 presumably occupies a role in outer membrane (OM) integrity maintenance which might involve the anchoring of the OM to the cell wall via the Surface layer homology domain (SLH). Other porin candidates can be connected to the uptake of metal irons or antibiotics. TonB2 malfunction affects porin transcription, lipopolysaccharide production and pigmentation, which links the protein function to these processes. SjdR likely is involved in peptidoglycan (PG) structure formation and affects the intracellular molecule transfer. **B** TonB3 as well as the TBDT SchT are involved in the translocation of schizokinen (green) and ferrichrome (yellow). The role of TonB4 in ferrichrome utilization and iron starvation regulation remains unclear. PM = plasma membrane.

Regarding the TonB-dependent transport in *Anabaena* it became obvious that the formerly assigned four TonB-like proteins are functionally diverse, because respective mutants partially exhibited specific phenotypes. It can be stated that SjdR (earlier annotated as TonB1) is a newly identified factor that influences PG ultrastructure (Fig 6A), which was made particularly apparent by the aberrant heterocyst morphology of the *sjdR* mutant. This again induces various cellular alterations (e.g. in intercellular diffusion velocity, diazotrophic growth and nanopore distribution) shaping the I-*sjdR* phenotype. Considering this in combination with the protein features (short periplasmic domain and homology to ZipA or GltJ proteins), we eliminate SjdR from the list of *Anabaena* TonB proteins. Next to SjdR, also TonB2 deletion causes specific effects that cannot entirely be explained through a canonical TonB function. I-*tonB2* was not hampered in siderophore transport, as assessed for ferric schizokinen and ferrichrome. However, next to alterations in the cellular metal and pigment concentration, the I-*tonB2* mutant demonstrates envelope modifications such as an

enhanced LPS abundance and a putative decrease of porin abundance, as judged from the lowered gene expression. That decreases the vulnerability of the strain towards antibiotics. An influence on porins and LPS is not described for *tonB* mutants in other organisms, whereas in *tol* mutants those modifications were described (Gaspar et al., 2000; Heyde et al., 1988). Therefore, we propose that TonB2 might hold a function related to the Tol system. Considering the absence of this system in cyanobacteria, other factors like TonB2 might partly adopt functional features ascribed to the Tol system (Fig. 6A). TonB3 can be considered as the essential component mediating the translocation of ferric compounds in *Anabaena* (Fig. 6B). Exemplarily, this was established for iron loaded schizokinen and ferrichrome; both compounds were not accessible to a *tonB3* mutant. A connection between TonB4 and schizokinen uptake could not be drawn, whereas ferrichrome appeared to be inaccessible to the *tonB4* mutant strain. The influence of TonB4 on ferrichrome transport, as well as the capacity of I-*tonB3* and I-*tonB4* to transport other substrates of *Anabaena* TBDTs, such as cobalamin and heme (unpublished results from Julia Graf), needs to be assessed in the future in order to comprehensively characterize TonB-dependent transport in *Anabaena*.

5. References

Achilles, K.M., Church, T.M., Wilhelm, S.W., Luther, G.W., Hutchins, D.A., 2003. Bioavailability of iron to *Trichodesmium* colonies in the western subtropical Atlantic Ocean. Limnol. Oceanogr. 48, 2250–2255.

Achouak, W., Heulin, T., Pagès, J.-M., 2001. Multiple facets of bacterial porins. FEMS Microbiol. Lett. 199, 1–7.

Ahmer, B.M.M., Thomas, M.G., Larsen, R.A., Postle, K., 1995. Characterization of the *exbBD* operon of *Escherichia coli* and the role of ExbB and ExbD in TonB function and stability. J. Bacteriol. 177, 4742–4747.

Ainsaar, K., Tamman, H., Kasvandik, S., Tenson, T., Hõrak, R., 2019. The $TonB_m$-pocAB system is required for maintenance of membrane integrity and polar position of flagella in *Pseudomonas putida*. J. Bacteriol. 201, e00303-19.

Al Shaer, D., Al Musaimi, O., de la Torre, B.G., Albericio, F., 2020. Hydroxamate siderophores: Natural occurrence, chemical synthesis, iron binding affinity and use as Trojan horses against pathogens. Eur. J. Med. Chem. 208, 112791.

Andrews, S.C., Robinson, A.K., Rodríguez-Quiñones, F., 2003. Bacterial iron homeostasis. FEMS Microbiol. Rev. 27, 215–237.

Arévalo, S., Nenninger, A., Nieves-Morión, M., Herrero, A., Mullineaux, C.W., Flores, E., 2021. Coexistence of Communicating and Noncommunicating Cells in the Filamentous Cyanobacterium *Anabaena*. mSphere 6, e01091-20.

Arunmanee, W., Pathania, M., Solovyova, A.S., Le Brun, A.P., Ridley, H., Baslé, A., Van Den Berg, B., Lakey, J.H., 2016. Gram-negative trimeric porins have specific LPS binding sites that are essential for porin biogenesis. Proc. Natl. Acad. Sci. U. S. A. 113, E5034–E5043.

Asmar, A.T., Ferreira, J.L., Cohen, E.J., Cho, S.H., Beeby, M., Hughes, K.T., Collet, J.F., 2017. Communication across the bacterial cell envelope depends on the size of the periplasm. PLoS Biol. 15, e2004303.

Babykin, M.M., Obando, T.S.A., Zinchenko, V. V., 2018. TonB-Dependent Utilization of Dihydroxamate Xenosiderophores in *Synechocystis* sp. PCC 6803. Curr. Microbiol. 75, 117–123.

Bagg, A., Neilands, J.B., 1987. Ferric uptake regulation protein acts as a repressor, employing iron(II) as a cofactor to bind the operator of an iron transport operon in *Escherichia coli*. Biochemistry 26, 5471–5477.

Baker, K.R., Postle, K., 2013. Mutations in *Escherichia coli* ExbB transmembrane domains identify scaffolding and signal transduction functions and exclude participation in a proton pathway. J. Bacteriol. 195, 2898–2911.

Basle, A., Qutub, R., Mehrazin, M., Wibbenmeyer, J., Delcour, A.H., 2004. Deletions of single extracellular loops affect pH sensitivity, but not voltage dependence, of the *Escherichia coli* porin OmpF. Protein Eng. Des. Sel. 17, 665–672.

Benevides-Matos, N., Wandersman, C., Biville, F., 2008. HasB, the *Serratia marcescens* TonB paralog, is specific to HasR. J. Bacteriol. 190, 21–27.

Benz, R., Schmid, A., Hancock, R.E.W., 1985. Ion selectivity of gram-negative bacterial porins. J. Bacteriol. 162, 722–727.

Berendt, S., Lehner, J., Zhang, Y.V., Rasse, T.M., Forchhammer, K., Maldener, I., 2012. Cell wall amidase AmiC1 is required for cellular communication and heterocyst development in the cyanobacterium *Anabaena* PCC 7120 but not for filament integrity. J. Bacteriol. 194, 5218–5227.

Bernadac, A., Gavioli, M., Lazzaroni, J.C., Raina, S., Lloubès, R., 1998. *Escherichia coli tol-pal* mutants form outer membrane vesicles. J. Bacteriol. 180, 4872–4878.

Bornikoel, J., Carrión, A., Fan, Q., Flores, E., Forchhammer, K., Mariscal, V., Mullineaux, C.W., Perez, R., Silber, N., Peter Wolk, C., Maldener, I., 2017. Role of two cell wall amidases in septal junction and nanopore formation in the multicellular cyanobacterium *Anabaena* sp. PCC 7120. Front. Cell. Infect. Microbiol. 7:e00386.

Boyd, P.W., Ellwood, M.J., 2010. The biogeochemical cycle of iron in the ocean. Nat. Geosci. 3, 675–682.

Braun, V., Gnirke, H., Henning, U., Rehn, K., 1973. Model for the structure of the shape-maintaining layer of the *Escherichia coli* cell envelope. J. Bacteriol. 114, 1264–1270.

Braun, V., Herrmann, C., 1993. Evolutionary relationship of uptake systems for biopolymers in *Escherichia coli*: cross-complementation between the TonB-ExbB-ExbD and the TolA-TolQ-TolR proteins. Mol. Microbiol. 8, 261–268.

Brenes-Álvarez, M., Vioque, A., Muro-Pastor, A.M., 2020. The integrity of the cell wall and its remodeling during heterocyst differentiation are regulated by phylogenetically conserved small RNA Yfr1 in *Nostoc* sp. strain PCC 7120. MBio 11, e02599-19.

Brockwell, D.J., Paci, E., Zinober, R.C., Beddard, G.S., Olmsted, P.D., Smith, D.A., Perham, R.N., Radford, S.E., 2003. Pulling geometry defines the mechanical resistance of a β-sheet protein. Nat. Struct. Biol. 10, 731–737.

Brouwer, E.M., Ngo, G., Yadav, S., Ladig, R., Schleiff, E., 2019. Tic22 from *Anabaena* sp. PCC 7120 with holdase function involved in outer membrane protein biogenesis shuttles between plasma membrane and Omp85. Mol. Microbiol. 111, 1302–1316.

Burnat, M., Herrero, A., Flores, E., 2014. Compartmentalized cyanophycin metabolism in the diazotrophic filaments of a heterocystforming cyanobacterium. Proc. Natl. Acad. Sci. U. S. A. 111, 3823–3828.

Cabeen, M.T., Jacobs-Wagner, C., 2005. Bacterial cell shape. Nat. Rev. Microbiol. 3, 601–610.

Cadieux, N., Kadner, R.J., 1999. Site-directed disulfide bonding reveals an interaction site between energy-coupling protein TonB and BtuB, the outer membrane cobalamin transporter. Proc. Natl. Acad. Sci. U. S. A. 96, 10673–10678.

Calvopiña, K., Dulyayangkul, P., Heesom, K.J., Avison, M.B., 2020. TonB-dependent uptake of β-lactam antibiotics in the opportunistic human pathogen *Stenotrophomonas maltophilia*. Mol. Microbiol. 113, 492–503.

Cascales, E., Gavioli, M., Sturgis, J.N., Lloubes, R., 2000. Proton motive force drives the interaction of the inner membrane TolA and outer membrane Pal proteins in *Escherichia coli*. Mol. Microbiol. 38, 904–915.

Cascales, E., Lloubès, R., Sturgis, J.N., 2001. The TolQ-TolR proteins energize TolA and share homologies with the flagellar motor proteins MotA-MotB. Mol. Microbiol. 42, 795–807.

Catel-Ferreira, M., Marti, S., Guillon, L., Jara, L., Coadou, G., Molle, V., Bouffartigues, E., Bou, G., Shalk, I., Jouenne, T., Vila-Farrés, X., Dé, E., 2016. The outer membrane porin OmpW of *Acinetobacter baumannii* is involved in iron uptake and colistin binding. FEBS Lett. 590, 224–231.

Cavet, J.S., Borrelly, G.P.M., Robinson, N.J., 2003. Zn, Cu and Co in cyanobacteria: selective control of metal availability. FEMS Microbiol. Rev. 27, 165–181.

Celia, H., Botos, I., Ni, X., Fox, T., De Val, N., Lloubes, R., Jiang, J., Buchanan, S.K., 2019. Cryo-EM structure of the bacterial Ton motor subcomplex ExbB–ExbD provides information on structure and stoichiometry. Commun. Biol. 2, 358.

Celia, H., Noinaj, N., Buchanan, S.K., 2020. Structure and stoichiometry of the Ton molecular motor. Int. J. Mol. Sci. 21, 375.

Celia, H., Noinaj, N., Zakharov, S.D., Bordignon, E., Botos, I., Santamaria, M., Barnard, T.J., Cramer, W.A., Lloubes, R., Buchanan, S.K., 2016. Structural insight into the role of the Ton complex in energy transduction. Nature 538, 60–65.

Chakilam, S.R., 2012. Metal effects on carotenoid content of Cyanobacteria. Int. J. Bot. 8, 192–197.

Chandrangsu, P., Rensing, C., Helmann, J.D., 2017. Metal homeostasis and resistance in bacteria. Nat. Rev. Microbiol. 15, 338–350.

Chang, C., Mooser, A., Plückthun, A., Wlodawer, A., 2001. Crystal structure of the dimeric C-terminal domain of TonB reveals a novel fold. J. Biol. Chem. 276, 27535–27540.

Chen, H.-Y.S., Bandyopadhyay, A., Pakrasi, H.B., 2018. Function, regulation and distribution of IsiA, a membrane-bound chlorophyll *a*-antenna protein in cyanobacteria. Photosynthetica 56, 322–333.

Chevalier, S., Bouffartigues, E., Bodilis, J., Maillot, O., Lesouhaitier, O., Feuilloley, M.G.J., Orange, N., Dufour, A., Cornelis, P., 2017. Structure, function and regulation of *Pseudomonas aeruginosa* porins. FEMS Microbiol. Rev. 41, 698–722.

Chimento, D.P., Kadner, R.J., Wiener, M.C., 2005. Comparative structural analysis of TonB-dependent outer membrane transporters: Implications for the transport cycle. Proteins Struct. Funct. Bioinforma. 59, 240–251.

Choi, U., Lee, C.R., 2019. Distinct roles of outer membrane porins in antibiotic resistance and membrane integrity in *Escherichia coli*. Front. Microbiol. 10, 1–9.

Chorev, D.S., Baker, L.A., Wu, D., Beilsten-Edmands, V., Rouse, S.L., Zeev-Ben-Mordehai, T., Jiko, C., Samsudin, F., Gerle, C., Khalid, S., Stewart, A.G., Matthews, S.J., Grünewald, K., Robinson, C. V., 2018. Protein assemblies ejected directly from native membranes yield complexes for mass spectrometry. Science 362, 829–834.

Chu, B.C.H., Peacock, R.S., Vogel, H.J., 2007. Bioinformatic analysis of the TonB protein family. BioMetals 20, 467–483.

Cohen, E.J., Ferreira, J.L., Ladinsky, M.S., Beeby, M., Hughes, K.T., 2017. Nanoscale-length control of the flagellar driveshaft requires hitting the tethered outer membrane. Science 356, 197–200.

Collins, R.F., Beis, K., Dong, C., Botting, C.H., McDonnell, C., Ford, R.C., Clarke, B.R., Whitfield, C., Naismith, J.H., 2007. The 3D structure of a periplasm-spanning platform required for assembly of group 1 capsular polysaccharides in *Escherichia coli*. Proc. Natl. Acad. Sci. U. S. A. 104, 2390–2395.

Costa, O.Y.A., Raaijmakers, J.M., Kuramae, E.E., 2018. Microbial extracellular polymeric substances: Ecological function and impact on soil aggregation. Front. Microbiol. 9, 1636.

Coughlin, R.T., Tonsager, S., McGroarty, E.J., 1983. Quantitation of metal cations bound to membranes and extracted lipopolysaccharide of *Escherichia coli*. Biochemistry 22, 2002–2007.

Cowan, S.W., Schirmer, T., Rummel, G., Steiert, M., Ghosh, R., Pauptit, R.A., Jansonius, J.N., Rosenbusch, J.P., 1992. Crystal structures explain functional properties of two *E. coli* porins. Nature 358, 727–733

Cowles, K.N., Moser, T.S., Siryaporn, A., Nyakudarika, N., Dixon, W., Turner, J.J., Gitai, Z., 2013. The putative Poc complex controls two distinct *Pseudomonas aeruginosa* polar motility mechanisms. Mol. Microbiol. 90, 923–938.

De Amorim, G.C., Prochnicka-Chalufour, A., Delepelaire, P., Lefèvre, J., Simenel, C., Wandersman, C., Delepierre, M., Izadi-Pruneyre, N., 2013. The structure of HasB reveals a new class of TonB protein fold. PLoS One 8, e58964.

De Cock, H., Tommassen, J., 1996. Lipopolysaccharides and divalent cations are involved in the formation of an assembly-competent intermediate of outer-membrane protein PhoE of *E. coli*. EMBO J. 15, 5567–5573.

Dong, Y., Li, Q., Geng, J., Cao, Q., Zhao, D., Jiang, M., Li, S., Lu, C., Liu, Y., 2021. The TonB system in *Aeromonas hydrophila* NJ-35 is essential for $MacA_2B_2$ efflux pump-mediated macrolide resistance. Vet. Res. 52, 63.

Duan, K., Lafontaine, E.R., Majumdar, S., Sokol, P.A., 2000. RegA, iron, and growth phase regulate expression of the *Pseudomonas aeruginosa tol-oprL* gene cluster. J. Bacteriol. 182, 2077–2087.

Durai, P., Batool, M., Choi, S., 2015. Structure and effects of cyanobacterial lipopolysaccharides. Mar. Drugs 13, 4217–4230.

Ehling-Schulz, M., Bilger, W., Scherer, S., 1997. UV-B-induced synthesis of photoprotective pigments and extracellular polysaccharides in the terrestrial cyanobacterium *Nostoc commune*. J. Bacteriol. 179, 1940–1945.

Ehrenreich, I.M., Waterbury, J.B., Webb, E.A., 2005. Distribution and diversity of natural product genes in marine and freshwater cyanobacterial cultures and genomes. Appl. Environ. Microbiol. 71, 7401–7413.

Eick-Helmerich, K., Braun, V., 1989. Import of biopolymers into *Escherichia coli*: nucleotide sequences of the *exbB* and *exbD* genes are homologous to those of the *tolQ* and *tolR* genes, respectively. J. Bacteriol. 171, 5117–5126.

Ertel, F., Mirus, O., Bredemeier, R., Moslavac, S., Becker, T., Schleiff, E., 2005. The evolutionarily related β-barrel polypeptide transporters from *Pisum sativum* and *Nostoc* PCC7120 contain two distinct functional domains. J. Biol. Chem. 280, 28281–28289.

Fanucci, G.E., Coggshall, K.A., Cadieux, N., Kim, M., Kadner, R.J., Cafiso, D.S., 2003. Substrate-induced conformational changes of the perplasmic N-terminus of an outer-membrane transporter by site-directed spin labeling. Biochemistry 42, 1391–1400.

Faure, L.M., Fiche, J.B., Espinosa, L., Ducret, A., Anantharaman, V., Luciano, J., Lhospice, S., Islam, S.T., Tréguier, J., Sotes, M., Kuru, E., Van Nieuwenhze, M.S., Brun, Y. V., Théodoly, O., Aravind, L., Nollmann, M., Mignot, T., 2016. The mechanism of force transmission at bacterial focal adhesion complexes. Nature 539, 530–535.

Fay, P., 1992. Oxygen relations of nitrogen fixation in cyanobacteria. Microbiol. Rev. 56, 340–373.

Ferguson, A.D., Deisenhofer, J., 2004. Metal Import through Microbial Membranes. Cell 116, 15–24.

Ferguson, A.D., Ködding, J., Walker, G., Bös, C., Coulton, J.W., Diederichs, K., Braun, V., Welte, W., 2001. Active transport of an antibiotic rifamycin derivative by the outer-membrane protein FhuA. Structure 9, 707–716.

Fernández, L., Hancock, R.E.W., 2012. Adaptive and mutational resistance: Role of porins and efflux pumps in drug resistance. Clin. Microbiol. Rev. 25, 661–681.

Finney, L.A., O'Halloran, T. V., 2003. Transition metal speciation in the cell: Insights from the chemistry of metal ion receptors. Science 300, 931–936.

Fischer, E., Günter, K., Braun, V., 1989. Involvement of ExbB and TonB in transport across the outer membrane of *Escherichia coli*: phenotypic complementation of *exb* mutants by overexpressed *tonB* and physical stabilization of TonB by ExbB. J. Bacteriol. 171, 5127–5134.

Flores, E., Herrero, A., Forchhammer, K., Maldener, I., 2016. Septal Junctions in Filamentous Heterocyst-Forming Cyanobacteria. Trends Microbiol. 24, 79–82.

Flores, E., Herrero, A., Wolk, C.P., Maldener, I., 2006. Is the periplasm continuous in filamentous multicellular cyanobacteria? Trends Microbiol. 14, 439–443.

Flores, E., Nieves-Morión, M., Mullineaux, C.W., 2018. Cyanobacterial septal junctions: Properties and regulation. Life 9, 1.

Flores, E., Pernil, R., Muro-Pastor, A.M., Mariscal, V., Maldener, I., Lechno-Yossef, S., Fan, Q., Wolk, C.P., Herrero, A., 2007. Septum-localized protein required for filament integrity and diazotrophy in the heterocyst-forming cyanobacterium *Anabaena* sp. strain PCC 7120. J. Bacteriol. 189, 3884–3890.

Foster, A.W., Osman, D., Robinson, N.J., 2014. Metal Preferences and Metallation. J. Biol. Chem. 289, 28095–28103.

Freed, D.M., Lukasik, S.M., Sikora, A., Mokdad, A., Cafiso, D.S., 2013. Monomeric TonB and the Ton box are required for the formation of a high-affinity transporter-TonB complex. Biochemistry 52, 2638–2648.

Fresenborg, L.S., Graf, J., Schätzle, H., Schleiff, E., 2020. Iron homeostasis of cyanobacteria: advancements in siderophores and metal transporters, in: Advances in Cyanobacterial Biology. Elsevier, pp. 85–117.

Galdiero, S., Falanga, A., Cantisani, M., Tarallo, R., Elena Della Pepa, M., D'Oriano, V., Galdiero, M., 2013. Microbe-Host Interactions: Structure and Role of Gram-Negative Bacterial Porins. Curr. Protein Pept. Sci. 13, 843–854.

Gallon, J.R., 1992. Reconciling the incompatible: N_2 fixation and O_2. New Phytol. 122, 571–609.

Gaspar, J.A., Thomas, J.A., Marolda, C.L., Valvano, M.A., 2000. Surface expression of O-specific lipopolysaccharide in *Escherichia coli* requires the function of the TolA protein. Mol. Microbiol. 38, 262–275.

Gerding, M.A., Ogata, Y., Pecora, N.D., Niki, H., de Boer, P.A.J., 2007. The trans-envelope Tol–Pal complex is part of the cell division machinery and required for proper outer-membrane invagination during cell constriction in *E. coli*. Mol. Microbiol. 63, 1008–1025.

Gerken, H., Vuong, P., Soparkar, K., Misra, R., 2020. Roles of the ENVZ/OMPR two-component system and porins in iron acquisition in *Escherichia coli*. MBio 11, 1–18.

Germon, P., Ray, M.C., Vianney, A., Lazzaroni, J.C., 2001. Energy-dependent conformational change in the TolA protein of *Escherichia coli* involves its N-terminal domain, TolQ, and TolR. J. Bacteriol. 183, 4110–4114.

Gledhill, M., Buck, K.N., 2012. The organic complexation of iron in the marine environment: A review. Front. Microbiol. 3, 1–17.

Godoy, P., Ramos-González, M.I., Ramos, J.L., 2001. Involvement of the TonB system in tolerance to solvents and drugs in *Pseudomonas putida* DOT-T1E. J. Bacteriol. 183, 5285–5292.

Goethe, E., Laarmann, K., Lührs, J., Jarek, M., Meens, J., Lewin, A., Goethe, R., 2020. Critical Role of Zur and SmtB in Zinc Homeostasis of *Mycobacterium smegmatis*. mSystems 5, e0080-19.

González-Sánchez, A., Cubillas, C.A., Miranda, F., Dávalos, A., García-de los Santos, A., 2018. The *ropAe* gene encodes a porin-like protein involved in copper transit in *Rhizobium etli* CFN42. Microbiologyopen 7, e00573.

González, A., Angarica, V.E., Sancho, J., Fillat, M.F., 2014. The FurA regulon in *Anabaena* sp. PCC 7120: In silico prediction and experimental validation of novel target genes. Nucleic Acids Res. 42, 4833–4846.

González, A., Bes, M.T., Barja, F., Peleato, M.L., Fillat, M.F., 2010. Overexpression of FurA in *Anabaena* sp. PCC 7120 Reveals New Targets for This Regulator Involved in Photosynthesis, Iron Uptake and Cellular Morphology. Plant Cell Physiol. 51, 1900–1914.

González, A., Bes, M.T., Luisa Peleato, M., Fillat, M.F., 2016. Expanding the role of FurA as essential global regulator in cyanobacteria. PLoS One 11, e0151384.

González, A., Bes, M.T., Valladares, A., Peleato, M.L., Fillat, M.F., 2012. FurA is the master regulator of iron homeostasis and modulates the expression of tetrapyrrole biosynthesis genes in *Anabaena* sp. PCC 7120. Environ. Microbiol. 14, 3175–3187.

González, A., Fillat, M.F., Bes, M.-T., Peleato, M.-L., Sevilla, E., 2018. The Challenge of Iron Stress in Cyanobacteria, in: Cyanobacteria. InTech.

Gray, A.N., Egan, A.J.F., van't Veer, I.L., Verheul, J., Colavin, A., Koumoutsi, A., Biboy, J., Altelaar, M.A.F., Damen, M.J., Huang, K.C., Simorre, J.P., Breukink, E., den Blaauwen, T., Typas, A., Gross, C.A., Vollmer, W., 2015. Coordination of peptidoglycan synthesis and outer membrane constriction during *Escherichia coli* cell division. Elife 4, e07118.

Gresock, M.G., Savenkova, M.I., Larsen, R.A., Ollis, A.A., Postle, K., 2011. Death of the Tonb Shuttle Hypothesis. Front. Microbiol. 2, 206.

Gumbart, J., Wiener, M.C., Tajkhorshid, E., 2007. Mechanics of force propagation in TonB-dependent outer membrane transport. Biophys. J. 93, 496–504.

Haeili, M., Speer, A., Rowland, J.L., Niederweis, M., Wolschendorf, F., 2015. The role of porins in copper acquisition by mycobacteria. Int. J. Mycobacteriology 4, 91–92.

Haeusser, D.P., Margolin, W., 2016. Splitsville: Structural and functional insights into the dynamic bacterial Z ring. Nat. Rev. Microbiol. 14, 305–319.

Hahn, A., Schleiff, E., 2014. The Cell Envelope, in: Flores, E., Herrero, A. (Eds.), The Cell Biology of Cyanobacteria. Caister Academic Press, U.K., Norfolk, pp. 29–87.

Hahn, A., Stevanovic, M., Mirus, O., Schleiff, E., 2012. The TolC-like protein HgdD of the cyanobacterium *Anabaena* sp. PCC 7120 is involved in secondary metabolite export and antibiotic resistance. J. Biol. Chem. 287, 41126–41138.

Hansel, A., Schmid, A., Tadros, M.H., Jürgens, U.J., 1994. Isolation and characterisation of porin from the outer membrane of *Synechococcus* PCC 6301. Arch. Microbiol. 161, 163–167.

Hansel, A., Tadros, M.H., 1998. Characterization of Two Pore-Forming Proteins Isolated from the Outer Membrane of *Synechococcus* PCC 6301. Curr. Microbiol. 36, 321–326.

Hantke, K., 2001. Iron and metal regulation in bacteria. Curr. Opin. Microbiol. 4, 172–177.

Hantke, K., 1981. Regulation of ferric iron transport in *Escherichia coli* K12: Isolation of a constitutive mutant. MGG Mol. Gen. Genet. 182, 288–292.

Herrero, A., Muro-Pastor, A.M., Flores, E., 2001. Nitrogen control in cyanobacteria. J. Bacteriol. 183, 411–425.

Herrero, A., Muro-Pastor, A.M., Valladares, A., Flores, E., 2004. Cellular differentiation and the NtcA transcription factor in filamentous cyanobacteria. FEMS Microbiol. Rev. 28, 469–487.

Herrero, A., Stavans, J., Flores, E., 2016. The multicellular nature of filamentous heterocyst-forming cyanobacteria. FEMS Microbiol. Rev. 40, 831–854.

Heyde, M., Lazzaroni, J.-C., Magnouloux-Blanc, B., Portalier, R., 1988. Regulation of porin gene expression over a wide range of extracellular pH in *Escherichia coli* K-12: Influence of a *tolA* mutation. FEMS Microbiol. Lett. 52, 59–66.

Hickman, S.J., Cooper, R.E.M., Bellucci, L., Paci, E., Brockwell, D.J., 2017. Gating of TonB-dependent transporters by substrate-specific forced remodelling. Nat. Commun. 8, 14804.

Hoiczyk, E., Baumeister, W., 1995. Envelope structure of four gliding filamentous cyanobacteria. J. Bacteriol. 177, 2387–2395.

Hoiczyk, E., Hansel, A., 2000. Cyanobacterial cell walls: news from an unusual prokaryotic envelope 182, 1191–1199.

Huang, B., Ru, K., Yuan, Z., Whitchurch, C.B., Mattick, J.S., 2004. TonB3 is required for normal twitching motility and extracellular assembly of type IV pili. J. Bacteriol. 186, 4387–4389.

Huang, F., Hedman, E., Funk, C., Kieselbach, T., Schröder, W.P., Norling, B., 2004. Isolation of outer membrane of *Synechocystis* sp. PCC 6803 and its proteomic characterization. Mol. Cell. Proteomics 3, 586–595.

Huff, J., Pavlenok, M., Sukumaran, S., Niederweis, M., 2009. Functions of the periplasmic loop of the porin MspA from *Mycobacterium smegmatis*. J. Biol. Chem. 284, 10223–10231.

Inoue, K., Potter, D., 2004. The chloroplastic protein translocation channel Toc75 and its paralog OEP80 represent two distinct protein families and are targeted to the chloroplastic outer envelope by different mechanisms. Plant J. 39, 354–365.

Izuhara, T., Kaihatsu, I., Jimbo, H., Takaichi, S., Nishiyama, Y., 2020. Elevated Levels of Specific Carotenoids During Acclimation to Strong Light Protect the Repair of Photosystem II in *Synechocystis* sp. PCC 6803. Front. Plant Sci. 11, 1030.

Jiang, H.B., Lou, W.J., Ke, W.T., Song, W.Y., Price, N.M., Qiu, B.S., 2015. New insights into iron acquisition by cyanobacteria: An essential role for ExbB-ExbD complex in inorganic iron uptake. ISME J. 9, 297–309.

Jiang, H.H., Zhou, Y., Liu, M., Larios-Valencia, J., Lee, Z., Wang, H., Gao, X.H., Zhu, J., 2020. *Vibrio cholerae* virulence activator toxr regulates manganese transport and resistance to reactive oxygen species. Infect. Immun. 88, e00944-19.

Johnstone, T.C., Nolan, E.M., 2015. Beyond iron: Non-classical biological functions of bacterial siderophores. Dalt. Trans. 44, 6320–6339.

Jones, C.M., Niederweis, M., 2010. Role of porins in iron uptake by *Mycobacterium smegmatis*. J. Bacteriol. 192, 6411–6417.

Jordan, L.D., Zhou, Y., Smallwood, C.R., Lill, Y., Ritchie, K., Yip, W.T., Newton, S.M., Klebba, P.E., 2013. Energy-dependent motion of TonB in the Gram-negative bacterial inner membrane. Proc. Natl. Acad. Sci. U. S. A. 110, 11553–11558.

Josts, I., Veith, K., Tidow, H., 2019. Ternary structure of the outer membrane transporter FoxA with resolved signaling domain provides insights into TonB-mediated siderophore uptake. Elife 8:e48528.

Jürgens, U.J., Drews, G., Weckesser, J., 1983. Primary structure of the peptidoglycan from the unicellular cyanobacterium *Synechocystis* sp. strain PCC 6714. J. Bacteriol. 154, 471–478.

Jürgens, U.J., Golecki, J.R., Weckesser, J., 1985. Characterization of the cell wall of the unicellular cyanobacterium *Synechocystis* PCC 6714. Arch. Microbiol. 142, 168–174.

Jürgens, U.J., Weckesser, J., 1985. Carotenoid-containing outer membrane of *Synechocystis* sp. strain PCC6714. J. Bacteriol. 164, 384–389.

Jüttner, F., 1983. ^{14}C-labeled metabolites in heterocysts and vegetative cells of *Anabaena cylindrica* filaments and their presumptive function as transport vehicles of organic carbon and nitrogen. J. Bacteriol. 155, 628–633.

Kamio, Y., Nikaido, H., 1977. Outer membrane of *Salmonella typhimurium*. Identification of proteins exposed on cell surface. BBA - Biomembr. 464, 589–601.

Kamio, Y., Nikaido, H., 1976. Outer membrane of *Salmonella typhimurium*: accessibility of phospholipid head groups to phospholipase C and cyanogen bromide activated dextran in the external medium. Biochemistry 15, 2561–2570.

Kampfenkel, K., Braun, V., 1993. Topology of the ExbB protein in the cytoplasmic membrane of *Escherichia coli*. J. Biol. Chem. 268, 6050–6057.

Kampfenkel, K., Braun, V., 1992. Membrane topology of the *Escherichia coli* ExbD protein. J. Bacteriol. 174, 5485–5487.

Karshikoff, A., Spassov, V., Cowan, S., Ladenstein, R., Schirmer, T., 1994. Electrostatic properties of two porin channels from *Escherichia coli*. J. Mol. Biol. 240, 372–384.

Kaushik, M.S., Singh, P., Tiwari, B., Mishra, A.K., 2016. Ferric Uptake Regulator (FUR) protein: properties and implications in cyanobacteria. Ann. Microbiol. 66, 61–75.

Kenney, C.D., Cornelissen, C.N., 2002. Demonstration and characterization of a specific interaction between gonococcal transferrin binding protein A and TonB. J. Bacteriol. 184, 6138–6145.

Khan, A., Singh, P., Srivastava, A., 2018. Synthesis, nature and utility of universal iron chelator – Siderophore: A review. Microbiol. Res. 212–213, 103–111.

Kim, Y.C., Tarr, A.W., Penfold, C.N., 2014. Colicin import into *E. coli* cells: A model system for insights into the import mechanisms of bacteriocins. Biochim. Biophys. Acta - Mol. Cell Res. 1843, 1717–1731.

Klebba, P.E., 2016. ROSET model of TonB action in Gram-negative bacterial iron acquisition. J. Bacteriol. 198, 1013–1021.

Ködding, J., Howard, P., Kaufmann, L., Polzer, P., Lustig, A., Welte, W., 2004. Dimerization of TonB is not essential for its binding to the outer membrane siderophore receptor FhuA of *Escherichia coli*. J. Biol. Chem. 279, 9978–9986.

Ködding, J., Killig, F., Polzer, P., Howard, S.P., Diederichs, K., Welte, W., 2005. Crystal structure of a 92-residue C-terminal fragment of TonB from *Escherichia coli* reveals significant conformational changes compared to structures of smaller TonB fragments. J. Biol. Chem. 280, 3022–3028.

Koebnik, R., 2005. TonB-dependent trans-envelope signalling: The exception or the rule? Trends Microbiol. 13, 343–347.

Koebnik, R., 1993. The molecular interaction between components of the TonB–ExbBD–dependent and of the TolQRA-dependent bacterial uptake systems. Mol. Microbiol. 9, 219–219.

Koebnik, R., Locher, K.P., Van Gelder, P., 2000. Structure and function of bacterial outer membrane proteins: Barrels in a nutshell. Mol. Microbiol. 37, 239–253.

Kojima, S., Blair, D.F., 2001. Conformational change in the stator of the bacterial flagellar Motor. Biochemistry 40, 13041–13050.

Kojima, S., Hayashi, K., Tochigi, S., Kusano, T., Kaneko, J., Kamio, Y., 2016. Peptidoglycan-associated outer membrane protein Mep45 of rumen anaerobe *Selenomonas ruminantium* forms a non-specific diffusion pore via its C-terminal transmembrane domain. Biosci. Biotechnol. Biochem. 80, 1954–1959.

Köster, W., 2001. ABC transporter-mediated uptake of iron, siderophores, heme and vitamin B_{12}. Res. Microbiol. 152, 291–301.

Kowata, H., Tochigi, S., Takahashi, H., Kojima, S., 2017. Outer membrane permeability of cyanobacterium *Synechocystis* sp. strain PCC 6803: Studies of passive diffusion of small organic nutrients reveal the absence of classical porins and intrinsically low permeability. J. Bacteriol. 199, e00371-17.

Kranzler, C., Lis, H., Finkel, O.M., Schmetterer, G., Shaked, Y., Keren, N., 2014. Coordinated transporter activity shapes high-affinity iron acquisition in cyanobacteria. ISME J. 8, 409–417.

Kranzler, C., Lis, H., Shaked, Y., Keren, N., 2011. The role of reduction in iron uptake processes in a unicellular, planktonic cyanobacterium. Environ. Microbiol. 13, 2990–2999.

Kranzler, C., Rudolf, M., Keren, N., Schleiff, E., 2013. Iron in Cyanobacteria, in: Advances in Botanical Research. pp. 57–105.

Krewulak, K.D., Vogel, H.J., 2008. Structural biology of bacterial iron uptake. Biochim. Biophys. Acta - Biomembr. 1778, 1781–1804.

Kumar, K., Mella-Herrera, R.A., Golden, J.W., 2010. Cyanobacterial heterocysts. Cold Spring Harb. Perspect. Biol. 2, a000315.

Ladomersky, E., Petris, M.J., 2015. Copper tolerance and virulence in bacteria. Metallomics 7, 957–964.

Lafontaine, E.R., Sokol, P.A., 1998. Effects of iron and temperature on expression of the *Pseudomonas aeruginosa tolQRA* genes: Role of the ferric uptake regulator. J. Bacteriol. 180, 2836–2841.

Larsen, R.A., Deckert, G.E., Kastead, K.A., Devanathan, S., Keller, K.L., Postle, K., 2007. His_{20} provides the sole functionally significant side chain in the essential TonB transmembrane domain. J. Bacteriol. 189, 2825–2833.

Larsen, R.A., Letain, T.E., Postle, K., 2003. *In vivo* evidence of TonB shuttling between the cytoplasmic and outer membrane in *Escherichia coli*. Mol. Microbiol. 49, 211–218.

Latifi, A., Jeanjean, R., Lemeille, S., Havaux, M., Zhang, C., 2005. Iron starvation leads to oxidative stress in *Anabaena* sp. strain PCC 7120. J. Bacteriol. 187, 6596–6598.

Lázaro, S., Fernández-Piñas, F., Fernández-Valiente, E., Blanco-Rivero, A., Leganés, F., 2001. *pbpB*, a gene coding for a putative penicillin-binding protein, is required for aerobic nitrogen fixation in the cyanobacterium *Anabaena* sp. strain PCC7120. J. Bacteriol. 183, 628–636.

Lazzaroni, J.C., Fognini-Lefebvre, N., Portalier, R., 1989. Cloning of the *excC* and *excD* genes involved in the release of periplasmic proteins by *Escherichia coli* K12. MGG Mol. Gen. Genet. 218, 460–464.

Lehner, J., Berendt, S., Dörsam, B., Pérez, R., Forchhammer, K., Maldener, I., 2013. Prokaryotic multicellularity: A nanopore array for bacterial cell communication. FASEB J. 27, 2293–2300.

Lehner, J., Zhang, Y., Berendt, S., Rasse, T.M., Forchhammer, K., Maldener, I., 2011. The morphogene AmiC2 is pivotal for multicellular development in the cyanobacterium *Nostoc punctiforme*. Mol. Microbiol. 79, 1655–1669.

Leonhardt, K., Straus, N., 1994. Photosystem II genes *isiA*, *psbDI* and *psbC* in *Anabaena* sp. PCC 7120: cloning, sequencing and the transcriptional regulation in iron-stressed and iron-repleted cells. Plant Mol. Biol. 24, 63–73.

Leonhardt, K., Straus, N.A., 1992. An iron stress operon involved in photosynthetic electron transport in the marine cyanobacterium *Synechococcus* sp. PCC 7002. J. Gen. Microbiol. 138, 1613–1621.

Letain, T.E., Postle, K., 1997. TonB protein appears to transduce energy by shuttling between the cytoplasmic membrane and the outer membrane in *Escherichia coli*. Mol. Microbiol. 24, 271–283.

Li, G.W., Burkhardt, D., Gross, C., Weissman, J.S., 2014. Quantifying absolute protein synthesis rates reveals principles underlying allocation of cellular resources. Cell 157, 624–635.

Li, T., Huang, X., Zhou, R., Liu, Y., Li, B., Nomura, C., Zhao, J., 2002. Differential expression and localization of Mn and Fe superoxide dismutases in the heterocystous cyanobacterium *Anabaena* sp. Strain PCC 7120. J. Bacteriol. 184, 5096–5103.

Lim, C.K., Hassan, K.A., Penesyan, A., Loper, J.E., Paulsen, I.T., 2013. The effect of zinc limitation on the transcriptome of *Pseudomonas protegens* Pf-5. Environ. Microbiol. 15, 702–715.

Lis, H., Kranzler, C., Keren, N., Shaked, Y., 2015. A comparative study of Iron uptake rates and mechanisms amongst marine and fresh water Cyanobacteria: prevalence of reductive Iron uptake. Life 5, 841–860.

Liu, X., Ferenci, T., 1998. Regulation of porin-mediated outer membrane permeability by nutrient limitation in *Escherichia coli*. J. Bacteriol. 180, 3917–3922.

Llamas, M.A., Ramos, J.L., Rodriguez-Herva, J.J., 2000. Mutations in each of the *tol* genes of *Pseudomonas putida* reveal that they are critical for maintenance of outer membrane stability. J. Bacteriol. 182, 4764–4772.

Lloubès, R., Cascales, E., Walburger, A., Bouveret, E., Lazdunski, C., Bernadac, A., Journet, L., 2001. The Tol-Pal proteins of the *Escherichia coli* cell envelope: An energized system required for outer membrane integrity? Res. Microbiol. 152, 523–529.

López-Igual, R., Flores, E., Herrero, A., 2010. Inactivation of a heterocyst-specific invertase indicates a principal role of sucrose catabolism in heterocysts of *Anabaena* sp. J. Bacteriol. 192, 5526–5533.

Lyons, N.A., Kolter, R., 2015. On the evolution of bacterial multicellularity. Curr. Opin. Microbiol. 24, 21–28.

Ma, Z., Jacobsen, F.E., Giedroc, D.P., 2009. Metal Transporters and Metal Sensors: How Coordination Chemistry Controls Bacterial Metal Homeostasis. Chem. Rev. 109, 4681-4681.

Maki-Yonekura, S., Matsuoka, R., Yamashita, Y., Shimizu, H., Tanaka, M., Iwabuki, F., Yonekura, K., 2018. Hexameric and pentameric complexes of the ExbBD energizer in the Ton system. Elife 7, e35419.

Marguerettaz, M., Dieppois, G., Que, Y.A., Ducret, V., Zuchuat, S., Perron, K., 2014. Sputum containing zinc enhances carbapenem resistance, biofilm formation and virulence of *Pseudomonas aeruginosa*. Microb. Pathog. 77, 36–41.

Mariscal, V., Herrero, A., Flores, E., 2007. Continuous periplasm in a filamentous, heterocyst-forming cyanobacterium. Mol. Microbiol. 65, 1139–1145.

Mariscal, V., Herrero, A., Nenninger, A., Mullineaux, C.W., Flores, E., 2011. Functional dissection of the three-domain SepJ protein joining the cells in cyanobacterial trichomes. Mol. Microbiol. 79, 1077–1088.

Mariscal, V., Nürnberg, D.J., Herrero, A., Mullineaux, C.W., Flores, E., 2016. Overexpression of SepJ alters septal morphology and heterocyst pattern regulated by diffusible signals in *Anabaena*. Mol. Microbiol. 101, 968–981.

Martin, J.H., 1990. Glacial-interglacial CO_2 change: The Iron Hypothesis. Paleoceanography 5, 1–13.

Martin, J.H., Fitzwater, S.E., 1988. Iron deficiency limits phytoplankton growth in the north-east pacific subarctic. Nature 331, 341–343.

Martin, K.A., Siefert, J.L., Yerrapragada, S., Lu, Y., McNeill, T.Z., Moreno, P.A., Weinstock, G.M., Widger, W.R., Fox, G.E., 2003. Cyanobacterial signature genes. Photosynth. Res. 75, 211–221.

Masilamani, R., Cian, M.B., Dalebroux, Z.D., 2018. *Salmonella* Tol-Pal reduces outer membrane glycerophospholipid levels for envelope homeostasis and survival during bacteremia. Infect. Immun. 86, e00173-18.

Mathelié-Guinlet, M., Asmar, A.T., Collet, J.F., Dufrêne, Y.F., 2020. Lipoprotein Lpp regulates the mechanical properties of the *E. coli* cell envelope. Nat. Commun. 11, 1–11.

Matias, V.R.F., Al-Amoudi, A., Dubochet, J., Beveridge, T.J., 2003. Cryo-transmission electron microscopy of frozen-hydrated sections of *Escherichia coli* and *Pseudomonas aeruginosa*. J. Bacteriol. 185, 6112–6118.

McBride, M.J., 2001. Bacterial gliding motility: Multiple mechanisms for cell movement over surfaces. Annu. Rev. Microbiol. 55, 49–75.

Merianos, H.J., Cadieux, N., Lin, C.H., Kadner, R.J., Cafiso, D.S., 2000. Substrate-induced exposure of an energy-coupling motif of a membrane transporter. Nat. Struct. Biol. 7, 205–209.

Merino-Puerto, V., Mariscal, V., Mullineaux, C.W., Herrero, A., Flores, E., 2010. Fra proteins influencing filament integrity, diazotrophy and localization of septal protein SepJ in the heterocyst-forming cyanobacterium *Anabaena* sp. Mol. Microbiol. 75, 1159–1170.

Merino-Puerto, V., Schwarz, H., Maldener, I., Mariscal, V., Mullineaux, C.W., Herrero, A., Flores, E., 2011. FraC/FraD-dependent intercellular molecular exchange in the filaments of a heterocyst-forming cyanobacterium, *Anabaena* sp. Mol. Microbiol. 82, 87–98.

Mesnage, S., Fontaine, T., Mignot, T., Delepierre, M., Mock, M., Fouet, A., 2000. Bacterial SLH domain proteins are non-covalently anchored to the cell surface via a conserved mechanism involving wall polysaccharide pyruvylation. EMBO J. 19, 4473–4484.

Miller, S.I., Salama, N.R., 2018. The gram-negative bacterial periplasm: Size matters. PLoS Biol. 16, 1–7.

Mirus, O., Strauss, S., Nicolaisen, K., von Haeseler, A., Schleiff, E., 2009. TonB-dependent transporters and their occurrence in cyanobacteria. BMC Biol. 7, 68.

Moeck, G., Coulton, J., Postle, K., 1997. Cell envelope signaling in *Escherichia coli*. Ligand binding to the ferrichrome-iron receptor FhuA promotes interaction with the energy-transducing protein TonB. J. Biol. Chem. 272, 28391–28397

Mokdad, A., Herrick, D.Z., Kahn, A.K., Andrews, E., Kim, M., Cafiso, D.S., 2012. Ligand-induced structural changes in the *Escherichia coli* ferric citrate transporter reveal modes for regulating protein-protein interactions. J. Mol. Biol. 423, 818–830.

Moore, J.K., Doney, S.C., Glover, D.M., Fung, I.Y., 2001. Iron cycling and nutrient-limitation patterns in surface waters of the world ocean. Deep. Res. Part II Top. Stud. Oceanogr. 49, 463–507.

Moslavac, S., Bredemeier, R., Mirus, O., Granvogl, B., Eichacker, L.A., Schleiff, E., 2005. Proteomic analysis of the outer membrane of *Anabaena* sp. strain PCC 7120. J. Proteome Res. 4, 1330–1338.

Moslavac, S., Reisinger, V., Berg, M., Mirus, O., Vosyka, O., Plöscher, M., Flores, E., Eichacker, L.A., Schleiff, E., 2007. The proteome of the heterocyst cell wall in *Anabaena* sp. PCC 7120. Biol. Chem. 388, 823–829.

Mühlradt, P.F., Golecki, J.R., 1975. Asymmetrical distribution and artifactual reorientation of lipopolysaccharide in the outer membrane bilayer of *Salmonella typhimurium*. Eur. J. Biochem. 51, 343–352.

Mullineaux, C.W., Mariscal, V., Nenninger, A., Khanum, H., Herrero, A., Flores, E., Adams, D.G., 2008. Mechanism of intercellular molecular exchange in heterocyst-forming cyanobacteria. EMBO J. 27, 1299–1308.

Nan, B., Chen, J., Neu, J.C., Berry, R.M., Oster, G., Zusman, D.R., 2011. Myxobacteria gliding motility requires cytoskeleton rotation powered by proton motive force. Proc. Natl. Acad. Sci. U. S. A. 108, 2498–2503.

Narayan, Prakash, O., Kumari, N., Rai, L.C., 2011. Iron starvation-induced proteomic changes in *Anabaena* (*Nostoc*) sp. PCC 7120: Exploring survival strategy. J. Microbiol. Biotechnol. 21, 136–146.

Navare, A.T., Chavez, J.D., Zheng, C., Weisbrod, C.R., Eng, J.K., Siehnel, R., Singh, P.K., Manoil, C., Bruce, J.E., 2015. Probing the protein interaction network of *Pseudomonas aeruginosa* cells by chemical cross-linking mass spectrometry. Structure 23, 762–773.

Nayar, A.S., Yamaura, H., Rajagopalan, R., Risser, D.D., Callahan, S.M., 2007. FraG is necessary for filament integrity and heterocyst maturation in the cyanobacterium *Anabaena* sp. strain PCC 7120. Microbiology 153, 601–607.

Neilands, J.B., 1981. Iron absorption and transport in microorganisms. Annu. Rev. Nutr. 1, 27–46.

Nevo, Y., Nelson, N., 2006. The NRAMP family of metal-ion transporters. Biochim. Biophys. Acta - Mol. Cell Res. 1763, 609–620.

Nickelsen, J., Rengstl, B., Stengel, A., Schottkowski, M., Soll, J., Ankele, E., 2011. Biogenesis of the cyanobacterial thylakoid membrane system - an update. FEMS Microbiol. Lett. 315, 1–5.

Nicolaisen, K., Hahn, A., Schleiff, E., 2009. The cell wall in heterocyst formation by *Anabaena* sp. PCC 7120. J. Basic Microbiol. 49, 5–24.

Nicolaisen, K., Hahn, A., Valdebenito, M., Moslavac, S., Samborski, A., Maldener, I., Wilken, C., Valladares, A., Flores, E., Hantke, K., Schleiff, E., 2010. The interplay between siderophore secretion and coupled iron and copper transport in the heterocyst-forming cyanobacterium *Anabaena* sp. PCC 7120. Biochim. Biophys. Acta - Biomembr. 1798, 2131–2140.

Nicolaisen, K., Moslavac, S., Samborski, A., Valdebenito, M., Hantke, K., Maldener, I., Muro-Pastor, A.M., Flores, E., Schleiff, E., 2008. Alr0397 is an outer membrane transporter for the siderophore schizokinen in *Anabaena* sp. strain PCC 7120. J. Bacteriol. 190, 7500–7507.

Nieves-Morión, M., Lechno-Yossef, S., López-Igual, R., Frías, J.E., Mariscal, V., Nürnberg, D.J., Mullineaux, C.W., Wolk, C.P., Flores, E., 2017a. Specific glucoside transporters influence septal structure and function in the filamentous, heterocyst-forming cyanobacterium *Anabaena* sp. strain PCC 7120. J. Bacteriol. 199, e00876-16.

Nieves-Morión, M., Mullineaux, C.W., Flores, E., 2017b. Molecular diffusion through cyanobacterial septal junctions. MBio 8, e01756-16.

Nieves-Morión, M., Flores, E., 2018. Multiple ABC glucoside transporters mediate sugar-stimulated growth in the heterocyst-forming cyanobacterium *Anabaena* sp. strain PCC 7120. Environ. Microbiol. Rep. 10, 40–48.

Nikaido, H., 2003. Molecular Basis of Bacterial Outer Membrane Permeability Revisited. Microbiol. Mol. Biol. Rev. 67, 593–656.

Nikaido, H., 1994. Porins and specific diffusion channels in bacterial outer membranes. J. Biol. Chem. 269, 3905–3908.

Nikaido, H., Saier, M.H., 1992. Transport proteins in bacteria: Common themes in their design. Science 258, 936–942.

Nikaido, H., Vaara, M., 1985. Molecular Basis of Bacterial Outer Membrane Permeability. Microbiol. Rev. 49, 1–32.

Noinaj, N., Guillier, M., Barnard, T.J., Buchanan, S.K., 2010. TonB-dependent transporters: regulation, structure, and function. Annu Rev Microbiol 64, 43–60.

Noinaj, N., Gumbart, J.C., Buchanan, S.K., 2017. The β-barrel assembly machinery in motion. Nat. Rev. Microbiol. 15, 197–204.

Norman, L., Cabanesa, D.J.E., Blanco-Ameijeiras, S., Moisset, S.A.M., Hassler, C.S., 2014. Iron Biogeochemistry in Aquatic Systems: From Source to Bioavailability. Chim. Int. J. Chem. 68, 764–771.

Nürnberg, D.J., Mariscal, V., Bornikoel, J., Nieves-Morión, M., Krauß, N., Herrero, A., Maldener, I., Flores, E., Mullineaux, C.W., 2015. Intercellular diffusion of a fluorescent sucrose analog via the septal junctions in a filamentous cyanobacterium. MBio 6, e02109-14.

Obando, T.A.S., Babykin, M.M., Zinchenko, V. V., 2018. A Cluster of Five Genes Essential for the Utilization of Dihydroxamate Xenosiderophores in *Synechocystis* sp. PCC 6803. Curr. Microbiol. 75, 1165–1173.

Occhino, D.A., Wyckoff, E.E., Henderson, D.P., Wrona, T.J., Payne, S.M., 1998. *Vibrio cholerae* iron transport: haem transport genes are linked to one of two sets of *tonB*, *exbB*, *exbD* genes. Mol. Microbiol. 29, 1493–1507.

Oeemig, J.S., Ollila, O.H.S., Iwaï, H., 2018. NMR structure of the C-terminal domain of TonB protein from *Pseudomonas aeruginosa*. PeerJ 2018, e5412.

Oh, E.T., Yun, H.S., Heo, T.-R., Koh, S.-C., Oh, K.-H., So, J.-S., 2002. Involvement of lipopolysaccharide of *Bradyrhizobium japonicum* in metal binding. J. Microbiol. Biotechnol. 12, 296–300.

Outten, C.E., O'Halloran, T. V., 2001. Femtomolar sensitivity of metalloregulatory proteins controlling zinc homeostasis. Science 292, 2488–2492.

Overbeeke, N., Lugtenberg, B., 1980. Expression of outer membrane protein e of *Escherichia coli* K12 by phosphate limitation. FEBS Lett. 112, 229–232.

Pagès, J.-M., James, C.E., Winterhalter, M., 2008. The porin and the permeating antibiotic: a selective diffusion barrier in Gram-negative bacteria. Nat. Rev. Microbiol. 6, 893–903.

Paquelin, A., Ghigo, J.M., Bertin, S., Wandersman, C., 2001. Characterization of HasB, a *Serratia marcescens* TonB-like protein specifically involved in the haemophore-dependent haem acquisition system. Mol. Microbiol. 42, 995–1005.

Pattanaik, B., Montgomery, B.L., 2010a. FdTonB is involved in the photoregulation of cellular morphology during complementary chromatic adaptation in Fremyella diplosiphon. Microbiology 156, 731–741.

Pattanaik, B., Montgomery, B.L., 2010b. A novel role for a TonB-family protein and photoregulation of iron acclimation in Fremyella diplosiphon. Plant Signal. Behav. 5, 851–853.

Pawelek, P.D., Croteau, N., Ng-Thow-Hing, C., Khursigara, C.M., Moiseeva, N., Allaire, M., Coulton, J.W., 2006. Structure of TonB in complex with FhuA, *E. coli* outer membrane receptor. Science 312, 1399–1402.

Payne, S.M., Mey, A.R., Wyckoff, E.E., 2016. *Vibrio* Iron Transport: Evolutionary Adaptation to Life in Multiple Environments. Microbiol. Mol. Biol. Rev. 80, 69–90.

Pereira, S., Zille, A., Micheletti, E., Moradas-Ferreira, P., De Philippis, R., Tamagnini, P., 2009. Complexity of cyanobacterial exopolysaccharides: Composition, structures, inducing factors and putative genes involved in their biosynthesis and assembly. FEMS Microbiol. Rev. 33, 917–941.

Pernil, R., Schleiff, E., 2019. Metalloproteins in the Biology of Heterocysts. Life 9, 32.

Phale, P.S., Philippsen, A., Kiefhaber, T., Koebnik, R., Phale, V.P., Schirmer, T., Rosenbusch, J.P., 1998. Stability of trimeric OmpF porin: The contributions of the latching loop L2. Biochemistry 37, 15663–15670.

Postle, K., Kastead, K.A., Gresock, M.G., Ghosh, J., Swayne, C.D., 2010. The TonB dimeric crystal structures do not exist *in vivo*. MBio 1, 307–317.

Postle, K., Larsen, R.A., 2007. TonB-dependent energy transduction between outer and cytoplasmic membranes. BioMetals 20, 453–465.

Pramanik, A., Hauf, W., Hoffmann, J., Cernescu, M., Brutschy, B., Braun, V., 2011. Oligomeric structure of ExbB and ExbB-ExbD isolated from *Escherichia coli* as revealed by LILBID mass spectrometry. Biochemistry 50, 8950–8956.

Qiu, G.-W., Lou, W.-J., Sun, C.-Y., Yang, N., Li, Z.-K., Li, D.-L., Zang, S.-S., Fu, F.-X., Hutchins, D.A., Jiang, H.-B., Qiu, B.-S., 2018. Outer Membrane Iron Uptake Pathways in the Model Cyanobacterium *Synechocystis* sp. Strain PCC 6803. Appl. enviormental Microbiol. 84, e01512-18.

Qiu, G., Jiang, H., Lis, H., Li, Z., Deng, B., Shang, J., Sun, C., Keren, N., Qiu, B., 2021. A unique porin meditates iron-selective transport through cyanobacterial outer membranes. Environ. Microbiol. 23, 376–390.

Rawling, E.G., Brinkman, F.S.L., Hancock, R.E.W., 1998. Roles of the carboxy-terminal half of Pseudomonas aeruginosa major outer membrane protein OprF in cell shape, growth in low-osmolarity medium, and peptidoglycan association. J. Bacteriol. 180, 3556–3562.

Razquin, P., Schmitz, S., Fillat, M.F., Peleato, M.L., Böhme, H., 1994. Transcriptional and translational analysis of ferredoxin and flavodoxin under iron and nitrogen stress in *Anabaena* sp. strain PCC 7120. J. Bacteriol. 176, 7411.

Resch, C.M., Gibson, J., 1983. Isolation of the carotenoid-containing cell wall of three unicellular cyanobacteria. J. Bacteriol. 155, 345–350.

Ries, W., Hotzy, C., Schocker, I., Sleytr, U.B., Sára, M., 1997. Evidence that the N-terminal part of the S-layer protein from Bacillus stearothermophilus PV72/p2 recognizes a secondary cell wall polymer. J. Bacteriol. 179, 3892–3898.

Rippka, R., Deruelles, J., Waterbury, J.B., Herdman, M., Stanier, R.Y., 1979. Generic Assignments, Strain Histories and Properties of Pure Cultures of Cyanobacteria. J. Gen. Microbiol. 111, 1–61.

Rosenfeld, Y., Shai, Y., 2006. Lipopolysaccharide (Endotoxin)-host defense antibacterial peptides interactions: Role in bacterial resistance and prevention of sepsis. Biochim. Biophys. Acta - Biomembr. 1758, 1513–1522.

Rudolf, M., Kranzler, C., Lis, H., Margulis, K., Stevanovic, M., Keren, N., Schleiff, E., 2015. Multiple modes of iron uptake by the filamentous, siderophore-producing cyanobacterium, *Anabaena* sp. PCC 7120. Mol. Microbiol. 97, 577–588.

Rudolf, M., Stevanovic, M., Kranzler, C., Pernil, R., Keren, N., Schleiff, E., 2016. Multiplicity and specificity of siderophore uptake in the cyanobacterium *Anabaena* sp. PCC 7120. Plant Mol. Biol. 92, 57–69.

Saha, R., Saha, N., Donofrio, R.S., Bestervelt, L.L., 2013. Microbial siderophores: a mini review. J. Basic Microbiol. 53, 303–317.

Samsudin, F., Ortiz-Suarez, M.L., Piggot, T.J., Bond, P.J., Khalid, S., 2016. OmpA: A Flexible Clamp for Bacterial Cell Wall Attachment. Structure 24, 2227–2235.

Sára, M., Sleytr, U.B., 2000. S-layer proteins. J. Bacteriol. 182, 859–868.

Sarver, J.L., Zhang, M., Liu, L., Nyenhuis, D., Cafiso, D.S., 2018. A Dynamic Protein-Protein Coupling between the TonB-Dependent Transporter FhuA and TonB. Biochemistry 57, 1045–1053.

Schalk, I.J., Guillon, L., 2013. Fate of ferrisiderophores after import across bacterial outer membranes: Different iron release strategies are observed in the cytoplasm or periplasm depending on the siderophore pathways. Amino Acids 44, 1267–1277.

Schauer, K., Rodionov, D.A., de Reuse, H., 2008. New substrates for TonB-dependent transport: do we only see the “tip of the iceberg”? Trends Biochem. Sci. 33, 330–338.

Schirrmeister, B.E., Gugger, M., Donoghue, P.C.J., 2015. Cyanobacteria and the Great Oxidation Event: Evidence from genes and fossils. Palaeontology 58, 769–785.

Schulz, G.E., 2002. The structure of bacterial outer membrane proteins. Biochim. Biophys. Acta - Biomembr. 1565, 308–317.

Sean Peacock, R., Weljie, A.M., Peter Howard, S., Price, F.D., Vogel, H.J., 2005. The solution structure of the C-terminal domain of TonB and interaction studies with TonB box peptides. J. Mol. Biol. 345, 1185–1197.

Seliger, S.S., Mey, A.R., Valle, A.-M., Payne, S.M., 2001. The two TonB systems of *Vibrio cholerae*: redundant and specific functions. Mol. Microbiol. 39, 801–812.

Shaked, Y., Lis, H., 2012. Disassembling iron availability to phytoplankton. Front. Microbiol. 3, 123.

Sharon, S., Salomon, E., Kranzler, C., Lis, H., Lehmann, R., Georg, J., Zer, H., Hess, W.R., Keren, N., 2014. The hierarchy of transition metal homeostasis: Iron controls manganese accumulation in a unicellular cyanobacterium. Biochim. Biophys. Acta - Bioenerg. 1837, 1990–1997.

Shcolnick, S., Shaked, Y., Keren, N., 2007. A role for mrgA, a DPS family protein, in the internal transport of Fe in the cyanobacterium *Synechocystis* sp. PCC6803. Biochim. Biophys. Acta - Bioenerg. 1767, 814–819.

Sherman, D.M., Tucker, D., Sherman, L.A., 2000. Heterocyst development and localization of cyanophycin in N_2-fixing cultures of *Anabaena* sp. PCC 7120 (cyanobacteria). J. Phycol. 36, 932–941.

Shi, H., Bratton, B.P., Gitai, Z., Huang, K.C., 2018. How to build a bacterial cell: MreB as the foreman of *E. coli* construction. Cell 172, 1294–1305.

Shrivastava, R., Jiang, X., Chng, S.-S., 2017. Outer membrane lipid homeostasis via retrograde phospholipid transport in *Escherichia coli*. Mol. Microbiol. 106, 395–408.

Shultis, D.D., Purdy, M.D., Banchs, C.N., Wiener, M.C., 2006. Outer membrane active transport: Structure of the BtuB:TonB complex. Science 312, 1396–1399.

Silhavy, T.J., Kahne, D., Walker, S., 2010. The bacterial cell envelope. Cold Spring Harb. Perspect. Biol. 2, a000414.

Singh, S., Mishra, A.K., 2014. Regulation of calcium ion and its effect on growth and developmental behavior in wild type and *ntcA* mutant of *Anabaena* sp. PCC 7120 under varied levels of $CaCl_2$. Microbiology 83, 235–246.

Smani, Y., Fàbrega, A., Roca, I., Sańchez-Encinales, V., Vila, J., Pachón, J., 2014. Role of OmpA in the multidrug resistance phenotype of *Acinetobacter baumannii*. Antimicrob. Agents Chemother. 58, 1806–1808.

Šmarda, J., Šmajs, D., Komrska, J., Krzyžánek, V., 2002. S-layers on cell walls of cyanobacteria. Micron 33, 257–277.

Smith, R.J., Hobson, S., Ellis, I.R., 1987. Evidence for Calcium-Mediated Regulation of Heterocyst Frequency and Nitrogenase Activity in Nostoc 6720. New Phytol. 105, 531–541.

Solov'eva, T., Likhatskaya, G., Khomenko, V., Guzev, K., Kim, N., Bystritskaya, E., Novikova, O., Stenkova, A., Rakin, A., Isaeva, M., 2018. The impact of length variations in the L2 loop on the structure and thermal stability of non-specific porins: The case of OmpCs from the *Yersinia pseudotuberculosis* complex. Biochim. Biophys. Acta - Biomembr. 1860, 515–525.

Speer, A., Rowland, J.L., Haeili, M., Niederweis, M., Wolschendorf, F., 2013. Porins increase copper susceptibility of *Mycobacterium tuberculosis*. J. Bacteriol. 195, 5133–5140.

Stebegg, R., Wurzinger, B., Mikulic, M., Schmetterer, G., 2012. Chemoheterotrophic growth of the cyanobacterium *Anabaena* sp. strain PCC 7120 dependent on a functional cytochrome c oxidase. J. Bacteriol. 194, 4601–4607.

Stevanovic, M., Hahn, A., Nicolaisen, K., Mirus, O., Schleiff, E., 2012. The components of the putative iron transport system in the cyanobacterium *Anabaena* sp. PCC 7120. Environ. Microbiol. 14, 1655–1670.

Stevanovic, M., Lehmann, C., Schleiff, E., 2013. The response of the TonB-dependent transport network in *Anabaena* sp. PCC 7120 to cell density and metal availability. BioMetals 26, 549–560.

Stock, J.B., Rauch, B., Roseman, S., 1977. Periplasmic space in *Salmonella typhimurium* and *Escherichia coli*. J. Biol. Chem. 252, 7850–7861.

Strain, S.M., Fesik, S.W., Armitage, I.M., 1983. Structure and metal-binding properties of lipopolysaccharides from heptoseless mutants of *Escherichia coli* studied by ^{13}C and ^{31}P nuclear magnetic resonance. J. Biol. Chem. 258, 13466–13477.

Street, J.H., Paytan, A., 2005. Iron, phytoplankton growth, and the carbon cycle, in: Metal Ions in Biological Systems. pp. 153–193.

Sugawara, E., Nestorovich, E.M., Bezrukov, S.M., Nikaido, H., 2006. *Pseudomonas aeruginosa* porin OprF exists in two different conformations. J. Biol. Chem. 281, 16220–16229.

Sutak, R., Camadro, J.M., Lesuisse, E., 2020. Iron Uptake Mechanisms in Marine Phytoplankton. Front. Microbiol. 11, 566691.

Sverzhinsky, A., Chung, J.W., Deme, J.C., Fabre, L., Levey, K.T., Plesa, M., Carter, D.M., Lypaczewski, P., Coulton, J.W., 2015. Membrane protein complex $ExbB_4$-$ExbD_1$-$TonB_1$ from *Escherichia coli* demonstrates conformational plasticity. J. Bacteriol. 197, 1873–1885.

Sverzhinsky, A., Fabre, L., Cottreau, A.L., Biot-Pelletier, D.M.P., Khalil, S., Bostina, M., Rouiller, I., Coulton, J.W., 2014. Coordinated rearrangements between cytoplasmic and periplasmic domains of the membrane protein complex ExbB-ExbD of *Escherichia coli*. Structure 22, 791–797.

Szatmári, D., Sárkány, P., Kocsis, B., Nagy, T., Miseta, A., Barkó, S., Longauer, B., Robinson, R.C., Nyitrai, M., 2020. Intracellular ion concentrations and cation-dependent remodelling of bacterial MreB assemblies. Sci. Rep. 10, 12002.

Szczepaniak, J., Press, C., Kleanthous, C., 2020. The multifarious roles of Tol-Pal in Gram-negative bacteria. FEMS Microbiol. Rev. 44, 490–506.

Thiolas, A., Bollet, C., La Scola, B., Raoult, D., Pagès, J.M., 2005. Successive emergence of *Enterobacter aerogenes* strains resistant to imipenem and colistin in a patient. Antimicrob. Agents Chemother. 49, 1354–1358.

Thomas, J., Meeks, J.C., Wolk, C.P., Shaffer, P.W., Austin, S.M., Chien, W.-S., 1977. Formation of Glutamine from [^{13}N]ammonia, [^{13}N]dinitrogen, and [^{14}C]glutamate by Heterocysts Isolated from *Anabaena cylindrica*. J. Bacteriol. 129, 1545–1555.

Torrecilla, I., Leganes, F., Bonilla, I., Fernandez-Pinas, F., 2004a. Light-to-dark transitions trigger a transient increase in intracellular Ca2+ modulated by the redox state of the photosynthetic electron transport chain in the cyanobacterium *Anabaena* sp. PCC7120. Plant, Cell Environ. 27, 810–819.

Torrecilla, I., Leganés, F., Bonilla, I., Fernández-Piñas, F., 2004b. A calcium signal is involved in heterocyst differentiation in the cyanobacterium *Anabaena* sp. PCC7120. Microbiology 150, 3731–3739.

Touati, D., 2000. Iron and oxidative stress in bacteria. Arch. Biochem. Biophys. 373, 1–6.

Tripp, J., Hahn, A., Koenig, P., Flinner, N., Bublak, D., Brouwer, E.M., Ertel, F., Mirus, O., Sinning, I., Tews, I., Schleiff, E., 2012. Structure and Conservation of the Periplasmic Targeting Factor Tic22 Protein from Plants and Cyanobacteria. J. Biol. Chem. 287, 24164–24173.

Vargas-Straube, M.J., Beard, S., Norambuena, R., Paradela, A., Vera, M., Jerez, C.A., 2020. High copper concentration reduces biofilm formation in *Acidithiobacillus ferrooxidans* by decreasing production of extracellular polymeric substances and its adherence to elemental sulfur. J. Proteomics 225, 103874.

Vergalli, J., Bodrenko, I. V., Masi, M., Moynié, L., Acosta-Gutiérrez, S., Naismith, J.H., Davin-Regli, A., Ceccarelli, M., van den Berg, B., Winterhalter, M., Pagès, J.M., 2020. Porins and small-molecule translocation across the outer membrane of Gram-negative bacteria. Nat. Rev. Microbiol. 18, 164–176.

Videau, P., Rivers, O.S., Ushijima, B., Oshiro, R.T., Kim, M.J., Philmus, B., Cozy, L.M., 2016. Mutation of the *murC* and *murB* genes impairs heterocyst differentiation in *Anabaena* sp. strain PCC 7120. J. Bacteriol. 198, 1196–1206.

Vollmer, W., Blanot, D., De Pedro, M.A., 2008. Peptidoglycan structure and architecture. FEMS Microbiol. Rev. 32, 149–167.

Von Meyenburg, K., Nikaido, H., 1977. Outer membrane of Gram-negative bacteria. XVII. Specificity of transport process catalyzed by the λ-receptor protein in *Escherichia coli*. Biochem. Biophys. Res. Commun. 78, 1100–1107.

Wachi, Y., Grant Burgess, J., Iwamoto, K., Yamada, N., Nakamura, N., Matsunaga, T., 1995. Effect of ultraviolet-A (UV-A) light on growth, photosynthetic activity and production of biopterin glucoside by the marine UV-A resistant cyanobacterium *Oscillatoria* sp. BBA - Gen. Subj. 1244, 165–168.

Wada, N., Sakamoto, T., Matsugo, S., 2013. Multiple roles of photosynthetic and sunscreen pigments in cyanobacteria focusing on the oxidative stress. Metabolites 3, 463–483.

Wager, B., Baslé, A., Delcour, A.H., 2010. Disulfide bond tethering of extracellular loops does not affect the closure of OmpF porin at acidic pH. Proteins Struct. Funct. Bioinforma. 78, 2886–2894.

Walsby, A.E., 2007. Cyanobacterial heterocysts: terminal pores proposed as sites of gas exchange. Trends Microbiol. 15, 340–349.

Walter, J., Lynch, F., Battchikova, N., Aro, E.M., Gollan, P.J., 2016. Calcium impacts carbon and nitrogen balance in the filamentous cyanobacterium *Anabaena* sp. PCC 7120. J. Exp. Bot. 67, 3997–4008.

Wang, Y., 2002. The function of OmpA in *Escherichia coli*. Biochem. Biophys. Res. Commun. 292, 396–401.

Weiss, G.L., Kieninger, A.-K., Maldener, I., Forchhammer, K., Pilhofer, M., 2019. Structure and Function of a Bacterial Gap Junction Analog. Cell 178, 374-384.

Wilcox, M., Mitchison, G.J., Smith, R.J., 1973. Pattern formation in the blue-green algae *Anabaena.* II. Controlled proheterocyst regression. J. Cell Sci. 13, 637–649.

Wilk, L., Strauss, M., Rudolf, M., Nicolaisen, K., Flores, E., Kühlbrandt, W., Schleiff, E., 2011. Outer membrane continuity and septosome formation between vegetative cells in the filaments of *Anabaena* sp. PCC 7120. Cell. Microbiol. 13, 1744–1754.

Wolk, C.P., Ernst, A., Elhai, J., 1994. Heterocyst Metabolism and Development, in: The Molecular Biology of Cyanobacteria. Springer Netherlands, pp. 769–823.

Wolk, C.P., Thomas, J., Shaffer, P.W., Austin, S.M., Galonsky, A., 1976. Pathway of nitrogen metabolism after fixation of ^{13}N labeled nitrogen gas by the cyanobacterium, *Anabaena cylindrica*. J. Biol. Chem. 251, 5027–5034.

Wylie, J.L., Worobec, E.A., 1995. The OprB porin plays a central role in carbohydrate uptake in *Pseudomonas aeruginosa*. J. Bacteriol. 117, 3021–3026.

Xu, Q., Ellena, J.F., Kim, M., Cafiso, D.S., 2006. Substrate-dependent unfolding of the energy coupling motif of a membrane transport protein determined by double electron-electron resonance. Biochemistry 45, 10847–10854.

Youderian, P., Burke, N., White, D.J., Hartzell, P.L., 2003. Identification of genes required for adventurous gliding motility in *Myxococcus xanthus* with the transposable element mariner. Mol. Microbiol. 49, 555–570.

Zhang, J.Y., Lin, G.M., Xing, W.Y., Zhang, C.C., 2018. Diversity of growth patterns probed in live cyanobacterial cells using a fluorescent analog of a peptidoglycan precursor. Front. Microbiol. 9, 791.

Zhao, Q., Li, X.Z., Mistry, A., Srikumar, R., Zhang, L., Lomovskaya, O., Poole, K., 1998. Influence of the tonB energy-coupling protein on efflux-mediated multidrug resistance in *Pseudomonas aeruginosa*. Antimicrob. Agents Chemother. 42, 2225–2231.

Zhao, Q., Poole, K., 2002a. Differential Effects of Mutations in *tonB1* on Intrinsic Multidrug Resistance and Iron Acquisition in *Pseudomonas aeruginosa*. J. Bacteriol. 184, 2045–2049.

Zhao, Q., Poole, K., 2002b. Mutational analysis of the TonB1 energy coupler of *Pseudomonas aeruginosa*. J. Bacteriol. 184, 1503–1513.

6. Appendix

Supplementary Material Manuscript 1

A TonB-like protein, SjdR, is involved in the structural definition of the intercellular septa in the heterocyst-forming cyanobacterium *Anabaena*

Schätzle Hannah, Arévalo Sergio, Flores Enrique, Schleiff Enrico

mBio (2021), 12(3):e00483-21

Supplementary Figures

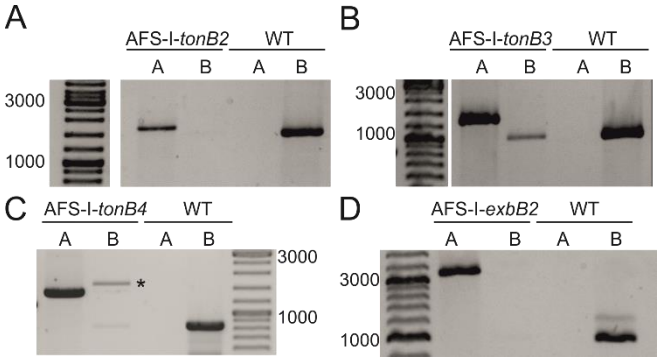

Figure S1. Genotypes of mutants utilized in this study. Genomic DNA from the wild type (WT) and I-*tonB2* (A), I-*tonB3* (B), I-*tonB4* (C), and I-*exbB2* (D) mutants was used as the PCR template. Oligonucleotides used for screening are listed in Table S1. The *tonB3* mutant was already mentioned in previous studies (44). For each mutant, an oligonucleotide combination specific for the gene of interest (lanes marked with B) or a combination where one oligonucleotide anneals in the plasmid used for insertion and the other oligonucleotide anneals in the gene (lanes marked with A) was used (imaged in Fig. 1). The gene-specific fragment in lanes B is expected in the wild-type strain and also in nonsegregated mutants, whereas fragment in lanes A is expected only in the mutant strains. I-*tonB2* and I-*exbB2* mutants are segregated, whereas I-*tonB3* and I-*tonB4* mutants are not segregated. The asterisk in panel C indicates an unspecific PCR product.

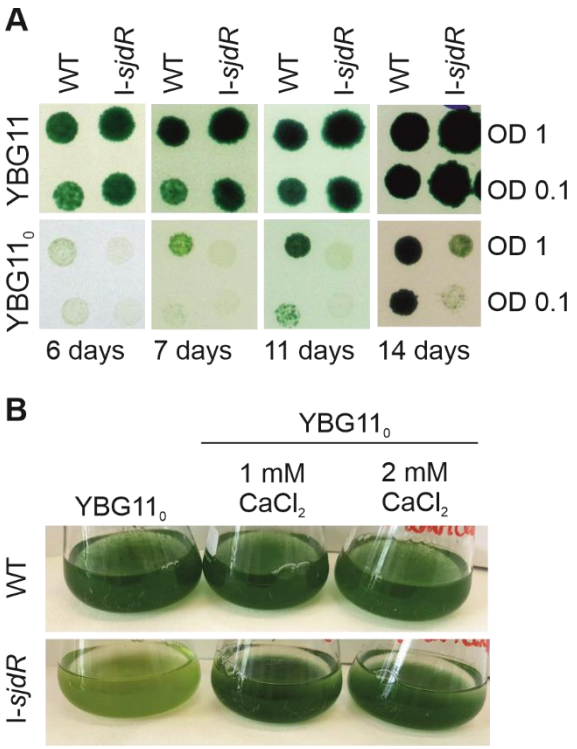

Figure S2. Growth of the wild type and the I-*sjdR* mutant in the presence and absence of combined nitrogen. (A) Five-microliter portions of cultures with an optical density at 750 nm of 1 or 0.1 were spotted on plates containing nitrate (YBG11) or on plates without combined nitrogen source (YBG11$_0$). The pictures for days 7 and 11 are taken from the same plate; the other pictures show independent plates. (B) Growth of the wild type and I-*sjdR* mutant in liquid cultures without a source of combined nitrogen with the indicated concentrations of calcium. YBG11$_0$ contains a final concentration of 245 µM $CaCl_2$.

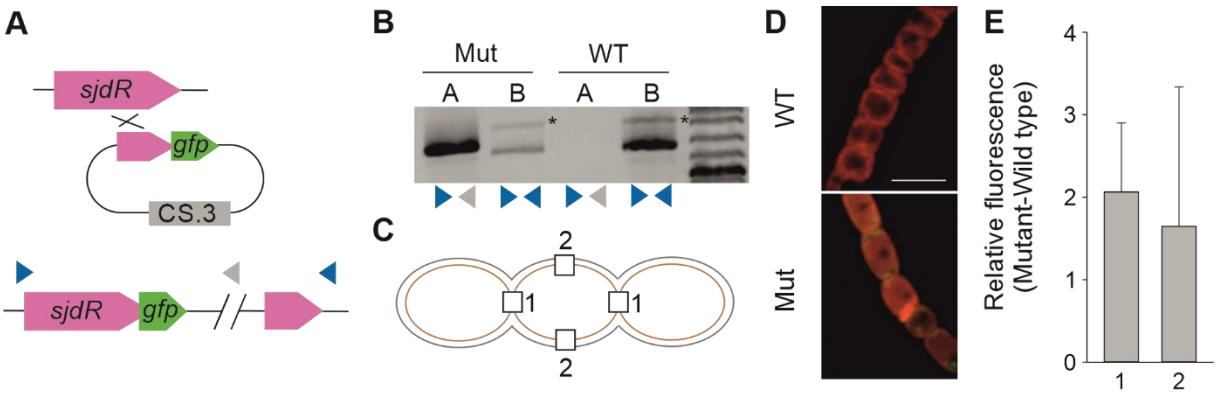

Figure S3. Construction and analysis of the *sjdR-gfp* strain. (A) Illustration of homologous recombination of plasmid pCSV3-sjdR-sf-gfp into the *Anabaena* genome. The genotype of the *sjdR-gfp* mutant strain is indicated at the bottom; the arrowheads indicate annealing sites of the oligonucleotides used for screening. (B) PCR on DNA of the *sjdR-gfp* mutant (Mut) and wild type (WT), an oligonucleotide pair indicating the plasmid insertion (A) or oligonucleotides annealing outside of the homologous region indicating the presence of the wild-type *sjdR* gene (B) were used. The asterisk marks an unspecific PCR product. (C) Schematic illustration of the regions where the GFP fluorescence was measured in the wild type and the *sjdR-gfp* strain. (D) Examples of fluorescence images for WT and *sjdR-gfp* strain, a merge of autofluorescence (red) and GFP (green) channels is shown. The reference bar indicates 5 µm. (E) GFP fluorescence was quantified at regions 1 and 2 as depicted in panel C, and the wild-type values were subtracted from the fluorescence in the mutant. A minimum of 120 measurements at the septum or the sidewall were taken from different filaments of each strain. The error bars indicate the standard deviations

Supplementary Tables

Table S1: Oligonucleotides used in this study

Oligonucleotide	Sequence (5'-3')	Purpose
sjdR-fw	GAATTCGTGTTAACCGTGATG	Cloning
sjdR-rv	GATATCGGAGAGGGACTAGG	
tonB2-fw	ATTAATAGATCTGTTGCAGTACCTCAGGGTTG	
tonB2-rv	ATTAATAGATCTGATTTACCTTGCAGCGATC	
tonB4-fw	AGATCTCCATTCCTTTGAATTC	
tonB4-rv	AGATCTGGAACAGCCTTTGGAA	
exbB2-fw	GGATCCGGCGTTCTCCTTATTAG	
exbB2-rv	GGATCCGCCGTCTTTGTTCCTCCC	
1636-fw	GGATCCGCATCATACTCGATCTCCC	
1636-rv	GGATCCGCTAGCCAATCATTTGCC	
1655-fw	GGATCCCCTTAGCCCGTTTAGATACC	
1655-rv	GGATCCCCTCAATCACTTCTGAACG	
sf-gfp-fw	GATATCGGTGGTGGTGGTGTGAGCAAGGGCGAGGAG	
sf-gfp-rv	CGGTACCTTACTTGTACAGCTCGTCC	
sjdR-gfp-fw	GCATCGATGGTAATACTCACACTAACG	
sjdR-gfp-rv	GCGATATCTTGACTAGGATTACTGTTTTG	
exbB2-s.fw	CTATTTACAGCCGGTGG	Screening
exbB2-s.rv	CCAAGCCAGATGCAGTAG	
pCSEL24-fw	GATACTTCGGCGATCACC	
pCSV3-1fw	CTGATGCCGCATAGTTAAGCC	
pCSV3-2fw	CCACGGAATGATGTCGTCGTG	
sjdR-s.fw	CCAGAATTTAACACTGGTGAG	
sjdR-s.rv	GCTCACGTCAATGCCTACC	
tonB2-s.fw	GGCAATACCCACCTTACGG	
tonB2-s.rv	GCGCTGTCGGACGTTATG	
tonB3-s.fw	GACTAAGTTGGTGAGAATAGG	
tonB3-s.rv	GGATCTGACTCTAGTTTCCC	
tonB4-s.fw	GTACAATCTCAATCATTCTGG	
tonB4-s.rv	CTGACGAAGTTGATCATTGC	
1636-s.fw	CCTCTGGTAGCACTTCTGG	
1636-s.rv	CTCAGTTACGCAATACAAAGC	
1655-s.fw	CCAGTTCCTATCAGCAGTCTC	
1655-s.rv	GCTCTAAACTGGCTAGACGG	
rnpB-qRT.fw	GTAGGCGTTGGCGGTTG	qRT PCR
rnpB-qRT.rv	CACTGGACGTTATCCAGC	
sjdR-qRT.fw	GCACCTGCTATTACTCCTCAGCC	
sjdR-qRT.rv	CCCGCTTTGTGACTGGTCTC	
nifH-qRT.fw	CGTATCCTACGACGTATTGG	
nifH-qRT.rv	CGCCATCATTTCACCAGAGG	
ntcA-qRT.fw	GTGGAGCAAGCACTGAAGG	
ntcA-qRT.rv	CATATCTCGGTGCGCTAAGG	
hepA-qRT.fw	CGCGGTGTCCGTTTATCTGG	
hepA-qRT.rv	CTGAATCTAGGGCGCTGGTG	

Table S2: *Anabaena* sp. strains used in this study

Strain	Resistance	Genotype	Reference
WT	-		
AFS-I-*sjdR*	Sp^R/Sm^R	*alr0248*::pCSEL24	This study
AFS-I-*tonB2*	Sp^R/Sm^R	*all3585*::pCSV3	This study
AFS-I-*tonB3*	Sp^R/Sm^R	*all5036*::pCSV3	Stevanovic, M., Hahn, A., Nicolaisen, K., Mirus, O., & Schleiff, E. (2012). Environmental Microbiology, 14, 1655–1670.
AFS-I-*tonB4*	Sp^R/Sm^R	*alr5329*::pCSV3	This study
AFS-I-*exbB2*	Sp^R/Sm^R	*alr4587*::pCSV3	This study
AFS-I-*1655*	Sp^R/Sm^R	*alr1655*::pCSV3	Kind gift from Leonard Fresenborg
AFS-I-*1636*	Sp^R/Sm^R	*all1636*::pCSV3	Kind gift from Leonard Fresenborg
AFS-*sjdR-gfp*	Sp^R/Sm^R	*alr0248*::pCSV3-gfp	This study

Table S3: Plasmids used in this study

Plasmid	Resistance	Insert	Purpose	Reference
pCSV3	Sp^R/Sm^R		Cloning	Valladares, A., Rodríguez, V., Camargo, S., Martínez-Noël, G. M. A., Herrero, A., & Luque, I. (2011). Journal of Bacteriology, 193, 1172–1182.
pCSEL24	Sp^R/Sm^R			Olmedo-Verd, E., Muro-Pastor, A. M., Flores, E., & Herrero, A. (2006). Journal of Bacteriology, 188, 6694–6699.
pCSEL21	Amp^R	*gfp-mut2*		Olmedo-Verd, E., Muro-Pastor, A. M., Flores, E., & Herrero, A. (2006). Journal of Bacteriology, 188, 6694–6699.
pCSEL21-sf-gfp	Amp^R	*sf-gfp*		In here
pCSEL24-alr0248	Sp^R/Sm^R	Internal fragment of *sjdR*	Generation of single-recombinant mutants	
pCSV3-all3585	Sp^R/Sm^R	Internal fragment of *tonB2*		
pCSV3-all5036	Sp^R/Sm^R	Internal fragment of *tonB3*		Stevanovic, M., Hahn, A., Nicolaisen, K., Mirus, O., & Schleiff, E. (2012). Environmental Microbiology, 14, 1655–1670.
pCSV3-alr5329	Sp^R/Sm^R	Internal fragment of *tonB4*		
pCSV3-alr4587	Sp^R/Sm^R	Internal fragment of *exbB2*		
pCSV3-all1636	Sp^R/Sm^R	Internal fragment of *all1636*		Kind gift from L. Fresenborg
pCSV3-alr1655	Sp^R/Sm^R	Internal fragment of *alr1655*		Kind gift from L. Fresenborg
pCSV3-sjdR-sf-gfp	Sp^R/Sm^R	*sjdR-sf-gfp*		In here

Table S4: Starvation status of cultures utilized for schizokinen uptake measurements

Strain (No. of replicates)	Chl at OD_{750}=1 (mg/ml)	Uptake rate (mol Fe/l*h) at OD_{750}=1	Avg. uptake rate ± SD (mol Fe/l*h)
Wild-type (15)	0.00087083	$1.1*10^{-8}$	$7±3.4*10^{-9}$
	0.0007723	$1.1*10^{-8}$	
	0.00066603	$6.6*10^{-9}$	
	0.00095435	$9.5*10^{-9}$	
	0.00088591	$5.8*10^{-9}$	
	0.00097211	$1.4*10^{-8}$	
	0.00084629	$4.3*10^{-9}$	
	0.0009489	$9.5*10^{-9}$	
	0.00073781	$5.1*10^{-9}$	
	0.00087414	$2.6*10^{-9}$	
	0.00063053	$2.5*10^{-9}$	
	0.00079717	$7.2*10^{-9}$	
	0.00067266	$4.7*10^{-9}$	
	0.00095444	$5.0*10^{-9}$	
	0.00068604	$9.1*10^{-9}$	
AFS-I-*sjdR* (6)	0.000668	$10.0*10^{-9}$	$6±2.5*10^{-9}$
	0.000769	$6.3*10^{-9}$	
	0.001005	$8.8*10^{-9}$	
	0.000769	$6.6*10^{-9}$	
	0.000703	$5.3*10^{-9}$	
	0.000721	$2.9*10^{-9}$	
AFS-I-*tonB3* (6)	0.00056119	$2.3*10^{-11}$	$4.0±0.1*10^{-11}$
	0.00064332	$1.2*10^{-10}$	
	0.00125149	$-7.4*10^{-11}$	
	0.00118604	$-9.6*10^{-11}$	
	0.00109563	$9.8*10^{-11}$	
	0.00093688	$1.7*10^{-10}$	

Table S5: Cyanobacteria with SjdR-like sequences

Order	Family	Genus	Species/Strain	
Nostocales	Nostocaceae	Nostoc	unclassified Nostoc	Nostoc sp. ATCC 43529
Nostocales	Nostocaceae	Nostoc	unclassified Nostoc	Nostoc sp. ATCC 53789
Nostocales	Nostocaceae	Nostoc	unclassified Nostoc	Nostoc sp. CENA543
Nostocales	Nostocaceae	Nostoc	unclassified Nostoc	Nostoc sp. HK-01
Nostocales	Nostocaceae	Nostoc	unclassified Nostoc	Nostoc sp. KVJ20
Nostocales	Nostocaceae	Nostoc	unclassified Nostoc	Nostoc sp. 'Lobaria pulmonaria (5183) cyanobiont'
Nostocales	Nostocaceae	Nostoc	unclassified Nostoc	Nostoc sp. MBR 210
Nostocales	Nostocaceae	Nostoc	unclassified Nostoc	Nostoc sp. NIES-4103
Nostocales	Nostocaceae	Nostoc	unclassified Nostoc	Nostoc sp. PA-18-2419
Nostocales	Nostocaceae	Nostoc	unclassified Nostoc	Nostoc sp. PCC 7107
Nostocales	Nostocaceae	Nostoc	unclassified Nostoc	Nostoc sp. PCC 7120
Nostocales	Nostocaceae	Nostoc	unclassified Nostoc	Nostoc sp. PCC 7524
Nostocales	Nostocaceae	Nostoc	unclassified Nostoc	Nostoc sp. 'Peltigera membranacea cyanobiont' 210A
Nostocales	Nostocaceae	Nostoc	unclassified Nostoc	Nostoc sp. 'Peltigera membranacea cyanobiont' 232
Nostocales	Nostocaceae	Nostoc	unclassified Nostoc	Nostoc sp. 'Peltigera malacea cyanobiont' DB3992
Nostocales	Nostocaceae	Nostoc	unclassified Nostoc	Nostoc sp. 'Peltigera membranacea cyanobiont' N6
Nostocales	Nostocaceae	Nostoc	unclassified Nostoc	Nostoc sp. RF31YmG
Nostocales	Nostocaceae	Nostoc	unclassified Nostoc	Nostoc sp. T09
Nostocales	Nostocaceae	Nostoc	unclassified Nostoc	Nostoc sp. TCL240-02
Nostocales	Nostocaceae	Nostoc	unclassified Nostoc	Nostoc sp. UIC 10630
Nostocales	Nostocaceae	Nostoc	Nostoc calcicola	
Nostocales	Nostocaceae	Nostoc	Nostoc carneum	
Nostocales	Nostocaceae	Nostoc	Nostoc commune	
Nostocales	Nostocaceae	Nostoc	Nostoc cycadae	
Nostocales	Nostocaceae	Nostoc	Nostoc flagelliforme	
Nostocales	Nostocaceae	Nostoc	Nostoc linckia	

Nostocales	Nostocaceae	Nostoc	Nostoc minutum NIES-26	
Nostocales	Nostocaceae	Nostoc	Nostoc piscinale	
Nostocales	Nostocaceae	Nostoc	Nostoc punctiforme NIES-2108	
Nostocales	Nostocaceae	Nostoc	Nostoc punctiforme	
Nostocales	Nostocaceae	Nostoc	Nostoc sphaeroides	
Nostocales	Nostocaceae	Nostoc	Nostoc sphaeroides CCNUC1	
Nostocales	Nostocaceae	Anabaena	unclassified Anabaena	Anabaena sp.
Nostocales	Nostocaceae	Anabaena	unclassified Anabaena	Anabaena sp. UHCC 0204
Nostocales	Nostocaceae	Anabaena	unclassified Anabaena	Anabaena sp. UHCC 0253
Nostocales	Nostocaceae	Cylindrospermum	Cylindrospermum stagnale	
Nostocales	Nostocaceae	Cylindrospermum	unclassified Cylindrospermum	Cylindrospermum sp. NIES-4074
Nostocales	Aphanizomenonaceae	Anabaenopsis	Anabaenopsis circularis	
Nostocales	Aphanizomenonaceae	Nodularia	unclassified Nodularia	Nodularia sp.
Nostocales	Calotrichaceae	Calothrix, Calothrix brevissima		
Nostocales	Calotrichaceae	Calothrix, Calothrix desertica		
Nostocales	Calotrichaceae	Calothrix	unclassified Calothrix	Calothrix sp. 336/3
Nostocales	Calotrichaceae	Calothrix	unclassified Calothrix	Calothrix sp. HK-06
Nostocales	Calotrichaceae	Calothrix	unclassified Calothrix	Calothrix sp. NIES-2100
Nostocales	Calotrichaceae	Calothrix	unclassified Calothrix	Calothrix sp. NIES-2098
Nostocales	Calotrichaceae	Calothrix	unclassified Calothrix	Calothrix sp. NIES-4101
Nostocales	Calotrichaceae	Calothrix	unclassified Calothrix	Calothrix sp. PCC 7103
Nostocales	Chlorogloeopsidaceae	Chlorogloeopsis	Chlorogloeopsis fritschii	
Nostocales	Hapalosiphonaceae	Fischerella	unclassified Fischerella	Fischerella sp. PCC 9431
Nostocales	Hapalosiphonaceae	Fischerella	Fischerella muscicola	
Nostocales	Hapalosiphonaceae	Fischerella	Fischerella thermalis	
Nostocales	Hapalosiphonaceae	Hapalosiphon	unclassified Hapalosiphon	Hapalosiphon sp. MRB220
Nostocales	Scytonemataceae	Scytonema	unclassified Scytonema	Scytonema sp. HK-05
Nostocales	Scytonemataceae	Scytonema	unclassified Scytonema	Scytonema sp. UIC 10036
Nostocales	Scytonemataceae	Scytonema	Scytonema millei	

Nostocales	Stigonemataceae	unclassified Stigonemataceae	Cyanobacterium PCC 7702	
Nostocales	Tolypothrichaceae	Hassallia	Hassallia byssoidea	
Nostocales	Tolypothrichaceae	Tolypothrix	Scytonema hofmanni	
Nostocales	Tolypothrichaceae	Tolypothrix	Tolypothrix bouteillei	
Nostocales	Tolypothrichaceae	Tolypothrix	unclassified Tolypothrix	Scytonema hofmanni UTEX B 1581
Nostocales	Tolypothrichaceae	Tolypothrix	unclassified Tolypothrix	Tolypothrix sp. PCC 7910
Nostocales	Tolypothrichaceae	Tolypothrix	unclassified Tolypothrix	Tolypothrix sp. NIES-4075
Oscillatoriophycideae	Chroococcales	unclassified Chroococcales	Chroococcales cyanobacterium IPPAS B-1203	
Oscillatoriophycideae	Chroococcales	Aphanothecaceae	Gloeothece	Gloeothece verrucosa
Oscillatoriophycideae	Chroococcales	Entophysalidaceae	Chlorogloea	unclassified Chlorogloea
Oscillatoriophycideae	Chroococcales	Chroococcaceae	Cyanosarcina	Cyanosarcina burmensis
Oscillatoriophycideae	Chroococcales	Chroococcaceae	Chroogloeocystis	Chroogloeocystis siderophila
Oscillatoriophycideae	Chroococcales	Chroococcaceae	Gloeocapsopsis	unclassified Gloeocapsopsis
Oscillatoriophycideae	Chroococcales	Chroococcaceae	Gloeocapsa	unclassified Gloeocapsa
Oscillatoriophycideae	Oscillatoriales	Desertifilaceae	Desertifilum	unclassified Desertifilum
Oscillatoriophycideae	Oscillatoriales	Desertifilaceae	Desertifilum	unclassified Desertifilum
Oscillatoriophycideae	Oscillatoriales	Oscillatoriaceae	Oscillatoria	unclassified Oscillatoria
Oscillatoriophycideae	Oscillatoriales	Oscillatoriaceae	Phormidium	Phormidium ambiguum
Oscillatoriophycideae	Oscillatoriales	Coleofasciculaceae	Geitlerinema	unclassified Geitlerinema
Oscillatoriophycideae	Oscillatoriales	Microcoleaceae	Microcoleus	unclassified Microcoleus
Oscillatoriophycideae	Oscillatoriales	Microcoleaceae	Kamptonema	unclassified Kamptonema
Chroococcidiopsidales	Chroococcidiopsidaceae	Chroococcidiopsis	Chroococcidiopsis cubana	
Chroococcidiopsidales	Chroococcidiopsidaceae	Aliterella	Aliterella atlantica	
Chroococcidiopsidales	Chroococcidiopsidaceae	Chroococcidiopsis	unclassified Chroococcidiopsis	Chroococcidiopsis sp. TS-821
Synechococcales	Merismopediaceae	Synechocystis	unclassified Synechocystis	Synechocystis sp. PCC 7509
Synechococcales	Leptolyngbyaceae	Phormidesmis	Phormidesmis priestleyi	

Synechococcales	Leptolyngbyaceae	Neosynechococcus	Neosynechococcus sphagnicola
Synechococcales	Leptolyngbyaceae	unclassified Leptolyngbyaceae	Leptolyngbyaceae cyanobacterium SL_7_1
unclassified Cyanobacteria	Cyanobacteria bacterium UBA11371		
unclassified Cyanobacteria	Cyanobacteria bacterium UBA11049		
unclassified Cyanobacteria	Cyanobacteria bacterium UBA9273		
unclassified Cyanobacteria	Cyanobacteria bacterium UBA11148		

Supplementary Material Manuscript 2

Functional diversity of TonB-like proteins in the heterocyst-forming cyanobacterium *Anabaena* sp. PCC 7120

Schätzle Hannah, Arévalo Sergio, Flores Enrique, Schleiff Enrico

Accepted for publication in mSphere (2021)

Supplemental Material

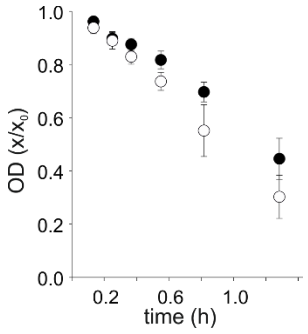

Figure S1. Sedimentation of I-*tonB2* (white symbols) and wild-type cultures (black symbols). The OD_{750} was measured in one cuvette after specific time points without further resuspension of the suspension. Average values of four biological replicates per strain with two technical replicates each are given, error bars show the standard deviation. Due to enhanced aggregation, I-*tonB2* filaments sediment faster in the cuvette than wild-type samples, which is indicated by a faster decrease of the OD_{750}.

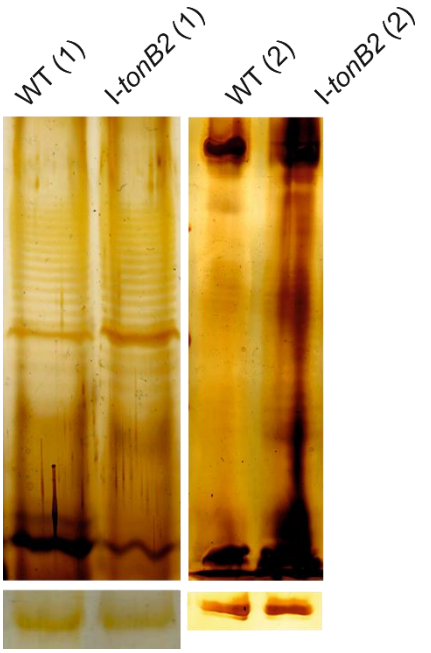

Figure S2. LPS extractions from wild-type *Anabaena* and I-*tonB2* cultures. (1) Cultures grown in tubes in the presence of 1% CO_2. (2) Cultures grown without bubbling in shaking flasks; a higher degree of aggregation was observed without CO_2 supplementation. The LPS isolated from the cultures was separated by SDS-PAGE and silver stained. The bottom panel shows the loading control (large subunit of Rubisco).

Table S1. Oligodeoxynucleotides used in the study

Oligonucleotide	Sequence (5'-3')	Purpose
tonB1-fw	GAATTCGTGTTAACCGTGATG	Cloning
tonB1-rv	GATATCGGAGAGGGACTAGG	
tonB2-fw	ATTAATAGATCTGTTGCAGTACCTCAGGGTTG	
tonB2-rv	ATTAATAGATCTGATTTACCTTGCAGCGATC	
tonB3-fw	ATTAATAGATCTCTGACACGAGTTCCTCAAGTTG	
tonB3-rv	ATTAATAGATCTCTTCGTCTAGTTCTCGATTACCGC	
tonB4-fw	AGATCTCCATTCCTTTGAATTC	
tonB4-rv	AGATCTGGAACAGCCTTTGGAA	
tonB1-s.fw	CCAGAATTTAACACTGGTGAG	Screening of *Anabaena* mutants
tonB1-s.rv	GCTCACGTCAATGCCTACC	
tonB2-s.fw	GGCAATACCCACCTTACGG	
tonB2-s.rv	GCGCTGTCGGACGTTATG	
tonB3-s.fw	GACTAAGTTGGTGAGAATAGG	
tonB3-s.rv	GGATCTGACTCTAGTTTCCC	
tonB4-s.fw	GTACAATCTCAATCATTCTGG	
tonB4-s.rv	CTGACGAAGTTGATCATTGC	
Vector-s	CTGATGCCGCATAGTTAAGCC	
rnpB-qRT.fw	GTAGGCGTTGGCGGTTG	qRT PCR
rnpB-qRT.rv	CACTGGACGTTATCCAGC	
tonB2-qRT.fw	GAACGGGTTGCAGTACCTC	
tonB2-qRT.rv	CAGCGTTTGGCGTAACAGG	
tonB3-qRT.fw	GCCAGATATTCCAGCACAG	
tonB3-qRT.rv	GGCAAACCTTCTGAACGAG	
tonB4-qRT.fw	CCAACGCCTGTCACTATTAC	
tonB4-qRT.rv	CTAACGAGACTGAAAGCACC	

Table S2. Plasmids used in this study

Plasmid	Resistance	Insert	Purpose	Reference
pCSV3	Sp^R/Sm^R		Cloning	(95)
pCSEL24	Sp^R/Sm^R			(96)
pCSEL24-alr0248	Sp^R/Sm^R	Internal fragment of *tonB1*	Generation of single-recombinant mutants	
pCSV3-all3585	Sp^R/Sm^R	Internal fragment of *tonB2*		
pCSV3-all5036	Sp^R/Sm^R	Internal fragment of *tonB3*		(38)
pCSV3-alr5329	Sp^R/Sm^R	Internal fragment of *tonB4*		

Table S3. *Anabaena* strains used in this study

Strain	Resistance	Genotype	Reference
WT	-		
AFS-I-*tonB1*	Sp^R/Sm^R	*alr0248*::pCSEL24	
AFS-I-*tonB2*	Sp^R/Sm^R	*all3585*::pCSV3	
AFS-I-*tonB3*	Sp^R/Sm^R	*all5036*::pCSV3	(38)
AFS-I-*tonB4*	Sp^R/Sm^R	*alr5329*::pCSV3	

Table S4. ^{55}Fe-Schizokinen uptake rates and normalized chlorophyll values

Strain	Uptake rates (mol Fe/l*h) at OD_{750}=1	Chl / OD_{750} (mg/ml)
Wild type	$1.6*10^{-8}$	0.0010
	$4.7*10^{-9}$	0.0011
	$9.5*10^{-9}$	0.0013
	$8.3*10^{-9}$	0.0013
	$1.8*10^{-9}$	0.0010
	$1.7*10^{-8}$	0.0010
	$6.4*10^{-9}$	0.0011
	$3.7*10^{-9}$	0.0013
I-*tonB2*	$4.9*10^{-9}$	0.0009
	$9.3*10^{-9}$	0.0009
	$4.8*10^{-9}$	0.0011
	$2.2*10^{-9}$	0.0006
	$8.2*10^{-9}$	0.0010
	$3.6*10^{-9}$	0.0006
	$1.4*10^{-9}$	0.0006
I-*tonB4*	$1.6*10^{-8}$	0.0008
	$4.8*10^{-9}$	0.0008
	$3.7*10^{-9}$	0.0006
	$3.7*10^{-9}$	0.0007
	$8.0*10^{-9}$	0.0009
	$7.3*10^{-9}$	0.0012
	$5.6*10^{-9}$	0.0012

Supplementary Material Manuscript 3

Comparative phenotypic analysis of *Anabaena* sp. PCC 7120 mutants of porin-like genes

Schätzle Hannah, Brouwer Eva-Maria, Liebhart Elisa, Stevanovic Mara, Schleiff Enrico

Journal of Microbiology and Biotechnology (2021), 31(5): 645-658

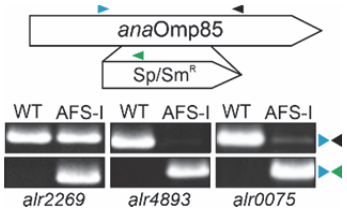

Figure S1. Segregation of *omp85* mutants. On top the orientation of the cassette is shown indicating the position of the primers used. The PCR product using gDNA isolated from the wild type (first lane, WT) or the indicated mutant strain (second lanes; AFS-I) using oligonucleotides flanking the recombination site (blue / black, upper panel) or using the gene specific forward and the cassette specific primer (blue, green) is shown. The strains are not segregated as judged from the occurrence of the wild-type gene with *alr2269* showing the lowest degree of segregation.

Table S1. Oligonucleotides used in this manuscript

purpose	name	sequence
mutagenesis	alr0834_FW	ATTTATAGATCTCAGCGATGTCTTATCAGGCG
	alr0834_RV	ATTTATAGATCTGGTCATTTGCTGTACCACTC
	alr2231_FW	AATTAAAGATCTGCATTGGCTAGTGTATTTGGC
	alr2231_RV	AATTAAAGATCTCGATGGGACAACGTAGCCAGCAG
	all4499_FW	AGATCTATCCCAACGGTACATACCGTGG
	all4499_RV	AGATCTGGATAGCATCGCTGAAGTTGAATGC
	alr4550_FW	AGATCTGGTTGAGCGCTACGGTTGTATTGC
	alr4550_RV	AGATCTCTGCTGCATAATGGCTATGTCG
	alr4741_FW	AGATCTGTGATTAGTGAAGATGCTC
	alr4741_RV	AGATCTGATATTAAGCCGATACG
	all5191_FW	AGATCTGGCACTACAAGCATTAAC
	all5191_RV	AGATCTCCAAAGCGTACAAAGTGACG
	all7614_FW	AGATCTGTTACATCAGTTTCC
	all7614_RV	AGATCTGAGAGTTGCCAACAGGGAAG
Screening of mutants	CS3_Rv	CTGATGCCGCATAGTTAAGCC
	alr0834_FW2	CTGCGGAACTAGCAAC
	alr0834_RV2	TTCGGATCCTTAGAAACTAAATGTGGTTCTC
	alr2231_FW2	TACTAAACTGCGGGGAGAAG
	alr2231_RV2	AATTAACTGCAGAAGCTTGAAACTAAAAGTAGTAC
	all4499_FW2	GGGCATTCCAAGCAC
	all4499_RV2	CTCAGCACCAGTAGC
	alr4550_FW2	CCGCTACAGTAACGAAG
	alr4550_RV2	CAATGCGGTAGATGGG
	alr4741_FW2	GGCGGAAGATATAGTC
	alr4741_RV2	CCAAGCTAATCTCGCC
	all5191_FW2	CCCATGATAGTTGGGC
	all5191_RV2	GGAAATTGAACCGTCTCC
	all7614_FW2	CAGCCATCACAAAC
	all7614_RV2	GCTGCATAGTTACCATCG
	alr0075_FW	ATGGATACGCCCAATATGGT
	alr0075_RV	TCCCAAGTCACCACGAAATA
	alr2269_FW	AGCCCAACCCCGTCTTA
	alr2269_RV	AGGCTGTCCATTCTGCTCTT
	alr4893_FW	ATCGGCAAACCCATCAG

	alr4893_RV	CCACGGACGGAGTTAGAA
qRT-PCR porins	0834-qRT-Fw	CGCGATTAGAACTTGTCTCC
	0834-qRT-Rw	GCTAGCGAAGAACAGGTTAC
	2231-qRT-Fw	TACTAAACTGCGGGGAGAAG
	2231-qRT-Rw	CCTCAAGATTCGGTCTGCTA
	4499-qRT-Fw	CAGGATTAGCCGCACTATTC
	4499-qRT-Rw	TATCTACCGCCAAGCCTATG
	4550-qRT-Fw	CGCGTATCTGACAACATC
	4550-qRT-Rw	GAAGGTGGTTCTCAGAGT
	4741-qRT-Fw	TGCTGATATCCAGGCTCAAC
	4741-qRT-Rw	CTCCATCACCTGGACGATTC
	5191-qRT-Fw	ATCGCGCCATAGGGACTAGC
	5191-qRT-Rw	GGTGCAGGTATCGGGATTTC
	7614-qRT-Fw	GCTGCATAGTTACCATCG
	7614-qRT-Rw	GTCCCATTTGGTAGTGGTAG
	rnpB-qRT-F1	GTAGGCGTTGGCGGTTG
	rnpB-qRT-R1	CACTGGACGTTATCCAGC

Table S2. Plasmids used in this study.

Plasmid Name	Marker	Properties	Reference
pCSV3	Sp^R Sm^R		[33]
pCSV3-*alr0834*	Sp^R Sm^R	pCSV3 with fragment of *alr0834*	
pCSV3-*alr2231*	Sp^R Sm^R	pCSV3 with fragment of *alr2231*	
pCSV3-*all4499*	Sp^R Sm^R	pCSV3 with fragment of *all4499*	
pCSV3-*alr4550*	Sp^R Sm^R	pCSV3 with fragment of *alr4550*	In here
pCSV3-*alr4741*	Sp^R Sm^R	pCSV3 with fragment of *alr4741*	
pCSV3-*all5191*	Sp^R Sm^R	pCSV3 with fragment of *all5191*	
pCSV3-*all7614*	Sp^R Sm^R	pCSV3 with fragment of *all7614*	

Table S3. *Anabaena* strains used in this study and their respective genotype

Name	Genotype	Segregated	Reference
Anabaena sp. PCC 7120	-	-	
AFS-I-*alr0075*	*alr0075*::CSV3	no	[56]
AFS-I-*alr2269*	*alr2269*::CSV3	no	[56]
AFS-I-*alr4893*	*alr4893*::CSV3	no	[56]
AFS-I-*alr0114*	*alr0114*::CSV3	no	[44]
AFS-I-*alr0834*	*alr0834*::CSV3	yes	In here
AFS-I-*alr2231*	*alr2231*::CSV3	no	In here
AFS-I-*all4499*	*all4499*::CSV3	no	In here
AFS-I-*alr4550*	*alr4550*::CSV3	yes	In here
AFS-I-*alr4741*	*alr4741*::CSV3	yes	In here
AFS-I-*all5191*	*all5191*::CSV3	yes	In here
AFS-I-*all7614*	*all7614*::CSV3	yes	In here